SYNTHESIS, CHARACTERIZATION, AND KINETICS OF ISOMERIZATION, C-H AND P-C BOND ACTIVATION FOR UNSATURATED DIPHOSPHINE-COORDINATED TRIOSMIUM CARBONYL CLUSTERS

Guanmin Wu

Dissertation Prepared for the Degree of

DOCTOR OF PHILOSOPHY

UNIVERSITY OF NORTH TEXAS

May 2008

APPROVED:

Michael G. Richmond, Major Professor and Chair
of the Department of Chemistry
William H. Watson, Committee Member
Diana S. Mason, Committee Member
Robert A. Stockland, Committee Member
Stephen A. Cooke, Committee Member
Sandra L. Terrell, Dean of the Robert B. Toulouse
School of Graduate Studies

Wu, Guanmin. Synthesis, characterization, and kinetics of isomerization, C-H and P-C bond activation for unsaturated diphosphine-coordinated triosmium carbonyl clusters. Doctor of Philosophy (Chemistry), May 2008, 177 pp., 18 tables, 41 figures, references, 172 titles.

Substitution of MeCN ligands in the activated cluster $Os_3(CO)10(MeCN)_2$ by the unsaturated diphosphine ligands (Z)-$Ph_2PCH=CHPPh_2$ (cDPPEn) or 4,5-bis(diphenylphosphino)-4-cyclopenten-1,3-dione (bpcd) proceeds rapidly at room temperature to furnish the ligand-bridged cluster 1,2-$Os_3(CO)_{10}$(P-P) (P-P represents cDPPEn or bpcd). Heating 1,2-$Os_3(CO)_{10}$(P-P) leads to the formation of the thermodynamically more stable chelating isomer 1,1-$Os_3(CO)_{10}$(P-P). Each compound of $Os_3(CO)_{10}$(P-P) has been characterized by x-ray diffraction, IR, ^{31}P NMR and ^{1}H NMR. Ligand isomerization kinetics have been investigated by UV-VIS and ^{31}P NMR (for cDPPEn) or ^{1}H NMR (for bpcd) spectroscopies. The isomerization mechanism is discussed based on the activation parameters and CO inhibition (for cDPPEn) or ligand trapping experiments (for bpcd).

Thermolysis of 1,1-$Os_3(CO)_{10}$(bpcd) in refluxing toluene gives the hydrido cluster $HOs_3(CO)_9[\mu$-$(PPh_2)C=C\{PPh(C_6H_4)\}C(O)CH_2C(O)]$ and the benzyne cluster $HOs_3(CO)_8(\mu_3$-$C_6H_4)[\mu_2,\eta^1$-$PPhC=C(PPh_2)C(O)CH_2C(O)]$. Photolysis of 1,1-$Os_3(CO)_{10}$(bpcd) using near UV light affords $HOs_3(CO)_9[\mu$-$(PPh_2)C=C\{PPh(C_6H_4)\}C(O)CH_2C(O)]$ as the sole product. $HOs_3(CO)_8(\mu_3$-$C_6H_4)[\mu_2,\eta^1$-$PPhC=C(PPh_2)C(O)CH_2C(O)]$ has been characterized in solution by IR and NMR spectroscopies. Furthermore its molecular structure has been determined by X-ray

crystallography. Reversible C-H bond formation in $HOs_3(CO)_9[\mu$-$(PPh_2)C{=}C\{PPh(C_6H_4)\}C(O)CH_2C(O)]$ is demonstrated by ligand trapping studies to give $1,1$-$Os_3(CO)_9L$(bpcd) (where L = CO, phosphine) via the unsaturated intermediate $1,1$-$Os_3(CO)_9$(bpcd). The kinetics for reductive coupling in $HOs_3(CO)_9[\gamma$-$(PPh_2)C{=}C\{PPh(C_6H_4)\}C(O)CH_2C(O)]$ and $DOs_3(CO)_9[\mu$-$(PPh_2$-$d_{10})C{=}C\{P(Ph$-$d_5)(C_6D_4)\}C(O)CH_2C(O)]$ in the presence of PPh_3 give rise to a k_H/k_D value of 0.88, whose magnitude supports the existence of a preequilibrium involving the hydride(deuteride) cluster and a transient arene-bound Os_3 species that precedes the rate-limiting formation of $1,1$-$Os_3(CO)_9$(bpcd). Strong proof for the proposed hydride(deuteride)/arene preequilibrium has been obtained from photochemical studies employing the isotopically labeled cluster $1,1$-$Os_3(CO)_{10}$(bpcd-$d_{4\textit{ortho}}$), whose bpcd phenyl groups each contain one *ortho* hydrogen and deuterium atom. Equilibrium and kinetic isotope effects in the orthometallation step has been determined by ^{1}H NMR in photochemical studies. Kinetics for the transformation from $HOs_3(CO)_9[\mu$-$(PPh_2)C{=}C\{PPh(C_6H_4)\}C(O)CH_2C(O)]$ to $HOs_3(CO)_8(\mu_3$-$C_6H_4)[\mu_2,\eta^1$-$PPhC{=}C(PPh_2)C(O)CH_2C(O)]$ has been studied by UV-VIS spectroscopy for which the mechanism is discussed.

ACKNOWLEDGMENTS

Firstly, I sincerely render my profound gratitude to Professor Michael G. Richmond, my major advisor, for his kind guidance, never-ending encouragement, assistance in directing the described research, and serving as the chairman of my advisory committee. I am especially grateful to Dr. Richmond for his model role as a professor and researcher, his efforts in stressing new knowledge, and his insistence for academic excellence, all of which do and will benefit me in my research and future endeavors. Drs. Diana Mason, Stephen Cooke, Robert Stockland, and William H. Watson are thanked for serving on my advisory committee. Dr. Watson is especially acknowledged for constantly supporting my research in single crystal structure determination and elucidation in the past several years. The help given to me by my group members including Dr. Jiancheng Wang, Jie Liu, Shih-huang Huang, Tao Chen, Dr. Srikanth Kandala, and Dr. Bhaskar Poola has been appreciated. I also want to thank Praveen K. Vadapalli and Alex Strugatskiy for their assistance during my time at UNT.

I am very grateful to my wife Fang Liu and my son Kevin for their love, support, and encouragement throughout the years.

Finally, I wish to thank the University of North Texas for support in the form of teaching assistantship and the Robert A. Welch Foundation for financial support in the form of a research assistantship. Novartis is thanked for support of my career development through its Tuition Reimbursement Program.

TABLE OF CONTENTS

LIST OF TABLES

Page

LIST OF FIGURES

Page

LIST OF SCHEMES

Page

CHAPTER I

INTRODUCTION

After the landmark discoveries of nickel tetracarbonyl and iron pentacarbonyl late in the 19th century, there was a period of development of the transition metal carbonyls that has led to a large number of interesting discoveries and diverse reaction chemistry. This chemistry has led not only to a substantial knowledge of the reactivity of bonded carbon monoxide but also to numerous applications in catalysis and organic synthesis. Carbonyl ligands have also played a significant and fundamental role in the development of transition metal cluster compounds and their applications.[1]

Cluster compounds, molecules containing three or more metal atoms connected by direct metal-metal bonds, provide a metal-metal framework in which ligands are able to coordinate to more than one metal center. The multisite coordination of ligands to a cluster frame has a profound effect on the structures, spectroscopic properties and chemical reactivity of the ligands and the cluster metal atoms. Moreover, certain molecules can be stabilized by clusters, which cannot be stabilized by mononuclear complexes. Both of the above factors may make clusters novel catalysts and platforms for the stabilization of reactive organic species.

Of all types of ligands, phosphines are the most common one associated with organotransition-metal compounds. Transition metals tend to coordinate trivalent phosphines with great affinity. Modified phosphine ligands are often utilized to change the activity or selectivity of homogeneous catalysts. The family of phosphine ligands consists of a great variety of substituted phosphines, which can be classified as

monodentate, bidentate and multidentate phosphines based on the binding capability of each phosphine ligand. These phosphine ligands exhibit a wide range of steric and electronic effects upon complexation to a metal center, be it a mononuclear or polynuclear entity.

A. Substitution Reactions of the Triosmium Dodecacarbonyl with Phosphine Ligands

1. Common Synthetic Methods for the Preparation of Substituted Triosmium Carbonyl Clusters and Pertinent Mechanisms

Simple substituted triosmium carbonyl clusters such as $Os_3(CO)_{11}L$, $Os_3(CO)_{10}L_2$ and $Os_3(CO)_9L_3$ (L = phosphine) and their reactions to give decarbonylation products containing ligand fragments from the original phosphine ligands have been known for a long time.[2-11]

Early studies on the substitution reactions of triosmium dodecacarbonyl had mainly been conducted by thermal or photochemical methods while attempting to maintain the integrity of the triosmium frame due to the great strength of Os-Os bonds.[12-13] However, subsequent ligand fragmentation and/or cluster decomposition was often observed during the course of these reactions.[14]

Thus, a synthetic strategy was sought by which the cluster platform could be activated under mild conditions to facilitate substitution reactions. In late 1970′s, new methods to prepare mono- and bis-substituted triosmium carbonyl clusters by using activated precursors such as $Os_3(CO)_{11}(NCMe)$, $Os_3(CO)_{10}(NCMe)_2$ and $Os_3(CO)_{10}(\eta^4\text{-}C_6H_8)$ to replace the parent triosmium dodecacarbonyl cluster in substitution reactions were developed in good yields. It turned out that $Os_3(CO)_{11}(NCMe)$ and

$Os_3(CO)_{10}(NCMe)_2$ represent the most valuable and earliest prepared of the activated triosmium clusters.[15-17] A simple substitution reaction scheme outlining this concept is shown below (Scheme 1.1).

Scheme 1.1. Synthesis of mono- and bis-substituted triosmium clusters with MeCN derivatives.

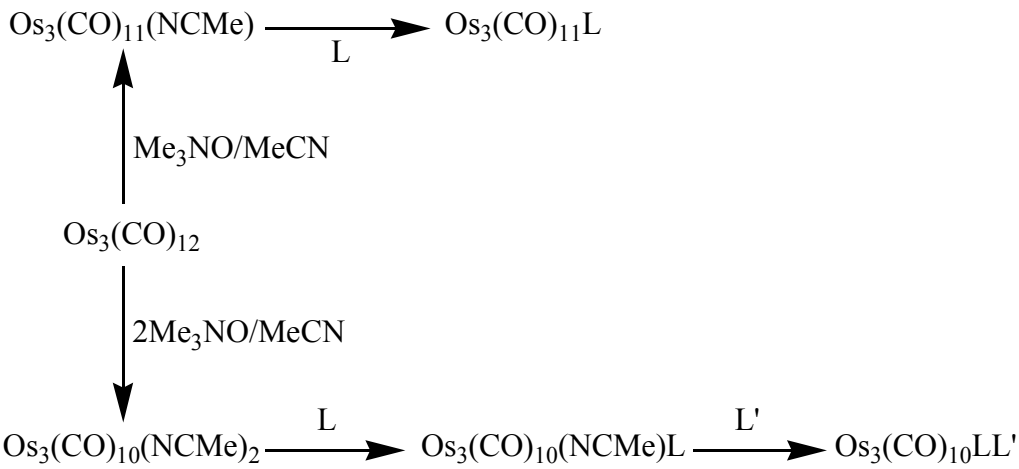

Since then, numerous studies on the synthesis of phosphine-substituted derivatives of $Os_3(CO)_{12}$ have appeared in the literature. The structural characterization, subsequent reactivities and reaction mechanisms of these clusters were exploited extensively.[2, 18-19] For example, Poë and Sekhar studied the kinetics for the reaction of $Os_3(CO)_{12}$ with PBu_3 and reaction of $Os_3(CO)_{11}PBu_3$ and $Os_3(CO)_{10}(PBu_3)_2$ with PBu_3 twenty years ago.[20-21] It was shown that when the reactions of $Os_3(CO)_{12}$ were carried out at high temperatures and low concentrations of PBu_3, the product $Os_3(CO)_9(PBu_3)_3$ was formed in quantitative yield via the stepwise dissociation of CO from $Os_3(CO)_{12}$, $Os_3(CO)_{11}PBu_3$ and $Os_3(CO)_{10}(PBu_3)_2$, followed by immediate capture of free phosphine ligand by the unsaturated intermediate. On the other hand, when the reactions of

$Os_3(CO)_{12}$ and $Os_3(CO)_{11}PBu_3$ were performed with high concentrations of PBu_3 and at low temperatures, a bimolecular process involving nucleophilic attack of the ligand on the cluster occurred, leading to complete fragmentation of the cluster and formation of the mononuclear complexes of $Os(CO)_4(PBu_3)$ and $Os(CO)_3(PBu_3)_2$. The reaction is presumed to take place via the ring-opened intermediate $Os_3(CO)_{11}(PBu_3)_2$ (Scheme 1.2). In the reaction of $Os_3(CO)_{10}(PBu_3)_2$ and PBu_3, no fragmentation was observed irrespective of the reaction conditions.

Scheme 1.2. Possible intermediate in the polyhedral opening of $Os_3(CO)_{11}PBu_3$ with PBu_3.

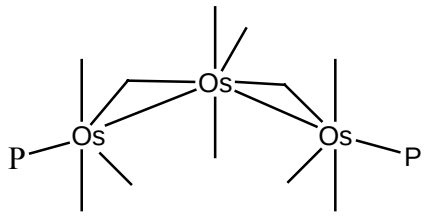

Poë and coworkers also studied the substitution kinetics for $Os_3(CO)_{11}(NCMe)$ and $Os_3(CO)_{10}(NCMe)_2$ with a variety of ligands.[22-23] For $Os_3(CO)_{11}(NCMe)$, it was found that substitution reactions proceeded through a simple dissociative mechanism, followed by the rapid ligand capture by the coordinatively unsaturated metal carbonyl cluster species $Os_3(CO)_{11}$, to furnish the corresponding monosubstituted cluster (Equations(1) and (2)).

$$Os_3(CO)_{11}(NCMe) \underset{k_{-1}}{\overset{k_1}{\rightleftharpoons}} Os_3(CO)_{11} + MeCN \qquad (1)$$

$$Os_3(CO)_{11} + L \xrightarrow{k_2} Os_3(CO)_{11}L \qquad (2)$$

In the case of substitution of $Os_3(CO)_{10}(NCMe)_2$, it was also suggested that the reversible dissociative step may be a concerted process in which a 'sideway on' or π-bound bridging CO group replaces the leaving MeCN ligand (Scheme 1.3).

Scheme 1.3. Possible intermediate in the substitution of $Os_3(CO)_{11}(NCMe)_2$.

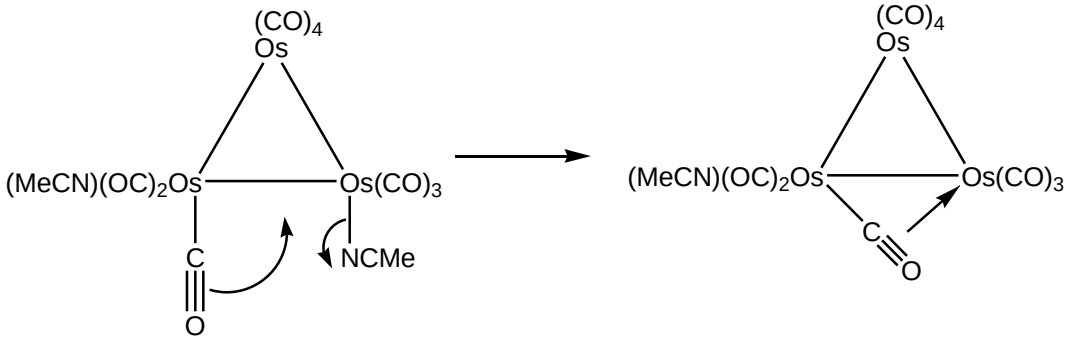

2. Triosmium Clusters Derived from Monodentate Phosphines

Multisubstituted triosmium carbonyl clusters have been prepared by using a variety of phosphine ligands. The maximal substitution number of phosphine ligands in a cluster was found to be six ligands because of the severe steric repulsion between equatorial ligands and the inability of phosphine ligands to occupy axial positions.[29] Monophosphine-substituted triosmium undecacarbonyl clusters are readily obtained by the easy displacement of the MeCN ligand in $Os_3(CO)_{11}(NCMe)$ by one phosphine ligand.[24-25] The phosphine ligand in the resulting product exclusively occupies one of the equatorial coordination sites in the phosphine-coordinated cluster (Scheme 1.4).

Scheme 1.4. Molecular structure of $Os_3(CO)_{11}P$.

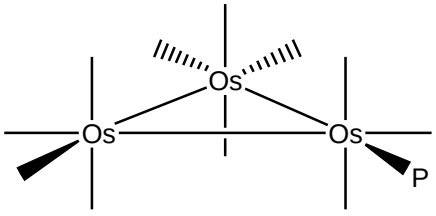

Within this family of $Os_3(CO)_{11}P$ clusters, the carbonyl ligands are fluxional in solution due to the labilizing influence of the phosphine ligand. Two mechanisms that account for the dynamic axial-equatorial carbonyl exchange have been proposed. The mechanism with the lowest energy barrier is depicted in Scheme 1.5. Here, the carbonyl exchange takes place via a bridging intermediate with two carbonyls bridging the Os_A-Os_B edge in the plane that contains the Os_A-Os_B edge and is perpendicular to the triosmium plane. The position of the phosphine ligand is unchanged in this process. Opening of the μ-CO intermediate leads to the effective scrambling of the six coplanar carbonyl ligands. There is another possible perpendicular plane along the Os_A-Os_C edge for the axial-equatorial exchange. However, the exchange in the third perpendicular plane along the Os_B-Os_C edge is blocked by the phosphine ligand.

Scheme 1.5. Terminal-bridge carbonyl exchange in $Os_3(CO)_{11}P$.

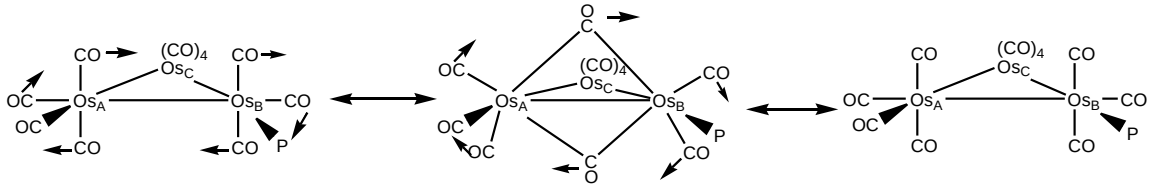

A second mechanism, which has a higher energy barrier, involves the exchange of all carbonyls. It has been suggested that a restricted trigonal twist by which the phosphine ligand rotates from one equatorial position to the other at the Os_B atom (Scheme 1.6) serves to assist in the equilibration of all the CO groups in $Os_3(CO)_{11}P$. This mechanism leads to an equilibrium between two conformers in which the phosphine ligand occupies different equatorial positions at the same osmium atom although they are indistinguishable in the case of monophosphine derivatives.

Reaction of $Os_3(CO)_{10}(NCMe)_2$ with two equivalents of a monodentate phosphine ligand leads to bisphosphine-substituted derivatives,[26] where the two phosphine ligands tend to occupy equatorial sites in the $Os_3(CO)_{10}P_2$ cluster. Four isomers are formed from different combinations of the coordination sites of the two phosphine ligands. These stereoisomers are shown in Scheme 1.7.

Scheme 1.6. Restricted trigonal twist mechanism of carbonyl exchange in $Os_3(CO)_{11}P$.

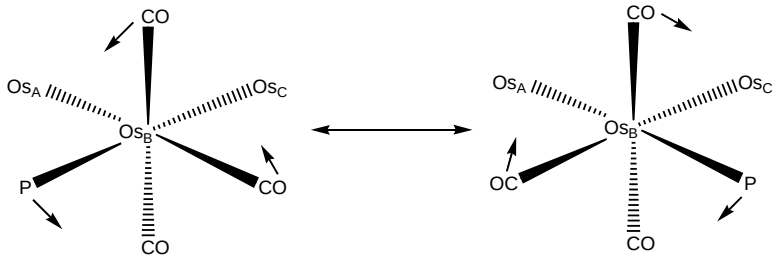

Scheme 1.7. Four isomers of $Os_3(CO)_{10}P_2$.

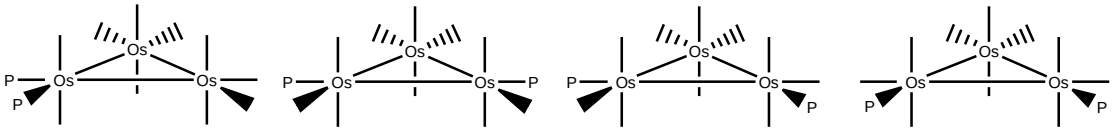

A B C D

Some clusters with structure A have been isolated, and clusters with structure D have only been observed for diphosphine ligands, while clusters with structures B and C have been shown to coexist in rapid equilibrium in solution.

The intramolecular phosphine ligand exchange can be explained by the same restricted trigonal twist mechanism as that of the monophosphine triosmium undecacarbonyl clusters (Scheme 1.8). Axial-equatorial carbonyl exchange takes place only in the vertical plane with the phosphine ligands remaining equatorially situated.[24, 27]

Scheme 1.8. Mechanism of phosphine ligand exchange in $Os_3(CO)_{10}P_2$.

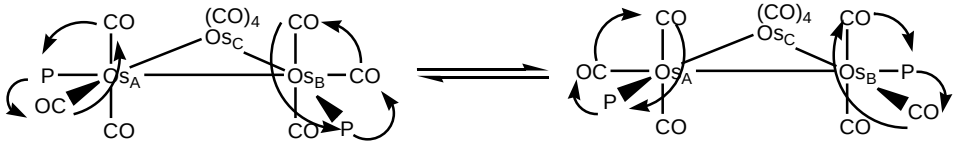

More highly substituted derivatives of $Os_3(CO)_{12}$ have been synthesized at elevated temperatures, under ultraviolet irradiation or a combination of thermal and photochemical methods.[24-25, 28-29] Based on ^{13}C and ^{31}P NMR studies, the structure of $Os_3(CO)_9P_3$ was suggested as follows (Scheme 1.9):

Scheme 1.9. Molecular structure of $Os_3(CO)_9P_3$.

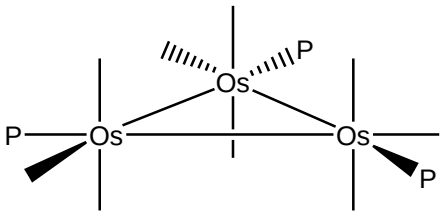

A synchronous phosphine scrambling mechanism was used to account for the dynamic behavior, in which each phosphine ligand simultaneously follows the restricted trigonal twist scheme at its own osmium atom (Scheme 1.10).

Scheme 1.10. Synchronous phosphine scrambling mechanism of $Os_3(CO)_9P_3$.

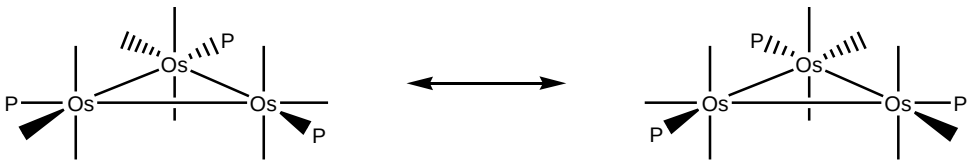

$Os_3(CO)_8P_4$ (where P = monophosphine ligands) exists as an isomeric mixture in solution, as is shown below (Scheme 1.11).

It was believed that the isomerization that equilibrates both A and B occurs via phosphine libration at an $Os(CO)_3P$ unit, and that this libration takes place only at one

osmium unit. There is terminal-bridge carbonyl exchange in the unique vertical plane in structure B, which has been demonstrated by VT ^{13}C NMR measurements.

The pentaphosphine-substituted triosmium carbonyl cluster $Os_3(CO)_7P_5$ (where P = monophosphine ligands) has one possible structure which is shown below (Scheme 1.12). In this structure, all of the phosphine ligands occupy equatorial positions, which leaves only one equatorial site to a carbonyl ligand. This structure is nonrigid with the P_1 ligand moving at the Os_A atom from one equatorial position to the other.

Scheme 1.11. Two isomers of $Os_3(CO)_8P_4$.

A B

Scheme 1.12. Molecular structure of $Os_3(CO)_7P_5$.

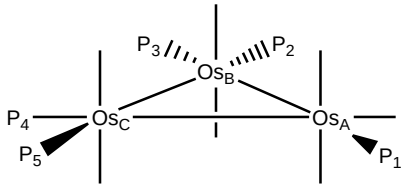

The only known hexaphosphite-substituted triosmium carbonyl cluster $Os_3(CO)_6P_6$ has been prepared from trimethylphosphite by UV activation of $Os_3(CO)_{12}$. This highly congested cluster is only accessible to the $P(OMe)_3$ ligand due to the inherent steric and electronic properties possessed by this ligand. All of the phosphite ligands are located at equatorial positions, and the structure is rigid due to the absence of the required vertical plane for terminal-bridge carbonyl exchange and an equatorial carbonyl site for the restricted trigonal twist mechanism.

3. Triosmium Clusters Derived from Bidentate Phosphines

Deeming, Kabir and coworkers have extensively investigated the synthesis and reactivity of triosmium carbonyl clusters containing diphosphine ligands, especially of the series of $Ph_2P(CH_2)_nPPh_2$ (n = 1 to 4).[30-39] The structures and associated abbreviations of some of the more common diphosphine ligands employed by researchers are shown as follows (Scheme 1.13 and Table 1.1):

Scheme 1.13. Bidentate diphosphine ligands.

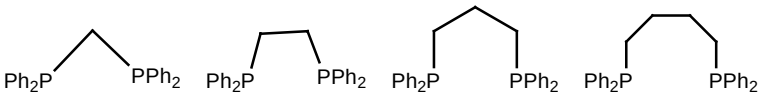

dppm (n=1) dppe (n=2) dppp (n=3) dppb (n=4)

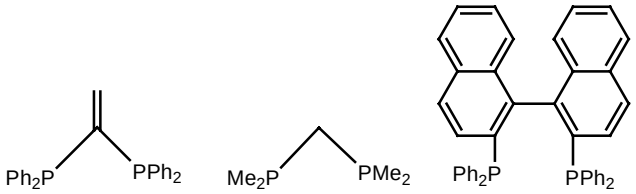

dppee dmpm BINAP

When only one of the phosphorus atoms is ligated to the triosmium carbonyl cluster, the resulting product is referred to as an η^1-diphosphine-coordinated triosmium undecacarbonyl cluster. The other "dangling" phosphorus atom of the bidentate ligand stays intact. This type of cluster has the same basic structural characteristics as that of monophosphine triosmium undecacarbonyl clusters. The pendent phosphorus atom can act as a donor moiety and coordinate to another $Os_3(CO)_{11}$ fragment to form dicluster products having the form of $Os_3(CO)_{11}(P\text{-}P)Os_3(CO)_{11}$, except in the case of the dppm

Table 1.1. Abbreviations and Names of Bidentate Diphosphine Ligands

Abbreviations	Name
dppee	1,1-bis(diphenylphosphino)ethene
dmpm	bis(dimethylphosphino)methane
dppm	bis(diphenylylphosphino)methane
dppe	bis(diphenylylphosphino)ethane
dppp	bis(diphenylylphosphino)propane
dppb	bis(diphenylylphosphino)butane
BINAP	2, 2′-bis(diphenylphosphino)-1,1′-binaphthyl

ligand due to steric effects, which prevent the coordination of another cluster entity and only exhibits ring closure with CO release to afford $Os_3(CO)_{10}$(dppm).

Diphosphine-substituted clusters $Os_3(CO)_{10}$(P-P) have a most outstanding feature where the diphosphine ligand can chelate to a single metal atom or bridge two adjacent metal atoms. The only exception where the bridging isomer exists without evidence for the chelating isomer is $Os_3(CO)_{10}$(dppm). Here the strain in the 4-member ring of the chelating isomer and the high steric favorability of the bridging isomer preclude formation of the aforementioned chelating isomer. However, the chelation of the dppm ligand has been demonstrated in the ruthenium and iridium clusters $Ru_5C(CO)_{12}$(dppm)[40] and $Ir_4(CO)_{10}$(dppm).[41] For these two clusters, X-ray diffraction analyses and NMR spectroscopic data have confirmed the chelating mode adopted by the ancillary dppm ligand.

The tendency for each ligand to act as a chelating or bridging ligand was studied by comparing the yields of the chelating and bridging isomers isolated from reactions of $Os_3(CO)_{10}(\eta^4\text{-}C_4H_6)$ and $Ph_2P(CH_2)_nPPh_2$ (n = 1 to 5). It was found that dppe acts predominantly as a chelating ligand, and that the chelating tendency decreases as the chain length at the diphosphine ligand increases so that $Ph_2P(CH_2)_5PPh_2$ functions only as a bridging ligand.[36] It was reported that the BINAP ligand gave only the chelating cluster.[42]

The fluxional behavior of 1,1-$Os_3(CO)_{10}$(P-P) and 1,2-$Os_3(CO)_{10}$(P-P) is similar to that of monosubstituted triosmium carbonyl clusters. However, there is only one vertical plane for axial-equatorial carbonyl exchange in these diphosphine-substituted clusters (Scheme 1.14). 1,1-$Os_3(CO)_{10}$(P-P) has two osmium atoms and 1,2-$Os_3(CO)_{10}$(P-P) has one osmium atom associated with a restricted trigonal twist because the rotation around the remaining osmium atoms is blocked by the equatorial phosphine ligands.

Scheme 1.14. Terminal-bridge carbonyl exchange of 1,1-$Os_3(CO)_{10}$(P-P) and 1,2-$Os_3(CO)_{10}$(P-P).

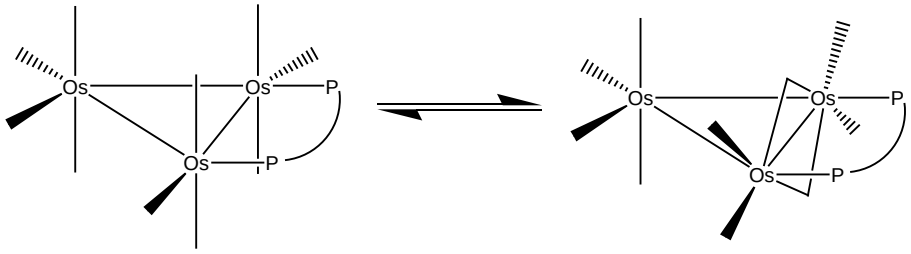

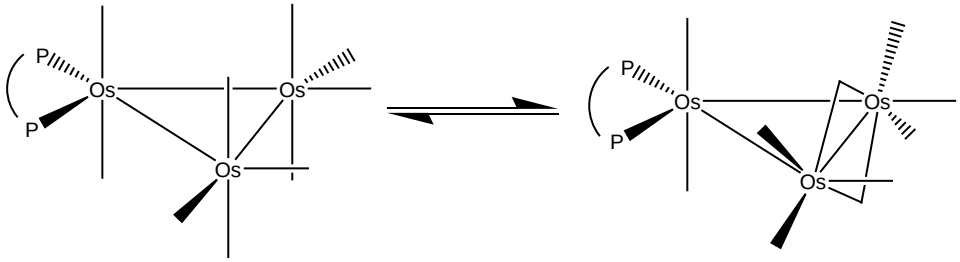

Multidentate phosphine ligands such as $Ph_2PCH_2CH_2PPhCH_2CH_2PPh_2$ (tripos) can act as monodentate or bidentate ligands. There are two isomers for the $Os_3(CO)_{11}(\eta^1$-triphos) cluster because there are two types of phosphorus atoms in the ligand. As a bidentate ligand, tripos can form two isomers for the bridging cluster 1,2-$Os_3(CO)_{10}$(tripos) in theory, although only one such isomer has been reported to date.[2]

While carbonyl ligands can rapidly move around metal atoms in these clusters, there has been no evidence for the intramolecular transfer of phosphine ligands between the metal atoms. This is probably due to the inertness of triosmium system and the negligible rates of opening of diphosphine chelates or bridges that would promote an overall isomerization.[30, 35]

Reaction of $Os_3(CO)_{10}(\mu$-P-P) with additional diphosphine ligand at high temperature leads to the formation of $Os_3(CO)_9(\mu$-P-P)(η^1-P-P) or $Os_3(CO)_8(\mu$-P-P)$_2$ in the case of the diphosphines dppee, dppm or $Ph_2P(CH_2)_5PPh_2$. In both types of clusters, the diphosphine ligands adopt equatorial positions and act as bridging ligands exclusively.[37, 43-44]

B. Chemical Properties of Phosphine-Substituted Triosmium Carbonyl Clusters

Except for further substitution of the carbonyl ligands, phosphine-substituted triosmium carbonyl clusters can react with acid and hydrogen to form hydride clusters, in

addition to undergoing orthometallation (C-H bond activation) and even P-C bond cleavage at coordinatively unsaturated osmium atoms that are formed from carbonyl loss. This part of the introduction will give a detailed description of these four types of reactions.

1. Protonation

1,1- and 1,2-$Os_3(CO)_{10}(PMe_2Ph)_2$ react with CF_3COOH in $CHCl_3$ to give 1,1- and 1,2-$[Os_3(\mu\text{-}H)(CO)_{10}(PMe_2Ph)_2]^+$, respectively.[45-46] The 1,2-isomer has two isomers in solution, the major one having equivalent phosphines at adjacent equatorial sites and the minor one having nonequivalent phosphines. The X-ray structure of the 1,2-isomer corresponds with that of the major isomer in solution. Protonation of an Os-Os bond creates a hydride-bridged moiety where the hydrido ligand causes an elongation at the bridged Os-Os bonds, typically making a protonated metal-metal bond the longest bond in a metal cluster. Protonation of 1,2-$Os_3(CO)_{10}P_2$, [P = PPh_3 or $P(OMe)_3$], and of the 1,2, 3- and 1,1,2-isomers of $[Os_3(CO)_9(PMe_2Ph)_3]$ was also examined. It was found that there is generally a marked preference for isomers that have the phosphines *cis* to the bridging hydride.

The hydrides 1,1-$[Os_3H(CO)_{10}(P\text{-}P)]^+$ were formed by addition of CF_3CO_2H to the chelating diphosphine compounds 1,1-$Os_3(CO)_{10}(P\text{-}P)$ [P-P = $Ph_2P(CH_2)_nPPh_2$, n = 2, 3] and have been isolated as the PF_6-salts. Unlike the parent clusters, the two phosphorus atoms in each of the hydride clusters are nonequivalent, as determined by spectroscopic and diffraction methods.[33]

1,2-$Os_3(CO)_{10}(P\text{-}P)$ [P-P = $Ph_2P(CH_2)_nPPh_2$ (n = 1 to 4)] show interesting

differences in their reactivity towards H^+.[32] Protonation leads to hydride complexes with the hydride bridging the two Os atoms coordinated by the diphosphine ligand when the diphosphine is dppe, dppp, or dppb. In comparison, the hydride and dppm ligands bridge different edges in $Os_3(\mu\text{-}H)(CO)_{10}(dppm)^+$.

Protonation of 1,2-$Os_3(CO)_{10}$(dppe) gives two independent isomers that have the general formula 1,2-$[Os_3H(CO)_{10}(dppe)]^+$.[47] One of the isomers has the hydride ligand bridging the two osmium atoms coordinated by the phosphorus atoms. This leads to the expansion of the Os-Os bond distance and the generation of equivalent phosphorus atoms and release of the Os_3 screw distortion found in the parent cluster. The other isomer has a bridging hydride ligand that connects one phosphine-coordinated osmium atom and the non-phosphine-substituted osmium atom that is not coordinated by phosphorus atoms, so that this isomer still exhibits significant distortion that can be seen from the staggered arrangement of the axial carbonyl ligands.

2. Hydrogenation

1,2-$Os_3(CO)_{10}$(P-P) can react with hydrogen to afford $Os_3(\mu\text{-}H)_2(CO)_8$(P-P) (P-P = dppm, dppe, dppp) but the dppb analog could not be made.[47] Interestingly, the direct hydrogenation of 1,1-$Os_3(CO)_{10}$(P-P) does not give dihydride clusters $Os_3(\mu\text{-}H)_2(CO)_8$(P-P).[48] Unlike the triosmium congener $Os_3(\mu\text{-}H)_2(CO)_{10}$, these dihydride derivatives neither react with CO, phosphines, etc.,[49-55] nor catalyze alkene isomerization[56-58] and alkyne insertion[59-60] at room temperature.

Hydrogenation of 1,1-$Os_3(CO)_{10}$(dppe) at atmospheric pressure in refluxing toluene does not give the simple dihydride $[Os_3H_2(CO)_8(dppe)]$ as found for the

corresponding 1,2- isomers.[33] Instead the cluster $Os_3H_3[Ph_2P(CH_2)_2PPh(C_6H_4)](CO)_8$ is obtained by loss of CO and addition of H_2 (Scheme 1.15).

Scheme 1.15. Hydrogenation of 1,1-$Os_3(CO)_{10}$(dppe).

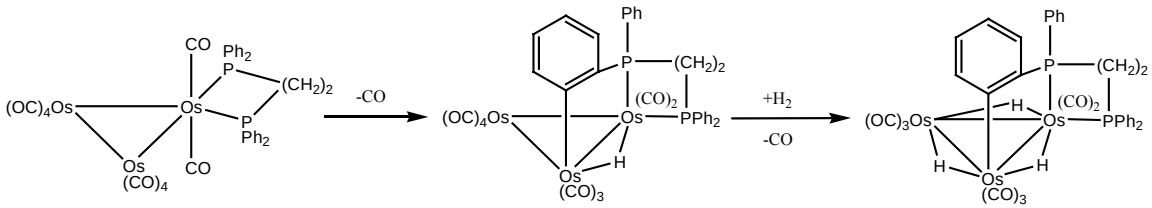

3. Orthometallation

Orthometallation often accompanies the formation of the unsaturated triosmium cluster $Os_3(CO)_8(H)[Ph_2PCH_2P(Ph)C_6H_4]$ from the thermolysis of 1,2-$Os_3(CO)_{10}$(dppm), in which the loss of two CO ligands is followed by the metallation of one of the ortho C-H bonds associated with one of the phenyl groups of the dppm ligand.[34] The reverse reaction with CO to form $Os_3(CO)_9(H)[Ph_2PCH_2P(Ph)C_6H_4]$ is quite facile and clearly reveals the inherent unsaturation associated with $Os_3(CO)_8(H)[Ph_2PCH_2P(Ph)C_6H_4]$. This was also observed in the thermolysis of 1,2-$Os_3(CO)_9$(dppm)(NCMe) in protic solvents.[61]

Metallation was also observed at the saturated carbon atom of the methylene group of the dmpm ligand in the conversion from 1,2-$Os_3(CO)_{10}$(dmpm) or 1,2-$Os_3(CO)_9$(dmpm)(C_2H_4) to afford $Os_3H(CO)_9(Me_2PCHPMe_2)$.[33] However, metallation occurs at one aryl C-H bond of one phenyl group of the dppm ligand in the conversion of 1,2-$Os_3(CO)_9$(dppm)(NCMe) to $Os_3H(CO)_9(Ph_2PCH_2PPh(C_6H_4))$.

4. P-C Bond Cleavage

In some cases, P-C bond cleavage is thermally and photochemically triggered in triosmium cluster systems. Accompanying the C-H bond activation in the hydrogenation

of 1,1-$Os_3(CO)_{10}[Ph_2P(CH_2)_nPPh_2]$ (n = 2, 3), P-C bond activation has also been observed at the bond between the orthometallated phosphorus atom and the attached phenyl group, ultimately giving the phosphido cluster $Os_3H_2[Ph_2P(CH_2)_nPPC_6H_4](CO)_8$ (n = 2, 3) (Scheme 1.16).[33] The observed benzene that accompanies these reactions comes from the activated aryl group.

Scheme 1.16. P-C bond cleavage of 1,1-$Os_3(CO)_{10}[Ph_2P(CH_2)_nPPh_2]$ (n = 2, 3).

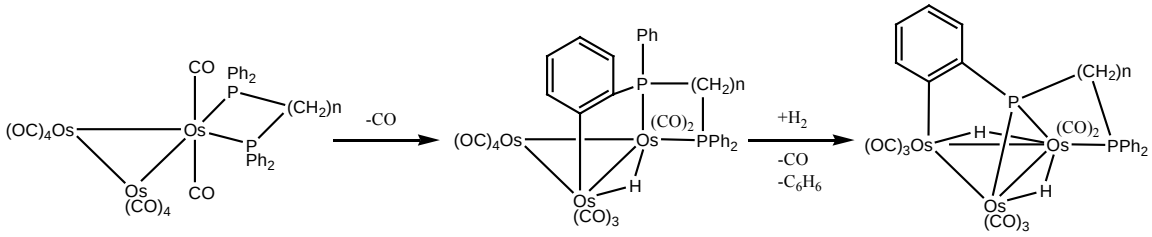

It was shown that 1,1-$Os_3(CO)_{10}(PMe_2Ph)_2$ undergoes orthometallation at its aryl groups at 110 °C to form $Os_3H(Me_2PC_6H_4)(PMe_2Ph)(CO)_9$ and that 1,2-$Os_3(CO)_{10}(PMe_2Ph)_2$ only reacts at higher temperature (125 °C) and then to give $Os_3(\mu_3\text{-}C_6H_4)(PMe_2)_2(CO)_7$ as the predominant product.[9] This latter product results from the orthometallation and P-C cleavage reaction of the aryl group at one of the PMe_2Ph ligands.

Thermolysis of the monosubstituted clusters $Os_3(CO)_{11}(PRPh_2)$ (R = Me, Ph) is accompanied by P-C bond cleavage to yield $Os_3H(\mu_3\text{-}C_6H_4PRPh)(CO)_9$, $Os_3(\mu_3\text{-}C_6H_4PR)(CO)_{10}$ and then $Os_3(\mu_3\text{-}C_6H_4)(\mu_3\text{-}PR)(CO)_9$. However, $HOs_3(\mu_3\text{-}C_6H_4)(PMe_2)(CO)_9$ was formed from P-C bond cleavage in the thermolysis of $Os_3(CO)_{11}(PMe_2Ph)$.[6] These data show a diverse course of reactivity in these phosphine ligand activations in comparison to the PMe_2Ph–substituted cluster.

C. Mechanistic Studies on Phosphine Ligand Activation

It is apparent that there is a saturated backbone connecting the phosphorus atoms in the majority of bidentate diphosphine ligands that have been employed in the preparation of derivatives of triosmium carbonyl clusters up to now. Steric effects of these ligands play an important role in the structures and chemical properties of these phosphine-substituted clusters. We can expect that electronic effects would have an influence on the reactivity of trisomium carbonyl clusters derived from bidentate diphosphine ligands that have rigid, unsaturated P-C=C-P backbones. However, studies on this type of clusters are limited. There is only one incomplete study on the synthesis of $Os_3(CO)_{10}$(cDPPEn) [cDPPEn = cis-bis(diphenylphosphino)ethylene].[62] There Bruce and coworkers have studied the reaction between $Os_3(CO)_{12}$ and the ligand cDPPEn. A product having the composition $Os_3(CO)_{10}$(cDPPEn) was characterized in solution by IR and ^{1}H NMR spectroscopy. With the introduction of different substituents at the carbon atoms of the P-C=C-P skeleton, many new types of diphosphine ligands[63] can be made such as bma [2, 3-bis(diphenylphosphino)maleic anhydride], bpcd [4, 5-bis(diphenylphosphino)-4-cyclopenten-1,3-dione], bmi [2, 3-bis(diphenylphosphino)maleimide], bpcbd [3, 4-bis(diphenylphosphino)cyclobutenedione] and bmf [3, 4-bis(diphenylphosphino)-5-methoxy-2(5H)-furanone] (Scheme 1.17). With the existence of a carbon-carbon double bond linking two phosphorus atoms, these four atoms (P-C-C-P) are always fixed in a plane during chemical conversion unless the C-C double bond is broken or activated by coordination to a metal center(s).

Scheme 1.17. Rigid bidentate diphosphine ligands.

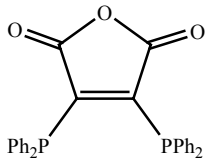

bma

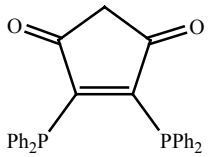

bpcd

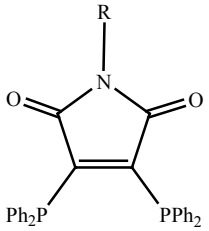

bmi

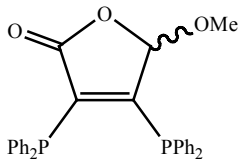

bmf

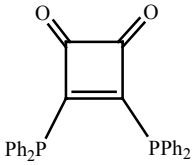

bpcbd

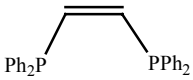

cDPPEn

In this dissertation, the rigid bidentate ligands bpcd and cDPPEn were chosen to study the substitution chemistry with triosmium carbonyl clusters and the subsequent chemical reactions of their triosmium derivatives. The presence of conjugated carbonyl groups relating to the P-C=C-P backbone in the bpcd ligand renders it a superior electron reservoir ligand, allowing for the potential orbital mixing of the ligand′s π^* system and suitable metal orbital. The structural and electronic differences between these two diphosphine ligands (i.e., bpcd versus cDPPEn) will allow reactivity comparisons to be made between the anticipated substituted clusters $Os_3(CO)_{10}$(P-P).

Presented in this dissertation are the in-depth studies on the synthesis and reactivity of diphosphine-substituted triosmium clusters. They include the areas of (1) the substitution of $Os_3(CO)_{10}(NCMe)_2$ by the rigid bidentate ligands bpcd and cDPPEn to form bridging clusters 1,2-$Os_3(CO)_{10}$(bpcd) and 1,2-$Os_3(CO)_{10}$(cDPPEn); (2) ligand

isomerization of 1,2-$Os_3(CO)_{10}$(bpcd) and 1,2-$Os_3(CO)_{10}$(cDPPEn) to produce the thermodynamically favored chelating clusters; (3) thermally and photochemically activated orthometallation of 1,1-$Os_3(CO)_{10}$(bpcd) and 1,1-$Os_3(CO)_{10}$(cDPPEn) to form the hydride clusters $HOs_3(CO)_9[\mu\text{-}(PPh_2)C{=}C\{PPh(C_6H_4)\}C(O)CH_2C(O)]$ and $HOs_3(CO)_9(Ph_2PCH{=}CHP(Ph)C_6H_4)$, repectively, via C-H bond oxidative addition following CO loss; (4) thermally promoted reductive coupling of the hydride clusters, coupled with CO capture, to furnish the 1,1-$Os_3(CO)_{10}$(P-P) clusters; and (5) mechanistic evidence for the P-C bond cleavage of the hydride cluster $HOs_3(CO)_9[\mu\text{-}(PPh_2)C{=}C\{PPh(C_6H_4)\}C(O)CH_2C(O)]$ to form the benzyne cluster $HOs_3(CO)_8(\mu_3\text{-}C_6H_4)[\mu_2,\eta^1\text{-}PPhC{=}C(PPh_2)C(O)CH_2C(O)]$.

D. Chapter References

1. Dyson, P. J.; McIndoe, J. S. *Transition Metal Carbonyl Cluster Chemistry*; Gordon and Breach Science Publishers: Amsterdam, The Netherlands, 2000; Chapter 1.
2. Deeming, A. J.; Donovan-Mtunzi, S.; Kabir, S. E. *J. Organomet. Chem.* **1987**, *333*, 253.
3. Bradford, C. W.; Nyholm, R. S.; Guss, J. M.; Ireland, P. R.; Mason, R. *J. Chem. Soc., Chem. Commun.* **1972**, *2*, 87.
4. Gainford, G. J.; Guss, J. M.; Ireland, P. R.; Mason, R.; Bradford, C. W.; Nyholm, R. S. *J. Organomet. Chem.* **1972**, *40*, C70.
5. Bradford, C. W.; Nyholm R. S. *J. Chem. Soc., Dalton Trans.* **1973**, 529.
6. Deeming, A. J.; Kimber, R. E.; Underhill, M. *J. Chem. Soc., Dalton Trans.* **1973**, 2589.

7. Deeming, A. J.; Underhill, M. *J. Chem. Soc., Dalton Trans.* **1973**, 2727.

8. Deeming, A. J. *J. Organomet. Chem.* **1977**, *128*, 63.

9. Deeming, A. J.; Kabir, S. E.; Powell, N. I.; Bates, P. A.; Hursthouse, M. B. *J. Chem. Soc., Dalton Trans.* **1987**, 1529.

10. Bruce, M. I.; Liddell, M. J.; Hughes, C. A.; Skelton, B. W.; White, A. H. *J. Organomet. Chem.* **1988**, *347*, 157.

11. Bruce, M. I.; Liddell, M. J.; Hughes, C. A.; Patrick, J. M.; Skelton, B. W.; White, A. H. *J. Organomet. Chem.* **1988**, *347*, 181.

12. Hughes, A. K.; Wade, K. *Coord. Chem. Rev.* **2000**, *197*, 191.

13. Housecroft, C. E.; Wade, K.; Smith, B. C. *J. Chem. Soc., Chem. Commun.* **1978**, 765.

14. Shriver, D. F.; Kaesz, H. D.; Adams, R. D. *The Chemistry of Metal Cluster Complexes*; VCH: New York, 1990.

15. Bryan, E. G.; Johnson, B. F. G.; Lewis, J. *J. Chem. Soc., Dalton Trans.* **1977**, 1328.

16. Johnson, B. F. G.; Lewis, J; Pippard, D. A. *J. Organomet. Chem.* **1978**, *145*, C4.

17. Tachikawa, M.; Shapley, J. R. *J. Organomet. Chem.* **1977**, *124*, C19.

18. Poë, A.; Sekhar, V. C. *J. Am. Chem. Soc.* **1984**, *106*, 5034.

19. Deeming, A. J. *Advances in Organometallic Chemistry*. **1986**, *26*, 1.

20. Poë, A.; Sekhar, V. C. *Inorg. Chem.* **1985**, *24*, 4376.

21. Brodie, N.; Poë, A.; Sekhar, V. *J. Chem. Soc., Chem. Commun.* **1985**, 1090.

22. Hudson, R. H. E.; Poë, A. J.; Sampson, C. N.; Siegel, A. J. *J. Chem. Soc., Dalton Trans.* **1989**, 2235.

23. Dahlinger, K.; Poë, A. J.; Sayal, P. K.; Sekhar, V. C. J. *J. Chem. Soc., Dalton Trans.* **1986**, 2145.

24. Alex, R. F.; Pomeroy, R. K. *Organometallics* **1987**, *6*, 2437.

25. Johnson, B. F. G.; Lewis, J.; Reichert, B. E.; Schorpp, K. T. *J. Chem. Soc., Dalton Trans.* **1976**, 1403.

26. Leong, W. K.; Liu, Y. *J. Organomet. Chem.* **1999**, *584*, 174.

27. Deeming, A. J.; Donovan-Mtunzi, S.; Kabir, S. E. *J. Organomet. Chem.* **1985**, *281*, C43.

28. Alex, R. F.; Pomeroy, R. K. *J. Organomet. Chem.* **1985**, *284*, 379.

29. Alex, R. F.; Einstein, F. W. B.; Jones, R. H.; Pomeroy, R. K. *Inorg. Chem.* **1987**, *26*, 3175.

30. Deeming, A. J.; Donovan-Mtunzi, S.; Kabir, S. E. *J. Organomet. Chem.* **1984**, *276*, C65.

31. Clucas, J. A.; Dawson, R. H.; Dolby, P. A.; Harding, M. M.; Pearson, K.; Smith, A. K. *J. Organomet. Chem.* **1986**, *311*, 153.

32. Deeming, A. J.; Donovan-Mtunzi, S.; Hardcastle, K. I.; Kabir, S. E.; Henrick, K.; McPartlin, M. *J. Chem. Soc., Dalton Trans.* **1988**, 579.

33. Deeming, A. J.; Hardcastle, K. I.; Kabir, S. E. *J. Chem. Soc., Dalton Trans.* **1988**, 827.

34. Clucas, J. A.; Foster, D. F.; Harding, M. M.; Smith, A. K. *J. Chem. Soc., Chem. Commun.* **1984**, 949.

35. Azam, K. A.; Hursthouse, M. B.; Kabir, S. E.; Malik, K. M. A.; Mottalib, M. A. *J. Chem. Crystallogr.* **1999**, *29*, 813.

36. Kabir, S. E.; Miah, A.; Nesa, L.; Uddin, K.; Hardcastle, K. I.; Rosenberg, E.; Deeming, A. J. *J. Organomet. Chem.* **1995**, *492*, 41.

37. Brown, M. P.; Dolby, P. A.; Harding, M. M.; Mathews, A. J.; Smith, A. K. *J. Chem. Soc., Dalton Trans.* **1993**, 1671.

38. Kabir, S. E.; Johns, C. A.; Malik, K. M. A.; Mottalib, M. A.; Rosenberg, E. *J. Organomet. Chem.* **2001**, *625*, 112.

39. Clucas, J. A.; Harding, M. M.; Smith, A. K. *J. Chem. Soc., Chem. Commun.* **1985**, 1280.

40. Evans, J.; Gracey, B. P.; Gray, L. R.; Webster, M. *J. Organomet. Chem.* **1982**, *240*, C61.

41. Tachikawa, M.; Shapley, J. R.; Haltiwanger, R. C.; Pierpont, C. G. *Inorg. Chem.* **1978**, *17*, 1976.

42. Deeming, A. J.; Stchedroff, M. *J. Chem. Soc., Dalton Trans.* **1998**, 3819.

43. Cartwright, S.; Clucas, J. A.; Dawson, R. H.; Foster, D. F.; Harding, M. M.; Smith, A. K. *J. Organomet. Chem.* **1986**, *302*, 403.

44. Harding, M. M.; Kariuki, B.; Mathews, A. J.; Smith, A. K.; Braunstein, P. *J. Chem. Soc., Dalton Trans.* **1994**, 33.

45. Lewis, J.; Deeming, A. J.; Johnson, B. F. G. *J. Chem. Soc. A* **1970**, *18*, 2967.

46. Deeming, A. J.; Donovan-Mtunzi, S.; Kabir, S. E.; Hursthouse, M. B.; Malik, K. M. A.; Walker, N. P. C. *J. Chem. Soc., Dalton Trans.* **1987**, 1869.

47. Deeming, A. J.; Kabir, S. E. *J. Organomet. Chem.* **1988**, *340*, 359.

48. Deeming, A. J.; Hasso, S. *J. Organomet. Chem.* **1975**, *88*, C21.

49. Deeming, A. J.; Hasso, S. *J. Organomet. Chem.* **1976**, *114*, 313.

50. Keister, J. B.; Shapley, J. R. *Inorg. Chem.* **1982**, *21*, 3304.

51. Shapley, J. R. Keister, J. B.; *J. Am. Chem. Soc.* **1975**, *97*, 4145.

52. Adams, R. D.; Golembeski, N. M. *Inorg. Chem.* **1979**, *18*, 1909.

53. Aime, S.; Osella, D.; Milone, L.; Rosenberg, E. *J. Organomet. Chem.* **1981**, *213*, 207.

54. Rosenberg, E.; Anslyn, E. V.; Barner-Thorsen, C.; Aime, S.; Osella, D.; Gobetto, R.; Milone, L. *Organometallics* **1984**, *3*,1790.

55. Bentsen, J. G.; Wrighton, M. S. *Inorg. Chem.* **1984**, *23*, 512.

56. Li, X. J.; Onuferko, J. H.; Gates, B. C. *J. Catal.* **1984**, *85*, 176.

57. Kiester, J. B.; Shapley, J. R. *J. Am. Chem. Soc.* **1976**, *98*, 1056.

58. Ferrari, R. P.; Vaglio, G. A.; Valle, M. *Inorg. Chim. Acta.* **1978**, *31*, 177.

59. Clauss, A. D.; Tachikawa, M.; Shapley, J. R. *Inorg. Chem.* **1981**, *20*. 1528.

60. Deeming, A. J.; Hasso, S.; Underhill, M. *J. Chem. Soc., Dalton Trans.* **1975**, 1614.

61. Hodge, S. R.; Johnson, B. F. G.; Lewis, J.; Raithby, P. R. *J. Chem. Soc., Dalton Trans.* **1987**, 931.

62. Bruce, M. I.; Williams, M. L.; Skelton, B. W.; White, A. H. *J. Organomet. Chem.* **1986**, *306*, 115.

63. (a) Fenske, D.; Becher, H. J. *Chem. Ber.* **1974**, *107*, 117. (b) Fenske, D.; Becher, H. J. *Chem. Ber.* **1975**, *108*, 2115. (c) Fenske, D. *Chem. Ber.* **1979**, *112*, 363.

CHAPTER II

EXPERIMENTAL

A. Materials

1. Solvents

CH_2Cl_2 and MeCN were distilled from CaH_2. THF, Et_2O, and toluene were distilled from sodium/benzophenone ketyl under argon. The deuterated solvent benzene-d_6 was vacuum distilled from CaH_2, while CD_2Cl_2 and $CDCl_3$ were distilled from P_2O_5 under vacuum. All distilled solvents were stored under argon in Schlenk vessels equipped with Teflon stopcocks.[1]

2. Reagents

The $Os_3(CO)_{12}$ used in the synthesis of $Os_3(CO)_{11}(NCMe)$ and $Os_3(CO)_{10}(NCMe)_2$ was prepared from carbonylation of OsO_4 according to the published procedure,[2] and the $Os_3(CO)_{11}(NCMe)$ and $Os_3(CO)_{10}(NCMe)_2$ were synthesized by following the known literature procedure.[3] Me_3NO was purchased from Aldrich Chemical Co. and OsO_4 was purchased from Engelhard Chemical Co. These chemicals were used as received. The Ph_2PTMS used in the synthesis of bpcd was prepared according to the published procedures.[4] The ligand bpcd was synthesized from 4,5-dichloro-4-cyclopenten-1,3-dione using the procedure of Fenske and Becher.[5] The diphosphine ligand cDPPEn, PPh_3, $P(OEt)_3$, PCy_3, *o*-bromo-chlorobenzene, D_2O, Mg, PCl_3, K, and Me_3SiCl were purchased from Aldrich Chemical Co., with the PCl_3 and Me_3SiCl purified by distillation before use and the others used as received. The ^{13}CO (>99%) used in the preparation of the ^{13}CO-enriched $Os_3(CO)_{12}$[6] was purchased from

Isotec, Inc. The tetra-*n*-butylammonium perchlorate (TBAP) used in the electrochemical studies was purchased from Johnson Matthey Electronics and recrystallized from ethyl acetate/petroleum ether, followed by drying 2 days under vacuum.

B. Instrumentation

Routine infrared spectra were recorded on a Nicolet 20SXB FT-IR spectrometer in 0.1 mm NaCl cells, using PC control and OMNIC software. ^{1}H and ^{13}C NMR spectra were recorded at 200 and 50 MHz, respectively, on a Varian Gemini-200 spectrometer and the ^{31}P NMR spectra recorded at 121 MHz on a Varian 300-VXR spectrometer. The reported ^{31}P chemical shifts are referenced to external PPh_3, whose chemical shift was set at δ = -6.0. Positive chemical shifts are to low field of the external standard. The high-resolution FAB mass spectra were obtained at the Mass Spectrometry facility at the University of California at San Diego using 3-nitrobenzyl alcohol as the sample matrix and polypropylene glycol as the reference. Cyclic voltammetric measurements were conducted with a PAR Model 273 potentiostat/galvanostat, equipped with positive feedback circuit to compensate for *iR* drop. The CV cell used was of airtight design and based on a three-electrode configuration, which enabled all cyclic voltammograms to be obtained free from oxygen and water. The CV experiments employed a platinum disk (area = 0.0079 cm^2) as the working electrode and a coiled platinum wire as the auxiliary electrode. All voltammograms utilized a silver wire quasi-reference electrode and all potential data are referenced relative to the formal potential of the Cp_2Fe/Cp_2Fe^+ redox couple run under identical conditions, taken to have an $E_{1/2}$ = 0.307 V.[7]

C. Photochemical Experiments and Determination of Quantum Yields

The photochemical experiments were carried out at the specified temperature using a suitable bath media or a temperature-controlled circulator bath with either GE blacklight bulbs, having a maximum output of 366 ± 20 nm, or a 200 W Oriel Hg(Xe) arc lamp. The GE blacklight bulbs used in the studies was configured with a variable-temperature customized UV-VIS cell holder that was connected to a VWR constant temperature circulator, by which the irradiation reaction temperature was regulated to within ± 0.5 °C. In the determination of the quantum yield, the light intensity was measured by ferioxalate actinometry[8] and was found to be on the order of ca. 1×10^{-7} einstein/min. The reported quantum yield represents the average value for three separate reactions.

D. Preparation of Compounds

1. $Os_3(CO)_{11}(\eta^1$-cDPPEn)

Into a Schlenk flask containing $Os_3(CO)_{11}$(NCMe), as prepared from 0.20 g (0.22 mmol) of $Os_3(CO)_{12}$ and 0.016 g (0.22 mmol) of Me_3NO according to the literature procedure,[3] was added 25 mL of dichloromethane by syringe, after which this solution was added to 0.087 g (0.22 mmol) cDPPEn in 25 mL of dichloromethane over 10 min, with stirring continued overnight at ambient temperature. The solvent was removed under vacuum and the residue separated by column chromatography over silica gel using 10% dichloromethane in hexane to give 0.13 g (0.10 mmol) of orange $Os_3(CO)_{11}(\eta^1$-cDPPEn) as the major product (yield: 46%), along with a minor amount of yellow 1,2-$Os_3(CO)_{10}$(cDPPEn) (0.032 g; 12%). $Os_3(CO)_{11}(\eta^1$-cDPPEn): IR (CH_2Cl_2): ν(CO) 2107

(m), 2053 (s), 2032 (s), 2016 (vs), 2001 (s,sh), 1989 (m), 1974 (m) cm^{-1}. ^{1}H NMR ($CDCl_3$, 298 K): δ 6.98 –7.60 (22H, m, vinyl and aryl). $^{31}P\{^{1}H\}$ NMR ($CDCl_3$, 298 K): δ -16.37 (1P, d, J_{P-P}=21 Hz), -30.65 (1P, d, J_{P-P}=21 Hz).

2. 1,2-$Os_3(CO)_{10}$(cDPPEn)

To a Schlenk flask containing 25 mL of dichloromethane of $Os_3(CO)_{10}(NCMe)_2$, as prepared from 0.50 g (0.55 mmol) of $Os_3(CO)_{12}$ and 0.091 g (1.2 mmol) of Me_3NO, was transferred a solution of 0.22 g of cDPPEn in 15 mL of dichloromethane by cannula, after which the solution was stirred overnight at ambient temperature. The solvent was then stripped and the residue separated by column chromatography over silica gel using 10% dichloromethane in hexane to give yellow 1,2-$Os_3(CO)_{10}$(cDPPEn) (0.47 g, 67%) and 0.025 g $Os_3(CO)_{11}(\eta^1$-cDPPEn) (yield: 3.6%). 1,2-$Os_3(CO)_{10}$(cDPPEn): IR (CH_2Cl_2): ν(CO) 2088 (s), 2025 (s), 2013 (vs), 2001 (vs), 1971 (s), 1949 (b, sh) cm^{-1}. ^{1}H NMR ($CDCl_3$, 298 K): δ 6.29 (2H, m, vinyl), 6.80 –7.45 (20H, m, aryl). $^{13}C\{^{1}H\}$ NMR (toluene-d_8, 243 K): 173.92 (s, 2C, equatorial), 178.91 (s, 2C, equatorial), 184.96 (s, 2C, axial), 191.49 (s, 4C, axial). $^{31}P\{^{1}H\}$ NMR ($CDCl_3$, 298 K): δ -6.45 (s). Anal. Calcd (found) for $C_{36}H_{22}O_{10}Os_3P_2$: C, 34.64 (34.95); H, 1.76 (1.78).

3. 1,1-$Os_3(CO)_{10}$(cDPPEn)

To a Carius tube was charged 0.20 g (0.16 mmol) of 1,2-$Os_3(CO)_{10}$(cDPPEn) in 15 mL of toluene that was saturated with CO. The solution was heated at ca. 100 °C for 22 hr, after which time the solvent was removed under vacuum and the residue separated by column chromatography over silica gel using 40% dichloromethane in hexane to give 0.14 g (0.11 mmol) a 7:1 mixture of 1,1-$Os_3(CO)_{10}$(cDPPEn) and 1,2-

$Os_3(CO)_{10}$(cDPPEn). Careful recrystallization of this mixture using dichloromethane and hexane afforded 0.080 g (0.064 mmol) of orange 1,1-$Os_3(CO)_{10}$(cDPPEn) (yield: 40%). 1,1-$Os_3(CO)_{10}$(cDPPEn): IR (CH_2Cl_2): ν(CO) 2092 (m), 2042 (vs), 2006 (vs, b), 1973 (m), 1957 (m), 1926 (w, b) cm^{-1}. ^1H NMR ($CDCl_3$, 298 K): δ 7.30 –7.80 (22H, m, vinyl and aryl). $^{13}C\{^1H\}$ NMR (toluene-d_8, 243 K): δ 171.24 (s, 2C, equatorial), 178.59 (s, 2C, equatorial), 185.34 (s, 4C, axial), 196.39 (t, 2C, axial, J_{P-C} = 9 Hz). $^{31}P\{^1H\}$ NMR ($CDCl_3$, 298 K): δ 37.39 (s). Anal. Calcd (found) for $C_{36}H_{22}O_{10}Os_3P_2$: C, 34.64 (34.71); H, 1.76 (1.68).

4. $Os_3(CO)_{11}(\eta^1$-bpcd)

Into a Schlenk flask containing $Os_3(CO)_{11}$(NCMe), as prepared from 0.20 g (0.22 mmol) of $Os_3(CO)_{12}$ and 0.016 g (0.22 mmol) of Me_3NO was added 100 mL of dichloromethane by syringe. This solution was slowly added to 0.51 g (1.10 mmol) of bpcd in 50 mL of dichloromethane over 6 hours, with stirring continued overnight. The solvent was then removed and the residue separated by column chromatography over silica gel using 40% dichloromethane in hexane to give the mixture of $Os_3(CO)_{11}(\eta^1$-bpcd) as the major component, along with minor amounts of 1,2-$Os_3(CO)_{10}$(bpcd) and an unknown species, all of which have the same R_f value and cannot be separated by column chromatography. Recrystallization from CH_2Cl_2/hexane affords 0.13 g (0.095 mmol) $Os_3(CO)_{11}(\eta^1$-bpcd). Yield: 43%. IR (CH_2Cl_2): ν(CO) 2010 (m), 2060 (s), 2042 (m), 2020 (s, b), 2006 (m, sh), 1993 (m, b), 1980 (m, b), 1949 (w, b), 1748 (w, symm bpcd), 1714 (m, antisymm bpcd) cm^{-1}. ^1H NMR ($CDCl_3$, 298 K): δ 7.00 –7.60 (20 H, m,

phenyl), 3.17 (2 H, s, methylene protons on the 5-membered ring). $^{31}P\{^{1}H\}$ NMR ($CDCl_3$, 298 K): δ -11.19 (1 P, d, J_{P-P}=14 Hz), -27.86 (1 P, d, J_{P-P}=14 Hz).

5. 1,2-$Os_3(CO)_{10}$(bpcd)

To a Schlenk flask containing 100 mL of benzene and $Os_3(CO)_{10}(NCMe)_2$, as prepared from 0.80 g (0.88 mmol) of $Os_3(CO)_{12}$ and 0.14 g (1.9 mmol) of Me_3NO, was added 0.41 g (0.88 mmol) of bpcd. The solution was stirred for 4 hours at ambient temperature, and the solvent removed under vacuum and the residue purified by column chromatography over silica gel using 40% dichloromethane in hexane. The green 1,2-$Os_3(CO)_{10}$(bpcd) isolated was recrystallized from CH_2Cl_2/hexane to give 0.56 g (0.43 mmol) of the product. Yield: 48%. 1,2-$Os_3(CO)_{10}$(bpcd): IR (CH_2Cl_2): ν(CO) 2091 (m), 2030 (m, sh), 2008 (vs,b), 1975 (m, b), 1958 (m, b), 1761 (w, symm bpcd), 1724 (m, antisymm bpcd) cm^{-1}. ^{1}H NMR ($CDCl_3$, 298 K): δ 3.06 (2H, s, methylene protons on the 5-membered ring), 7.25 –7.70 (20H, m, phenyl). $^{13}C\{^{1}H\}$ NMR (toluene-d_8, 233 K): 193.07 (s, 4C, axial), 184.78 (s, 2C, axial), 178.17 (s, 2C, equatorial), 173.12 (s, 2C, equatorial). $^{31}P\{^{1}H\}$ NMR ($CDCl_3$, 298 K): δ -17.55 (s).

6. 1,1-$Os_3(CO)_{10}$(bpcd)

A CO-saturated benzene solution containing 0.56 g (0.43 mmol) of 1,2-$Os_3(CO)_{10}$(bpcd) was heated at 50 °C for 20 hours to effect isomerization to the chelating isomer. The solvent was removed under vacuum and the residue separated by column chromatography over silica gel using 40% dichloromethane in hexane to give 0.42 g (0.32 mmol) of brown solid, 1,1-$Os_3(CO)_{10}$(bpcd). Yield: 74%. 1,1-$Os_3(CO)_{10}$(bpcd): IR (CH_2Cl_2): ν(CO) 2096 (m), 2047 (vs), 2010 (vs,b), 1992 (m), 1977 (m), 1964 (w, b),

1925 (m,b), 1749 (w, symm bpcd), 1717 (m, antisymm bpcd) cm^{-1}. ^{1}H NMR ($CDCl_3$, 298 K): δ 3.74 (2H, s, methylene protons on the 5-membered ring), 7.25 –7.70 (20H, m, phenyl). $^{13}C\{^{1}H\}$ NMR (toluene-d_8, 253 K): 198.59 (t, 2C, axial, J_{P-C} = 8 Hz), 185.03 (s, 4C, axial), 177.02 (s, 2C, equatorial), 171.02 (s, 2C, equatorial). $^{31}P\{^{1}H\}$ NMR ($CDCl_3$, 298 K): δ 17.97 (s). Anal. Calcd (found) for $C_{39}H_{22}O_{12}Os_3P_2$: C, 35.62 (35.56); H, 1.69 (1.74).

7. $HOs_3(CO)_9[\mu\text{-}(PPh_2)C{=}C\{PPh(C_6H_4)\}C(O)CH_2C(O)]$

To a Schlenk flask containing 50 mL of benzene and $Os_3(CO)_{10}(NCMe)_2$, as prepared from 0.25 g (0.28 mmol) of $Os_3(CO)_{12}$ and 0.060 g (0.80 mmol) of Me_3NO according to the literature procedure,[3] was transferred the solution of 0.13 g (0.28 mmol) of bpcd in 15 mL of benzene by cannula, after which the solution was stirred for 3 days at 45 °C. The solvent was then stripped and the residue separated by column chromatography over silica gel using 40% dichloromethane in hexane to give a 7:1 mixture of 1,1-$Os_3(CO)_{10}$(bpcd) and $HOs_3(CO)_9[\mu\text{-}(PPh_2)C{=}C\{PPh(C_6H_4)\}C(O)CH_2C(O)]$, as determined by ^{1}H NMR spectroscopy. The cluster mixtute was dissolved in 40 mL of dichloromethane in a Schlenk tube and irradiated with two black lights for 7 days at 40 °C. The solvent was removed under vacuum and the residue was filtered through silica gel using dichloromethane and recrystallized from benzene to afford 0.082 g (0.064 mmol) of brown solid, identified as $HOs_3(CO)_9[\mu\text{-}(PPh_2)C{=}C\{PPh(C_6H_4)\}C(O)CH_2C(O)]$. Yield: 23%. IR ($CH_2Cl_2$): ν(CO) 2084 (s), 2042 (s), 2019 (vs), 2003 (m), 1751 (w, symm bpcd), 1719 (m, antisymm bpcd) cm^{-1}. ^{1}H NMR ($CDCl_3$, 298 K): δ 6.90 –8.30 (19H, m, phenyl), 3.54 (2H, s, methylene on

the 5-membered ring), -16.28 (1H, t, hydride, J_{H-P}=13 Hz). $^{13}C\{^{1}H\}$ NMR (toluene-d_8, 223 K): 185.32 (m, 3C), 179.02 (s, 1C), 178.24 (d, 1C, J_{P-C} = 9 Hz), 176.88 (s, broad, 1C), 176.09 (s, broad, 1C), 175.31 (s, 1C), 173.79 (s, 1C). $^{31}P\{^{1}H\}$ NMR ($CDCl_3$, 298 K): δ 26.71 (1 P, d, J_{P-P}=15 Hz), 19.18 (1 P, d, J_{P-P}=15 Hz). Anal. Calcd (found) for $C_{38}H_{22}O_{11}Os_3P_2 \cdot 0.5C_6H_6$: C, 37.13 (37.07); H, 1.90 (2.08).

8. $HOs_3(CO)_8(\mu_3\text{-}C_6H_4)[\mu_2,\eta^1\text{-}PPhC{=}C(PPh_2)C(O)CH_2C(O)]$

0.16 g (0.12 mmol) of 1,1-$Os_3(CO)_{10}$(bpcd) was charged to a screw-capped NMR tube, followed by 0.7 mL of toluene-d_8. The NMR tube was heated at 110 °C and the progress of the reaction was monitored by ^{1}H NMR. Upon completion, the solvent was then removed and the residue was separated by column chromatography over silica gel using 50% dichloromethane in hexane. Recrystallization from benzene gave 0.062 g (0.049 mmol) of $HOs_3(CO)_8(\mu_3\text{-}C_6H_4)[\mu_2,\eta^1\text{-}PPhC{=}C(PPh_2)C(O)CH_2C(O)]$ as a brown solid. Yield: 40%. IR (CH_2Cl_2): ν(CO) 2077 (s), 2042 (vs), 2030 (m), 1999 (m), 1990 (m), 1977 (m) 1748 (w, symm bpcd), 1715 (m, antisymm bpcd) cm^{-1}. ^{1}H NMR ($CDCl_3$, 298 K): δ 3.66 (2 H, AB quartet, J_{H-H} = 22 Hz), 6.50 –9.20 (19 H, m, aryl), -16.68 (1 H, dd, J_{H-P}= 14, 6.7 Hz). $^{13}C\{^{1}H\}$ NMR (toluene-d_8, 253 K): 184.41 (d, 1C, J_{P-C} = 7 Hz), 182.42 (s, 1C), 180.86 (d, 1C, J_{P-C} = 74 Hz), 179.98 (d, 1C, J_{P-C} = 74 Hz), 175.64 (s, broad, 1C), 175.10 (d, 1C, J_{P-C} = 7 Hz), 174.70 (s, 1C), 171.44 (s, 1C). $^{31}P\{^{1}H\}$ NMR ($CDCl_3$, 298 K): δ 10.96 (1 P, d, J_{P-P}=12 Hz), -72.18 (1 P, d, J_{P-P}=12 Hz). Anal. Calcd (found) for $C_{37}H_{22}O_{10}Os_3P_2 \cdot 0.5C_6H_6$: C, 37.01 (36.58); H, 1.94 (1.90).

9. bpcd-d_{20}

To a Schlenk flask containing 150 mL of THF and 1.3 g (4.7 mmol) of $P(C_6D_5)_3$, which was prepared according to the literature procedure,[9] was added 0.55 g (14 mmol) of potassium. The reaction mixture was stirred overnight at ambient temperature and filtered through a sintered funnel to remove the unreacted potassium. The filtrate was cooled to 0 °C with an ice/water bath and to this solution was added 4 equivalents (2.5 mL, 19 mmol) of TMSCl dropwise with a syringe in order to promote the consumption of the $(C_6D_5)_2P^-$ anion that was formed from the reduction of triphenylphosphine-d_{15}. After stirring at 0 °C for 1 hour, the bath was removed and the reaction mixture was stirred for an additional 2 hours with warming. The solvent and unreacted TMSCl were removed under vacuum and the residue was dissolved in 5 mL of Et_2O. The resulting solution was cooled to 0 °C with an ice/water bath and then treated with 0.33 g (2.0 mmol) of 4,5-dichloro-4-cyclopenten-1,3-dione in a solvent mixture of 20 mL of Et_2O and 3 mL of THF dropwise by a pressure-equilibrated addition funnel over 30 minutes. The solution was stirred overnight at ambient temperature, followed by solvent removal and chromatographic separation over silica gel using 50% dichloromethane in hexane as the eluent. The yellow bpcd-d_{20} (0.31 g) was isolated in 32% yield. (based on the consumption of 4,5-dichloro-4-cyclopenten-1,3-dione). ^{1}H NMR ($CDCl_3$, 298 K): δ 2.92 (methylene protons on the 5-membered ring). $^{31}P\{^1H\}$ NMR ($CDCl_3$, 298 K): δ -22.76 (s). FAB-MS (*m/z*): 484.2344 (calc for $C_{29}H_2D_{20}O_2P_2$: 484.2345).

10. 1,1-$Os_3(CO)_{10}$(bpcd-d_{20})

To a Schlenk flask containing 50 mL of dichloromethane and $Os_3(CO)_{10}(NCMe)_2$, as prepared from 0.28 g (0.31 mmol) of $Os_3(CO)_{12}$ and 0.053 g (0.71 mmol) of Me_3NO,[3]

was added 0.15 g (0.31 mmol) of bpcd-d_{20} in 15 mL of dichloromethane by cannula, followed by stirring for 6 hours at 40 °C. The solvent was then stripped and the residue separated by column chromatography over silica gel using 40% dichloromethane in hexane to give a 1:1 mixture of 1,1-$Os_3(CO)_{10}$(bpcd-d_{20}) and 1,2-$Os_3(CO)_{10}$(bpcd-d_{20}). The isomeric clusters were dissolved in 40 mL of CO-saturated dichloromethane in a Schlenk flask and heated for 3 days at 45 °C under 1 atm CO. The solvent was removed under vacuum and the residue was separated by column chromatography over silica gel using 40-50% dichloromethane in hexane to afford 0.24 g (0.18 mmol) of 1,1-$Os_3(CO)_{10}$(bpcd-d_{20}) and 0.023 g (0.048 mmol) of unreacted bpcd-d_{20}. 1,1-$Os_3(CO)_{10}$(bpcd-d_{20}): yield: 58% (Based on the consumption of Os), IR (CH_2Cl_2): (CO) 2096 (m), 2047 (vs), 2011 (vs, b), 1992 (m), 1977 (m), 1963 (w, b), 1926 (m, b), 1749 (w, symm dione carbonyl), 1717 (m, antisymm dione carbonyl) cm^{-1}. ^1H NMR ($CDCl_3$, 298 K): δ 3.73 (methylene protons on the 5-membered ring). $^{31}P\{^1H\}$ NMR ($CDCl_3$, 298 K): δ 17.03 (s).

11. $DOs_3(CO)_9[\mu\text{-}(PPh_2\text{-}d_{10})C{=}C\{P(Ph\text{-}d_5)(C_6D_4)\}C(O)CH_2C(O)]$

To a Schlenk tube containing 0.24 g (0.18 mmol) of 1,1-$Os_3(CO)_{10}$(bpcd-d_{20}) was charged a solvent mixture of 4 mL of toluene-d_8 and 8 mL of benzene-d_6. The resulting solution was irradiated by two Black lights for 10 days, during which time the CO released from the cluster was periodically removed by bubbling argon through the solution. The reaction process was monitored by ^1H NMR spectroscopy and when the starting cluster had been completely consumed, the solvent was removed under vacuum and the residue was separated by column chromatography over silica gel using 40-50%

dichloromethane in hexane to afford 0.20 g (0.15 mmol) of $DOs_3(CO)_9[\mu$-$(PPh_2$-$d_{10})C{=}C\{P(Ph$-$d_5)(C_6D_4)\}C(O)CH_2C(O)]$. Yield: 83%. ^{1}H NMR ($CDCl_3$, 298 K): δ 3.55 (methylene protons on the 5-membered ring). $^{31}P\{^1H\}$ NMR ($CDCl_3$, 298 K): δ 26.21 (1P, d, $J_{P\text{-}P}$=14 Hz), 18.92 (1P, d, $J_{P\text{-}P}$=14 Hz).

12. bpcd-d_{4ortho}

To a Schlenk flask containing 1.4 g (5.3 mmol) of $P(Ph$-$d_{1ortho})_3$[10] was added 150 mL of THF, followed by 0.62 g (16.0 mmol) of potassium in small pieces. The reaction mixture was stirred overnight at ambient temperature and filtered through a sintered funnel to remove unreacted potassium. The filtrate was cooled to 0 °C with an ice/water bath and to this solution was added 5 equivalents (3.5 mL, 27 mmol) of TMSCl dropwise with a syringe in order to promote the consumption of $(C_6D_5)_2P^-$ anion. After stirring at 0 °C for 1 hour, the bath was removed and the reaction mixture was stirred for an additional 2 hours with warming. The solvent and unreacted TMSCl were removed under vacuum and the residue was dissolved in 5 mL of Et_2O. The resulting solution was cooled to 0 °C with an ice/water bath and then treated with 0.26 g (1.6 mmol) of 4,5-dichloro-4-cyclopenten-1,3-dione dissolved in a mixture of 20 mL of Et_2O and 3 mL of THF dropwise by a pressure-equilibrated addition funnel over 30 minutes. The solution was stirred overnight at ambient temperature. The solvent was then stripped and the residue was separated by column chromatography over silica gel with 50% dichloromethane in hexane as the eluent to afford 0.16 g (0.34 mmol) of yellow bpcd-d_{4ortho}. Yield: 22% (based on the consumption of 4,5-dichloro-4-cyclopenten-1,3-dione). ^{1}H NMR ($CDCl_3$, 298 K): δ 7.15-7.45 (16H, m, phenyl), 2.93 (2H, s, methylene protons on the 5-membered

ring). $^{31}P\{^{1}H\}$ NMR ($CDCl_3$, 298 K): δ -22.48 (s). FAB-MS (m/z): 468.1341 (calc for $C_{29}H_{18}D_4O_2P_2$: 468.1341).

13. 1,1-$Os_3(CO)_{10}$(bpcd-d_{4ortho})

To a Schlenk flask containing $Os_3(CO)_{10}(NCMe)_2$, as prepared from 0.31 g (0.34 mmol) of $Os_3(CO)_{12}$ and 0.053 g (0.71 mmol) of Me_3NO,[3] and 50 mL of dichloromethane was added a solution of 0.16 g (0.34 mmol) of bpcd-d_{4ortho} in 15 mL of dichloromethane. The reaction was stirred for 6 hours at 40 °C. All volatiles were then removed and the residue separated by column chromatography over silica gel using 40% dichloromethane in hexane to give a mixture of 1,1-$Os_3(CO)_{10}$(bpcd-d_{4ortho}) and 1,2-$Os_3(CO)_{10}$(bpcd-d_{4ortho}), which was dissolved in 40 mL of CO-saturated dichloromethane in a Schlenk flask and heated for 2 days at 55 °C under 1 atm CO. The solvent was removed under vacuum and the residue was separated by column chromatography over silica gel using 40-50% dichloromethane in hexane to afford 0.22 g (0.17 mmol) of 1,1-$Os_3(CO)_{10}$(bpcd-d_{4ortho}). Yield: 48% (based on the consumption of bpcd-d_{4ortho}). IR (CH_2Cl_2): ν(CO) 2096 (m), 2047 (vs), 2010 (vs,b), 1992 (m), 1977 (m), 1964 (w, b), 1926 (m,b), 1749 (w, symm bpcd), 1717 (m, antisymm bpcd) cm^{-1}. ^{1}H NMR ($CDCl_3$, 298 K): δ 7.35-7.70 (16H, m, phenyl), 3.75 (2H, s, methylene protons on the 5-membered ring). $^{31}P\{^{1}H\}$ NMR ($CDCl_3$, 298 K): 17.32.

E. Kinetic Studies

1. Isomerization of $Os_3(CO)_{10}$(cDPPEn) by UV-VIS Spectroscopy

The UV-visible kinetic studies were conducted using 1.0 cm quartz UV-visible cells that were equipped with a high-vacuum Teflon stopcock to facilitate material

transfer on the vacuum line and in the glove box. A stock solution of 1,2-$Os_3(CO)_{10}$(cDPPEn), having a concentration of ca. 1.0×10^{-4} M, was prepared by dissolving 0.0062 g of the cluster in 50 mL of CO-saturated toluene under a CO atmosphere. The stock solution when not in use was stored in the dark and under CO. All samples for UV-VIS kinetic experiments were saturated with CO prior to heating to suppress the formation of the hydride-bridged cluster $HOs_3(CO)_9$[μ-(Z)-$PhP(C_6H_4)CH=CHPPH_2$] (*vide infra*). The Hewlett-Packard 8452A diode array spectrophotometer used in the kinetic studies was configured with a variable-temperature UV-VIS cell holder that was assembled with a VWR constant temperature circulator by which the reaction temperature was regulated to within ± 0.5 °C. The spectrophotometer was interfaced with a computer, by which the UV-VIS kinetic measurements were conducted in the kinetics mode using the UV-visible ChemStation software (Rev. A. 10.01 [81]), which was developed by the Agilent Technologies. The kinetics were monitored by following the absorbance increase at 368 nm as a function of time for a minimum of 6 half-lives. The rate to equilibrium (k_e) was determined by non-linear regression analysis with Origin® software using the single exponential function (equation 1):

$$A(t) = A_\infty + \Delta A \times e^{(-k_e t)} \qquad (1)$$

2. Isomerization of $Os_3(CO)_{10}$(cDPPEn) by ^{31}P NMR Spectroscopy

The ^{31}P NMR kinetic and equilibration experiments were carried out in 5 mm NMR tubes equipped with a J-Young valve for the easy admission of CO gas. All NMR samples were prepared by dissolving 0.050 g of 1,2-$Os_3(CO)_{10}$(cDPPEn) in 0.7 mL of

toluene-d_8, followed by deoxygenation by 3 freeze-pump-thaw cycles and a final admission of CO to the tube. The NMR samples were heated in a VWR constant temperature circulator bath. Samples for analysis were removed at the desired time and quenched in an external ice/water bath immediately before NMR analysis. The relative molar ratio of 1,2-$Os_3(CO)_{10}$(cDPPEn), 1,1-$Os_3(CO)_{10}$(cDPPEn), and $HOs_3(CO)_9$[μ-(Z)-$PhP(C_6H_4)CH{=}CHPPH_2$] was calculated on the basis of the integration values of each species relative to the total integration value of all the Os_3 species present in the ^{31}P NMR spectrum. The data were analyzed and the rate to equilibrium (k_e) determined by non-linear regression analysis with Origin® software using the single exponential function (equation 1). The equilibrium ratio of 1,1-$Os_3(CO)_{10}$(cDPPEn) to 1,2-$Os_3(CO)_{10}$(cDPPEn) at the examined temperatures was calculated by averaging 3 measurements after the samples had reached equilibrium (>10 half-lifes).

3. Isomerization of $Os_3(CO)_{10}$(bpcd) in the Absence of Trapping Ligands by UV-VIS Spectroscopy

A stock solution of 1,2-$Os_3(CO)_{10}$(bpcd), having a concentration of ca. 1.0×10^{-4} M, was prepared by dissolving 0.0063 g of the cluster in 40 mL of benzene under Ar. The stock solution when not in use was stored in the dark and under Ar. The kinetics was monitored by following the increase of the absorbance at 364 nm as a function of time for at least 3 half-lifes.

4. Isomerization of $Os_3(CO)_{10}$(bpcd) in the Presence of Trapping Ligands by UV-VIS Spectroscopy

A stock solution of 1,2-$Os_3(CO)_{10}$(bpcd) (ca. 1.0×10^{-4} M) in 40 mL of benzene solution was treated with a measured excess of PPh_3, $P(OEt)_3$ or PCy_3. The solution containing only the trapping ligand was used as the blank for all UV-VIS measurements. The stock solution when not in use was stored in the dark and under Ar. The kinetics were monitored by following the increase of the 364 nm absorbance as a function of time for at least 3 half-lifes.

5. Isomerization of $Os_3(CO)_{10}$(bpcd) in the Absence of Trapping Ligands by ^{1}H NMR Spectroscopy

The ^{1}H NMR kinetic experiments were carried out in 5 mm NMR tubes. All NMR samples were prepared by dissolving 0.020 g of 1,2-$Os_3(CO)_{10}$(bpcd) cluster and an internal standard (*tert*-butylbenzne, 1,4-di-*tert*-butylbenzene or 1,4-dimethoxybenzene) in 0.7 mL of bezene-d_6. After 3 freeze-pump-thaw degassing cycles, the tube was flame-sealed under vacuum. The NMR samples were heated in a VWR constant temperature circulator, which allowed the reaction temperature to be regulated to within ± 0.5 °C. The samples were quenched in an external ice bath prior to NMR analysis. The relative molar ratio of 1,2-$Os_3(CO)_{10}$(bpcd) and 1,1-$Os_3(CO)_{10}$(bpcd) was calculated based on the integration value of the methylene proton peak of each species relative to the internal standard. The first-order rate constants were determined by least-squares analysis using the trendline feature in Microsoft Excel®.

6. Isomerization of $Os_3(CO)_{10}$(bpcd) in the Presence of Trapping Ligands by ^{1}H NMR Spectroscopy

The ^{1}H NMR kinetic experiments were carried out in 5 mm NMR tubes. All NMR samples were prepared by dissolving 0.020 g 1,2-$Os_3(CO)_{10}$(bpcd) cluster, the internal standard (*tert*-butylbenzne, 1,4-di-*tert*-butylbenzene or 1,4-dimethoxybenzene) and 10 equivalents of the trapping ligand (PPh_3, $P(OEt)_3$ or PCy_3) in 0.7 mL of bezene-d_6. The data were treated by the method of least-squares analysis to calculate the rate constants (*k*).

7. Thermolysis of 1,1-$Os_3(CO)_{10}$(bpcd) and $HOs_3(CO)_9[\mu$-$(PPh_2)C{=}C\{PPh(C_6H_4)\}C(O)CH_2C(O)]$ by ^{1}H NMR Spectroscopy

The NMR samples were prepared as described above by dissolving 0.020 g of 1,1-$Os_3(CO)_{10}$(bpcd) cluster or 0.020 g of $HOs_3(CO)_9[\mu$-$(PPh_2)C{=}C\{PPh(C_6H_4)\}C(O)CH_2C(O)]$ cluster with the internal standard (*tert*-butylbenzne, 1,4-di-*tert*-butylbenzene or 1,4-dimethoxybenzene) in 0.7 mL of toluene-d_8. The samples were heated at 90.0 °C and analyzed hourly for a total of 40 hours.

8. Ligand Trapping Studies Using $HOs_3(CO)_9[\mu$-$(PPh_2)C{=}C\{PPh(C_6H_4)\}C(O)CH_2C(O)]$ in the Presence of PPh_3, PCy_3, and $P(OEt)_3$

The UV-visible kinetic studies were conducted using 1.0 cm quartz UV-visible cells that were equipped with a high-vacuum Teflon stopcock. A stock solution of $HOs_3(CO)_9[\mu$-$(PPh_2)C{=}C\{PPh(C_6H_4)\}C(O)CH_2C(O)]$ (ca. 1.0×10^{-4} M) in toluene was treated with a measured excess of PPh_3, $P(OEt)_3$ or PCy_3 (>10 equivalents). The kinetics were monitored by following the decrease of the absorbance at 396 nm as a function of time for at least 3 half-lifes. The data were treated by non-linear regression analysis, which furnished the quoted first-order rate constants (*k*).

9. UV-VIS Investigation of $HOs_3(CO)_9[\mu\text{-}(PPh_2)C{=}C\{PPh(C_6H_4)\}C(O)CH_2C(O)]$ to $HOs_3(CO)_8(\mu_3\text{-}C_6H_4)[\ \mu_2,\eta^1\text{-}PPhC{=}C(PPh_2)C(O)CH_2C(O)]$

These kinetic studies were carried out similarly as described for the ligand-trapping studies using $HOs_3(CO)_9[\mu\text{-}(PPh_2)C{=}C\{PPh(C_6H_4)\}C(O)CH_2C(O)]$. The kinetics were monitored by following the decrease in the 396 nm absorbance band of the starting cluster for at least 3 half-lifes. The rate constants were determined by non-linear regression analysis of the absorbance data as a function of time.

10. Ligand Trapping Studies of $DOs_3(CO)_9[\mu\text{-}(PPh_2\text{-}d_{10})C{=}C\{P(Ph\text{-}d_5)(C_6D_4)\}C(O)CH_2C(O)]$ with PPh_3 Using UV-VIS Spectroscopy

The UV-visible kinetic studies described here were carried out in an analogous fashion as for the protio-isotopomer. The reaction of $DOs_3(CO)_9[\mu\text{-}(PPh_2\text{-}d_{10})C{=}C\{P(Ph\text{-}d_5)(C_6D_4)\}C(O)CH_2C(O)]$ in the presence of PPh_3 (25-fold excess) was investigated. The kinetics were monitored by following the decrease of the 396 nm absorbance band belonging to the starting deuteride cluster for at least 3 half-lifes.

11. Kinetic Isotope Effect Study for the Orthometallation of 1,1-$Os_3(CO)_{10}(bpcd\text{-}d_{4ortho})$

0.020 g (0.015 mmol) of 1,1-$Os_3(CO)_{10}(bpcd\text{-}d_{4ortho})$ and 0.50 mL of toluene-d_8 were added to a 5 mm NMR tube equipped with a J-Young valve. The solution was freeze-pump-thaw degassed three times and then cooled to 0 °C in a quartz dewar, after which the sample was irradiated with a 200 W Oriel Hg(Xe) arc lamp until ca. 5% of the starting cluster remained. The amount of hydride, $HOs_3(CO)_9[\mu\text{-}(PPh_2\text{-}d_{2ortho})C{=}C\{P(Ph\text{-}d_{1ortho})(C_6H_3D)\}C(O)CH_2C(O)]$, versus the amount of deuteride, $DOs_3(CO)_9[\mu\text{-}(PPh_2\text{-}d_{2ortho})C{=}C\{P(Ph\text{-}d_{1ortho})(C_6H_4)\}C(O)CH_2C(O)]$, was then determined by measuring the

area under the hydride resonance and the methylene group associated with the bpcd ring of both isotopomers.[11] Under these conditions, the amount of hydride-to-deuteride cluster was found to be 55:45.

12. Equilibrium Isotope Effect between $HOs_3(CO)_9[\mu\text{-}(PPh_2\text{-}d_{2ortho})C{=}C\{P(Ph\text{-}d_{1ortho})(C_6H_3D)\}C(O)CH_2C(O)]$ and $DOs_3(CO)_9[\mu\text{-}(PPh_2\text{-}d_{2ortho})C{=}C\{P(Ph\text{-}d_{1ortho})(C_6H_4)\}C(O)CH_2C(O)]$

The equilibrium experiments were performed in 5 mm NMR tubes with samples that were irradiated by a Mercury Arc lamp in a temperature-controlled water bath at 40 °C. All NMR samples were prepared by dissolving 0.020 g of 1,1-$Os_3(CO)_{10}(bpcd\text{-}d_{4ortho})$ in 0.7 mL of toluene-d_8, followed by 3 freeze-pump-thaw cycles prior to flame sealing of the NMR tube. The progress of the irradiation reaction was monitored by NMR spectroscopy. The relative molar ratio of $HOs_3(CO)_9[\mu\text{-}(PPh_2\text{-}d_{2ortho})C{=}C\{P(Ph\text{-}d_{1ortho})(C_6H_3D)\}C(O)CH_2C(O)]$ versus $DOs_3(CO)_9[\mu\text{-}(PPh_2\text{-}d_{2ortho})C{=}C\{P(Ph\text{-}d_{1ortho})(C_6H_4)\}C(O)CH_2C(O)]$ was calculated using the integration value of hydride ligand in $HOs_3(CO)_9[\mu\text{-}(PPh_2\text{-}d_{2ortho})C{=}C\{P(Ph\text{-}d_{1ortho})(C_6H_3D)\}C(O)CH_2C(O)]$ and of the total integral for the methylene protons from $HOs_3(CO)_9[\mu\text{-}(PPh_2\text{-}d_{2ortho})C{=}C\{P(Ph\text{-}d_{1ortho})(C_6H_3D)\}C(O)CH_2C(O)]$ and $DOs_3(CO)_9[\mu\text{-}(PPh_2\text{-}d_{2ortho})C{=}C\{P(Ph\text{-}d_{1ortho})(C_6H_4)\}C(O)CH_2C(O)]$.

F. X-Ray Crystallography

1. 1,2-$Os_3(CO)_{10}(cDPPEn)\cdot CH_2Cl_2$

Single crystals of 1,2-$Os_3(CO)_{10}(cDPPEn)\cdot CH_2Cl_2$ suitable for X-ray diffraction analysis were grown from a dichloromethane solution containing pure 1,2-

$Os_3(CO)_{10}$(cDPPEn) that had been layered with hexane. An orange crystal of dimensions 0.43 x 0.18 x 0.17 mm^3 was selected and the Mo Kα radiation used was monochromatized by a crystal of graphite. Intensity data in the range of $2.7 < 2\theta < 56.6^\circ$ were collected at 297 K using the θ/2θ scan technique in the variable-scan speed mode on a Bruker SMART™ 1000 CCD-based diffractometer. The frames were integrated with the available SAINT software package using a narrow-frame algorithm,[12] and the structure was solved and refined using the SHELXTL program package.[13] The molecular structure was checked by using PLATON,[14] and all nonhydrogen atoms were refined anisotropically. All hydrogen atoms were assigned calculated positions and allowed to ride on the attached heavy atom. Refinement converged at $R = 0.0342$ and $R_w = 0.0685$ for 8518 independent reflections with $I > 2\sigma(I)$.

2. 1,1-$Os_3(CO)_{10}$(cDPPEn)

Single crystals of 1,1-$Os_3(CO)_{10}$(cDPPEn) suitable for X-ray diffraction analysis were grown from a dichloromethane solution containing a 1:7 mixture of 1,2-$Os_3(CO)_{10}$(cDPPEn) and 1,1-$Os_3(CO)_{10}$(cDPPEn) that had been layered with hexane. An orange crystal of dimensions 0.31 x 0.14 x 0.12 mm^3 was selected and the Mo Kα radiation used was monochromatized by a crystal of graphite. Intensity data in the range of $3.3 < 2\theta < 56.6^\circ$ were collected at 213 K using the θ/2θ scan technique in the variable-scan speed mode on a Bruker SMART™ 1000 CCD-based diffractometer. The frames were integrated with the available SAINT software package using a narrow-frame algorithm,[12] and the structure was solved and refined using the SHELXTL program package.[13] The molecular structure was checked by using PLATON,[14] and all

nonhydrogen atoms were refined anisotropically. The remaining hydrogen atoms were assigned calculated positions and allowed to ride on the attached heavy atom. Refinement converged at $R = 0.0448$ and $R_w = 0.0585$ for 8180 independent reflections with $I > 2\sigma(I)$.

3. 1,2-$Os_3(CO)_{10}$(bpcd)

Single crystals of 1,2-$Os_3(CO)_{10}$(bpcd), as the *m*-xylene solvate, suitable for X-ray diffraction analysis were grown from the slow evaporation of a test tube containing dichloromethane/hexane solution of 1,2-$Os_3(CO)_{10}$(bpcd) that had been placed inside a sealed Schlenk tube containing *m*-xylene. A green crystal of dimensions 0.28 x 0.17 x 0.10 mm^3 was selected and the Mo Kα radiation used was monochromatized by a crystal of graphite. Intensity data in the range of $2.6 < 2\theta < 54.0^\circ$ were collected at 213 K using the $\theta/2\theta$ scan technique in the variable-scan speed mode on a Bruker SMART^{TM} 1000 CCD-based diffractometer. The frames were integrated with the available SAINT software package using a narrow-frame algorithm,[12] and the structure was solved and refined using the SHELXTL program package.[13] The molecular structure was checked by using PLATON,[14] and all nonhydrogen atoms were refined anisotropically. All hydrogen atoms were assigned calculated positions and allowed to ride on the attached heavy atom. Refinement converged at $R = 0.0477$ and $R_w = 0.0782$ for 10128 independent reflections with $I > 2\sigma(I)$.

4. 1,1-$Os_3(CO)_{10}$(bpcd)

Single crystals of 1,1-$Os_3(CO)_{10}$(bpcd) suitable for X-ray diffraction analysis were grown from a dichloromethane solution containing the pure 1,1-$Os_3(CO)_{10}$(bpcd)

cluster that had been layered with hexane. A brown crystal of dimensions 0.36 x 0.28 x 0.20 mm^3 was selected. The Mo Kα radiation used was monochromatized by a crystal of graphite. Intensity data in the range of $3.0 < 2\theta < 45.0^{\circ}$ were collected at 300 K using the θ/2θ scan technique in the variable-scan speed mode on a Bruker SMART™ 1000 CCD-based diffractometer. The frames were integrated with the available SAINT software package using a narrow-frame algorithm,[12] and the structure was solved and refined using the SHELXTL program package.[13] The molecular structure was checked by using PLATON,[14] and all nonhydrogen atoms were refined anisotropically, while the hydrogen atoms were assigned calculated positions and allowed to ride on the attached heavy atom. Refinement converged at $R = 0.0249$ and $R_w = 0.0582$ for 5120 independent reflections with $I > 2\sigma(I)$.

5. $HOs_3(CO)_8(\mu_3\text{-}C_6H_4)[\mu_2,\eta^1\text{-}PPhC{=}C(PPh_2)C(O)CH_2C(O)]\cdot(C_7H_8)$

Single crystals of $HOs_3(CO)_8(\mu_3\text{-}C_6H_4)[\mu_2,\eta^1\text{-}PPhC{=}C(PPh_2)C(O)CH_2C(O)]\cdot(C_7H_8)$ suitable for X-ray diffraction analysis were grown from the slow evaporation of a toluene/hexane solution containing the $HOs_3(CO)_8(\mu_3\text{-}C_6H_4)[\mu_2,\eta^1\text{-}PPhC{=}C(PPh_2)C(O)CH_2C(O)]$. A brown crystal of dimensions 0.31 x 0.16 x 0.03 mm^3 was selected. The Mo Kα radiation used was monochromatized by a crystal of graphite. Intensity data in the range of $4.0 < 2\theta < 56.6^{\circ}$ were collected at 213 K using the θ/2θ scan technique in the variable-scan speed mode on a Bruker SMART™ 1000 CCD-based diffractometer. The frames were integrated with the available SAINT software package using a narrow-frame algorithm,[12] and the structure was solved and refined using

the SHELXTL program package.[13] The molecular structure was checked by using PLATON,[14] and all nonhydrogen atoms were refined anisotropically. With the exception of the bridging hydride that was not located during data refinement, all other hydrogen atoms were assigned calculated positions and allowed to ride on the attached heavy atom. Refinement converged at $R = 0.0780$ and $R_w = 0.1643$ for 9724 independent reflections with $I > 2\sigma(I)$.

G. Chapter References

1. Shriver, D. F. *The Manipulation of Air-Sensitive Compounds*; McGraw-Hill: New York, 1969.
2. Drake, S. R.; Loveday, P. A. *Inorg. Synth.* **1990**, *28*, 230.
3. Nicholls, J. N.; Vargas, M. D. *Inorg. Synth.* **1989**, *26*, 289.
4. Kuchen, W.; Buchward, H. *Chem. Ber.* **1959**, *92*, 227.
5. (a) Fenske, D.; Becher, H. J. *Chem. Ber.* **1974**, *107*, 117. (b) Fenske, D. *Chem. Ber.* **1979**, *112*, 363.
6. (a) Alex, R. F.; Pomeroy, R. K. *Organometallics* **1987,** *6*, 2437. (b) Walter, T. H.; Reven, L.; Oldfield, E. *J. Phys. Chem.* **1989**, *93*, 1320.
7. Bard, A. J.; Faulkner, L. R. *Electrochemical Methods*; Wiley: New York, 1980.
8. (a) Calvert, J. G.; Pitts, J. N. *Photochemistry*; Wiley: New York, 1966. (b) Parker, C. A. *Proc. R. Soc. London Ser. A* **1953**, *220*, 104. (c) Hatchard, C. G.; Parker, C. A. *Proc. R. Soc. London Ser. A* **1956**, *235*, 518.
9. (a) Bianco, V. D.; Doronzo, S. *Inorg. Synth*. **1976**, *16*, 164. (b) Siedle, A. R.; Newmark, R. A. *J. Am. Chem. Soc.* **1989**, *111*, 2058.

10. Bennett, M. A.; Milner D. L. *J. Am. Chem. Soc.* **1969**, *91*, 6983.

11. A ^{1}H spin-lattice (T_1) relaxation study on cluster $HOs_3(CO)_9[\mu$-$(PPh_2)C{=}C\{PPh(C_6H_4)\}C(O)CH_2C(O)]$ in benzene-d_6 was conducted and the T_1 values for the hydride (1.9 s) and the methylene (0.3 s) groups were determined by using the standard inversion-recovery pulse sequence. Accurate integration intensities, free from saturation effects, were thus obtained for the KIE and EIE experiments with $Os_3(CO)_{10}$(bpcd-d_{4ortho}) by employing an acquisition delay of 10 s (>5 T_1).

12. Saint Version 6.02, Bruker Analytical X-ray Systems, Inc., Madison, WI, 1997-1999.

13. SHELXTL Version 5.1, Bruker Analytical X-ray Systems, Inc., Madison, WI, 1998.

14. PLATON - A Multipurpose Crystallographic Tool, Utrecht University, Utrecht, The Netherlands, Speck, A. L., 2001.

CHAPTER III

RESULTS

A. Synthesis and Spectroscopic Properties of $Os_3(CO)_{11}(\eta^1$-cDPPEn)

The reaction between $Os_3(CO)_{11}(NCMe)$ and the unsaturated diphosphine ligand cDPPEn proceeds rapidly at room temperature to furnish $Os_3(CO)_{11}(\eta^1$-cDPPEn) as the predominant product. The ligand-bridged cluster 1,2-$Os_3(CO)_{10}$(cDPPEn) that accompanies this reaction results from the bis(acetonitrile) derivative $Os_3(CO)_{10}(NCMe)_2$ that was formed as a side product in the preparation of $Os_3(CO)_{11}(NCMe)$. $Os_3(CO)_{11}(\eta^1$-cDPPEn) was purified by chromatography over silica gel and characterized in solution by IR and NMR spectroscopies. The ^{31}P NMR spectrum of $Os_3(CO)_{11}(\eta^1$-cDPPEn) reveals the existence of two coupled phosphorus resonances ($J_{P\text{-}P}$ = 21 Hz), one of which is a dangling phosphorus atom represented by the up-field ^{31}P resonance at δ -30.65 and the other one is the phosphorus atom that is coordinated to one osmium atom, appearing down-field at δ -16.37. By comparison with the ^{31}P chemical shift of the free cDPPEn ligand, the $Os_3(CO)_{11}(\eta^1$-cDPPEn) cluster shows an up-field shift of 7.91 ppm for its dangling phosphorus atom and a down-field shift of 6.37 ppm for its coordinated phosphorus atom, the latter of which is similar to the previously reported ^{31}P chemical shifts of monophosphine-substituted triosmium clusters.[1] The IR spectrum of $Os_3(CO)_{11}(\eta^1$-cDPPEn) in CH_2Cl_2 shows terminal ν(CO) bands at 2107 (m), 2053 (s), 2032 (s), 2016 (vs), 2001 (s,sh), 1989 (m), and 1974 (m) cm^{-1}, fully consistent with those reported carbonyl frequency patterns of related triosmium carbonyl clusters.[2]

B. Synthesis and Spectroscopic Properties of 1,2-$Os_3(CO)_{10}$(cDPPEn)

The synthesis of 1,2-$Os_3(CO)_{10}$(cDPPEn) was fulfilled by the facile substitution of the two adjacent acetonitrile ligands in the $Os_3(CO)_{10}(MeCN)_2$ cluster with the unsaturated diphosphine ligand cDPPEn. The reaction proceeds rapidly and without complications at room temperature to give the ligand-bridged cluster as the predominant product, along with minor amounts of $Os_3(CO)_{11}(\eta^1$-cDPPEn), whose origin is derived from the monoacetonitrile derivative $Os_3(CO)_{11}(MeCN)$ that accompanies the preparation of $Os_3(CO)_{10}(MeCN)_2$. 1,2-$Os_3(CO)_{10}$(cDPPEn) was purified by chromatography over silica gel and characterized in solution by IR and NMR spectroscopies. The IR spectrum of 1,2-$Os_3(CO)_{10}$(cDPPEn) in CH_2Cl_2 shows terminal ν(CO) bands at 2088 (s), 2025 (s), 2013 (vs), 2001 (vs), 1971 (s), and 1949 (b, sh) cm^{-1}, completely consistent with the previously reported carbonyl frequencies of 1,2-diphosphine-substituted triosmium clusters.[3] Particularly diagnostic in the characterization of 1,2-$Os_3(CO)_{10}$(cDPPEn) was the up-field ^{31}P resonance at δ -6.45 that supports the bridging of adjacent osmium centers by the ancillary diphosphine ligand, with the ^1H NMR spectrum revealing the two vinyl hydrogens of the ethylene bridge at δ 6.29 as part of an AA′XX′ multiplet due to coupling with the two phosphorus centers. The ^{31}P NMR chemical shift of 1,2-$Os_3(CO)_{10}$(cDPPEn) shows a down-field shift of 29.03 ppm with respect to the free cDPPEn ligand. Four singlet carbonyl resonances were observed in the ^{13}C NMR spectrum of a ^{13}CO-enriched sample of 1,2-$Os_3(CO)_{10}$(cDPPEn) at δ 191.49, 184.96, 178.91 and 173.92 with an integral ratio of 4:2:2:2, fully consistent with the structure of 1,2-$Os_3(CO)_{10}$(cDPPEn). Based on the VT ^{13}C NMR study of ^{13}CO-enriched 1,2-$Os_3(CO)_{10}$(cDPPEn) (Figure 3.1), the assignments of these resonances are shown in

Scheme 3.1.

Scheme 3.1. ^{13}C NMR assignments of 1,2-$Os_3(CO)_{10}$(cDPPEn).

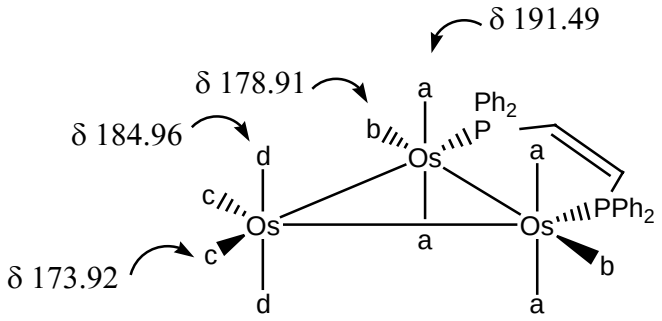

The ^{31}P NMR and ^{13}C NMR results of 1,2-$Os_3(CO)_{10}$(cDPPEn) indicate that the structure of 1,2-$Os_3(CO)_{10}$(cDPPEn) in solution has idealized C_{2v} symmetry, where the major symmetry axis bisects the triosmium plane along the line connecting the middle point of the two phosphorus-coordinated osmium atoms and the third osmium atom.

C. Synthesis and Spectroscopic Properties of 1,1-$Os_3(CO)_{10}$(cDPPEn)

The transformation of 1,2-$Os_3(CO)_{10}$(cDPPEn) into the chelating isomer 1,1-$Os_3(CO)_{10}$(cDPPEn) was found based on the results from a routine thermolysis study. Heating a sample of 1,2-$Os_3(CO)_{10}$(cDPPEn) in benzene-d_6 in a sealed NMR tube at 75 °C overnight indicated a diminution in the intensity of the vinyl protons in the ^1H NMR spectrum along with the appearance of a new ^{31}P resonance at δ 37.39, whose large down-field shift of 43.8 ppm with respect to the bridging isomer, is consistent with the formation of a chelating diphosphine ligand. Continued heating of this same mixture for over one week led to the slow growth of 1,1-$Os_3(CO)_{10}$(cDPPEn) at the expense of 1,2-

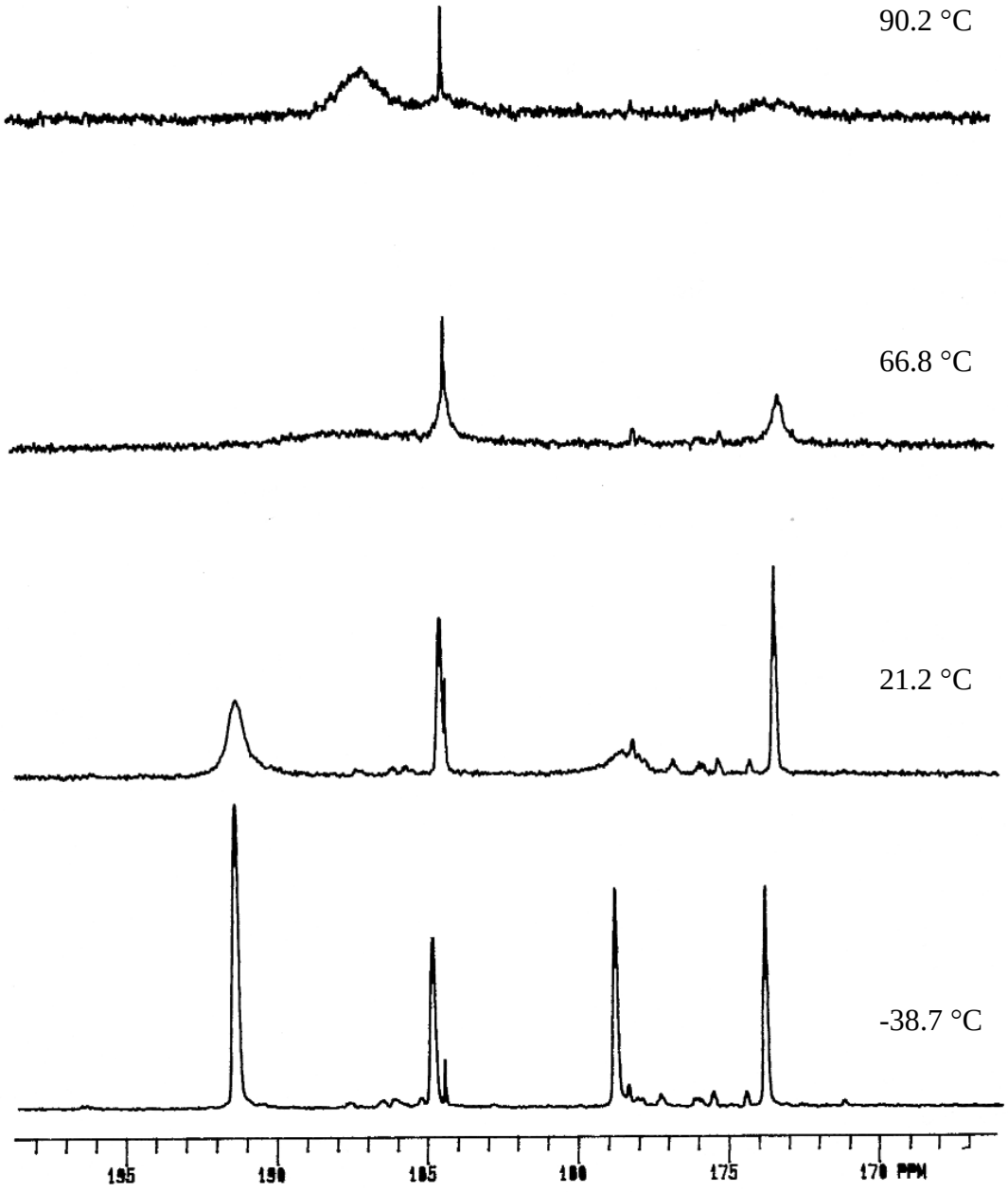

Figure 3.1. VT $^{13}C\{^{1}H\}$ NMR (50 MHz) of ^{13}CO-enriched 1,2-$Os_3(CO)_{10}$(cDPPEn) recorded in toluene-d_8.

$Os_3(CO)_{10}$(cDPPEn) and establishment of an equilibrium that favored the chelating isomer 1,1-$Os_3(CO)_{10}$(cDPPEn). Interestingly, TLC examination of parallel thermolysis reactions conducted in Schlenk vessels starting with 1,2-$Os_3(CO)_{10}$(cDPPEn) showed only a single spot for the equilibrium mixture of 1,2-$Os_3(CO)_{10}$(cDPPEn) and 1,1-$Os_3(CO)_{10}$(cDPPEn). If TLC had been the sole method of analysis, the isomerization reaction would have been missed. A trace amount of a third cluster (<1%) was also detected spectroscopically under these conditions and assigned to that of $HOs_3(CO)_9$[(Z)-$PhP(C_6H_4)CH=CHPPh_2$], on the basis of a high-field triplet at δ -17.00 ($^2J_{P-H}$ = 13 Hz) in the ^{1}H NMR spectrum and two nonequivalent ^{31}P resonances at δ 43.31 and 54.13 in the ^{31}P NMR spectrum. The orthometallation of the ancillary cDPPEn ligand in 1,1-$Os_3(CO)_{10}$(cDPPEn) is a phenomenon that has been observed in related triosmium clusters containing the diphosphine ligands dppm, dppe, and dppp. Thermolysis of 1,2-$Os_3(CO)_{10}$(cDPPEn) in the presence of 1 atm of CO greatly suppressed the amount of hydride cluster formed without adversely affecting the formation of 1,1-$Os_3(CO)_{10}$(cDPPEn). The origin of $HOs_3(CO)_9$[(Z)-$PhP(C_6H_4)CH=CHPPh_2$] was unequivocally demonstrated through the irradiation of samples of pure 1,1-$Os_3(CO)_{10}$(cDPPEn) (*vide infra*) using near-UV light. Here the same NMR resonances (^{1}H and ^{31}P) for the hydride cluster were reproduced. The possibility of 1,2-$Os_3(CO)_{10}$(cDPPEn) serving as the source of the hydride cluster was ruled out by UV-VIS and ^{31}P NMR spectroscopic studies. Irradiation of 1,2-$Os_3(CO)_{10}$(cDPPEn) with 366 nm light led to a slow bleaching of the absorption bands for 1,2-$Os_3(CO)_{10}$(cDPPEn) with no evidence for the formation of the hydride cluster. Taken collectively, these

observations strongly support the involvement of the two equilibria depicted in Scheme 3.2.

The IR spectrum of 1,1-$Os_3(CO)_{10}$(cDPPEn) in CH_2Cl_2 exhibits terminal ν(CO) bands at 2092 (m), 2042 (vs), 2006 (vs,b), 1973 (m), 1957 (m), 1926 (w, b) cm^{-1}, which are consistent with the carbonyl frequency patterns of other 1,1-bisphosphine-substituted triosmium carbonyl clusters.[4,1e] Four carbonyl resonances were observed in the ^{13}C NMR spectrum of a ^{13}CO-enriched sample of 1,1-$Os_3(CO)_{10}$(cDPPEn) at δ 196.39, 185.34, 178.59, 171.24, with an integral ratio of 2:4:2:2 at ca. -40 °C, which are fully consistent with the structure of 1,1-$Os_3(CO)_{10}$(cDPPEn). On the basis of VT ^{13}C NMR (Figure 3.2) and 2D-EXSY ^{13}C NMR (Figure 3.3) studies on the ^{13}CO-enriched 1,1-$Os_3(CO)_{10}$(cDPPEn), the proposed assignments of these resonances are shown in Scheme 3.3.

The ^{31}P NMR and ^{13}C NMR data of 1,1-$Os_3(CO)_{10}$(cDPPEn) support the identity of 1,1-$Os_3(CO)_{10}$(cDPPEn) and indicate that the cluster possesses C_{2v} symmetry in solution. Here the major symmetry axis bisects the triosmium plane through the phosphorus-coordinated osmium atom and the mid point of the non-phosphine-substituted Os-Os bond.

D. X-Ray Diffraction Structure of 1,2-$Os_3(CO)_{10}$(cDPPEn)·CH_2Cl_2

Single crystals of 1,2-$Os_3(CO)_{10}$(cDPPEn)·CH_2Cl_2 were successfully grown from a CH_2Cl_2 solution containing the pure 1,2-$Os_3(CO)_{10}$(cDPPEn) clusters that had been layered with hexanes. The molecular structure of 1,2-$Os_3(CO)_{10}$(cDPPEn)·CH_2Cl_2 was determined by X-ray diffraction analysis, with 1,2-$Os_3(CO)_{10}$(cDPPEn) existing as

discrete molecules in the unit cell with no unusually short inter- or intramolecular contacts. The X-ray data processing and collection parameters are listed in Table 3.1, and selected bond distances and angles given in Table 3.2. The molecular configuration and the numbering scheme of 1,2-$Os_3(CO)_{10}$(cDPPEn) are presented in the ORTEP diagram of Figure 3.4.

Scheme 3.2. Phosphine migration and orthometallation equilibria involving cDPPEn-coordinated triosmium carbonyl clusters.

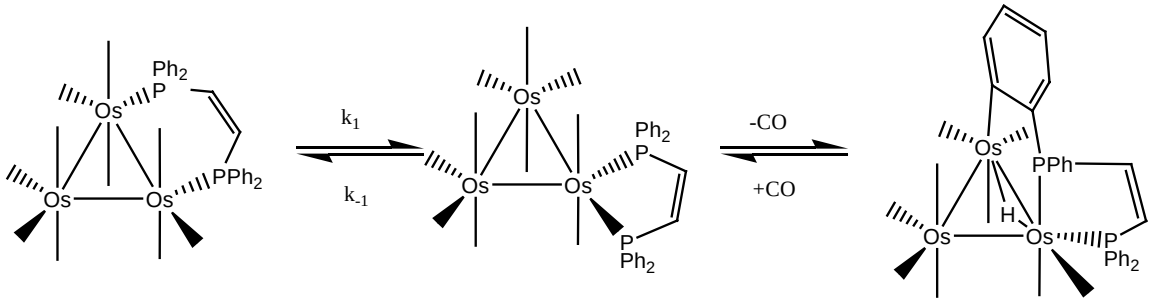

Scheme 3.3. ^{13}C NMR assignments of 1,1-$Os_3(CO)_{10}$(cDPPEn).

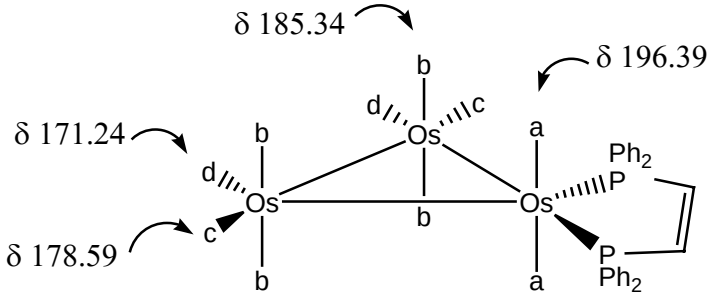

The Os-Os bond distances in 1,2-$Os_3(CO)_{10}$(cDPPEn) range from 2.8642(6) Å [Os(1)-Os(2)] to 2.8774(6) Å [Os(2)-Os(3)] and display a mean distance of 2.8717 Å. The Os-Os distances are normal relative to those in other simple polynuclear osmium clusters,[5,1h] which indicate that the triosmium frame itself does not experience any significantly adverse perturbation due to the coordination of the cDPPEn. The ten

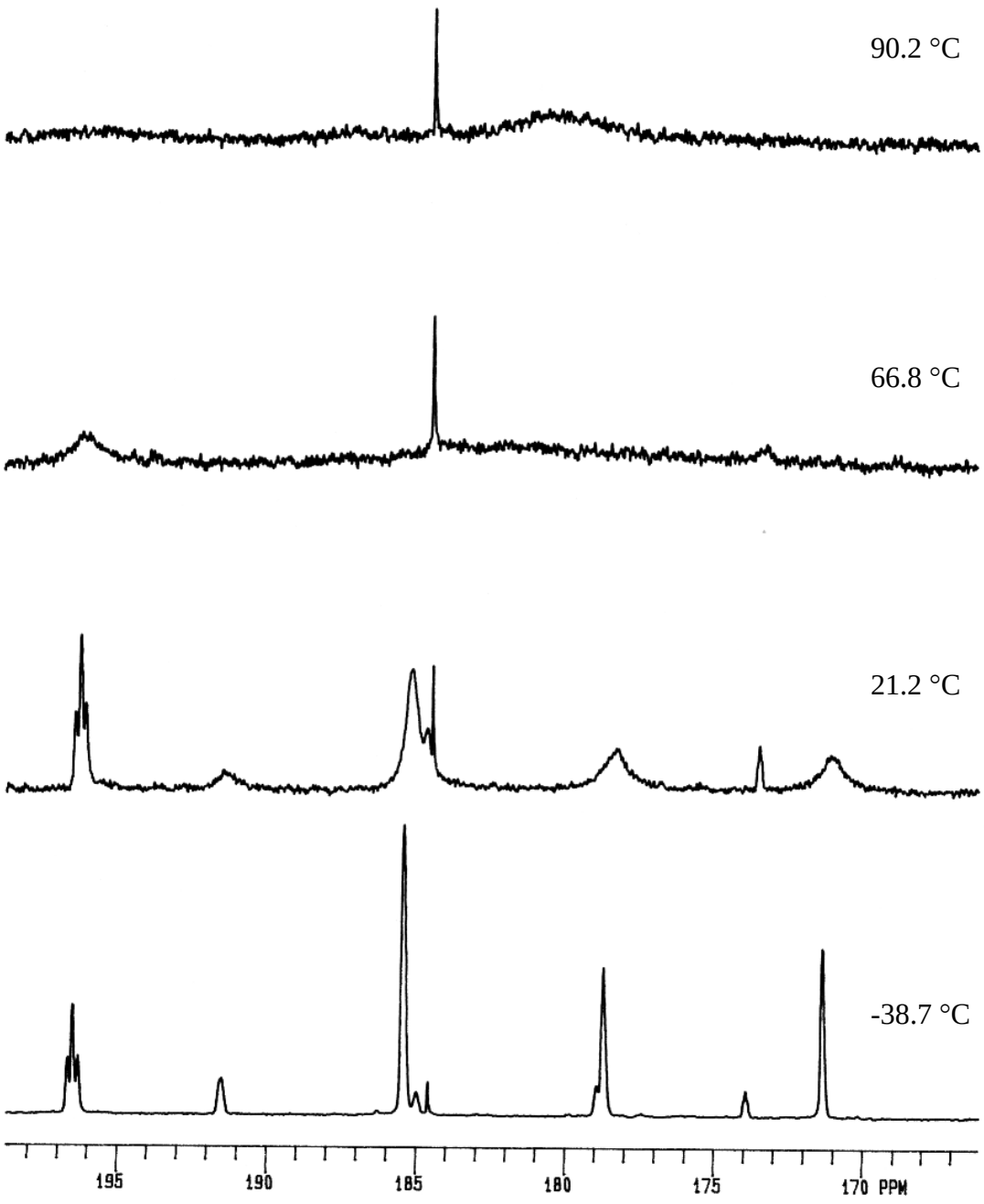

Figure 3.2. VT $^{13}C\{^{1}H\}$ NMR (50 MHz) of ^{13}CO-enriched mixture of 1,1-$Os_3(CO)_{10}$(cDPPEn) and 1,2-$Os_3(CO)_{10}$(cDPPEn) at equilibrium (after at least 5 half-lifes at 100 °C) recorded in toluene-d_8.

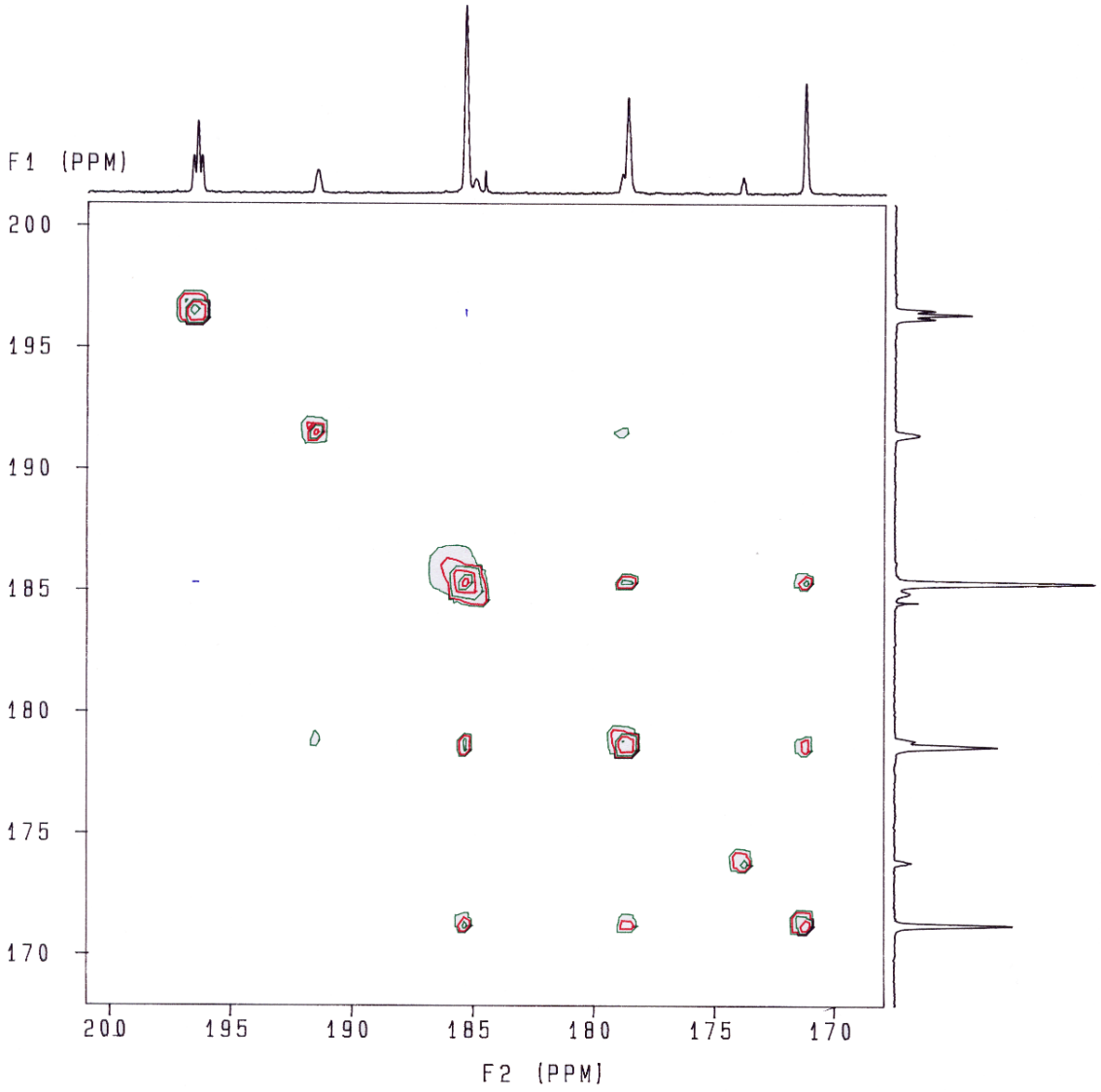

Figure 3.3. Contour map of the two-dimensional phase-sensitive $^{13}C\{^{1}H\}$ EXSY NMR (50 MHz) spectrum of ^{13}CO-enriched mixture of 1,1-$Os_3(CO)_{10}$(cDPPEn) and 1,2-$Os_3(CO)_{10}$(cDPPEn) at equilibrium (after at least 5 half-lifes at 100 °C) recorded in toluene-d_8 at –38.7 °C (t_m= 0.70 s).

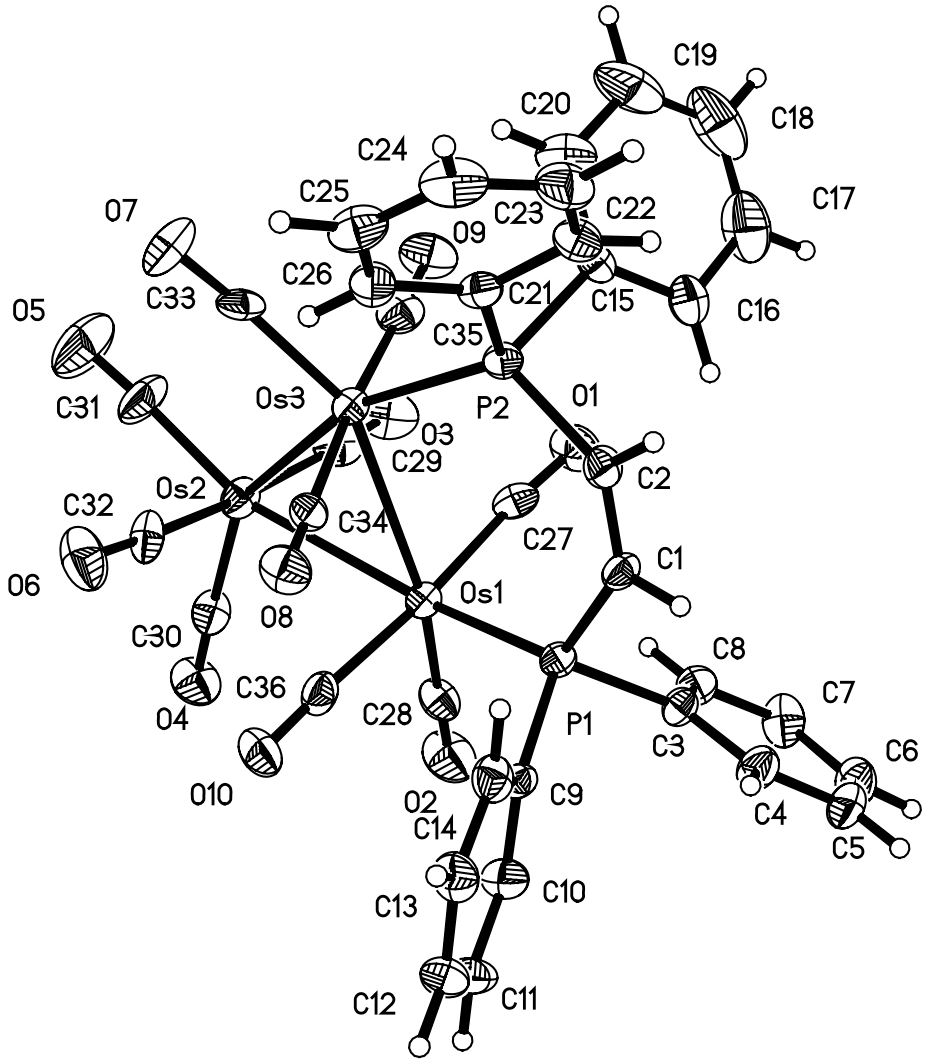

Figure 3.4. ORTEP diagram of 1,2-$Os_3(CO)_{10}$(cDPPEn) showing the thermal ellipsoids at the 50% probability level. (Reprinted with permission from *Organometallics* **2005**, 24, 5431-5439. Copyright 2005 American Chemical Society.)

Table 3.1. Crystal Data and Structure Refinement for 1,2-$Os_3(CO)_{10}$(cDPPEn)·CH_2Cl_2

Empirical formula	$Os_3C_{36}H_{22}O_{10}P_2 \cdot CH_2Cl_2$	
Formula weight	1332.00	
Temperature	297(2) K	
Wavelength	0.71073 Å	
Crystal system	Monoclinic	
Space group	P2(1)	
Unit cell dimensions	a = 12.715(3) Å	α = 90°
	b = 10.606(2) Å	β = 99.982(4)°
	c = 15.128(3) Å	γ = 90°
Volume	2009.2(8) $Å^3$	
Z	2	
Density (calculated)	2.202 Mg/m^3	
Absorption coefficient	9.729 mm^{-1}	
F(000)	1236	
Crystal size	0.43 x 0.18 x 0.17 mm^3	
Theta range for data collection	1.37 to 28.34°	
Index ranges	$-16 \le h \le 16$, $-14 \le k \le 13$, $-20 \le l \le 19$	
Reflections collected	16299	
Independent reflections	8518 [R(int) = 0.0670]	
Completeness to theta = 28.34°	91.0%	
Absorption correction	Empirical	
Max. and min. transmission	0.8112 and 0.2635	
Refinement method	Full-matrix least-squares on F^2	
Data / restraints / parameters	8518 / 1 / 488	
Goodness-of-fit on F^2	0.965	
Final R indices [I > 2sigma(I)]	R1 = 0.0342, wR2 = 0.0685	
R indices (all data)	R1 = 0.0412, wR2 = 0.0708	
Absolute structure parameter	-0.004(8)	
Extinction coefficient	0.00000(6)	
Largest diff. peak and hole	1.473 and -1.797 e. $Å^{-3}$	

Table 3.2. Bond Lengths [Å] and Angles [°] for 1,2-$Os_3(CO)_{10}$(cDPPEn)·CH_2Cl_2[a]

Bond Distances			
Os(1)-C(28)	1.874(11)	O(7)-C(33)	1.149(11)
Os(1)-C(27)	1.930(10)	O(8)-C(34)	1.157(10)
Os(1)-C(36)	1.962(10)	O(9)-C(35)	1.152(12)
Os(1)-P(1)	2.307(2)	O(10)-C(36)	1.122(11)
Os(1)-Os(2)	2.8642(6)	C(1)-C(2)	1.317(12)
Os(1)-Os(3)	2.8734(7)	C(3)-C(4)	1.393(12)
Os(2)-C(30)	1.892(10)	C(3)-C(8)	1.394(12)
Os(2)-C(31)	1.898(10)	C(4)-C(5)	1.386(13)
Os(2)-C(32)	1.929(9)	C(5)-C(6)	1.357(15)
Os(2)-C(29)	1.949(12)	C(6)-C(7)	1.376(15)
Os(2)-Os(3)	2.8774(6)	C(7)-C(8)	1.385(12)
Os(3)-C(33)	1.885(9)	C(9)-C(14)	1.373(12)
Os(3)-C(34)	1.912(9)	C(9)-C(10)	1.374(13)
Os(3)-C(35)	1.940(11)	C(10)-C(11)	1.383(14)
Os(3)-P(2)	2.314(2)	C(11)-C(12)	1.361(15)
Cl(1)-C(37)	1.714(17)	C(12)-C(13)	1.366(15)
Cl(2)-C(37)	1.726(18)	C(13)-C(14)	1.372(13)
P(1)-C(3)	1.822(8)	C(15)-C(20)	1.358(14)
P(1)-C(1)	1.826(8)	C(15)-C(16)	1.399(12)
P(1)-C(9)	1.829(8)	C(16)-C(17)	1.395(17)
P(2)-C(2)	1.826(9)	C(17)-C(18)	1.36(2)
P(2)-C(21)	1.838(9)	C(18)-C(19)	1.34(2)
P(2)-C(15)	1.841(8)	C(19)-C(20)	1.394(17)
O(1)-C(27)	1.160(11)	C(21)-C(26)	1.375(12)
O(2)-C(28)	1.154(12)	C(21)-C(22)	1.411(12)
O(3)-C(29)	1.146(12)	C(22)-C(23)	1.390(13)
O(4)-C(30)	1.141(11)	C(23)-C(24)	1.354(15)
O(5)-C(31)	1.139(12)	C(24)-C(25)	1.333(15)
O(6)-C(32)	1.139(11)	C(25)-C(26)	1.398(12)

Table 3.2. Con′t.

Bond Angles			
C(28)-Os(1)-C(27)	95.0(4)	C(2)-P(2)-C(21)	96.8(4)
C(28)-Os(1)-C(36)	90.0(4)	C(2)-P(2)-C(15)	100.8(4)
C(27)-Os(1)-C(36)	174.5(4)	C(21)-P(2)-C(15)	101.4(4)
C(28)-Os(1)-P(1)	98.4(3)	C(2)-P(2)-Os(3)	121.7(3)
C(27)-Os(1)-P(1)	91.9(3)	C(21)-P(2)-Os(3)	117.4(3)
C(36)-Os(1)-P(1)	89.6(2)	C(15)-P(2)-Os(3)	115.1(3)
C(28)-Os(1)-Os(2)	100.3(3)	C(2)-C(1)-P(1)	134.2(6)
C(27)-Os(1)-Os(2)	93.8(3)	C(1)-C(2)-P(2)	134.0(6)
C(36)-Os(1)-Os(2)	83.0(2)	C(4)-C(3)-C(8)	117.8(7)
P(1)-Os(1)-Os(2)	159.83(5)	C(4)-C(3)-P(1)	120.6(6)
C(28)-Os(1)-Os(3)	159.3(3)	C(8)-C(3)-P(1)	121.6(6)
C(27)-Os(1)-Os(3)	80.4(3)	C(5)-C(4)-C(3)	120.1(9)
C(36)-Os(1)-Os(3)	94.1(3)	C(6)-C(5)-C(4)	121.1(10)
P(1)-Os(1)-Os(3)	101.88(6)	C(5)-C(6)-C(7)	120.3(9)
Os(2)-Os(1)-Os(3)	60.198(14)	C(6)-C(7)-C(8)	119.3(9)
C(30)-Os(2)-C(31)	103.6(5)	C(7)-C(8)-C(3)	121.4(9)
C(30)-Os(2)-C(32)	96.1(4)	C(14)-C(9)-C(10)	117.9(8)
C(31)-Os(2)-C(32)	89.6(5)	C(14)-C(9)-P(1)	123.0(7)
C(30)-Os(2)-C(29)	92.5(4)	C(10)-C(9)-P(1)	118.9(7)
C(31)-Os(2)-C(29)	90.6(5)	C(9)-C(10)-C(11)	121.1(10)
C(32)-Os(2)-C(29)	171.1(4)	C(12)-C(11)-C(10)	119.7(10)
C(30)-Os(2)-Os(1)	90.9(3)	C(11)-C(12)-C(13)	120.0(9)
C(31)-Os(2)-Os(1)	164.1(4)	C(12)-C(13)-C(14)	120.0(9)
C(32)-Os(2)-Os(1)	95.3(3)	C(13)-C(14)-C(9)	121.3(9)
C(29)-Os(2)-Os(1)	82.3(3)	C(20)-C(15)-C(16)	119.7(9)
C(30)-Os(2)-Os(3)	149.1(3)	C(20)-C(15)-P(2)	119.5(8)
C(31)-Os(2)-Os(3)	106.5(4)	C(16)-C(15)-P(2)	120.5(8)
C(32)-Os(2)-Os(3)	77.7(3)	C(17)-C(16)-C(15)	117.8(12)
C(29)-Os(2)-Os(3)	93.7(3)	C(18)-C(17)-C(16)	122.2(13)

Table 3.2. Con′t.

Os(1)-Os(2)-Os(3)	60.060(15)	C(19)-C(18)-C(17)	118.9(13)
C(33)-Os(3)-C(34)	93.8(4)	C(18)-C(19)-C(20)	121.4(16)
C(33)-Os(3)-C(35)	91.1(4)	C(15)-C(20)-C(19)	120.0(12)
C(34)-Os(3)-C(35)	175.1(4)	C(26)-C(21)-C(22)	118.0(8)
C(33)-Os(3)-P(2)	104.9(2)	C(26)-C(21)-P(2)	123.1(7)
C(34)-Os(3)-P(2)	88.2(2)	C(22)-C(21)-P(2)	118.9(6)
C(35)-Os(3)-P(2)	90.4(3)	C(23)-C(22)-C(21)	119.5(9)
C(33)-Os(3)-Os(1)	153.5(2)	C(24)-C(23)-C(22)	120.9(9)
C(34)-Os(3)-Os(1)	78.6(3)	C(25)-C(24)-C(23)	120.2(9)
C(35)-Os(3)-Os(1)	97.0(3)	C(24)-C(25)-C(26)	121.3(10)
P(2)-Os(3)-Os(1)	100.27(6)	C(21)-C(26)-C(25)	120.0(9)
C(33)-Os(3)-Os(2)	96.8(2)	O(1)-C(27)-Os(1)	174.8(8)
C(34)-Os(3)-Os(2)	97.6(2)	O(2)-C(28)-Os(1)	178.5(9)
C(35)-Os(3)-Os(2)	81.9(3)	O(3)-C(29)-Os(2)	175.1(9)
P(2)-Os(3)-Os(2)	157.10(5)	O(4)-C(30)-Os(2)	177.4(9)
Os(1)-Os(3)-Os(2)	59.743(14)	O(5)-C(31)-Os(2)	175.6(12)
C(3)-P(1)-C(1)	98.8(4)	O(6)-C(32)-Os(2)	175.6(8)
C(3)-P(1)-C(9)	101.6(4)	O(7)-C(33)-Os(3)	175.4(8)
C(1)-P(1)-C(9)	100.7(4)	O(8)-C(34)-Os(3)	171.9(8)
C(3)-P(1)-Os(1)	117.6(3)	O(9)-C(35)-Os(3)	175.8(9)
C(1)-P(1)-Os(1)	122.1(3)	O(10)-C(36)-Os(1)	176.7(9)
C(9)-P(1)-Os(1)	112.8(2)	Cl(1)-C(37)-Cl(2)	115.3(10)

[a]Numbers in parentheses are estimated standard deviations in the least significant digits.

terminal carbonyl groups may be considered as linear with standard distances. The observed distortion or twisting of the axial CO groups in 1,2-$Os_3(CO)_{10}$(cDPPEn) from idealized D_{3h} to D_3 symmetry, relative to $Os_3(CO)_{12}$, is a feature commonly found in many structurally characterized phosphine-substituted triosmium and triruthenium clusters,[6] as supported by molecular mechanics calculations.[7] The P(1)-Os(1) [2.307(2) Å] and P(2)-Os(3) [2.314(2) Å] distances are in excellent agreement with the average lengths reported for those in a variety of phosphine-substituted osmium compounds.[1,3, 8] Coordination of the diphosphine ligand across the Os(1)-Os(3) bond in 1,2-$Os_3(CO)_{10}$(cDPPEn) leads to a significant stretching of the cDPPEn ligand that causes ground-state destabilization relative to the chelating isomer 1,1-$Os_3(CO)_{10}$(cDPPEn). The internuclear P(1)···P(2) distance of 3.863(4) Å found for 1,2-$Os_3(CO)_{10}$(cDPPEn) is ca. 0.58 Å longer than the corresponding distance reported for the free ligand cDPPEn, while the P(1)-C(1)-C(2) and P(2)-C(2)-C(1) bond angles of 134.2(6)° and 134.0(6)°, respectively, associated with the unsaturated backbone of the diphosphine ligand are ca. 11° larger as compared to the analogous linkages in cDPPEn.[9] Additional evidence supporting the unfavorable bridging mode of coordination of the unsaturated phosphine to the metal frame in 1,2-$Os_3(CO)_{10}$(cDPPEn) is seen in the C(1)-P(1)-Os(1) [122.1(3)°] and C(2)-P(2)-Os(2) [121.7(3)°] bond angles that exhibit a substantial deviation from the anticipated bond angle of ca. 109° expected for a tetracoordinate phosphorus center.

E. X-Ray Diffraction Structure of 1,1-$Os_3(CO)_{10}$(cDPPEn)

Single crystals of 1,1-$Os_3(CO)_{10}$(cDPPEn) were grown from a CH_2Cl_2 solution containing the equilibrated mixture (7:1 ratio) of 1,1-$Os_3(CO)_{10}$(cDPPEn) and 1,2-

$Os_3(CO)_{10}$(cDPPEn) that had been layered with hexane. The molecular structure of 1,1-$Os_3(CO)_{10}$(cDPPEn) was determined by X-ray diffraction analysis. 1,1-$Os_3(CO)_{10}$(cDPPEn) exists as discrete molecules in the unit cell with no unusually short inter- or intramolecular contacts. The X-ray data processing and collection parameters are listed in Table 3.3, and selected bond distances and angles given in Table 3.4. The molecular composition and the numbering scheme of 1,1-$Os_3(CO)_{10}$(cDPPEn) are presented in the ORTEP diagram shown in Figure 3.5.

The molecular structure of 1,1-$Os_3(CO)_{10}$(cDPPEn) confirms the attendant migration of the diphosphine ligand upon heating cluster 1,2-$Os_3(CO)_{10}$(cDPPEn). The mean Os-Os and Os-P bond lengths of 2.9139 Å and 2.296 Å, respectively, and are unremarkable with respect to those bond distances in 1,2-$Os_3(CO)_{10}$(cDPPEn) and other phosphine-substituted osmium clusters.[3] The ten ancillary carbonyls are all linear in nature and display a slight twist or canting of the axial CO groups, albeit much less pronounced than the twist observed in 1,2-$Os_3(CO)_{10}$(cDPPEn). The internuclear non-bonding P(1)···P(2) distance of 3.092(6) Å in 1,1-$Os_3(CO)_{10}$(cDPPEn) is nearly 0.77 Å shorter than the internuclear P(1)···P(2) separation in 1,2-$Os_3(CO)_{10}$(cDPPEn), in keeping with the trend reported for the free ligand (*vide supra*) and other mono- and polynuclear compounds containing a chelating cDPPEn ligand.[10] Consistent with the premise concerning the greater stability for chelation of the cDPPEn ligand in the 1,1-$Os_3(CO)_{10}$(cDPPEn) cluster vis-á-vis the 1,2-$Os_3(CO)_{10}$(cDPPEn) cluster are the bond angles of 109.0(3)°, 107.8(3)°, 120.2(6)°, 118.1(6)° found for the Os(1)-P(1)-C(1), Os(1)-P(2)-C(2), P(1)-C(1)-C(2), and P(2)-C(2)-C(1) linkages, respectively. These values show

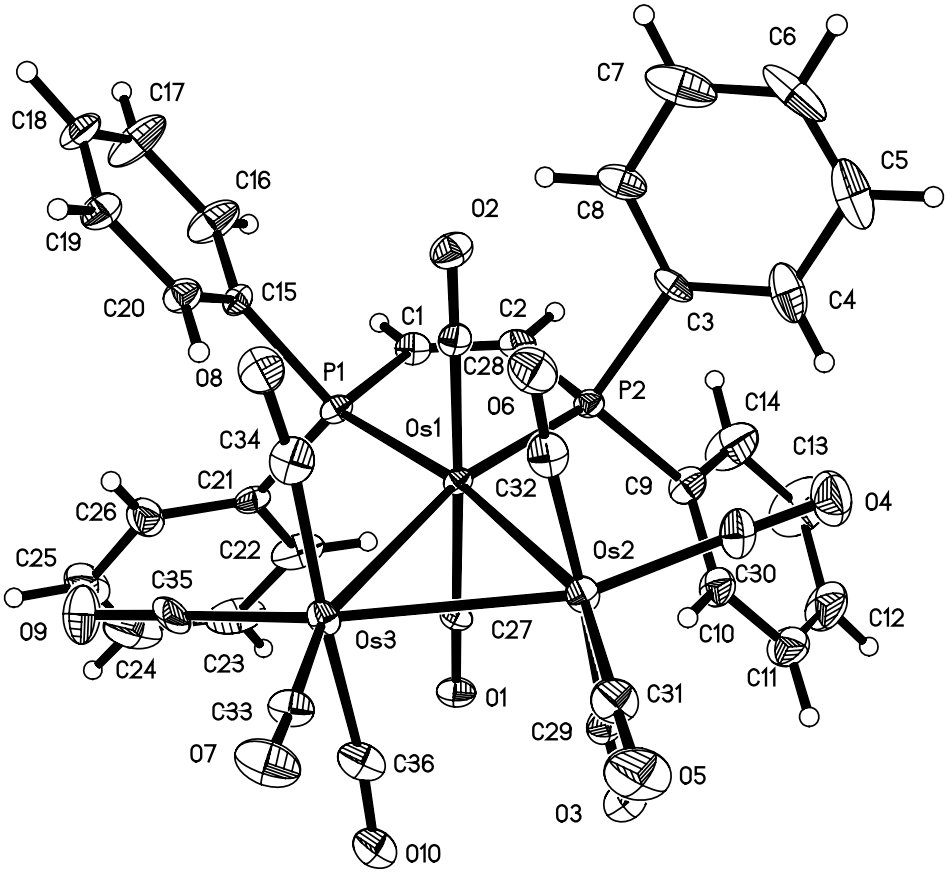

Figure 3.5. ORTEP diagram of 1,1-$Os_3(CO)_{10}$(cDPPEn) showing the thermal ellipsoids at the 50% probability level. (Reprinted with permission from *Organometallics* **2005**, 24, 5431-5439. Copyright 2005 American Chemical Society.)

Table 3.3. Crystal Data and Structure Refinement for 1,1-$Os_3(CO)_{10}$(cDPPEn)

Empirical formula	$C_{36}H_{22}O_{10}Os_3P_2$	
Formula weight	1247.08	
Temperature	213(2) K	
Wavelength	0.71073 Å	
Crystal system	Monoclinic	
Space group	P2(1)/n	
Unit cell dimensions	a = 10.444(1) Å	α= 90°
	b = 24.115(3) Å	β= 100.940(2)°
	c = 14.370(2) Å	γ = 90°
Volume	3553.6(9) $Å^3$	
Z	4	
Density (calculated)	2.331 Mg/m^3	
Absorption coefficient	10.848 mm^{-1}	
F(000)	2304	
Crystal size	0.31 x 0.14 x 0.12 mm^3	
Theta range for data collection	1.67 to 28.30°	
Index ranges	$-13 \le h \le 13$, $-32 \le k \le 31$, $-19 \le l \le 18$	
Reflections collected	29748	
Independent reflections	8180 [R(int) = 0.0872]	
Completeness to theta = 28.30°	92.6%	
Absorption correction	Empirical	
Max. and min. transmission	0.8804 and 0.2609	
Refinement method	Full-matrix least-squares on F^2	
Data / restraints / parameters	8180 / 0 / 461	
Goodness-of-fit on F^2	0.921	
Final R indices [I > 2sigma(I)]	R1 = 0.0448, wR2 = 0.0585	
R indices (all data)	R1 = 0.0869, wR2 = 0.0658	
Extinction coefficient	0.000177(11)	
Largest diff. peak and hole	1.508 and -1.178 e. $Å^{-3}$	

Table 3.4. Bond Lengths [Å] and Angles [°] for 1,1-$Os_3(CO)_{10}$(cDPPEn)[a]

Bond Distances			
Os(1)-C(27)	1.925(8)	O(8)-C(34)	1.142(8)
Os(1)-C(28)	1.942(8)	O(9)-C(35)	1.143(9)
Os(1)-P(1)	2.293(2)	O(10)-C(36)	1.155(8)
Os(1)-P(2)	2.299(2)	C(1)-C(2)	1.322(9)
Os(1)-Os(2)	2.9218(5)	C(3)-C(4)	1.381(10)
Os(1)-Os(3)	2.9286(5)	C(3)-C(8)	1.386(10)
Os(2)-C(31)	1.881(9)	C(4)-C(5)	1.424(13)
Os(2)-C(30)	1.899(9)	C(5)-C(6)	1.367(14)
Os(2)-C(32)	1.942(9)	C(6)-C(7)	1.345(14)
Os(2)-C(29)	1.956(10)	C(7)-C(8)	1.371(12)
Os(2)-Os(3)	2.8914(5)	C(9)-C(10)	1.371(11)
Os(3)-C(33)	1.887(8)	C(9)-C(14)	1.378(11)
Os(3)-C(35)	1.908(9)	C(10)-C(11)	1.381(9)
Os(3)-C(36)	1.932(9)	C(11)-C(12)	1.359(13)
Os(3)-C(34)	1.951(9)	C(12)-C(13)	1.383(14)
P(1)-C(1)	1.811(8)	C(13)-C(14)	1.392(11)
P(1)-C(15)	1.832(7)	C(15)-C(20)	1.362(10)
P(1)-C(21)	1.839(8)	C(15)-C(16)	1.380(10)
P(2)-C(2)	1.816(8)	C(16)-C(17)	1.377(10)
P(2)-C(9)	1.827(7)	C(17)-C(18)	1.371(12)
P(2)-C(3)	1.827(8)	C(18)-C(19)	1.364(11)
O(1)-C(27)	1.148(8)	C(19)-C(20)	1.376(9)
O(2)-C(28)	1.132(7)	C(21)-C(26)	1.374(10)
O(3)-C(29)	1.136(9)	C(21)-C(22)	1.401(10)
O(4)-C(30)	1.151(9)	C(22)-C(23)	1.409(13)
O(5)-C(31)	1.160(9)	C(23)-C(24)	1.374(13)

Table 3.4. Con′t.

O(6)-C(32)	1.150(8)	C(24)-C(25)	1.350(14)
O(7)-C(33)	1.161(9)	C(25)-C(26)	1.376(11)
	Bond Angles		
C(27)-Os(1)-C(28)	177.5(3)	C(2)-P(2)-C(9)	101.1(4)
C(27)-Os(1)-P(1)	88.5(2)	C(2)-P(2)-C(3)	100.6(4)
C(28)-Os(1)-P(1)	91.7(2)	C(9)-P(2)-C(3)	102.1(4)
C(27)-Os(1)-P(2)	92.8(2)	C(2)-P(2)-Os(1)	107.8(3)
C(28)-Os(1)-P(2)	89.7(2)	C(9)-P(2)-Os(1)	122.3(3)
P(1)-Os(1)-P(2)	84.66(7)	C(3)-P(2)-Os(1)	119.5(2)
C(27)-Os(1)-Os(2)	92.9(2)	C(2)-C(1)-P(1)	118.1(6)
C(28)-Os(1)-Os(2)	86.4(2)	C(1)-C(2)-P(2)	120.2(6)
P(1)-Os(1)-Os(2)	167.54(5)	C(4)-C(3)-C(8)	118.7(8)
P(2)-Os(1)-Os(2)	107.62(5)	C(4)-C(3)-P(2)	122.8(7)
C(27)-Os(1)-Os(3)	85.2(2)	C(8)-C(3)-P(2)	118.4(6)
C(28)-Os(1)-Os(3)	92.4(2)	C(3)-C(4)-C(5)	120.0(10)
P(1)-Os(1)-Os(3)	108.61(5)	C(6)-C(5)-C(4)	117.4(10)
P(2)-Os(1)-Os(3)	166.48(5)	C(7)-C(6)-C(5)	123.5(11)
Os(2)-Os(1)-Os(3)	59.236(13)	C(6)-C(7)-C(8)	118.7(11)
C(31)-Os(2)-C(30)	102.4(4)	C(7)-C(8)-C(3)	121.6(10)
C(31)-Os(2)-C(32)	90.5(3)	C(10)-C(9)-C(14)	118.3(7)
C(30)-Os(2)-C(32)	91.7(3)	C(10)-C(9)-P(2)	120.8(6)
C(31)-Os(2)-C(29)	91.2(4)	C(14)-C(9)-P(2)	120.9(7)
C(30)-Os(2)-C(29)	91.0(3)	C(9)-C(10)-C(11)	121.3(8)
C(32)-Os(2)-C(29)	176.4(3)	C(12)-C(11)-C(10)	120.6(9)
C(31)-Os(2)-Os(3)	99.3(3)	C(11)-C(12)-C(13)	119.2(9)
C(30)-Os(2)-Os(3)	158.1(2)	C(12)-C(13)-C(14)	119.9(10)
C(32)-Os(2)-Os(3)	84.9(2)	C(9)-C(14)-C(13)	120.6(9)
C(29)-Os(2)-Os(3)	91.7(2)	C(20)-C(15)-C(16)	118.3(7)
C(31)-Os(2)-Os(1)	159.5(3)	C(20)-C(15)-P(1)	120.3(6)
C(30)-Os(2)-Os(1)	98.0(2)	C(16)-C(15)-P(1)	121.4(6)
C(32)-Os(2)-Os(1)	90.7(2)	C(17)-C(16)-C(15)	120.3(8)

Table 3.4. Con′t.

C(29)-Os(2)-Os(1)	86.5(2)	C(18)-C(17)-C(16)	120.9(9)
Os(3)-Os(2)-Os(1)	60.499(12)	C(19)-C(18)-C(17)	118.7(8)
C(33)-Os(3)-C(35)	102.0(3)	C(18)-C(19)-C(20)	120.4(8)
C(33)-Os(3)-C(36)	91.4(3)	C(15)-C(20)-C(19)	121.4(8)
C(35)-Os(3)-C(36)	90.4(3)	C(26)-C(21)-C(22)	119.4(8)
C(33)-Os(3)-C(34)	91.5(3)	C(26)-C(21)-P(1)	120.8(6)
C(35)-Os(3)-C(34)	91.1(3)	C(22)-C(21)-P(1)	119.8(7)
C(36)-Os(3)-C(34)	176.3(3)	C(21)-C(22)-C(23)	118.4(9)
C(33)-Os(3)-Os(2)	96.6(2)	C(24)-C(23)-C(22)	120.2(10)
C(35)-Os(3)-Os(2)	161.1(2)	C(25)-C(24)-C(23)	120.5(10)
C(36)-Os(3)-Os(2)	85.3(2)	C(24)-C(25)-C(26)	120.5(11)
C(34)-Os(3)-Os(2)	92.2(2)	C(21)-C(26)-C(25)	120.9(9)
C(33)-Os(3)-Os(1)	156.3(2)	O(1)-C(27)-Os(1)	177.4(6)
C(35)-Os(3)-Os(1)	101.5(2)	O(2)-C(28)-Os(1)	176.6(7)
C(36)-Os(3)-Os(1)	91.6(2)	O(3)-C(29)-Os(2)	173.7(8)
C(34)-Os(3)-Os(1)	84.8(2)	O(4)-C(30)-Os(2)	178.6(8)
Os(2)-Os(3)-Os(1)	60.265(12)	O(5)-C(31)-Os(2)	178.2(8)
C(1)-P(1)-C(15)	102.5(4)	O(6)-C(32)-Os(2)	175.4(7)
C(1)-P(1)-C(21)	100.0(4)	O(7)-C(33)-Os(3)	176.8(7)
C(15)-P(1)-C(21)	101.5(3)	O(8)-C(34)-Os(3)	172.9(7)
C(1)-P(1)-Os(1)	109.0(3)	O(9)-C(35)-Os(3)	177.5(8)
C(15)-P(1)-Os(1)	120.6(3)	O(10)-C(36)-Os(3)	174.3(7)
C(21)-P(1)-Os(1)	120.1(2)		

[a]Numbers in parentheses are estimated standard deviations in the least significant digits.

minimal deviation from the idealized bond angles of 109° associated with an sp^3 hybridized central phosphorus atom and 120° associated with an sp^2 hybridized central carbon atom.

F. Synthesis and Spectroscopic Properties of $Os_3(CO)_{11}(\eta^1$-bpcd)

The reaction of an equimolar amount of $Os_3(CO)_{12}$ and Me_3NO in the presence of the unsaturated diphosphine ligand bpcd at ambient temperature leads to formation of $Os_3(CO)_{11}(\eta^1$-bpcd) as the predominant product. Attempts to purify $Os_3(CO)_{11}(\eta^1$-bpcd) by column chromatography gave a mixture of 80% of η^1-$Os_3(CO)_{11}$(bpcd), 20% of 1,2-$Os_3(CO)_{10}$(bpcd), and another unknown species, all of which possess identical R_f values. Recrystallization of the chromatographed mixture from CH_2Cl_2/hexanes afforded pure $Os_3(CO)_{11}(\eta^1$-bpcd). The resulting cluster was characterized in solution by IR and NMR spectroscopies. Comparison of the IR stretching frequency pattern of carbonyl ligands of $Os_3(CO)_{11}(\eta^1$-bpcd) with known monosubstituted $Os_3(CO)_{11}P$ clusters indicates that $Os_3(CO)_{11}(\eta^1$-bpcd) contains one phosphine group coordinated at an equatorial position of the triosmium frame.[1] The IR spectrum of $Os_3(CO)_{11}(\eta^1$-bpcd) reveals that the stretching frequencies of the two carbonyl groups associated with the dione moiety exhibit a blue shift of ca. 7 and 9 cm^{-1} for the symmetric stretching and antisymmetric stretching modes, respectively (Figure 3.6). The ^1H NMR spectrum of $Os_3(CO)_{11}(\eta^1$-bpcd) (Figure 3.7) indicates that the resonance assigned to the methylene protons on the dione ring is shifted down-field by 0.24 ppm with respect to the free ligand. The ^{31}P NMR spectrum of $Os_3(CO)_{11}(\eta^1$-bpcd) (Figure 3.9) reveals the existence of two doublets

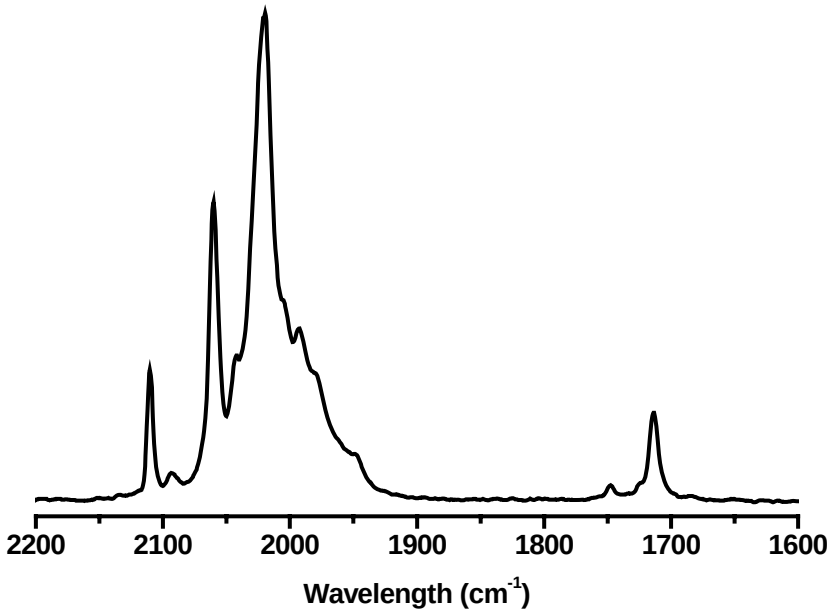

Figure 3.6. Infrared spectrum of the carbonyl region for $Os_3(CO)_{11}(\eta^1$-bpcd) in CH_2Cl_2.

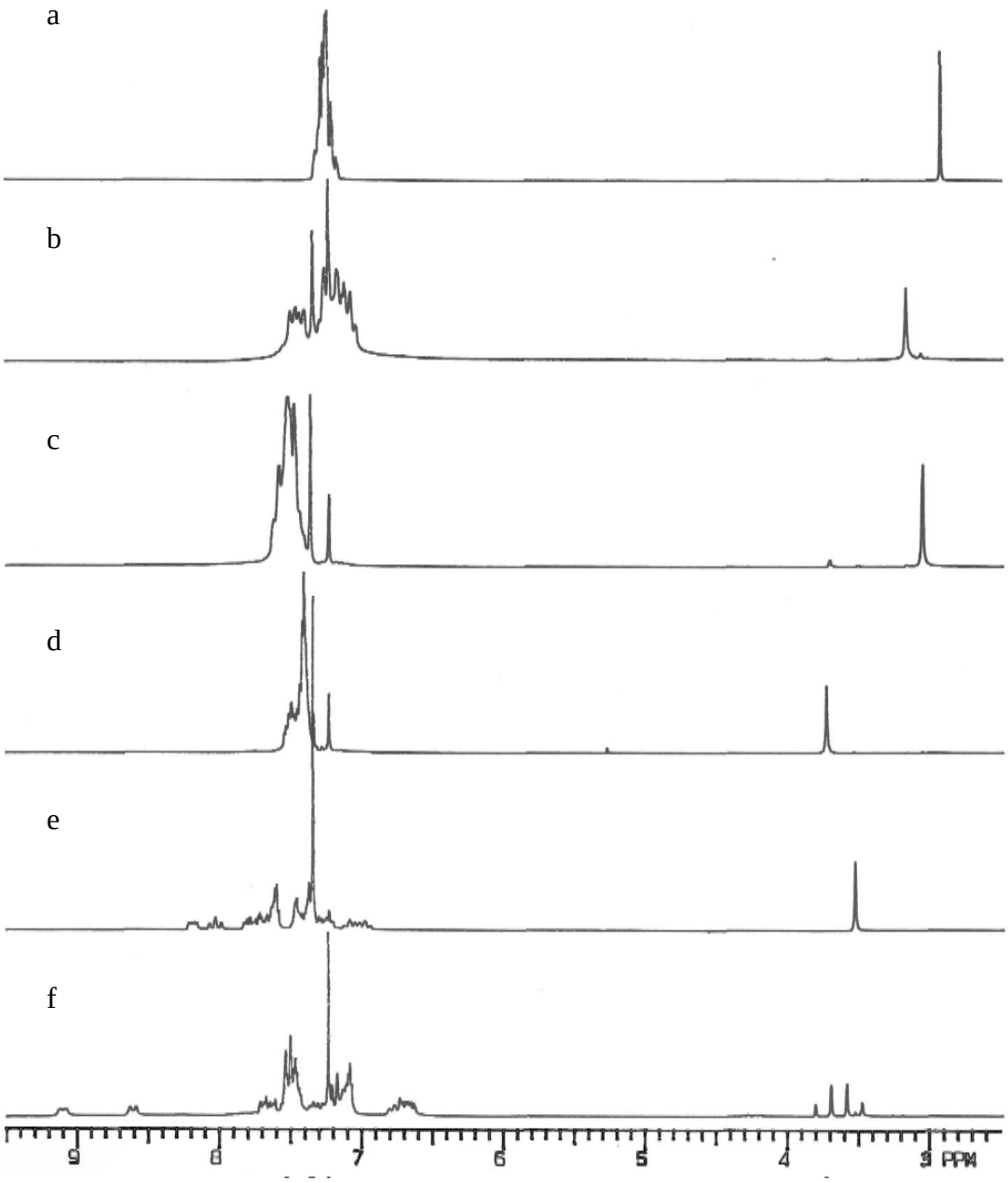

Figure 3.7. ^{1}H NMR spectra from δ 2.5—9.5 in $CDCl_3$: (a) free bpcd, (b) $Os_3(CO)_{11}(\eta^1$-bpcd), (c) 1,2-$Os_3(CO)_{10}$(bpcd), (d) 1,1-$Os_3(CO)_{10}$(bpcd), (e) $HOs_3(CO)_9[\mu$-$(PPh_2)C{=}C\{PPh(C_6H_4)\}C(O)CH_2C(O)]$, and (f) $HOs_3(CO)_8(\mu_3$-$C_6H_4)[\mu_2,\eta^1$-$PPhC{=}C(PPh_2)C(O)CH_2C(O)]$.

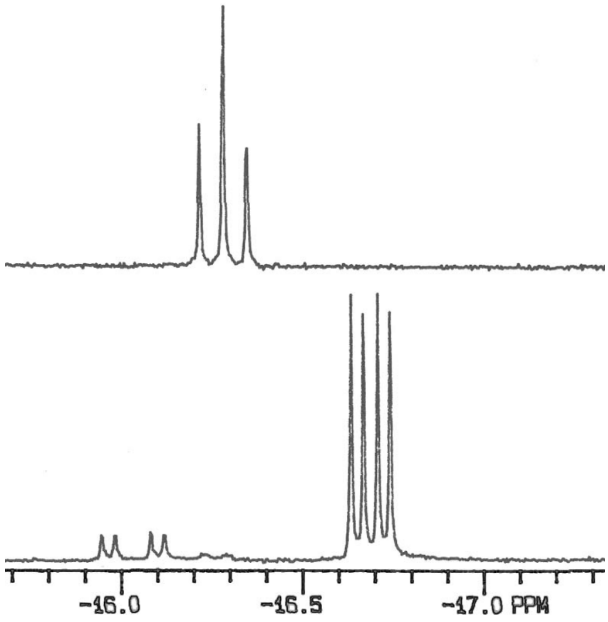

Figure 3.8. Hydride region of ^{1}H NMR spectra for $HOs_3(CO)_9[\mu$-$(PPh_2)C{=}C\{PPh(C_6H_4)\}C(O)CH_2C(O)]$ (top) and $HOs_3(CO)_8(\mu_3$-$C_6H_4)[\mu_2,\eta^1$-$PPhC{=}C(PPh_2)C(O)CH_2C(O)]$ (bottom) in $CDCl_3$.

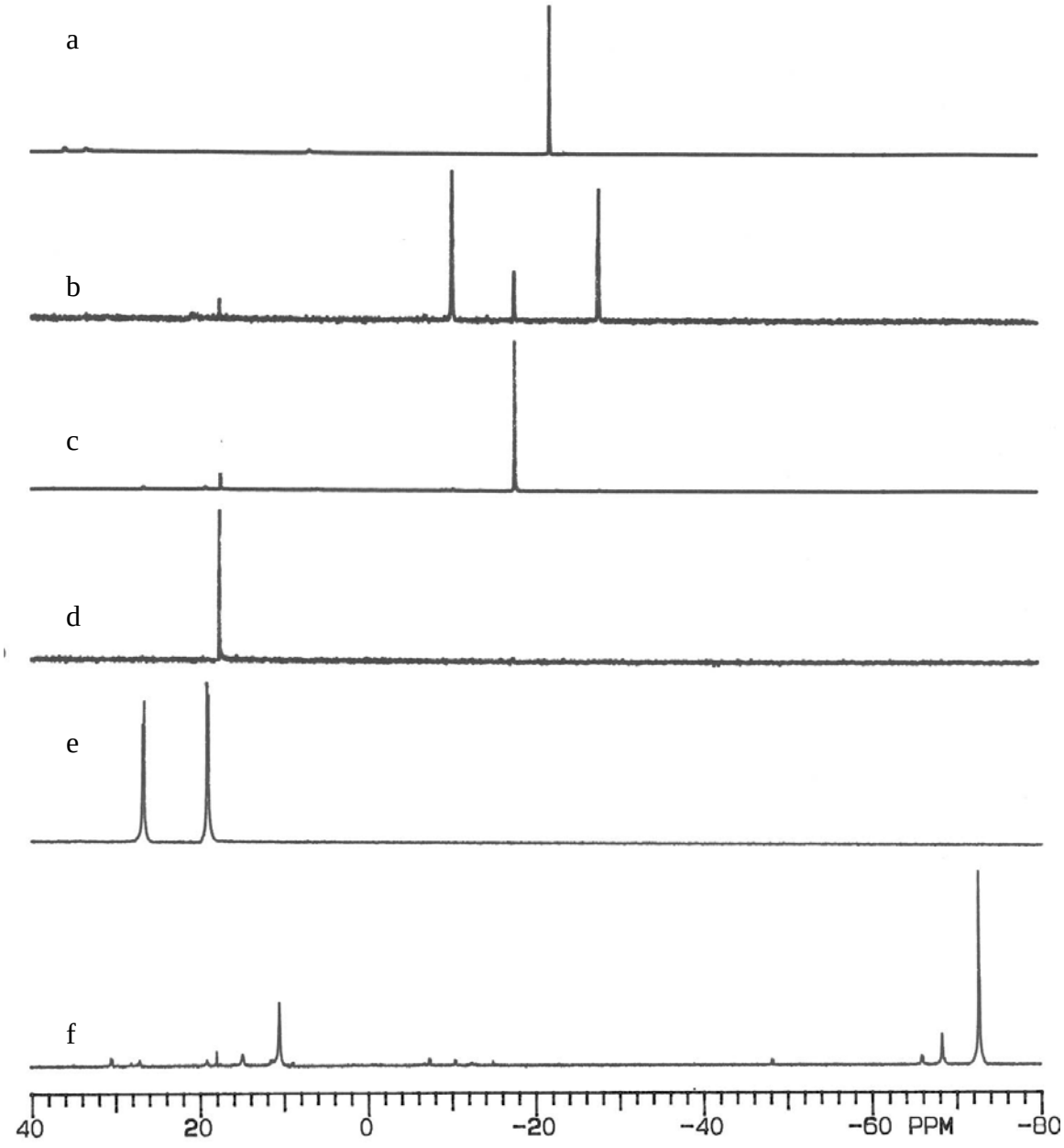

Figure 3.9. ^{31}P NMR in $CDCl_3$: (a) free bpcd, (b) $Os_3(CO)_{11}(\eta^1$-bpcd), (c) 1,2-$Os_3(CO)_{10}$(bpcd), (d) 1,1-$Os_3(CO)_{10}$(bpcd), (e) $HOs_3(CO)_9[\mu$-$(PPh_2)C{=}C\{PPh(C_6H_4)\}C(O)CH_2C(O)]$, and (f) $HOs_3(CO)_8(\mu_3$-$C_6H_4)[\mu_2,\eta^1$-$PPhC{=}C(PPh_2)C(O)CH_2C(O)]$.

having a J_{P-P} = 15 Hz. The up-field resonance at δ -27.86 is assigned to the dangling phosphorus atom, while the down-field resonance at δ -11.19, which is comparable to the previously reported ^{31}P chemical shifts for monophosphine-substituted triosmium carbonyl clusters, is assigned to the PPh_2 group attached to the osmium cluster. The two-dimensional ^{31}P-$^{31}P\{^1H\}$ COSY NMR spectrum (Figure 3.10) of $Os_3(CO)_{11}(\eta^1$-bpcd) verifies the coupling of these two phosphorus atoms in the cluster.

G. Synthesis and Spectroscopic Properties of 1,2-$Os_3(CO)_{10}$(bpcd)

The reaction of $Os_3(CO)_{10}(MeCN)_2$ with an equimolar amount of bpcd proceeds rapidly and without complications at room temperature to give a green product, 1,2-$Os_3(CO)_{10}$(bpcd), along with minor amounts of $Os_3(CO)_{11}(\eta^1$-bpcd). 1,2-$Os_3(CO)_{10}$(bpcd) was purified by chromatography over silica gel free from the minor product $Os_3(CO)_{11}(\eta^1$-bpcd) that decomposed on contact with silica gel. 1,2-$Os_3(CO)_{10}$(bpcd) was characterized in solution by IR and NMR spectroscopies. The pattern for the cabonyl stretching frequencies in 1,2-$Os_3(CO)_{10}$(bpcd) is similar to those of previously reported diphosphine-bridged clusters,[3] which suggests that the bpcd ligand spans two osmium atoms and coordinates by both phosphine moieties. The vibrational frequencies for the carbonyl groups of the bpcd ligand are blue shifted by 20 and 19 cm^{-1} for the symmetric stretching and antisymmetric stretching modes, respectively, upon coordination to the cluster (Figure 3.11). The ^1H NMR spectrum of 1,2-$Os_3(CO)_{10}$(bpcd) (Figure 3.7) reveals that the singlet assigned to the methylene protons of bpcd ligand is shifted down-field by 0.13 ppm upon coordination to the cluster. The ^{31}P NMR spectrum (Figure 3.9) of 1,2-$Os_3(CO)_{10}$(bpcd) shows a singlet at –17.55 ppm, that is 4.6 ppm down-field with respect

to the free bpcd ligand. Four types of carbonyl resonances were observed in the ^{13}C NMR spectrum of a ^{13}CO-enriched sample of 1,2-$Os_3(CO)_{10}$(bpcd) recorded at -61 °C. Here resonances were observed at δ 193.07, 184.78, 178.17 and 173.12 with an integral ratio of 4:2:2:2, fully consistent with the structure of 1,2-$Os_3(CO)_{10}$(bpcd). The results of VT ^{13}C NMR measurements on a ^{13}CO-enriched sample of 1,2-$Os_3(CO)_{10}$(bpcd) are shown in Figure 3.12, with the assignments for these resonances depicted below in Scheme 3.4.

The magnetic equivalence of the two phosphorus atoms and the two methylene protons in 1,2-$Os_3(CO)_{10}$(bpcd) indicates that the structure of 1,2-$Os_3(CO)_{10}$(bpcd) possesses C_{2v} symmetry in solution.

H. Synthesis and Spectroscopic Properties of 1,1-$Os_3(CO)_{10}$(bpcd)

1,2-$Os_3(CO)_{10}$(bpcd) slowly converts to the new cluster 1,1-$Os_3(CO)_{10}$(bpcd) in solution at ambient temperature. Gently heating 1,2-$Os_3(CO)_{10}$(bpcd) in solution in the

Scheme 3.4. ^{13}C NMR assignments of 1,2-$Os_3(CO)_{10}$(bpcd).

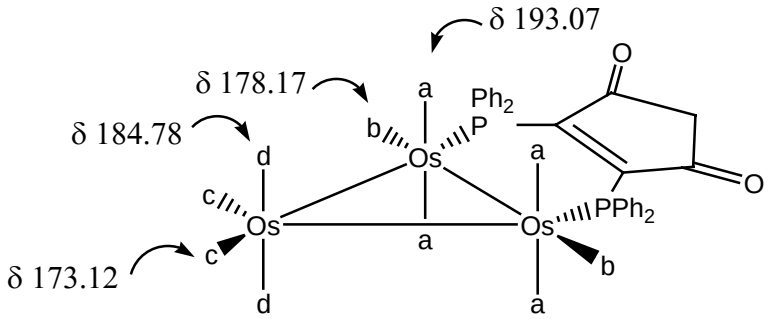

presence of CO leads to the formation of 1,1-$Os_3(CO)_{10}$(bpcd), which upon CO loss furnishes the hydride cluster $HOs_3(CO)_9[\mu\text{-}(PPh_2)C{=}C\{PPh(C_6H_4)\}C(O)CH_2C(O)]$

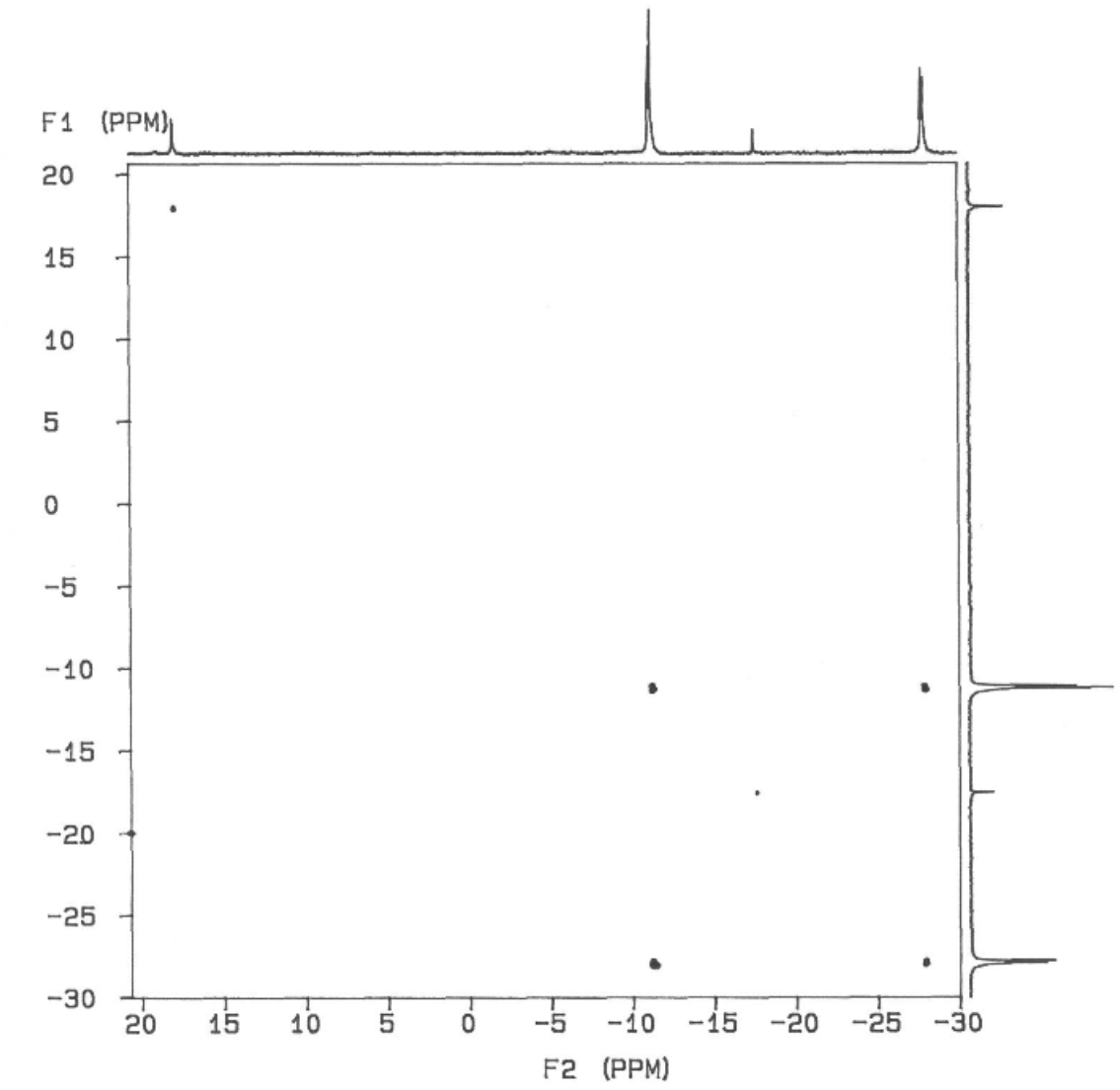

Figure 3.10. ^{31}P-$^{31}P\{^{1}H\}$ COSY NMR data for a mixture of $Os_3(CO)_{11}(\eta^1$-bpcd), 1,2-$Os_3(CO)_{10}$(bpcd) and 1,1-$Os_3(CO)_{10}$(bpcd) in $CDCl_3$.

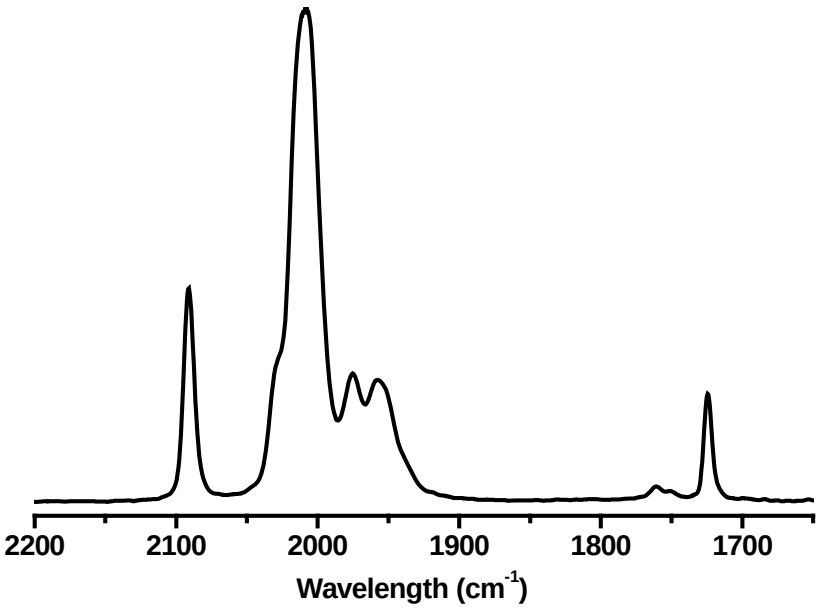

Figure 3.11. Infrared spectrum of the carbonyl region for 1,2-$Os_3(CO)_{10}$(bpcd) recorded in CH_2Cl_2.

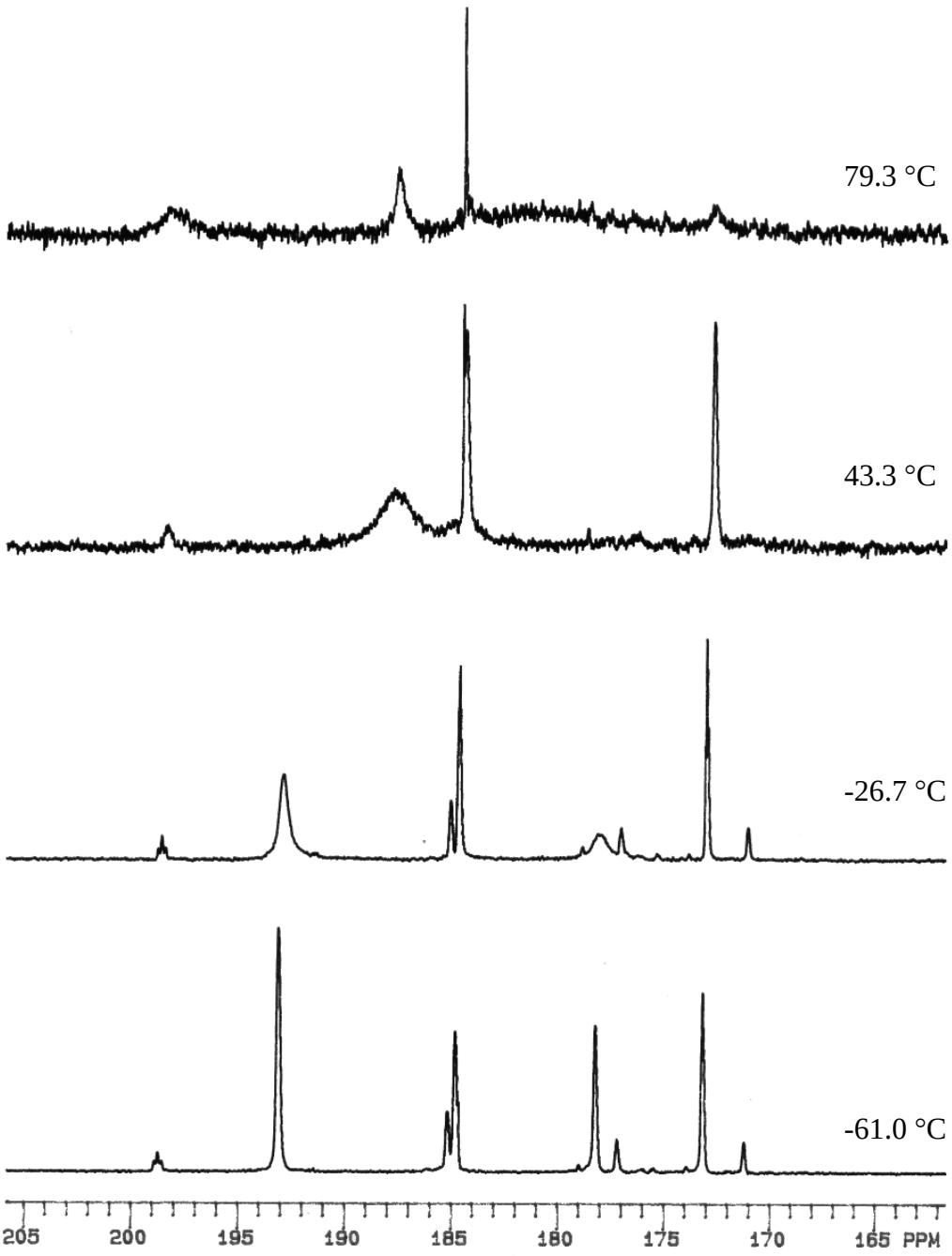

Figure 3.12. VT $^{13}C\{^{1}H\}$ NMR spectra (50 MHz) of ^{13}CO-enriched 1,2-$Os_3(CO)_{10}$(bpcd) recorded in C_7D_8.

through an orthometallation sequence. The role of the CO is to suppress the formation of the hydride cluster. Chromatographic separation and recrystallization of the 1,1-$Os_3(CO)_{10}$(bpcd) from CH_2Cl_2 afforded the chelating isomer as an orange-red, air-stable solid. Interestingly, TLC examination of parallel thermolysis reactions conducted in Schlenk vessels starting with 1,2-$Os_3(CO)_{10}$(bpcd) showed only a single spot for coexistent mixtures of 1,2-$Os_3(CO)_{10}$(bpcd) and 1,1-$Os_3(CO)_{10}$(bpcd). However, monitoring the thermolysis reaction of 1,2-$Os_3(CO)_{10}$(bpcd) by ^{1}H NMR (Figure 3.13) and ^{31}P NMR unambiguously confirms the isomerization from 1,2-$Os_3(CO)_{10}$(bpcd) to 1,1-$Os_3(CO)_{10}$(bpcd). The ^{1}H NMR spectrum of 1,1-$Os_3(CO)_{10}$(bpcd) shows a singlet at 3.74 ppm that is assigned to the two equivalent methylene protons of the bpcd ligand. This resonance is shifted down-field by 0.68 ppm and 0.81 ppm with respect to those of 1,2-$Os_3(CO)_{10}$(bpcd) and free bpcd ligand, respectively (Figure 3.7). Comparison of the ^{31}P NMR spectrum of 1,1-$Os_3(CO)_{10}$(bpcd) with that of 1,2-$Os_3(CO)_{10}$(bpcd) indicates a remarkable down-field shift of the ^{31}P resonance by 35.5 ppm relative to the latter cluster (Figure 3.9). Four types of carbonyl resonances were observed in the ^{13}C NMR spectrum of a ^{13}CO-enriched sample of 1,1-$Os_3(CO)_{10}$(bpcd) recorded at -15.4 °C. Terminal carbonyl resonances were found at δ 198.59, 185.03, 177.02, 171.02, with an integral ratio of 2:4:2:2, fully consistent with the structure of 1,1-$Os_3(CO)_{10}$(bpcd). The data from VT ^{13}C NMR (Figure 3.14) and 2D-EXSY ^{13}C NMR (Figure 3.15) studies on a ^{13}CO-enriched sample of 1,1-$Os_3(CO)_{10}$(bpcd) have allowed assignments of these resonances, as depicted in Scheme 3.5. The IR spectrum of 1,1-$Os_3(CO)_{10}$(bpcd) shows blue shifts for the two carbonyl groups on the dione ring by 8 and 12 cm^{-1} for symmetric and

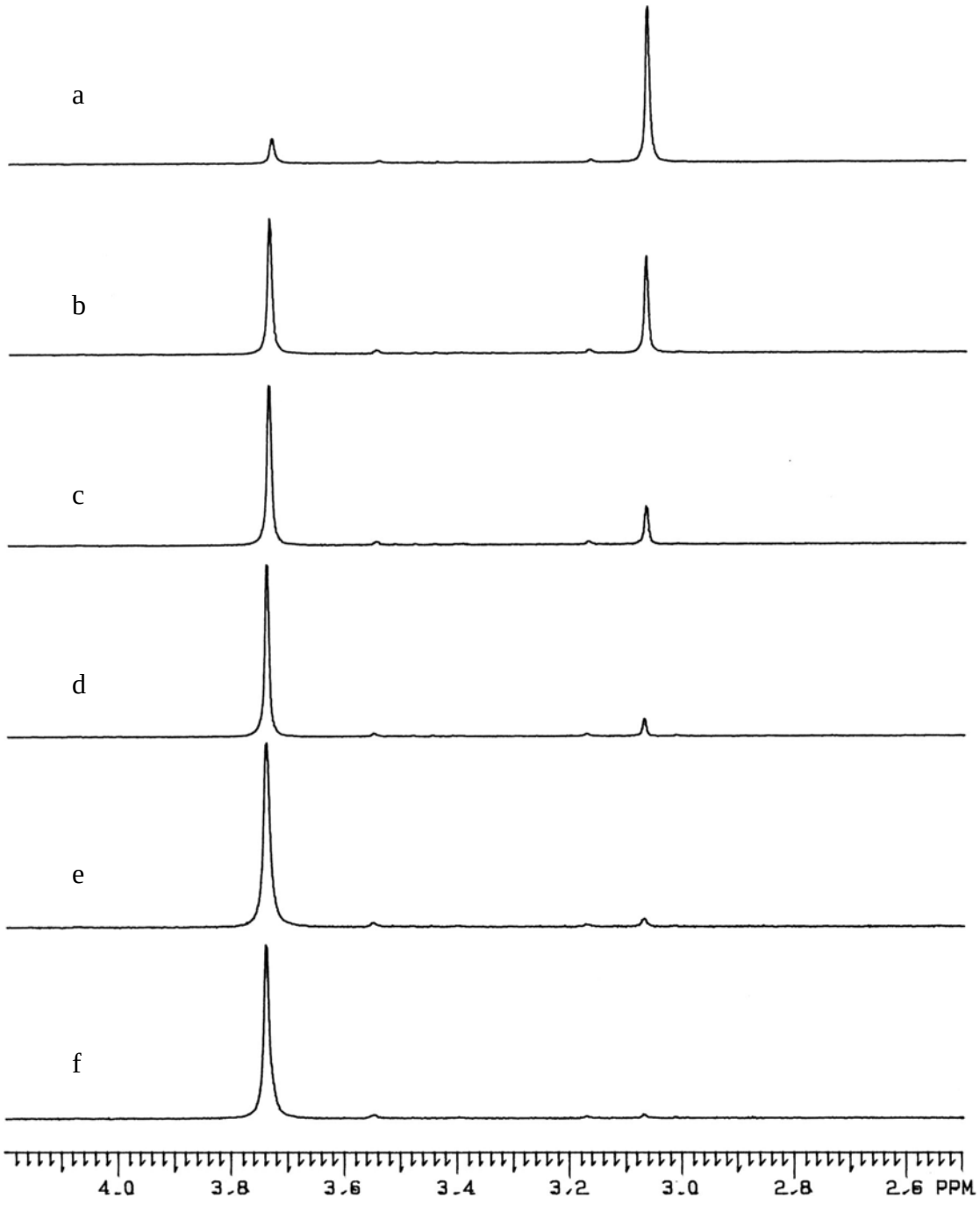

Figure 3.13. Stacked ^{1}H NMR spectra of 1,2-$Os_3(CO)_{10}$(bpcd) on heating in $CDCl_3$ at 65.0°C: (a) 0 hr, (b) 0.5 hr, (c) 1.0 hr, (d) 1.5 hr, (e) 2.0 hr, and (f) 2.5 hr.

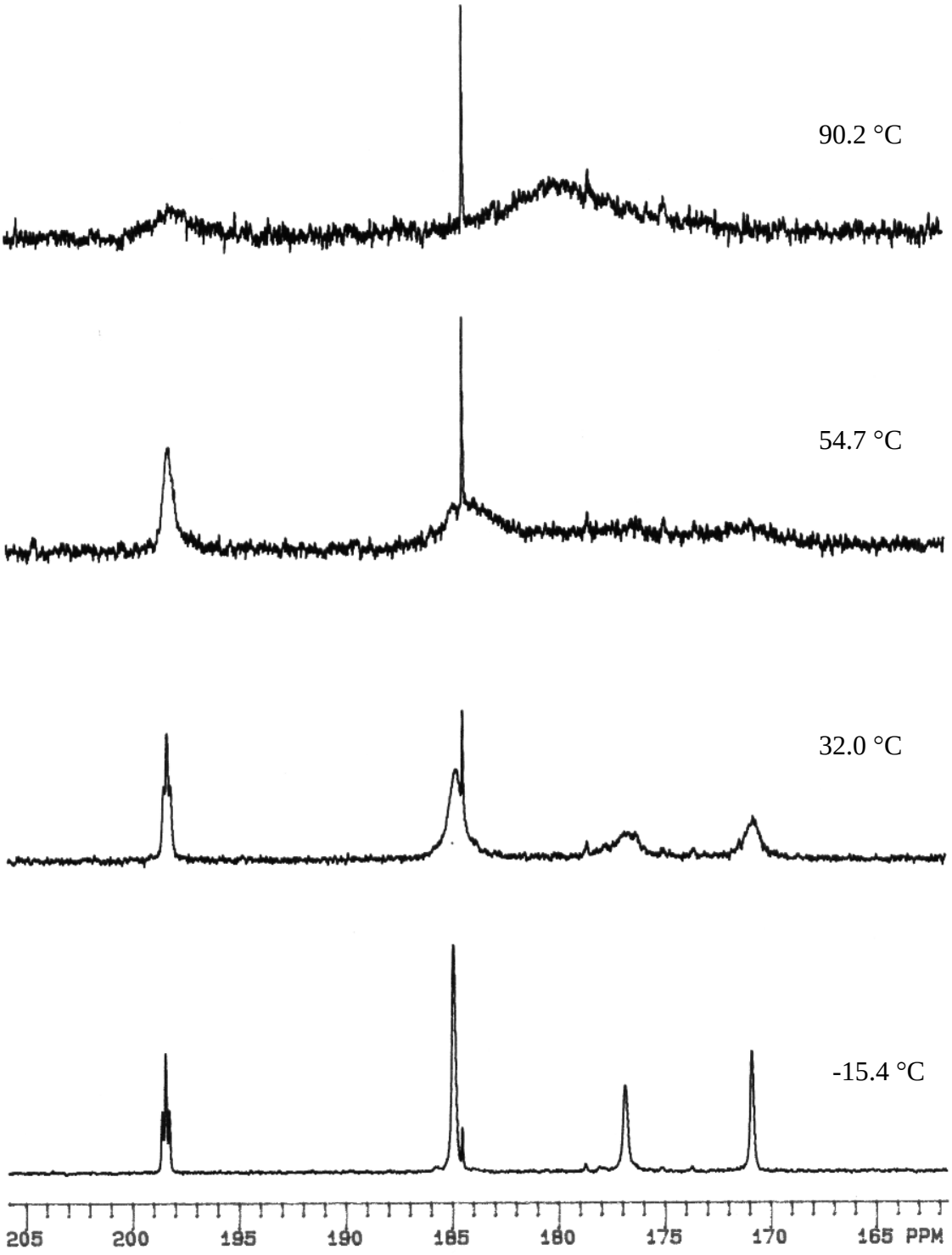

Figure 3.14. VT $^{13}C\{^{1}H\}$ NMR spectra (50 MHz) of ^{13}CO-enriched 1,1-$Os_3(CO)_{10}$(bpcd).

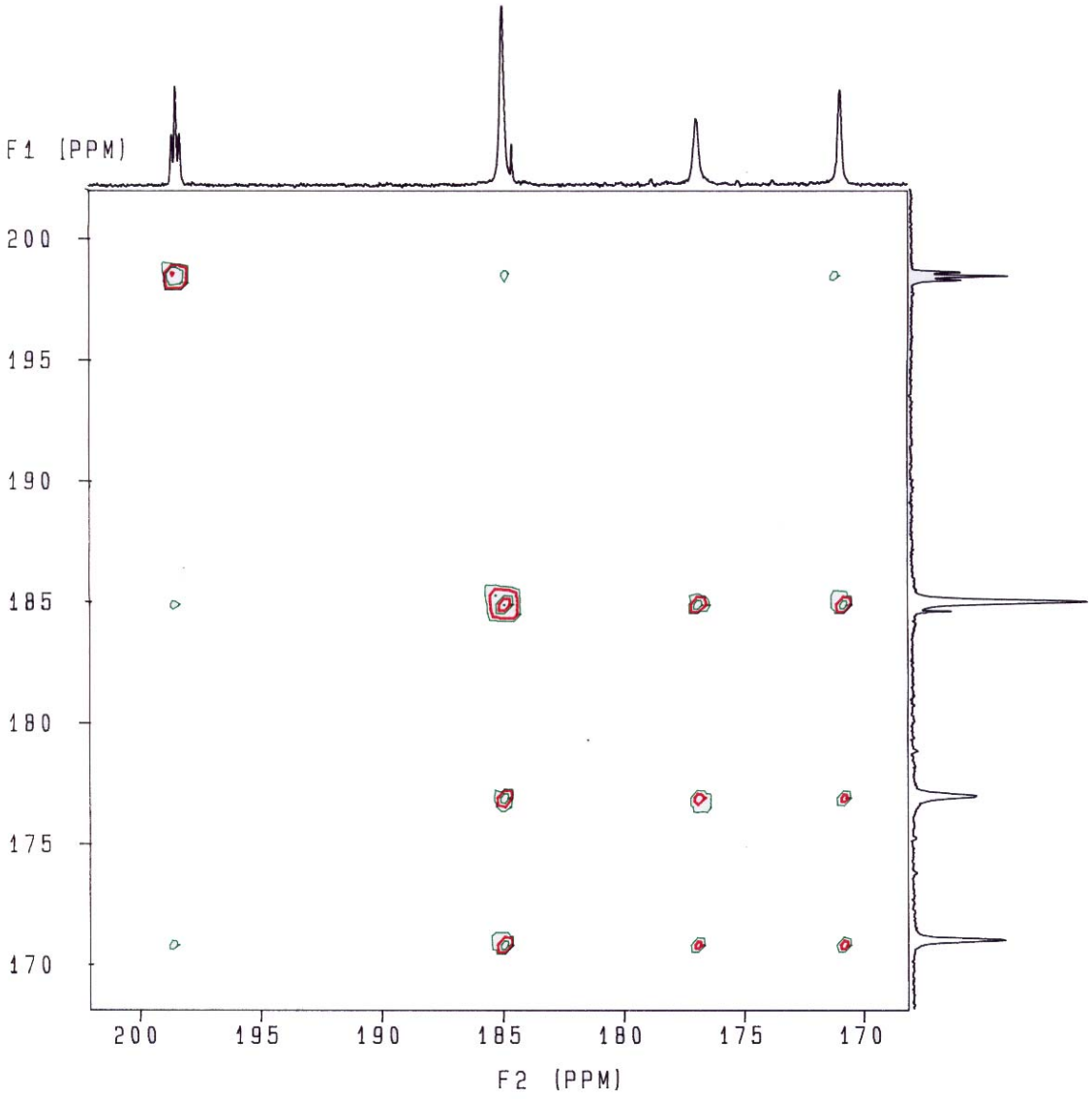

Figure 3.15. Contour map of the two-dimensional phase-sensitive $^{13}C\{^{1}H\}$ EXSY NMR (50 MHz) spectrum of ^{13}CO-enriched 1,1-$Os_3(CO)_{10}$(bpcd) recorded at –15.4 °C (t_m = 0.70s).

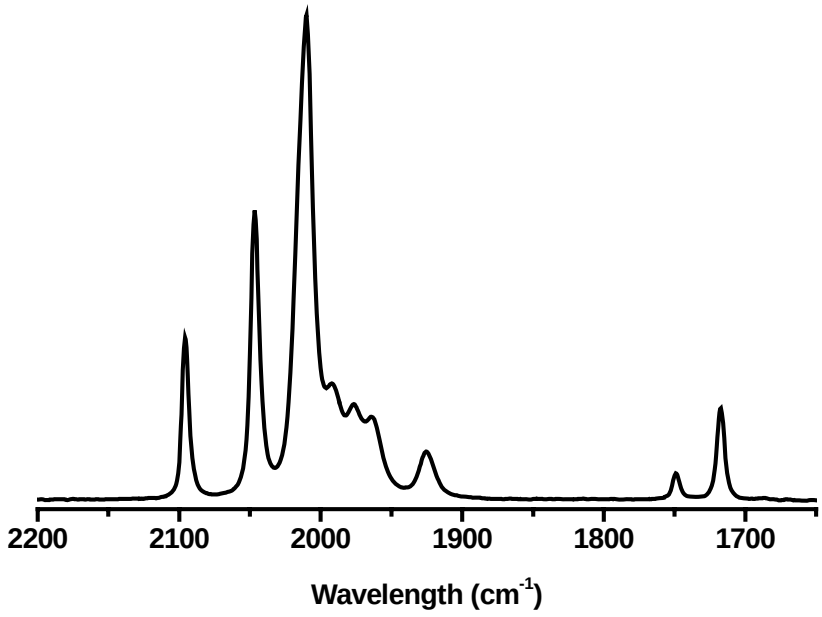

Figure 3.16. Infrared spectrum of the carbonyl region for 1,1-$Os_3(CO)_{10}$(bpcd) recorded in CH_2Cl_2.

antisymmetric stretching modes, respectively (Figure 3.16), with respect to the free bpcd ligand.

I. Synthesis and Spectroscopic Properties of $HOs_3(CO)_9[\mu$-$(PPh_2)C{=}C\{PPh(C_6H_4)\}C(O)CH_2C(O)]$

Thermolysis of 1,1-$Os_3(CO)_{10}$(bpcd) at ca. 80 °C affords the hydride cluster $HOs_3(CO)_9[\mu$-$(PPh_2)C{=}C\{PPh(C_6H_4)\}C(O)CH_2C(O)]$ due to CO loss and subsequent orthometallation. A complication arising from the thermolysis method for the preparation of the hydride cluster is the accompanying formation of the benzyne cluster due to Scheme 3.5. ^{13}C NMR assignments of 1,1-$Os_3(CO)_{10}$(bpcd).

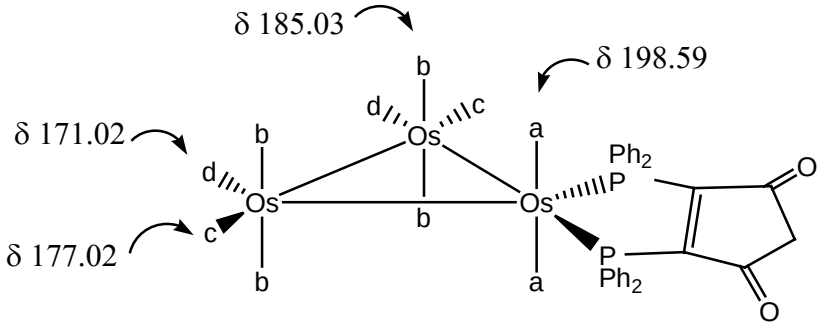

P-C bond cleavage of the coordinated bpcd ligand. However, photolysis of 1,1-$Os_3(CO)_{10}$(bpcd) with near-UV light provides a clean route for the synthesis of the hydride cluster without any complications (Figure 3.17). Chromatographic separation, followed by recrystallization of the irradiation product from CH_2Cl_2/hexane, yields the pure hydride cluster as a brown solid. The hydride cluster was characterized in solution by IR and NMR spectroscopies. The IR spectrum of the hydride cluster shows a blue shift of 10 and 14 cm^{-1} for the symmetric and antisymmetric stretching modes for the two carbonyl groups belonging to the bpcd ligand, respectively (Figure 3.18). The ^{1}H NMR

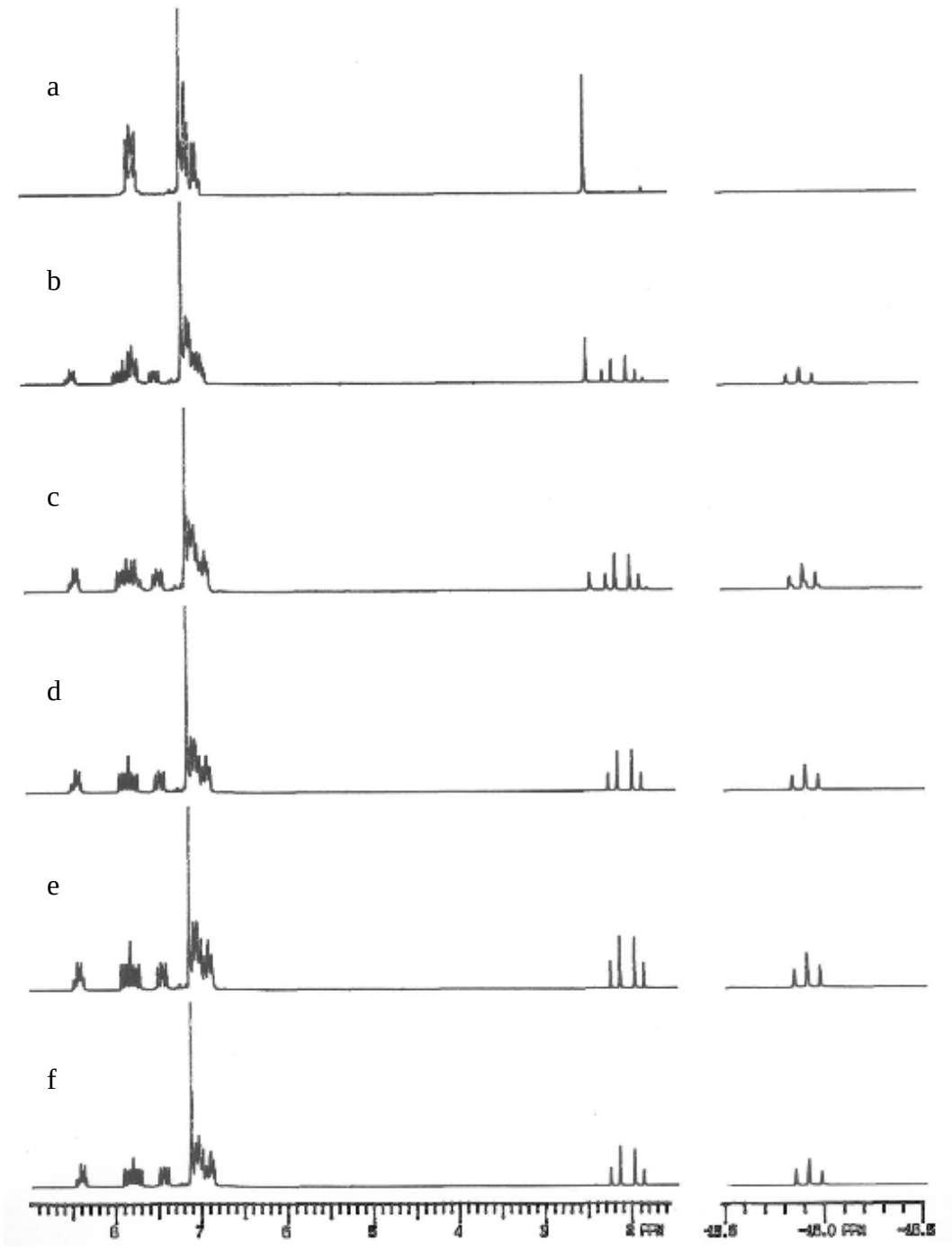

Figure 3.17. ^{1}H NMR spectra of 1,1-$Os_3(CO)_{10}$(bpcd) under irradiation with blacklights in C_6D_6 for (a) 0 hr, (b) 3 hr, (c) 6 hr, (d) 27 hr, (e) 30 hr, and (f) 150 hr.

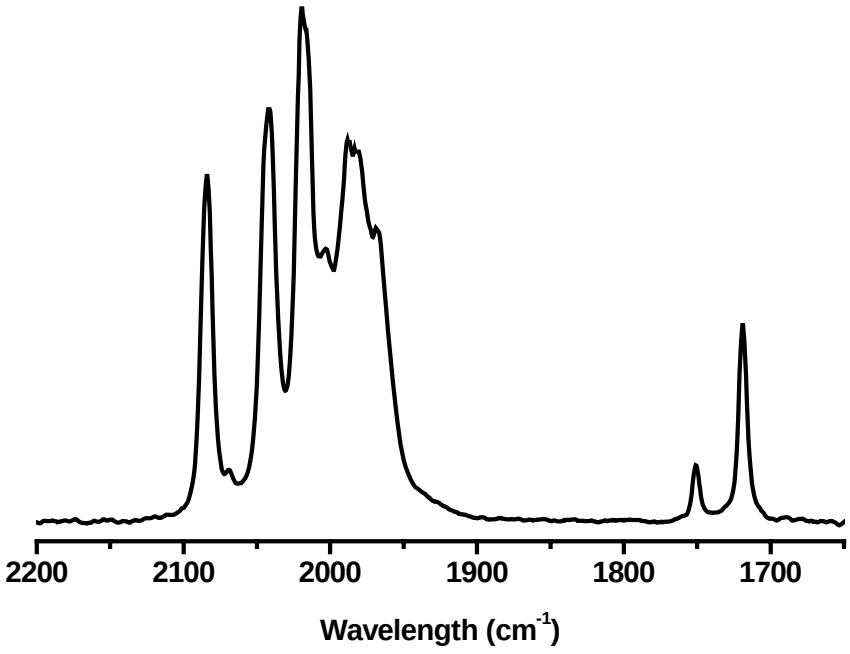

Figure 3.18. Infrared spectrum of the carbonyl region for $HOs_3(CO)_9[\mu\text{-}(PPh_2)C{=}C\{PPh(C_6H_4)\}C(O)CH_2C(O)]$ recorded in CH_2Cl_2.

spectrum of the hydride cluster clearly shows an up-field triplet centered at –16.28 ppm (J_{H-P} = 13 Hz) (Figure 3.8), which is assigned to a bridging hydrido ligand that spans two osmium atoms, with equal coupling to the two phosphorus atoms. Interestingly, there is a distinct solvent effect on the appearance of the methylene protons of the dione ring in the ^{1}H NMR spectrum. The two methylene protons appear as a singlet at 3.54 ppm in $CDCl_3$ (Figure 3.7) and as an AB quartet centered at 2.07 ppm (J_{H-H} = 21 Hz) in benzene-d_6 or toluene-d_8. A down-field shift of 0.61 ppm in the ^{1}H NMR spectrum was observed for the methylene protons in the hydride cluster compared to those of the free bpcd ligand in $CDCl_3$ solvent. The ^{31}P NMR spectrum of the hydride cluster reveals two different resonances at 26.71 ppm and 19.18 ppm (J_{P-P} = 15 Hz) (Figure 3.9).

J. Synthesis and Spectroscopic Properties of $HOs_3(CO)_8(\mu_3\text{-}C_6H_4)[\ \mu_2,\eta^1\text{-}PPhC{=}C(PPh_2)C(O)CH_2C(O)]$

Direct heating of 1,1-$Os_3(CO)_{10}$(bpcd) or $HOs_3(CO)_9[\mu\text{-}(PPh_2)C{=}C\{PPh(C_6H_4)\}C(O)CH_2C(O)]$ at 110 °C affords the benzyne cluster $HOs_3(CO)_8(\mu_3\text{-}C_6H_4)[\mu_2,\eta^1\text{-}PPhC{=}C(PPh_2)C(O)CH_2C(O)]$ as the major product, along with minor amounts of the chelated and hydride clusters. Chromatographic separation, followed by recrystallization, yielded the benzyne cluster as a brown solid. The benzyne cluster was characterized in solution by IR and NMR spectroscopies. The absorption bands for the C-O bonds of the terminal carbonyl ligands and the dione ring were observed at 2077 (s), 2042 (vs), 2030 (m), 1999 (m), 1990 (m), 1977 (m), 1748 (w, symm bpcd), and 1715 (m, antisymm bpcd) cm^{-1}, with the latter two blue shifted by 7 and 10 cm^{-1} with respect to the free bpcd ligand (Figure 3.19). The ^{1}H NMR spectrum of the

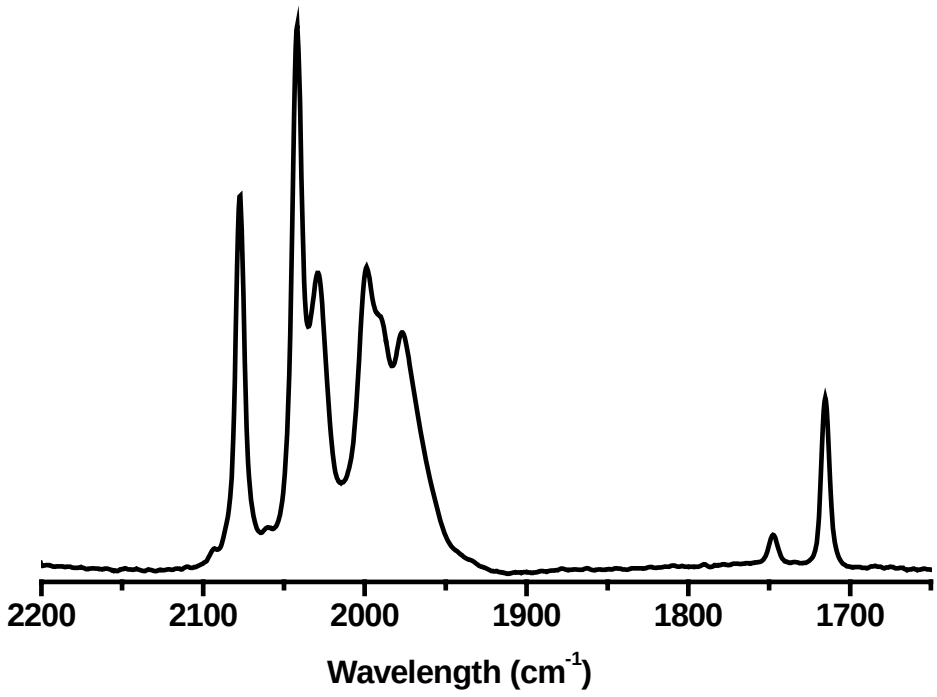

Figure 3.19. Infrared spectrum of the carbonyl region for $HOs_3(CO)_8(\mu_3\text{-}C_6H_4)[\mu_2,\eta^1\text{-}PPhC{=}C(PPh_2)C(O)CH_2C(O)]$ recorded in CH_2Cl_2.

benzyne cluster exhibits an up-field doublet of doublets centered at -16.68 ppm ($J_{H\text{-}P}$ = 14, 6.7 Hz) (Figure 3.8), consistent with a bridging hydrido ligand spanning an osmium-osmium bond. The AB quartet centered at 3.66 ppm (J_{H-H} = 22 Hz) (Figure 3.7) is readily assigned to the diasterotopic methylene protons of the bpcd ligand. The benzyne hydrogens exhibit an ABXY spin system, with the AB protons buried under the aromatic protons belonging to the other three phenyl groups. The ^{31}P NMR spectrum of the benzyne cluster shown in Figure 3.9 confirms the presence of two coupled resonances at 10.96 ppm and –72.18 ppm (J_{P-P} = 12 Hz), with the former assigned to the phosphorus atom of the phosphine ligand and the latter assigned to the phosphorus atom of the phosphido ligand. Comparison of the ^{31}P chemical shifts of the benzyne cluster with that of the free bpcd ligand shows an up-field shift of 50.1 ppm for the phosphido ligand and a down-field shift of 33.1 ppm for the normal phosphine moiety. The high-field shift found for the phosphido moiety supports the bridging of non-bonded osmium atoms.[11]

K. X-Ray Diffraction Structure of 1,2-$Os_3(CO)_{10}$(bpcd)

Single crystals of 1,2-$Os_3(CO)_{10}$(bpcd), as the *m*-xylene solvate, were successfully grown from the slow evaporation of a CH_2Cl_2/hexane solution containing the 1,2-$Os_3(CO)_{10}$(bpcd) that was surrounded with *m*-xylene. The molecular structure of 1,2-$Os_3(CO)_{10}$(bpcd) was determined by X-ray diffraction analysis. Complex 1,2-$Os_3(CO)_{10}$(bpcd) exists as discrete molecules in the unit cell with no unusually short inter- or intramolecular contacts. The X-ray data processing and collection parameters are listed in Table 3.5, and selected bond distances and angles given in Table 3.6. The

molecular configuration and the numbering scheme of 1,2-$Os_3(CO)_{10}$(bpcd)·(*m*-xylene) are presented in the ORTEP diagram of Figure 3.20.

The Os-Os bond distances in 1,2-$Os_3(CO)_{10}$(bpcd) range from 2.8535(8) Å [Os(2)-Os(3)] to 2.8633(8) Å [Os(1)-Os(3)] and display a mean distance of 2.8572 Å. The Os-Os distances are normal relative to those in other simple polynuclear osmium clusters, which indicate that the triosmium frame itself does not experience any significantly adverse perturbation due to the coordination of the bpcd. The ten terminal carbonyl groups may be considered as linear with standard distances. The observed distortion or twisting of the axial CO groups in 1,2-$Os_3(CO)_{10}$(bpcd) from idealized D_{3h} to D_3 symmetry is a feature common to many structurally characterized phosphine-substituted triosmium and triruthenium clusters, as supported by molecular mechanics calculations. The determined P-Os bond distances of P(1)-Os(1) [2.318(2) Å] and P(2)-Os(2) [2.322(2) Å] are in excellent agreement with the average lengths reported for a variety of P-substituted osmium compounds. Coordination of the diphosphine ligand across the Os(1)-Os(2) bond in 1,2-$Os_3(CO)_{10}$(bpcd) leads to a significant stretching of the bpcd ligand, causing ground-state destabilization relative to the chelating isomer 1,1-$Os_3(CO)_{10}$(bpcd). The internuclear P(1)···P(2) distance of 3.797(7) Å found for 1,2-$Os_3(CO)_{10}$(bpcd)·(*m*-xylene) is ca. 0.60 Å longer than the corresponding distance reported for the free ligand cDPPEn, while the P(1)-C(2)-C(3) and P(2)-C(3)-C(2) bond angles of 131.3(7)$^\circ$ and 130.8(7)$^\circ$, respectively, associated with the unsaturated backbone of the diphosphine ligand are ca. 10° larger as compared to the analogous linkages in the free cDPPEn. Additional evidence supporting the unfavorable bridging mode of

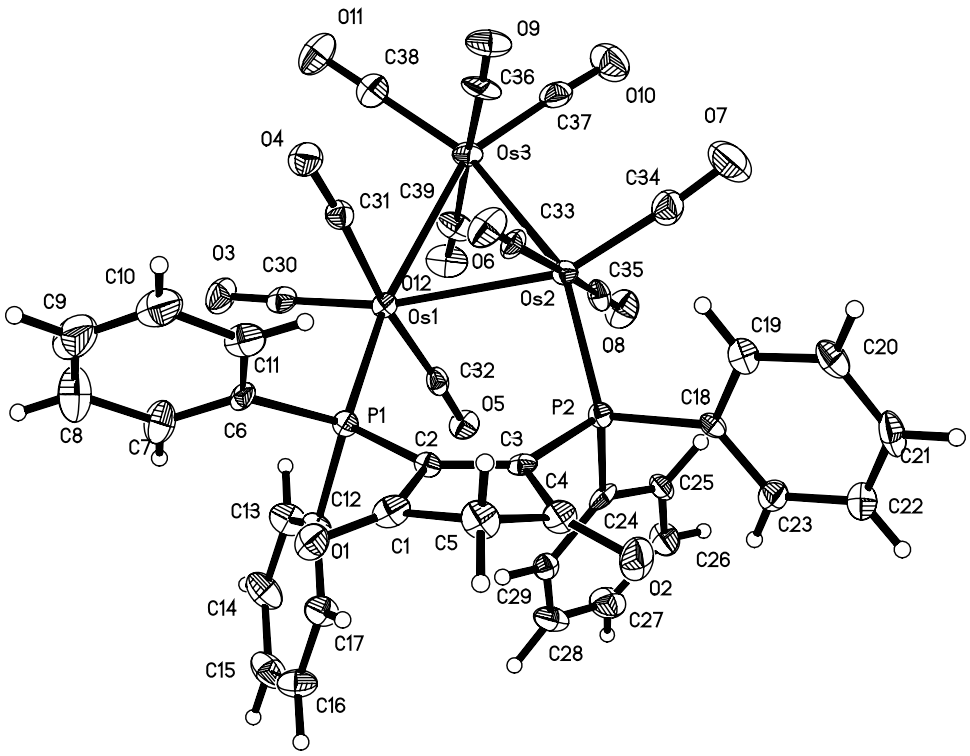

Figure 3.20. ORTEP diagram of 1,2-$Os_3(CO)_{10}$(bpcd) showing the thermal ellipsoids at the 50% probability level. (Reprinted with permission from *Organometallics* **2006**, 25, 930-945. Copyright 2006 American Chemical Society.)

Table 3.5. Crystal Data and Structure Refinement for 1,2-$Os_3(CO)_{10}$(bpcd)·(*m*-xylene)

Empirical formula	$C_{39}H_{22}O_{12}Os_3P_2$·(*m*-xylene)	
Formula weight	1411.19	
Temperature	213(2) K	
Wavelength	0.71073 Å	
Crystal system	Monoclinic	
Space group	P2(1)/c	
Unit cell dimensions	a = 14.031(4) Å	α = 90°
	b = 30.89(1) Å	β = 115.05(2)°
	c = 11.881(4) Å	γ = 90°
Volume	4665(3) $Å^3$	
Z	4	
Density (calculated)	2.009 Mg/m^3	
Absorption coefficient	8.279 mm^{-1}	
F(000)	2632	
Crystal size	0.28 x 0.17 x 0.10 mm^3	
Theta range for data collection	1.32 to 26.99°	
Index ranges	$-17 \le h \le 17$, $-39 \le k \le 39$, $-14 \le l \le 15$	
Reflections collected	37461	
Independent reflections	10128 [R(int) = 0.0998]	
Completeness to theta = 26.99°	99.4%	
Absorption correction	empirical	
Max. and min. transmission	.975 1 and .4934	
Refinement method	Full-matrix least-squares on F^2	
Data / restraints / parameters	10128 / 0 / 537	
Goodness-of-fit on F^2	0.923	
Final R indices [I > 2sigma(I)]	R1 = 0.0477, wR2 = 0.0782	
R indices (all data)	R1 = 0.1031, wR2 = 0.0880	
Largest diff. peak and hole	1.779 and -0.891 e. $Å^{-3}$	

Table 3.6. Bond Lengths [Å] and Angles [°] for 1,2-$Os_3(CO)_{10}$(bpcd)·(*m*-xylene)[a]

Bond Distances			
Os(1)-C(30)	1.881(11)	C(3)-C(4)	1.507(12)
Os(1)-C(31)	1.927(10)	C(4)-C(5)	1.493(13)
Os(1)-C(32)	1.940(10)	C(6)-C(7)	1.362(13)
Os(1)-P(1)	2.318(2)	C(6)-C(11)	1.380(12)
Os(1)-Os(2)	2.8549(10)	C(7)-C(8)	1.393(15)
Os(1)-Os(3)	2.8633(8)	C(8)-C(9)	1.365(18)
Os(2)-C(34)	1.850(12)	C(9)-C(10)	1.360(17)
Os(2)-C(35)	1.922(10)	C(10)-C(11)	1.390(14)
Os(2)-C(33)	1.931(10)	C(12)-C(17)	1.394(11)
Os(2)-P(2)	2.322(2)	C(12)-C(13)	1.401(12)
Os(2)-Os(3)	2.8535(8)	C(13)-C(14)	1.395(13)
Os(3)-C(37)	1.877(12)	C(14)-C(15)	1.363(14)
Os(3)-C(38)	1.919(12)	C(15)-C(16)	1.382(13)
Os(3)-C(39)	1.955(11)	C(16)-C(17)	1.372(12)
Os(3)-C(36)	1.959(11)	C(18)-C(23)	1.383(12)
P(1)-C(6)	1.808(9)	C(18)-C(19)	1.403(11)
P(1)-C(12)	1.825(8)	C(19)-C(20)	1.358(12)
P(1)-C(2)	1.849(9)	C(20)-C(21)	1.376(14)
P(2)-C(24)	1.809(9)	C(21)-C(22)	1.374(13)
P(2)-C(18)	1.817(9)	C(22)-C(23)	1.375(13)
P(2)-C(3)	1.863(9)	C(24)-C(25)	1.360(12)
O(1)-C(1)	1.183(11)	C(24)-C(29)	1.390(12)
O(2)-C(4)	1.211(11)	C(25)-C(26)	1.375(12)
O(3)-C(30)	1.146(11)	C(26)-C(27)	1.386(13)
O(4)-C(31)	1.135(10)	C(27)-C(28)	1.348(14)
O(5)-C(32)	1.139(10)	C(28)-C(29)	1.377(12)
O(6)-C(33)	1.137(10)	C(40)-C(47)	1.32(3)
O(7)-C(34)	1.159(11)	C(40)-C(45)	1.46(2)
O(8)-C(35)	1.155(10)	C(40)-C(41)	1.51(2)

Table 3.6. Con′t.

O(9)-C(36)	1.124(10)	C(41)-C(42)	1.38(2)
O(10)-C(37)	1.171(12)	C(42)-C(43)	1.59(2)
O(11)-C(38)	1.126(11)	C(42)-C(44)	2.06(3)
O(12)-C(39)	1.134(10)	C(43)-C(44)	1.30(3)
C(1)-C(2)	1.521(12)	C(44)-C(45)	1.27(2)
C(1)-C(5)	1.536(13)	C(44)-C(46)	1.71(3)
C(2)-C(3)	1.359(11)		
	Bond Angles		
C(30)-Os(1)-C(31)	89.4(4)	C(2)-C(3)-P(2)	130.8(7)
C(30)-Os(1)-C(32)	94.0(4)	C(4)-C(3)-P(2)	120.9(7)
C(31)-Os(1)-C(32)	173.3(4)	O(2)-C(4)-C(5)	125.9(8)
C(30)-Os(1)-P(1)	97.1(3)	O(2)-C(4)-C(3)	125.8(9)
C(31)-Os(1)-P(1)	93.6(3)	C(5)-C(4)-C(3)	107.9(8)
C(32)-Os(1)-P(1)	91.7(3)	C(4)-C(5)-C(1)	101.2(7)
C(30)-Os(1)-Os(2)	159.3(3)	C(7)-C(6)-C(11)	119.0(10)
C(31)-Os(1)-Os(2)	93.5(3)	C(7)-C(6)-P(1)	119.9(8)
C(32)-Os(1)-Os(2)	81.3(3)	C(11)-C(6)-P(1)	120.8(8)
P(1)-Os(1)-Os(2)	103.09(6)	C(6)-C(7)-C(8)	121.1(11)
C(30)-Os(1)-Os(3)	101.0(3)	C(9)-C(8)-C(7)	117.9(13)
C(31)-Os(1)-Os(3)	77.5(3)	C(8)-C(9)-C(10)	123.0(14)
C(32)-Os(1)-Os(3)	96.1(3)	C(9)-C(10)-C(11)	117.8(13)
P(1)-Os(1)-Os(3)	159.62(6)	C(6)-C(11)-C(10)	121.1(11)
Os(2)-Os(1)-Os(3)	59.87(2)	C(17)-C(12)-C(13)	117.2(8)
C(34)-Os(2)-C(35)	91.1(4)	C(17)-C(12)-P(1)	122.6(7)
C(34)-Os(2)-C(33)	93.3(4)	C(13)-C(12)-P(1)	120.1(7)
C(35)-Os(2)-C(33)	173.4(4)	C(14)-C(13)-C(12)	121.4(9)
C(34)-Os(2)-P(2)	103.2(3)	C(15)-C(14)-C(13)	119.2(10)
C(35)-Os(2)-P(2)	95.0(3)	C(14)-C(15)-C(16)	120.8(10)
C(33)-Os(2)-P(2)	88.8(3)	C(17)-C(16)-C(15)	120.0(10)
C(34)-Os(2)-Os(3)	101.2(3)	C(16)-C(17)-C(12)	121.4(9)

Table 3.6. Con′t.

C(35)-Os(2)-Os(3)	76.7(3)	C(23)-C(18)-C(19)	117.6(9)
C(33)-Os(2)-Os(3)	97.7(3)	C(23)-C(18)-P(2)	123.6(7)
P(2)-Os(2)-Os(3)	154.38(6)	C(19)-C(18)-P(2)	118.8(7)
C(34)-Os(2)-Os(1)	158.2(3)	C(20)-C(19)-C(18)	121.9(10)
C(35)-Os(2)-Os(1)	94.9(3)	C(19)-C(20)-C(21)	118.7(10)
C(33)-Os(2)-Os(1)	79.3(3)	C(22)-C(21)-C(20)	121.5(10)
P(2)-Os(2)-Os(1)	97.13(6)	C(21)-C(22)-C(23)	119.1(10)
Os(3)-Os(2)-Os(1)	60.211(15)	C(22)-C(23)-C(18)	121.2(9)
C(37)-Os(3)-C(38)	101.5(4)	C(25)-C(24)-C(29)	117.4(8)
C(37)-Os(3)-C(39)	92.7(4)	C(25)-C(24)-P(2)	118.4(7)
C(38)-Os(3)-C(39)	89.2(4)	C(29)-C(24)-P(2)	124.2(7)
C(37)-Os(3)-C(36)	91.4(4)	C(24)-C(25)-C(26)	123.0(9)
C(38)-Os(3)-C(36)	95.1(4)	C(25)-C(26)-C(27)	117.9(10)
C(39)-Os(3)-C(36)	173.4(4)	C(28)-C(27)-C(26)	120.7(10)
C(37)-Os(3)-Os(2)	99.9(3)	C(27)-C(28)-C(29)	120.2(10)
C(38)-Os(3)-Os(2)	157.1(3)	C(28)-C(29)-C(24)	120.7(9)
C(39)-Os(3)-Os(2)	98.0(3)	O(3)-C(30)-Os(1)	179.2(9)
C(36)-Os(3)-Os(2)	76.2(3)	O(4)-C(31)-Os(1)	174.8(9)
C(37)-Os(3)-Os(1)	154.9(3)	O(5)-C(32)-Os(1)	177.4(8)
C(38)-Os(3)-Os(1)	101.1(3)	O(6)-C(33)-Os(2)	174.5(8)
C(39)-Os(3)-Os(1)	77.0(3)	O(7)-C(34)-Os(2)	175.3(11)
C(36)-Os(3)-Os(1)	97.2(3)	O(8)-C(35)-Os(2)	177.0(9)
Os(2)-Os(3)-Os(1)	59.92(2)	O(9)-C(36)-Os(3)	176.4(8)
C(6)-P(1)-C(12)	104.0(4)	O(10)-C(37)-Os(3)	176.0(9)
C(6)-P(1)-C(2)	102.9(4)	O(11)-C(38)-Os(3)	179.0(10)
C(12)-P(1)-C(2)	102.4(4)	O(12)-C(39)-Os(3)	175.0(9)
C(6)-P(1)-Os(1)	109.9(3)	C(47)-C(40)-C(45)	126(2)
C(12)-P(1)-Os(1)	117.2(3)	C(47)-C(40)-C(41)	114(2)
C(2)-P(1)-Os(1)	118.6(3)	C(45)-C(40)-C(41)	119.7(19)
C(24)-P(2)-C(18)	104.0(4)	C(42)-C(41)-C(40)	111.0(17)

Table 3.6. Con′t.

C(24)-P(2)-C(3)	104.5(4)	C(41)-C(42)-C(43)	134.0(19)
C(18)-P(2)-C(3)	102.0(4)	C(41)-C(42)-C(44)	95.0(14)
C(24)-P(2)-Os(2)	116.2(3)	C(43)-C(42)-C(44)	39.1(10)
C(18)-P(2)-Os(2)	114.3(3)	C(44)-C(43)-C(42)	91(2)
C(3)-P(2)-Os(2)	114.4(3)	C(45)-C(44)-C(43)	157(3)
O(1)-C(1)-C(2)	127.1(9)	C(45)-C(44)-C(46)	112(2)
O(1)-C(1)-C(5)	126.9(9)	C(43)-C(44)-C(46)	91(2)
C(2)-C(1)-C(5)	106.0(8)	C(45)-C(44)-C(42)	107.3(17)
C(3)-C(2)-C(1)	109.5(8)	C(43)-C(44)-C(42)	50.3(14)
C(3)-C(2)-P(1)	131.3(7)	C(46)-C(44)-C(42)	141(2)
C(1)-C(2)-P(1)	119.3(7)	C(44)-C(45)-C(40)	106.8(19)
C(2)-C(3)-C(4)	108.3(8)		

[a]Numbers in parentheses are estimated standard deviations in the least significant digits.

coordination of the unsaturated phosphine to the metal frame in 1,2-$Os_3(CO)_{10}$(bpcd) is seen in the C(2)-P(1)-Os(1) [118.6(3)°] and C(3)-P(2)-Os(2) [114.4(3)°] bond angles that exhibit a substantial deviation from the anticipated bond angle of ca. 109° expected for a tetracoordinate phosphorus center. The five-membered ring of the coordinated bpcd ligand in the 1,2-$Os_3(CO)_{10}$(bpcd) is tilted out of plane defined by the three osmium atoms. The two phosphorus atoms of the 1,2-$Os_3(CO)_{10}$(bpcd) lie at the top and bottom sides of the triosmium plane, respectively, with a dihedral angle of 24.82° observed for the P(1)-Os(1)-Os(2)-P(2) atoms.

L. X-Ray Diffraction Structure of 1,1-$Os_3(CO)_{10}$(bpcd)

Single crystals of 1,1-$Os_3(CO)_{10}$(bpcd) were successfully grown by the slow diffusion of hexane into a CH_2Cl_2 solution containing pure 1,1-$Os_3(CO)_{10}$(bpcd). The molecular structure of 1,1-$Os_3(CO)_{10}$(bpcd) was determined by X-ray diffraction analysis. 1,1-$Os_3(CO)_{10}$(bpcd) exists as discrete molecules in the unit cell with no unusually short inter- or intramolecular contacts. The X-ray data processing and collection parameters are listed in Table 3.7, and selected bond distances and angles given in Table 3.8. The molecular structure and the numbering scheme of 1,1-$Os_3(CO)_{10}$(bpcd) are presented in the ORTEP diagram of Figure 3.21.

The ORTEP diagram of 1,1-$Os_3(CO)_{10}$(bpcd) confirms the attendant migration of the diphosphine ligand upon heating the bridged-cluster. The mean Os-Os and Os-P bond lengths were found to be 2.9074 Å and 2.2987 Å, respectively, and are unremarkable with respect to those bonds in 1,2-$Os_3(CO)_{10}$(bpcd) and other phosphine-substituted osmium clusters. The internuclear non-bonding P(1)···P(2) distance of 3.169(4) Å in 1,1-

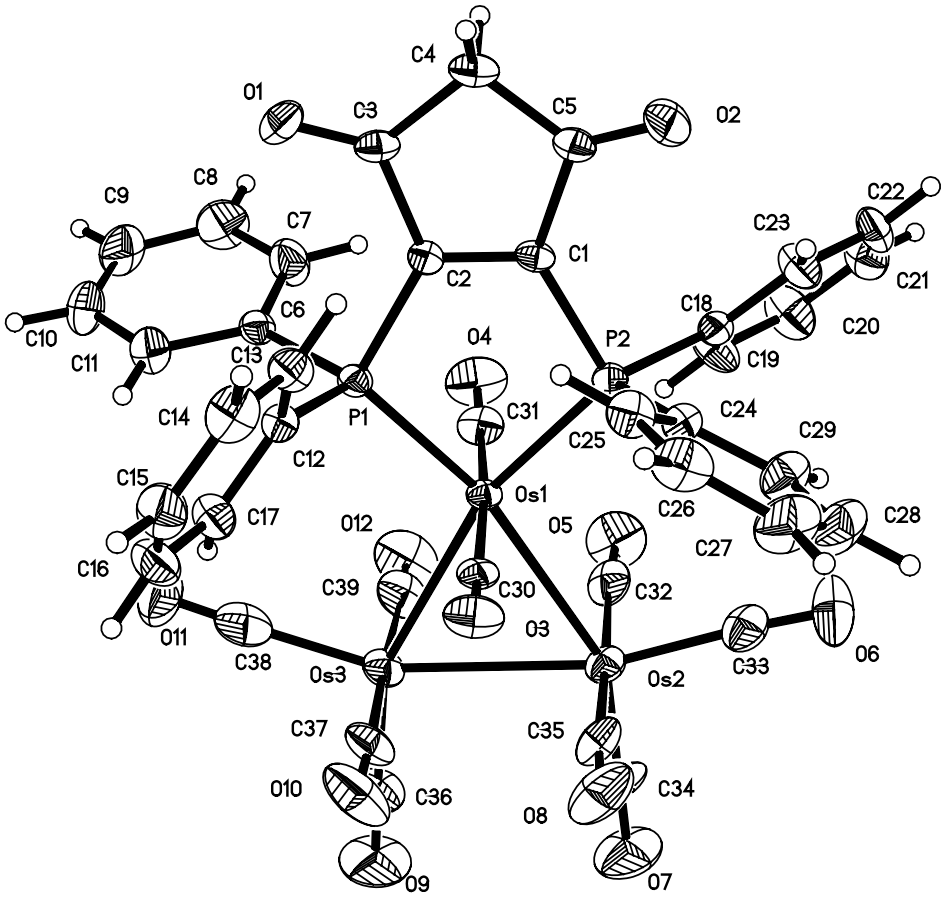

Figure 3.21. ORTEP diagram of 1,1-$Os_3(CO)_{10}$(bpcd) showing the thermal ellipsoids at the 50% probability level. (Reprinted with permission from *Organometallics* **2006**, 25, 930-945. Copyright 2006 American Chemical Society.)

Table 3.7. Crystal Data and Structure Refinement for 1,1-$Os_3(CO)_{10}$(bpcd)

Empirical formula	$Os_3C_{39}H_{22}O_{12}P_2$	
Formula weight	1315.11	
Temperature	300(2) K	
Wavelength	0.71073 Å	
Crystal system	Monoclinic	
Space group	P2(1)/n	
Unit cell dimensions	a = 11.028(1) Å	α= 90°
	b = 19.913(3) Å	β= 104.107(2)°
	c = 18.382(3) Å	γ = 90°
Volume	3915.0(10) $Å^3$	
Z	4	
Density (calculated)	2.231 Mg/m^3	
Absorption coefficient	9.857 mm^{-1}	
F(000)	2440	
Crystal size	0.36 x 0.28 x 0.20 mm^3	
Theta range for data collection	1.53 to 22.50°	
Index ranges	$-11 \le h \le 11$, $-21 \le k \le 21$, $-19 \le l \le 19$	
Reflections collected	22472	
Independent reflections	5120 [R(int) = 0.0596]	
Completeness to theta = 22.50°	100.0%	
Absorption correction	Empirical	
Max. and min. transmission	0.7019 and 0.1409	
Refinement method	Full-matrix least-squares on F^2	
Data / restraints / parameters	5120 / 0 / 506	
Goodness-of-fit on F^2	0.966	
Final R indices [I > 2sigma(I)]	R1 = 0.0249, wR2 = 0.0582	
R indices (all data)	R1 = 0.0336, wR2 = 0.0619	
Extinction coefficient	0.00045(3)	
Largest diff. peak and hole	1.298 and -1.127 e. $Å^{-3}$	

Table 3.8. Bond Lengths [Å] and Angles [°] for 1,1-$Os_3(CO)_{10}$(bpcd)[a]

Bond Distances			
Os(1)-C(30)	1.916(7)	O(11)-C(38)	1.144(10)
Os(1)-C(31)	1.903(7)	O(12)-C(39)	1.138(9)
Os(1)-P(1)	2.2947(17)	C(1)-C(2)	1.340(8)
Os(1)-P(2)	2.3027(17)	C(1)-C(5)	1.517(9)
Os(1)-Os(3)	2.9092(5)	C(2)-C(3)	1.516(9)
Os(1)-Os(2)	2.9143(5)	C(3)-C(4)	1.509(9)
Os(2)-C(34)	1.869(9)	C(4)-C(5)	1.503(9)
Os(2)-C(33)	1.893(9)	C(6)-C(7)	1.367(9)
Os(2)-C(32)	1.917(9)	C(6)-C(11)	1.391(9)
Os(2)-C(35)	1.923(9)	C(7)-C(8)	1.377(10)
Os(2)-Os(3)	2.8988(6)	C(8)-C(9)	1.382(11)
Os(3)-C(36)	1.895(9)	C(9)-C(10)	1.328(10)
Os(3)-C(38)	1.918(11)	C(10)-C(11)	1.378(9)
Os(3)-C(39)	1.915(9)	C(12)-C(17)	1.375(9)
Os(3)-C(37)	1.932(9)	C(12)-C(13)	1.375(9)
P(1)-C(6)	1.823(6)	C(13)-C(14)	1.397(10)
P(1)-C(12)	1.818(6)	C(14)-C(15)	1.356(11)
P(1)-C(2)	1.824(6)	C(15)-C(16)	1.372(11)
P(2)-C(24)	1.815(6)	C(16)-C(17)	1.363(9)
P(2)-C(18)	1.827(6)	C(18)-C(19)	1.371(9)
P(2)-C(1)	1.849(6)	C(18)-C(23)	1.402(9)
O(1)-C(3)	1.192(8)	C(19)-C(20)	1.378(9)
O(2)-C(5)	1.183(8)	C(20)-C(21)	1.336(11)
O(3)-C(30)	1.149(7)	C(21)-C(22)	1.363(11)
O(4)-C(31)	1.166(8)	C(22)-C(23)	1.391(9)
O(5)-C(32)	1.151(9)	C(24)-C(25)	1.369(9)
O(6)-C(33)	1.150(9)	C(24)-C(29)	1.385(9)
O(7)-C(34)	1.151(9)	C(25)-C(26)	1.389(10)
O(8)-C(35)	1.146(8)	C(26)-C(27)	1.359(12)

Table 3.8. Con′t.

O(9)-C(36)	1.136(10)	C(27)-C(28)	1.375(11)
O(10)-C(37)	1.134(9)	C(28)-C(29)	1.391(10)
	Bond Angles		
C(30)-Os(1)-C(31)	175.9(3)	C(1)-P(2)-Os(1)	106.0(2)
C(30)-Os(1)-P(1)	88.37(19)	C(2)-C(1)-C(5)	109.9(5)
C(31)-Os(1)-P(1)	90.0(2)	C(2)-C(1)-P(2)	118.7(5)
C(30)-Os(1)-P(2)	89.9(2)	C(5)-C(1)-P(2)	131.3(5)
C(31)-Os(1)-P(2)	93.7(2)	C(1)-C(2)-C(3)	110.8(5)
P(1)-Os(1)-P(2)	87.15(6)	C(1)-C(2)-P(1)	120.9(5)
C(30)-Os(1)-Os(3)	88.07(19)	C(3)-C(2)-P(1)	128.2(4)
C(31)-Os(1)-Os(3)	88.9(2)	O(1)-C(3)-C(4)	127.1(6)
P(1)-Os(1)-Os(3)	108.68(4)	O(1)-C(3)-C(2)	126.7(6)
P(2)-Os(1)-Os(3)	163.97(4)	C(4)-C(3)-C(2)	106.3(5)
C(30)-Os(1)-Os(2)	87.58(19)	C(5)-C(4)-C(3)	105.5(6)
C(31)-Os(1)-Os(2)	93.3(2)	O(2)-C(5)-C(4)	127.7(7)
P(1)-Os(1)-Os(2)	167.82(4)	O(2)-C(5)-C(1)	125.6(6)
P(2)-Os(1)-Os(2)	104.32(4)	C(4)-C(5)-C(1)	106.7(6)
Os(3)-Os(1)-Os(2)	59.706(13)	C(7)-C(6)-C(11)	117.9(6)
C(34)-Os(2)-C(33)	102.0(4)	C(7)-C(6)-P(1)	119.3(5)
C(34)-Os(2)-C(32)	92.6(4)	C(11)-C(6)-P(1)	122.8(5)
C(33)-Os(2)-C(32)	88.7(3)	C(6)-C(7)-C(8)	121.3(7)
C(34)-Os(2)-C(35)	92.7(4)	C(9)-C(8)-C(7)	119.6(7)
C(33)-Os(2)-C(35)	90.8(3)	C(10)-C(9)-C(8)	119.5(7)
C(32)-Os(2)-C(35)	174.7(3)	C(9)-C(10)-C(11)	121.6(7)
C(34)-Os(2)-Os(3)	93.9(3)	C(10)-C(11)-C(6)	119.9(7)
C(33)-Os(2)-Os(3)	164.1(2)	C(17)-C(12)-C(13)	117.3(6)
C(32)-Os(2)-Os(3)	90.6(2)	C(17)-C(12)-P(1)	119.4(5)
C(35)-Os(2)-Os(3)	88.5(2)	C(13)-C(12)-P(1)	123.2(5)
C(34)-Os(2)-Os(1)	153.9(3)	C(12)-C(13)-C(14)	120.8(7)
C(33)-Os(2)-Os(1)	104.1(2)	C(15)-C(14)-C(13)	120.1(8)

Table 3.8. Con′t.

C(32)-Os(2)-Os(1)	86.5(2)	C(14)-C(15)-C(16)	119.5(7)
C(35)-Os(2)-Os(1)	88.5(2)	C(17)-C(16)-C(15)	120.0(7)
Os(3)-Os(2)-Os(1)	60.059(12)	C(16)-C(17)-C(12)	122.2(7)
C(36)-Os(3)-C(38)	103.9(4)	C(19)-C(18)-C(23)	117.9(6)
C(36)-Os(3)-C(39)	92.0(4)	C(19)-C(18)-P(2)	121.7(5)
C(38)-Os(3)-C(39)	90.5(4)	C(23)-C(18)-P(2)	120.4(5)
C(36)-Os(3)-C(37)	90.3(4)	C(18)-C(19)-C(20)	121.3(7)
C(38)-Os(3)-C(37)	91.1(4)	C(21)-C(20)-C(19)	121.1(8)
C(39)-Os(3)-C(37)	176.8(3)	C(20)-C(21)-C(22)	119.3(7)
C(36)-Os(3)-Os(2)	96.0(3)	C(21)-C(22)-C(23)	121.4(7)
C(38)-Os(3)-Os(2)	160.0(2)	C(22)-C(23)-C(18)	118.9(7)
C(39)-Os(3)-Os(2)	87.0(2)	C(25)-C(24)-C(29)	118.9(6)
C(37)-Os(3)-Os(2)	90.5(2)	C(25)-C(24)-P(2)	120.2(5)
C(36)-Os(3)-Os(1)	156.3(3)	C(29)-C(24)-P(2)	120.6(5)
C(38)-Os(3)-Os(1)	99.8(2)	C(24)-C(25)-C(26)	121.0(7)
C(39)-Os(3)-Os(1)	87.8(2)	C(27)-C(26)-C(25)	119.7(8)
C(37)-Os(3)-Os(1)	89.2(2)	C(26)-C(27)-C(28)	120.6(7)
Os(2)-Os(3)-Os(1)	60.236(9)	C(29)-C(28)-C(27)	119.6(8)
C(6)-P(1)-C(12)	106.5(3)	C(28)-C(29)-C(24)	120.2(8)
C(6)-P(1)-C(2)	101.9(3)	O(3)-C(30)-Os(1)	174.6(6)
C(12)-P(1)-C(2)	102.6(3)	O(4)-C(31)-Os(1)	176.3(6)
C(6)-P(1)-Os(1)	122.0(2)	O(5)-C(32)-Os(2)	175.7(7)
C(12)-P(1)-Os(1)	115.5(2)	O(6)-C(33)-Os(2)	175.9(7)
C(2)-P(1)-Os(1)	105.8(2)	O(7)-C(34)-Os(2)	179.3(9)
C(24)-P(2)-C(18)	103.6(3)	O(8)-C(35)-Os(2)	175.3(6)
C(24)-P(2)-C(1)	102.7(3)	O(9)-C(36)-Os(3)	178.1(9)
C(18)-P(2)-C(1)	104.3(3)	O(10)-C(37)-Os(3)	176.1(7)
C(24)-P(2)-Os(1)	115.7(2)	O(11)-C(38)-Os(3)	176.9(9)
C(18)-P(2)-Os(1)	122.3(2)	O(12)-C(39)-Os(3)	173.2(7)

[a]Numbers in parentheses are estimated standard deviations in the least significant digits.

$Os_3(CO)_{10}$(bpcd) is nearly 0.63 Å shorter than the internuclear P(1)···P(2) separation in 1,2-$Os_3(CO)_{10}$(bpcd) and in keeping with the trend reported for the free ligand (*vide supra*) and other mono- and polynuclear compounds containing a chelating bpcd ligand. Consistent with the premise concerning the greater stability for chelation of the bpcd ligand in the 1,1-$Os_3(CO)_{10}$(bpcd) cluster vis-á-vis the 1,2-$Os_3(CO)_{10}$(bpcd) cluster are the angles of 105.8(2)°, 106.0(2)°, 120.9(5)°, 118.7(5)° found for the Os(1)-P(1)-C(2), Os(1)-P(2)-C(1), P(1)-C(2)-C(1), and P(2)-C(1)-C(2) linkages, respectively. These values show minimal deviation from the idealized bond angles of 109° associated with an sp^3 hybridized central phosphorus atom and 120° associated with an sp^2 hybridized central carbon atom. Contrary to 1,2-$Os_3(CO)_{10}$(bpcd), the five-membered ring of the coordinated bpcd ligand is essentially coplanar with the triosmium plane in the 1,1-$Os_3(CO)_{10}$(bpcd) cluster.

M. X-Ray Diffraction Structure of $HOs_3(CO)_8(\mu_3\text{-}C_6H_4)[\mu_2,\eta^1\text{-}PPhC{=}C(PPh_2)C(O)CH_2C(O)]$

Single crystals of $HOs_3(CO)_8(\mu_3\text{-}C_6H_4)[\mu_2,\eta^1\text{-}PPhC{=}C(PPh_2)C(O)CH_2C(O)]$ were successfully grown by the slow evaporation method using a toluene/hexanes solution containing pure $HOs_3(CO)_8(\mu_3\text{-}C_6H_4)[\mu_2,\eta^1\text{-}PPhC{=}C(PPh_2)C(O)CH_2C(O)]$. The molecular structure of $HOs_3(CO)_8(\mu_3\text{-}C_6H_4)[\mu_2,\eta^1\text{-}PPhC{=}C(PPh_2)C(O)CH_2C(O)]$ was determined by X-ray diffraction analysis. $HOs_3(CO)_8(\mu_3\text{-}C_6H_4)[\mu_2,\eta^1\text{-}PPhC{=}C(PPh_2)C(O)CH_2C(O)]$ exists as discrete molecules in the unit cell with no unusually short inter- or intramolecular contacts. The X-ray data processing and collection parameters are listed in Table 3.9, and selected bond distances and angles

given in Table 3.10. The molecular composition and the numbering scheme for $HOs_3(CO)_8(\mu_3\text{-}C_6H_4)[\mu_2,\eta^1\text{-}PPhC{=}C(PPh_2)C(O)CH_2C(O)]$ are presented in the ORTEP diagram in Figure 3.22.

The solid-state structure of $HOs_3(CO)_8(\mu_3\text{-}C_6H_4)[\mu_2,\eta^1\text{-}PPhC{=}C(PPh_2)C(O)CH_2C(O)]$ reveals that there are two Os-Os bonds, one benzyne ligand, and one phosphido ligand in this open triangular cluster, with the latter two groups coming from the cleavage of a P-Ph bond of one of the ancillary phenyl groups. The 3.809(1) Å separation between Os(1) and Os(3) atoms accounts for the opened polyhedron found in $HOs_3(CO)_8(\mu_3\text{-}C_6H_4)[\mu_2,\eta^1\text{-}PPhC{=}C(PPh_2)C(O)CH_2C(O)]$. The three osmium atoms and the phosphorus atom of the phosphido ligand form a square plane, that is face-capped by the benzyne ligand. The benzyne ligand, acting formally as a four-electron donor, coordinates to the Os(1) and Os(3) atoms with two σ bonds and to Os(2) by a π bond. The bond distances between the benzyne ligand and the Os_3 frame are 2.169(14) Å, 2.160(13) Å, 2.313(14) Å, and 2.332(15) Å for Os(1)-C(24), Os(3)-C(25), Os(2)-C(24), and Os(2)-C(25) vectors, respectively. The bond distances for Os(1)-Os(2) and Os(2)-Os(3) vectors are 2.9188(10) Å and 2.8184(10) Å, respectively, with an average distance of 2.8686 Å, which is comparable with those bond distances in other triosmium clusters.[8] The bond angle of 83.18(2)$^\circ$ for Os(1)-Os(2)-Os(3) linkage further supports the ring-opened structure for this triosmium cluster. The phosphorus atom of the phosphido ligand coordinates to Os(1) and Os(3) with distances of 2.373(4) and 2.374(3) Å, respectively. The phosphorus atom of the phosphine ligand that is σ-bonded to the

Os(1) center exhibits a bond distance of 2.350(3) Å, which is slightly shorter than the other two P-Os bond distances.

N. Cyclic Voltammetric Investigation of bpcd, $Os_3(CO)_{11}(\eta^1$-bpcd), 1,2-$Os_3(CO)_{10}$(bpcd) ,1,2-$Os_3(CO)_{10}$(bpcd), $HOs_3(CO)_9[\mu$-$(PPh_2)C{=}C\{PPh(C_6H_4)\}C(O)CH_2C(O)]$ and $HOs_3(CO)_8(\mu_3$-$C_6H_4)[\mu_2,\eta^1$-$PPhC{=}C(PPh_2)C(O)CH_2C(O)]$

Cyclic voltammetry (CV) studies on the free bpcd ligand and the bpcd-coordinated triosmium carbonyl clusters were performed at a platinum-disk electrode in CH_2Cl_2 solvent containing 0.25 M *tetra*-n-butylammonium perchlorate (TBAP) as the supporting electrolyte. The results of these CV experiments are summarized in Table3.11. The bpcd ligand and all the clusters exhibit a reversible, one-electron reduction, based on peak current (I_p^a / I_p^c) ratios of unity and linear plots of the current function (I_p) versus the square root of the scan rate over the scan rates of 0.05-1.00 V/s.[12] The ΔE_p values of around 90 mV for the bpcd ligand and the bpcd coordinated-clusters suggest that the reduction in these compounds may be kinetically slow (i.e., k_{het} is slow) given that each of these values is greater than the 80 mV peak-to-peak separation observed for the one-electron standard ferrocene. For all of these clusters, the possession of an uncoordinated 4-cyclopenten-1,3-dione ring leads to a reversible one-electron reduction due to electron accession involving the π^* system of the redox-active carbocyclic ring.[13,10a] The disappearance of the reduction behavior upon the coordination of the C=C π bond of the dione moiety has been demonstrated in the study of $Ru_2(CO)_6$(bpcd) by Richmond et al.[14] It is typically observed that electron transfer leads to fragmentation of a majority of

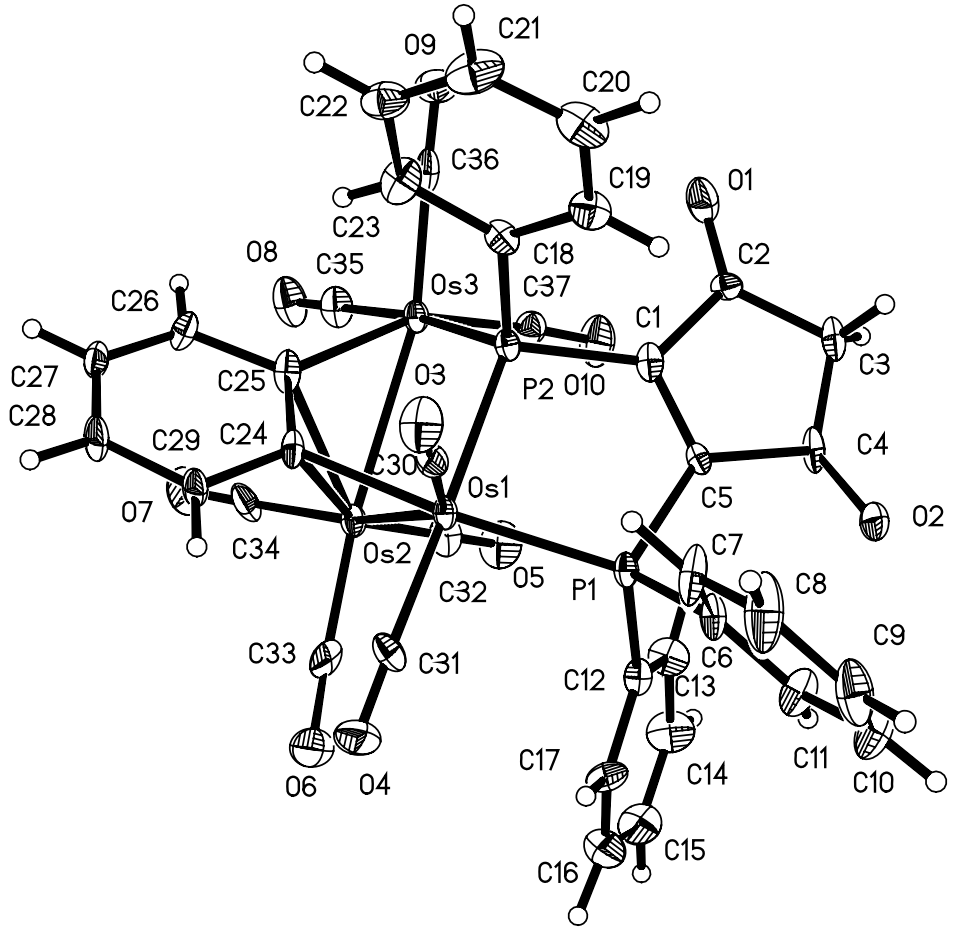

Figure 3.22. ORTEP diagram of $HOs_3(CO)_8(\mu_3\text{-}C_6H_4)[\mu_2,\eta^1\text{-}PPhC{=}C(PPh_2)C(O)CH_2C(O)]$ showing the thermal ellipsoids at the 50% probability level. (Reprinted with permission from *Organometallics* **2006**, 25, 930-945. Copyright 2006 American Chemical Society.)

Table 3.9. Crystal Data and Structure Refinement for $HOs_3(CO)_8(\mu_3\text{-}C_6H_4)[\mu_2,\eta^1\text{-}PPhC{=}C(PPh_2)C(O)CH_2C(O)]$

Empirical formula	$Os_3C_{44}H_{29}O_{10}P_2$	
Formula weight	1350.21	
Temperature	213(2) K	
Wavelength	0.71073 Å	
Crystal system	Monoclinic	
Space group	P2(1)/c	
Unit cell dimensions	a = 22.350(6) Å	α = 90°
	b = 11.511(3) Å	β = 111.281(5)°
	c = 17.383(5) Å	γ = 90°
Volume	4167(2) $Å^3$	
Z	4	
Density (calculated)	2.152 Mg/m^3	
Absorption coefficient	9.260 mm^{-1}	
F(000)	2524	
Crystal size	0.31 x 0.16 x 0.03 mm^3	
Theta range for data collection	2.02 to 28.29°	
Index ranges	$-29 \le h \le 29$, $-15 \le k \le 15$, $-22 \le l \le 22$	
Reflections collected	34779	
Independent reflections	9724 [R(int) = 0.2122]	
Completeness to theta = 28.29°	93.8%	
Absorption correction	Empirical	
Max. and min. transmission factors	1.000, 0.515	
Refinement method	Full-matrix least-squares on F^2	
Data / restraints / parameters	9724 / 0 / 534	
Goodness-of-fit on F_2	0.993	
Final R indices [I > 2sigma(I)]	R1 = 0.0780, wR2 = 0.1643	
R indices (all data)	R1 = 0.1181, wR2 = 0.1809	
Extinction coefficient	0.00000(6)	
Largest diff. peak and hole	7.498 and -2.449 e. $Å^{-3}$	

Table 3.10. Bond Lengths [Å] and Angles [°] for $HOs_3(CO)_8(\mu_3\text{-}C_6H_4)[\mu_2,\eta^1\text{-}PPhC{=}C(PPh_2)C(O)CH_2C(O)]$[a]

Bond Distances			
Os(1)-C(30)	1.880(17)	C(2)-C(3)	1.521(19)
Os(1)-C(31)	1.909(15)	C(3)-C(4)	1.49(2)
Os(1)-C(24)	2.169(13)	C(4)-C(5)	1.521(17)
Os(1)-P(1)	2.350(3)	C(6)-C(11)	1.37(2)
Os(1)-P(2)	2.373(4)	C(6)-C(7)	1.38(2)
Os(1)-Os(2)	2.9188(10)	C(7)-C(8)	1.39(2)
Os(2)-C(33)	1.864(17)	C(8)-C(9)	1.36(3)
Os(2)-C(32)	1.879(16)	C(9)-C(10)	1.42(3)
Os(2)-C(34)	1.909(17)	C(10)-C(11)	1.42(2)
Os(2)-C(24)	2.313(14)	C(12)-C(17)	1.353(19)
Os(2)-C(25)	2.332(15)	C(12)-C(13)	1.40(2)
Os(2)-Os(3)	2.8184(10)	C(13)-C(14)	1.35(2)
Os(3)-C(37)	1.905(16)	C(14)-C(15)	1.33(2)
Os(3)-C(35)	1.915(16)	C(15)-C(16)	1.36(3)
Os(3)-C(36)	1.924(18)	C(16)-C(17)	1.34(2)
Os(3)-C(25)	2.160(13)	C(18)-C(19)	1.36(2)
Os(3)-P(2)	2.374(3)	C(18)-C(23)	1.41(2)
P(1)-C(5)	1.815(13)	C(19)-C(20)	1.41(2)
P(1)-C(6)	1.821(13)	C(20)-C(21)	1.40(3)
P(1)-C(12)	1.829(14)	C(21)-C(22)	1.39(3)
P(2)-C(18)	1.811(13)	C(22)-C(23)	1.37(2)
P(2)-C(1)	1.826(14)	C(24)-C(25)	1.394(19)
O(1)-C(2)	1.218(15)	C(24)-C(29)	1.442(18)
O(2)-C(4)	1.184(17)	C(25)-C(26)	1.465(19)
O(3)-C(30)	1.150(18)	C(26)-C(27)	1.32(2)
O(4)-C(31)	1.134(17)	C(27)-C(28)	1.40(2)
O(5)-C(32)	1.141(19)	C(28)-C(29)	1.40(2)
O(6)-C(33)	1.173(18)	C(38)-C(43)	1.35(2)

Table 3.10. Con't.

O(7)-C(34)	1.127(19)	C(38)-C(39)	1.39(3)
O(8)-C(35)	1.163(19)	C(38)-C(44)	1.47(3)
O(9)-C(36)	1.108(18)	C(39)-C(40)	1.33(3)
O(10)-C(37)	1.156(19)	C(40)-C(41)	1.39(3)
C(1)-C(5)	1.375(18)	C(41)-C(42)	1.35(3)
C(1)-C(2)	1.497(18)	C(42)-C(43)	1.33(3)
	Bond Angles		
C(30)-Os(1)-C(31)	89.2(6)	O(1)-C(2)-C(1)	123.3(13)
C(30)-Os(1)-C(24)	95.0(6)	O(1)-C(2)-C(3)	129.1(12)
C(31)-Os(1)-C(24)	95.7(6)	C(1)-C(2)-C(3)	107.6(11)
C(30)-Os(1)-P(1)	102.4(5)	C(4)-C(3)-C(2)	104.9(11)
C(31)-Os(1)-P(1)	94.8(5)	O(2)-C(4)-C(3)	127.8(13)
C(24)-Os(1)-P(1)	159.8(4)	O(2)-C(4)-C(5)	124.5(14)
C(30)-Os(1)-P(2)	92.2(4)	C(3)-C(4)-C(5)	107.7(12)
C(31)-Os(1)-P(2)	177.8(4)	C(1)-C(5)-C(4)	109.5(12)
C(24)-Os(1)-P(2)	82.5(4)	C(1)-C(5)-P(1)	120.0(10)
P(1)-Os(1)-P(2)	86.56(12)	C(4)-C(5)-P(1)	130.1(10)
C(30)-Os(1)-Os(2)	146.5(5)	C(11)-C(6)-C(7)	120.0(13)
C(31)-Os(1)-Os(2)	94.9(4)	C(11)-C(6)-P(1)	121.4(10)
C(24)-Os(1)-Os(2)	51.5(4)	C(7)-C(6)-P(1)	118.6(11)
P(1)-Os(1)-Os(2)	110.35(9)	C(6)-C(7)-C(8)	119.9(16)
P(2)-Os(1)-Os(2)	82.98(9)	C(9)-C(8)-C(7)	121.2(19)
C(33)-Os(2)-C(32)	98.1(7)	C(8)-C(9)-C(10)	120.0(18)
C(33)-Os(2)-C(34)	94.7(6)	C(11)-C(10)-C(9)	117.9(16)
C(32)-Os(2)-C(34)	93.0(7)	C(6)-C(11)-C(10)	120.9(14)
C(33)-Os(2)-C(24)	99.9(6)	C(17)-C(12)-C(13)	117.8(14)
C(32)-Os(2)-C(24)	153.8(6)	C(17)-C(12)-P(1)	119.7(11)
C(34)-Os(2)-C(24)	104.3(6)	C(13)-C(12)-P(1)	122.3(11)
C(33)-Os(2)-C(25)	130.5(6)	C(14)-C(13)-C(12)	119.9(16)
C(32)-Os(2)-C(25)	131.4(6)	C(15)-C(14)-C(13)	120.9(17)

Table 3.10. Con't.

C(34)-Os(2)-C(25)	84.3(6)	C(14)-C(15)-C(16)	119.7(16)
C(24)-Os(2)-C(25)	34.9(5)	C(17)-C(16)-C(15)	120.7(17)
C(33)-Os(2)-Os(3)	170.3(4)	C(16)-C(17)-C(12)	120.8(16)
C(32)-Os(2)-Os(3)	83.7(5)	C(19)-C(18)-C(23)	117.5(14)
C(34)-Os(2)-Os(3)	94.7(5)	C(19)-C(18)-P(2)	122.7(12)
C(24)-Os(2)-Os(3)	75.5(4)	C(23)-C(18)-P(2)	119.5(11)
C(25)-Os(2)-Os(3)	48.5(3)	C(18)-C(19)-C(20)	121.8(16)
C(33)-Os(2)-Os(1)	87.5(4)	C(21)-C(20)-C(19)	118.9(17)
C(32)-Os(2)-Os(1)	115.2(4)	C(22)-C(21)-C(20)	119.5(16)
C(34)-Os(2)-Os(1)	151.2(5)	C(23)-C(22)-C(21)	120.0(17)
C(24)-Os(2)-Os(1)	47.3(3)	C(22)-C(23)-C(18)	122.0(16)
C(25)-Os(2)-Os(1)	72.8(3)	C(25)-C(24)-C(29)	120.4(12)
Os(3)-Os(2)-Os(1)	83.18(2)	C(25)-C(24)-Os(1)	122.9(10)
C(37)-Os(3)-C(35)	89.8(7)	C(29)-C(24)-Os(1)	116.5(10)
C(37)-Os(3)-C(36)	95.6(6)	C(25)-C(24)-Os(2)	73.3(8)
C(35)-Os(3)-C(36)	95.1(7)	C(29)-C(24)-Os(2)	122.0(10)
C(37)-Os(3)-C(25)	156.2(6)	Os(1)-C(24)-Os(2)	81.2(4)
C(35)-Os(3)-C(25)	92.5(6)	C(24)-C(25)-C(26)	116.5(12)
C(36)-Os(3)-C(25)	107.8(6)	C(24)-C(25)-Os(3)	124.7(10)
C(37)-Os(3)-P(2)	95.0(5)	C(26)-C(25)-Os(3)	118.8(10)
C(35)-Os(3)-P(2)	172.9(5)	C(24)-C(25)-Os(2)	71.8(8)
C(36)-Os(3)-P(2)	89.6(4)	C(26)-C(25)-Os(2)	123.6(10)
C(25)-Os(3)-P(2)	81.0(4)	Os(3)-C(25)-Os(2)	77.6(4)
C(37)-Os(3)-Os(2)	102.5(4)	C(27)-C(26)-C(25)	122.6(14)
C(35)-Os(3)-Os(2)	88.7(5)	C(26)-C(27)-C(28)	121.3(14)
C(36)-Os(3)-Os(2)	161.6(4)	C(27)-C(28)-C(29)	119.7(13)
C(25)-Os(3)-Os(2)	53.9(4)	C(28)-C(29)-C(24)	119.4(13)
P(2)-Os(3)-Os(2)	85.20(9)	O(3)-C(30)-Os(1)	178.5(14)
C(5)-P(1)-C(6)	104.4(6)	O(4)-C(31)-Os(1)	178.3(14)
C(5)-P(1)-C(12)	105.8(6)	O(5)-C(32)-Os(2)	178.1(14)

Table 3.10. Con′t.

C(6)-P(1)-C(12)	103.5(6)	O(6)-C(33)-Os(2)	176.2(16)
C(5)-P(1)-Os(1)	106.5(4)	O(7)-C(34)-Os(2)	179.2(16)
C(6)-P(1)-Os(1)	123.7(5)	O(8)-C(35)-Os(3)	179.2(14)
C(12)-P(1)-Os(1)	111.5(4)	O(9)-C(36)-Os(3)	176.7(13)
C(18)-P(2)-C(1)	102.0(6)	O(10)-C(37)-Os(3)	175.6(14)
C(18)-P(2)-Os(1)	111.0(5)	C(43)-C(38)-C(39)	120(2)
C(1)-P(2)-Os(1)	105.2(5)	C(43)-C(38)-C(44)	123(2)
C(18)-P(2)-Os(3)	116.7(5)	C(39)-C(38)-C(44)	117(2)
C(1)-P(2)-Os(3)	114.7(4)	C(40)-C(39)-C(38)	118(2)
Os(1)-P(2)-Os(3)	106.73(13)	C(39)-C(40)-C(41)	122(2)
C(5)-C(1)-C(2)	109.6(12)	C(42)-C(41)-C(40)	119(2)
C(5)-C(1)-P(2)	121.2(10)	C(43)-C(42)-C(41)	120(2)
C(2)-C(1)-P(2)	129.0(10)	C(42)-C(43)-C(38)	121(2)

[a]Numbers in parentheses are estimated standard deviations in the least significant digits.

carbonyl clusters because a metal-metal antibonding orbital is populated upon reduction.[15] However, no fragmentation of these bpcd-coordinated triosmium carbonyl clusters was observed during the CV time scale in these experiments due to the redox-active 4-cyclopenten-1,3-dione ring, which provides an alternate ligand-based LUMO. The cyclic voltammogram of 1,1-$Os_3(CO)_{10}$(bpcd) and ferrocene taken at ambient temperature is shown in Figure 3.23.

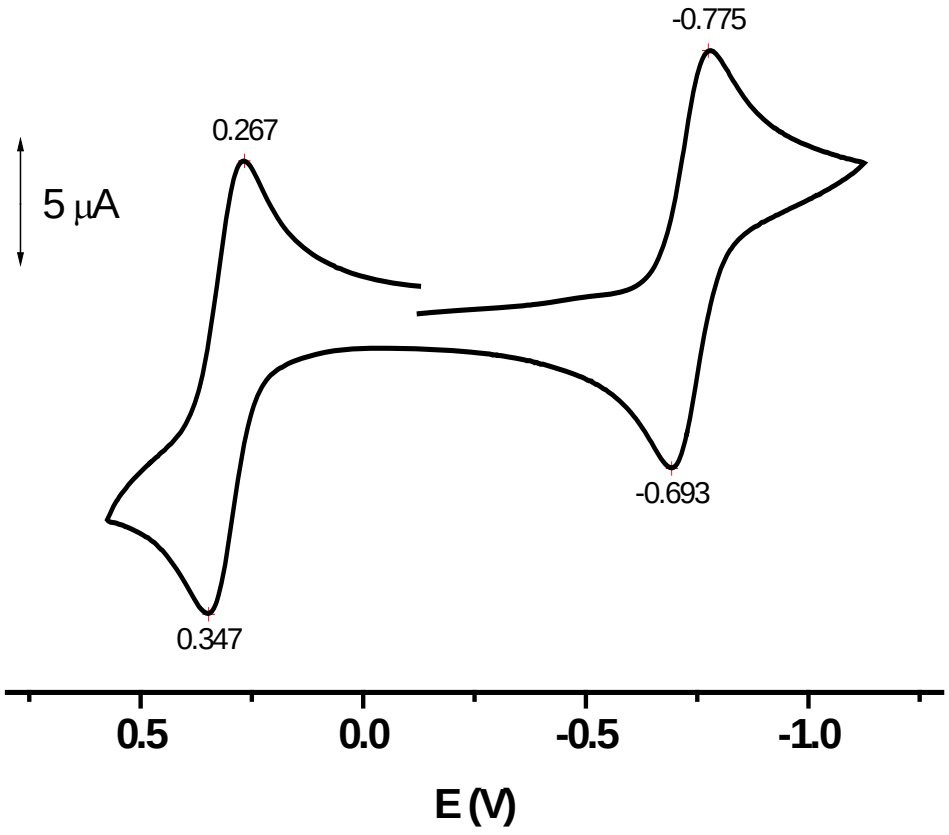

Figure 3.23. Cyclic voltammogram of 1,1-$Os_3(CO)_{10}$(bpcd) and ferrocene (ca. 10^{-3} M) at ambient temperature in CH_2Cl_2 containing 0.25 M TBAP and a scan rate of 0.25 V/s.

Table 3.11. CV Data for the bpcd Ligand and Os_3 Clusters (Volts)[a]

	Redox couple (0/1$^-$)[b]		
Compound[c]	E_p^c	E_p^a	$E_{1/2}$
a	-1.149	-1.057	-1.103
b	-0.955	-0.855	-0.905
c	-0.720	-0.626	-0.673
d	-0.775	-0.693	-0.734
e	-0.757	-0.669	-0.713
f	-0.887	-0.787	-0.837

[a]In ca. 10^{-3} M of CH_2Cl_2 solution containing 0.25 M TBAP at ambient temperature and a scan rate of 0.25 V/s. Potentials are in volts relative to a silver wire quasi-reference electrode, calibrated against ferrocene. [b] E_p^c and E_p^a refer to the cathodic and anodic peak potentials of the CV waves. The half-wave potential $E_{1/2}$, which represents the chemically redox couple, is defined as $(E_p^c + E_p^a)/2$. [c](a) bpcd, (b) $Os_3(CO)_{11}(\eta^1$-bpcd), (c) 1,2-$Os_3(CO)_{10}$(bpcd), (d) 1,1-$Os_3(CO)_{10}$(bpcd), (e) $HOs_3(CO)_9[\mu$-$(PPh_2)C{=}C\{PPh(C_6H_4)\}C(O)CH_2C(O)]$, and (f) $HOs_3(CO)_8(\mu_3$-$C_6H_4)[\mu_2,\eta^1$-$PPhC{=}C(PPh_2)C(O)CH_2C(O)]$.

O. Chapter References

1. (a) Cartwright, S.; Clucas, J. A.; Dawson, R. H.; Foster, D. F.; Harding, M. M.; Smith, A. K. *J. Organomet. Chem.* **1986**, *302*, 403. (b) Clucas, J. A.; Foster, D. F.; Harding, M. M.; Smith, A. K. *J. Chem. Soc., Chem. Commun.* **1984**, 949. (c) Foster, D. F.; Harrison, J.; Nicholls, B. S.; Smith, A. K. *J. Organomet. Chem.* **1985**, *295*, 99. (d) Clucas, J. A.; Harding, M. M.; Smith, A. K. *J. Chem. Soc., Chem. Commun.* **1985**, 1280. (e) Deeming, A. J.; Donovan-Mtunzi, S.; Kabir, S. E. *J. Organomet. Chem.* **1984**, *276*, C65. (f) Deeming, A. J.; Hardcastle, K. I.; Kabir, S. E. *J. Chem. Soc., Dalton Trans.* **1988**, 827. (g) Deeming, A. J.; Kabir, S. E. *J. Organomet. Chem.* **1988**, *340*, 359. (h) Churchill, M. R.; DeBoer, B. G. *Inorg. Chem.* **1977**, *16*, 878.

2. (a) Alex, R. F.; Pomeroy, R. K. *Organometallics* **1987**, *6*, 2437. (b) Johnson, B. F. G.; Lewis, J.; Reichert, B. E.; Schorpp, K. T. *J. Chem. Soc., Dalton Trans.* **1976**, 1403. (c) Nordlander, E.; Johnson, B. F. G.; Lewis, J.; Owen, S. M.; Raithby, P. R. *J. Chem. Soc., Dalton Trans.* **1996**, 3825. (d) Bruce, M. I.; Matisons, J. G.; Nicholson, B. K. *J. Organomet. Chem.* **1983**, *247*, 321. (e) Persson, R.; Monari, M.; Gobetto, R.; Russo, A.; Aime, S.; Calhorda, M. J.; Nordlander, E. *Organometallics* **2001**, *20*, 4150.

3. (a) Deeming, A. J.; Donovan-Mtunzi, S.; Kabir, S. E. *J. Organomet. Chem.* **1987**, *333*, 253. (b) Azam, K. A.; Hursthouse, M. B.; Kabir, S. E.; Malik, K. M. A.; Mottalib, M. A. *J. Chem. Crystallogr.* **1999**, *29*, 813. (c) Deeming, A. J. *Adv. Organomet. Chem.* **1986**, *26*, 1. (d) Deeming, A. J.; Donovan-Mtunzi, S.; Hardcastle, K. I.; Kabir, S. E.; Henrick, K.; McPartlin, M. *J. Chem. Soc., Dalton Trans.* **1988**, 579. (e) Kabir, S. E.;

Miah, A.; Nesa, L.; Uddin, K.; Hardcastle, K. I.; Rosenberg, E.; Deeming, A. J. *J. Organomet. Chem.* **1995**, *492*, 41.

4. Clucas, J. A.; Dawson, R. H.; Dolby, P. A.; Harding, M. M.; Pearson, K.; Smith, A. K. *J. Organomet. Chem.* **1986**, *311*, 153.

5. (a) Green, M.; Orpen, A. G.; Schaverien, C. J. *J. Chem. Soc., Dalton Trans.* **1989**, 1333. (b) Bruce, M. I.; Pain, G. N.; Hughes, C. A.; Patrick, J. M.; Skelton, B. W.; White, A. H. *J. Organomet. Chem.* **1986**, *307*, 343. (c) Adams, R. D.; Tanner, J. T. *Organometallics* **1989**, *8*, 563. (d) Constable, E. C.; Johnson, B. F. G.; Khan, F. K.; Lewis, J.; Raithby, P. R.; Mikulcik, P. *J. Organomet. Chem.* **1991**, *403*, 15. (e) Biradha, K.; Hansen, V. M.; Leong, W. K.; Pomeroy, R. K.; Zaworotko, M. J. *J. Clust. Sci.* **2000**, *11*, 285.

6. (a) Alex, R. F.; Einstein, F. W. B.; Jones, R. H.; Pomeroy, R. K. *Inorg. Chem.* **1987**, *26*, 3175. (b) Bruce, M. I.; Liddell, M. J.; Hughes, C. A.; Skelton, B. H.; White, A. H. *J. Organomet. Chem.* **1988**, *347*, 157. (c) Bruce, M. I.; Liddell, M. J.; Hughes, C. A.; Patrick, J. M.; Skelton, B. H.; White, A. H. *J. Organomet. Chem.* **1988**, *347*, 181. (d) Bruce, M. I.; Liddell, M. J.; Skawkataly, O. B.; Hughes, C. A.; Skelton, B. H.; White, A. H. *J. Organomet. Chem.* **1988**, *347*, 207.

7. Lauher, J. W. *J. Am. Chem. Soc.* **1986**, *108*, 1521.

8. (a) Brown, M. P.; Dolby, P. A.; Harding, M. M.; Mathews, A. J.; Smith, A. K. *J. Chem. Soc., Dalton Trans.* **1993**, 1671. (b) Kabir, S. E.; Johns, C. A.; Malik, K. M. A.; Mottalib, M. A.; Rosenberg, E. *J. Organomet. Chem.* **2001**, *625*, 112. (c) Orpen, A. G.;

Brammer, L.; Allen, F. K.; Kennard, O.; Watson, D. G.; Taylor, R. *J. Chem. Soc., Dalton Trans.* **1989**, S1.

9. Berners, S. J.; Colquhoun, L. A.; Healy, P. C.; Byriel, K. A.; Hanna, J. V. *J. Chem. Soc., Dalton Trans.* **1992**, 3357.

10. (a) Yang, K.; Bott, S. G.; Richmond, M. G.; *Organometallics* **1994**, *13*, 3788. (b) Watson, W. H.; Ejsmont, K.; Liu, J.; Richmond, M. G. *J. Chem. Crystallogr.* **2003**, *33*, 775.

11. (a) Kabir, S. E.; Miah, M. A.; Sarker, N. C.; Hussain, G. M. G.; Hardcastle, K. I.; Nordlander, E.; Rosenberg, E. *Organometallics* **2005**, *24*, 3315. (b) Ang, S. G.; Zhong, X.; Ang, H. G. *J. Organomet. Chem.* **2003**, *665*, 218. (c) Akter, J.; Azam, K. A.; Kabir, S. E.; Abdul Malik, K. M.; Abdul M. M. *Inorg. Chem. Commun.* **2000**, *3*, 553. (d) Ang, H. G.; Ang, S. G.; Wang, X. *J. Chem. Soc., Dalton Trans.* **2000**, 3429. (e) Deeming, A. J.; Smith, M. B. *J. Chem. Soc., Dalton Trans.* **1993**, 3383. (f) Deeming, A. J.; Powell, N. I.; Arce, A. J.; De Sanctis, Y.; Manzur, J. *J. Chem. Soc., Dalton Trans.* **1991**, 3381.

12. Bard, A. J.; Faulkner, L. R. *Electrochemical Methods*; Wiley: New York, 1980.

13. Shen, H.; Williams, T. J.; Bott, S. G.; Richmond, M. G. *J. Organomet. Chem.* **1995**, *505*, 1.

14. Shen, H.; Bott, S. G.; Richmond, M. G. *Organometallics* **1995**, 14, 4625.

15. (a) Cyr, J. E.; Rieger, P. H. *Organometallics* **1991**, *10*, 2153. (b) Bond, A. M.; Dawson, P. A.; Peake, B. M.; Robinsin, B. H.; Simpson, J. *Inorg. Chem.* **1977**, *16*, 2199. (c) Cyr, J. E.; DeGray, J. A.; Gosser, D. K.; Lee, E. S.; Rieger, P. H.

Organometallics **1985**, *4*, 950. (d) Zanello, P.; Aime, S.; Osella, D. *Organometallics* **1984**, *3*, 1374.

CHAPTER IV

DISCUSSION AND CONCLUSION

A. Fluxional Mechanism of CO Scrambling in 1,2-$Os_3(CO)_{10}$(cDPPEn) and 1,1-$Os_3(CO)_{10}$(cDPPEn)

The fluxionality of CO in 1,2-$Os_3(CO)_{10}$(cDPPEn) and 1,1-$Os_3(CO)_{10}$(cDPPEn) was studied by VT $^{13}C\{^1H\}$ NMR spectroscopy. The limiting ^{13}C NMR spectrum for 1,2-$Os_3(CO)_{10}$(cDPPEn) obtained at –38.7 °C shows four sharp singlets at δ 191.49, 184.96, 178.91 and 173.92 with an integral ratio of 4:2:2:2 (Figure 4.1). This suggests the 1,2-$Os_3(CO)_{10}$(cDPPEn) molecule has C_{2v} symmetry in solution. Warming the sample leads to line broadening of peaks a and c, whereas peaks b and d remain sharp up to 66.8 °C. Coalescence of peaks a and c was observed at 54.7 °C. Line broadening of peaks b and d was observed when the temperature was increased above 43.3 °C, with coalescence for peaks b and d estimated at ca. 90.2 °C. The fluxional behavior of the CO ligands in 1,2-$Os_3(CO)_{10}$(cDPPEn) is similar to that found in 1,2-$Os_3(CO)_{10}[Ph_2P(CH_2)_nPPh_2]$ (n = 1, 2, 3, or 4) and 1,2-$Os_3(CO)_{10}(PEt_3)_2$, except that 1,2-$Os_3(CO)_{10}$(dppe) gives five singlets in its limiting ^{13}C NMR spectrum due to the fact that its symmetry is lower than C_{2v} in solution.[1]

There are two mechanisms that account for the CO scrambling behavior in 1,2-$Os_3(CO)_{10}$(cDPPEn). The lower energy mechanism operates by exchanging two equatorial and four axial CO ligands over the two cDPPEn-bridged osmium atoms (Scheme 4.1) in a vertical plane, as shown in Scheme 4.2. Exchange of the CO ligands in the other two vertical planes is blocked by the equatorial phosphine ligands. The other

higher energy exchange process is a turnstile mechanism, which is observed at temperatures (> 50 °C). This promotes the scrambling of the CO groups (labeled as b and d). This mechanism exchanges the two equatorial and one axial carbonyl ligands at the unique, non-phosphine-substituted osmium center (Scheme 4.3). Rate constants and free energies of activation at the estimated coalescence temperature for each operating CO exchange mechanism in 1,2- $Os_3(CO)_{10}$(cDPPEn) are shown in Table 4.1.[2]

Scheme 4.1. Terminal-bridge CO exchange of 1,2-$Os_3(CO)_{10}$(diphosphine) via a di-μ-CO bridged intermediate where the diphosphine is cDPPEn or bpcd.

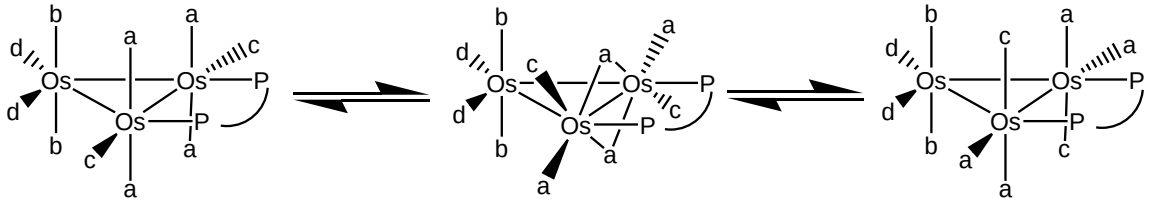

Scheme 4.2. 1,1- and 1,2-$Os_3(CO)_{10}$(diphosphine) isomers; o = CO, P—P = diphosphine. The planes illustrated each contain six CO ligands allowing a 'merry-go-round' mechanism via a di-μ-CO bridged intermediate where the diphosphine is cDPPEn or bpcd.

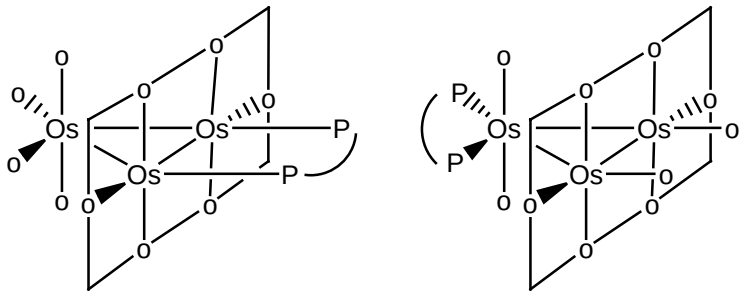

1,2-$Os_3(CO)_{10}$(diphosphine) 1,1-$Os_3(CO)_{10}$(diphosphine)

The limiting ^{13}C NMR spectrum of 1,1-$Os_3(CO)_{10}$(cDPPEn) recorded at –38.7 °C

shows one triplet and three singlet resonances at δ 196.39, 185.34, 178.59, and 171.24,

Scheme 4.3. Turnstile mechanism for axial-equatorial CO exchange around a single osmium metal center in 1,2-$Os_3(CO)_{10}$(diphosphine) where the diphosphine is cDPPEn or bpcd.

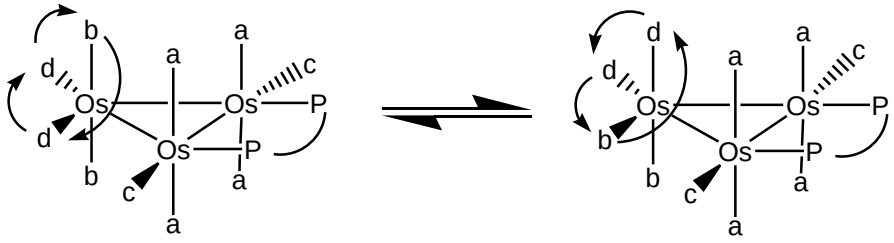

with a ratio of 2:4:2:2 (Figure 4.2). A detailed VT $^{13}C\{^1H\}$ NMR study shows line broadening for peak b, c and d on warming, while peak a still remains sharp up to 21.2 °C. Coalescence of the b, c, and d resonances was observed at 66.8 °C, which can be explained by the two-center, merry-go-round and the turnstile exchange mechanisms that operate simultaneously (see Scheme 4.4 and 4.5). In this case, the vertical plane for the two-center CO exchange is contained by two nonphosphine-coordinated osmium atoms, whereas there are two single-metal centers for the one-center turnstile exchange. Interestingly, peak a at δ 196.39 starts to broaden above 32.0 °C and disappears into the baseline at temperatures > 90 °C. This may be interpreted by a three-center exchange of the three axial CO ligands in a conical surface on the same side of the metal plane via tri-μ-CO intermediates.[3] The calculated rate constants and the free energies of activation at

the estimated coalescence temperature for each operating CO exchange mechanism in 1,2- $Os_3(CO)_{10}$(cDPPEn) were calculated, with the data displayed in Table 4.1.[2]

B. Kinetic Investigation for the Reversible Isomerization between 1,2-$Os_3(CO)_{10}$(cDPPEn) and 1,1-$Os_3(CO)_{10}$(cDPPEn) and the Associated Diphosphine Isomerization Mechanism

The kinetic study on the isomerization reaction involving 1,2-$Os_3(CO)_{10}$(cDPPEn) and 1,1-$Os_3(CO)_{10}$(cDPPEn) was conducted by using both UV-VIS and ^{31}P NMR spectroscopies, the latter of which method provides unequivocal evidence for the reversible equilibrium between 1,2-$Os_3(CO)_{10}$(cDPPEn) and 1,1-$Os_3(CO)_{10}$(cDPPEn). The approach to equilibrium for the isomerization between 1,2-$Os_3(CO)_{10}$(cDPPEn) and 1,1-$Os_3(CO)_{10}$(cDPPEn) was monitored by ^{31}P NMR spectroscopy in toluene-d_8 over the temperature range of 358.0 and 373.0 K, with the data from the experiment at the latter temperature displayed in Figure 4.3. The plot of the concentration of each species over total Os_3 concentration versus time reveals smooth exponential decay and growth curves for the consumption of cluster 1,2-$Os_3(CO)_{10}$(cDPPEn) and formation of cluster 1,1-$Os_3(CO)_{10}$(cDPPEn), respectively. Non-linear regression analysis of these data afforded a first-order rate constant for the consumption of 1,2-$Os_3(CO)_{10}$(cDPPEn) [k_e = 1.82 (4) x 10^{-4} s^{-1}] that was nearly identical to the rate determined for the formation of 1,1-$Os_3(CO)_{10}$(cDPPEn) [k_e = 1.74 (2) x 10^{-4} s^{-1}] (Figure 4.4). The rate constants (k_e) reported for the two ^{31}P NMR experiments in Table 4.2 represent an average of the reaction rates from the decay and growth curves of cluster of 1,2-$Os_3(CO)_{10}$(cDPPEn) and 1,1-$Os_3(CO)_{10}$(cDPPEn). The final ^{31}P NMR spectrum in Figure 4.3 recorded after

11 hr of thermolysis (> 10 half-lives) clearly favors the chelating isomer (δ 37.86) and affords a K_{eq} = 6.9 for the 1,2-$Os_3(CO)_{10}$(cDPPEn)⇆1,1-$Os_3(CO)_{10}$(cDPPEn) isomerization. An identical K_{eq} value was determined from the ^{31}P NMR experiment conducted at 358.0 K. With the K_{eq} value in hand, the first-order rate constants k_1 and k_{-1}, for the forward and reverse reactions, respectively, are readily extracted and are reported

Scheme 4.4. Terminal-bridge CO exchange of 1,1-$Os_3(CO)_{10}$(diphosphine) via a di-μ-CO bridged intermediate where the diphosphine is cDPPEn or bpcd.

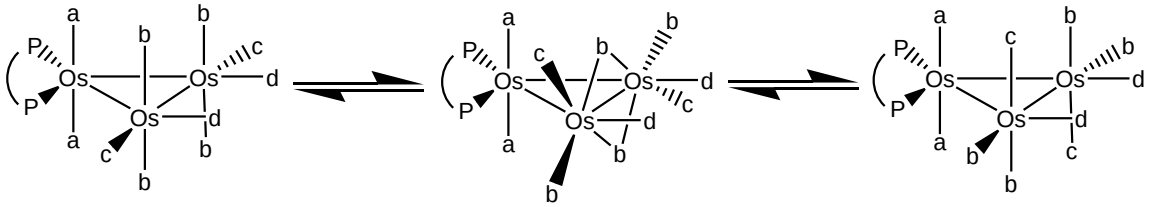

Scheme 4.5. Turnstile mechanism for axial-equatorial CO exchange of 1,1-$Os_3(CO)_{10}$(diphosphine) around a single osmium metal center where the diphosphine is cDPPEn or bpcd.

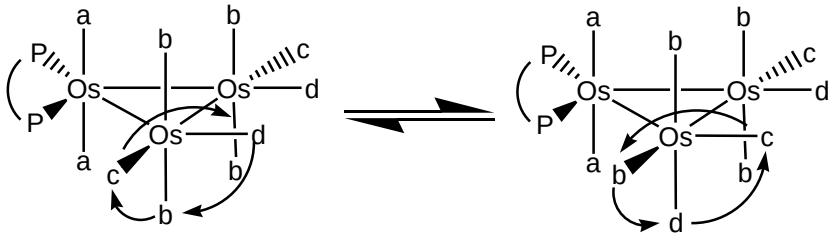

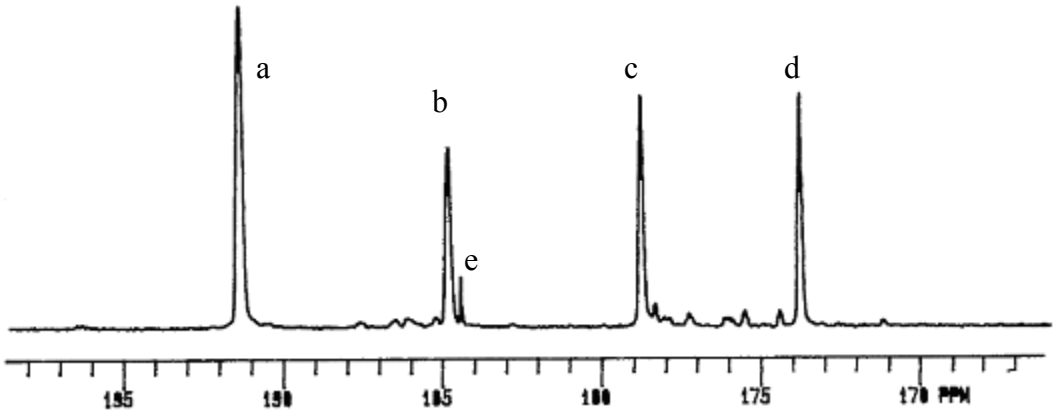

Figure 4.1. $^{13}C\{^{1}H\}$ NMR spectrum of ^{13}CO-enriched 1,2-$Os_3(CO)_{10}$(cDPPEn) recorded in C_7D_8 at –38.7 °C and under 1 atm ^{13}CO. (a) δ 191.49 (axial), (b) δ 184.96 (axial), (c) δ 178.91 (equatorial), (d) δ 173.92 (equatorial) and ^{13}CO dissolved in solution: (e) δ 184.56.

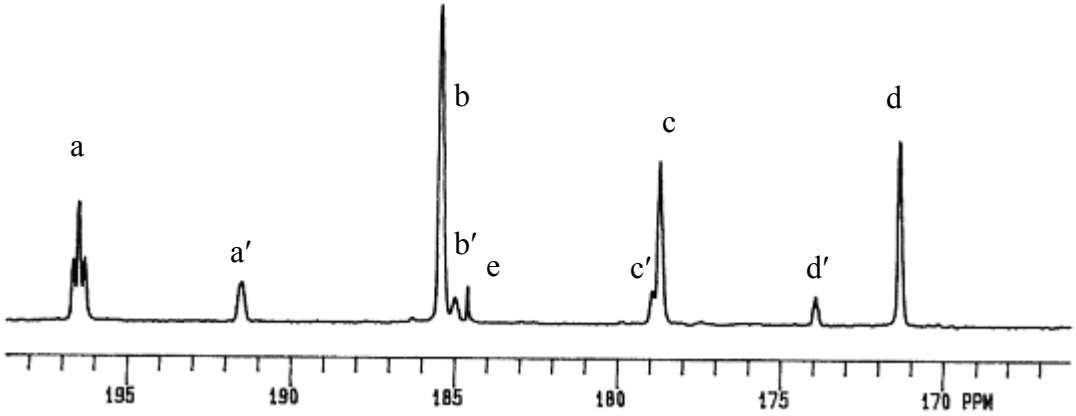

Figure 4.2. $^{13}C\{^{1}H\}$ NMR spectrum of ^{13}CO-enriched mixture of 1,2-$Os_3(CO)_{10}$(cDPPEn) and 1,1-$Os_3(CO)_{10}$(cDPPEn) in equilibrium with a ratio of 1:7 recorded in C_7D_8 at –38.7 °C and under 1 atm ^{13}CO. Cluster 1,1-$Os_3(CO)_{10}$(cDPPEn): (a) δ 196.39, (b) δ 185.34, (c) δ 178.59, and (d) δ 171.24; peak a′, b′, c′ and d′ from 1,2-$Os_3(CO)_{10}$(cDPPEn); peak e from ^{13}CO.

Table 4.1. The Estimated Coalescence Temperature (T_c), Rate Constant (k), and Free energy of Activation ($\Delta G^{\ddagger}$) for CO Scrambling in $Os_3(CO)_{10}$(cDPPEn)

Compound	Mechanism[a]	T_c (°C)	k (s^{-1})	$\Delta G^{\ddagger}$ (Kcal/mol)
1,2-isomer	a	54.7	1.40×10^3	14.6
	b	90.2	1.23×10^3	16.3
1,1-isomer	a	54.7	7.49×10^2	15.0
	b	66.8	8.16×10^2	15.5
	c	90.2	1.23×10^3	16.3

[a]Mechanism a---two-center terminal-bridge-terminal exchange involving 6 CO ligands; b---one-center turnstile exchange involving 3 CO ligands; c---three-center exchange of three axial CO ligands.

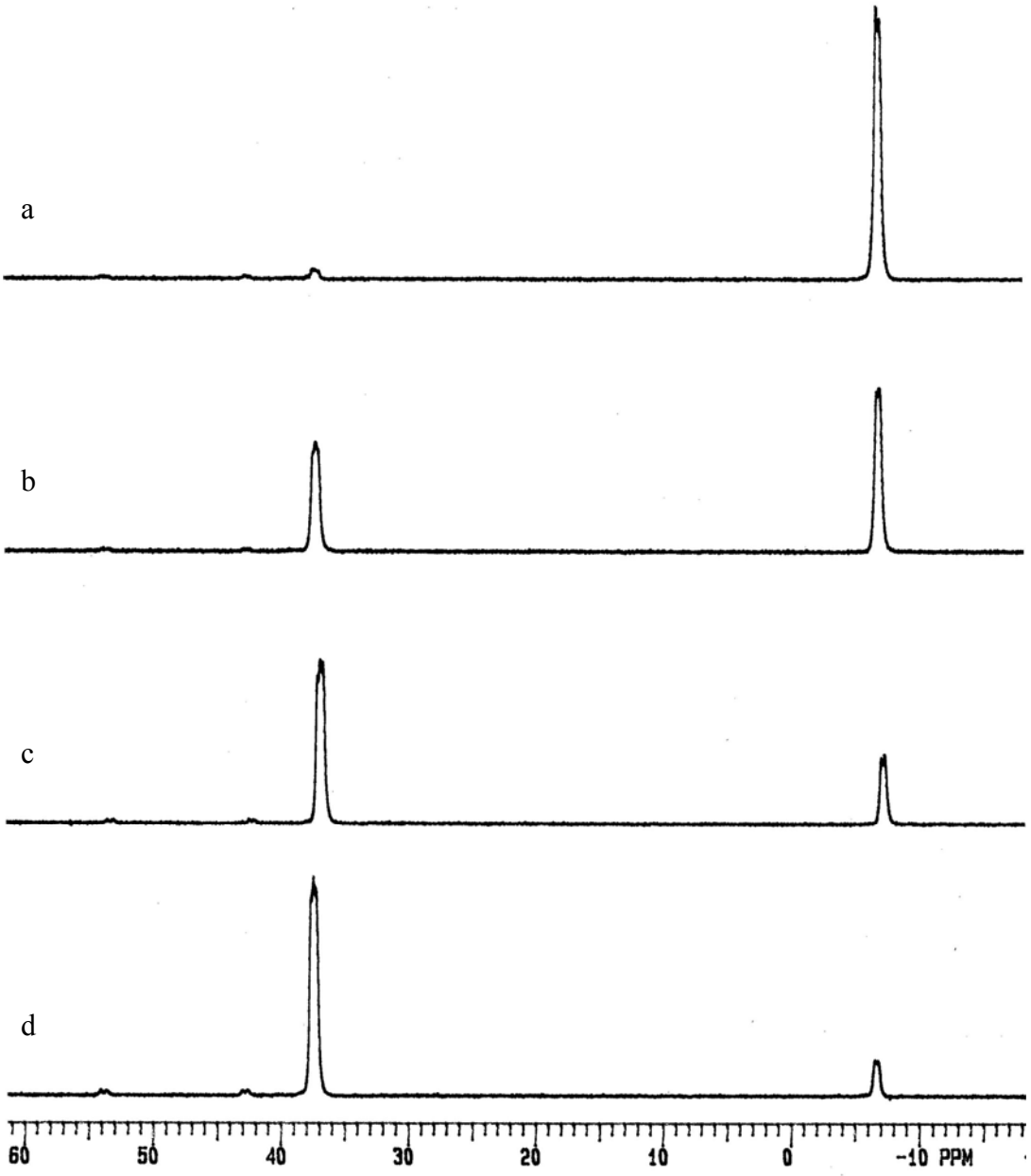

Figure 4.3. Representative ^{31}P NMR spectra recorded at 100 °C in toluene-d_8 for thermolysis of 1,2-$Os_3(CO)_{10}$(cDPPEn). (a) 0.0 hr, (b) 1.0 hr, (c) 3.0 hr, (d) 11.0 hr.

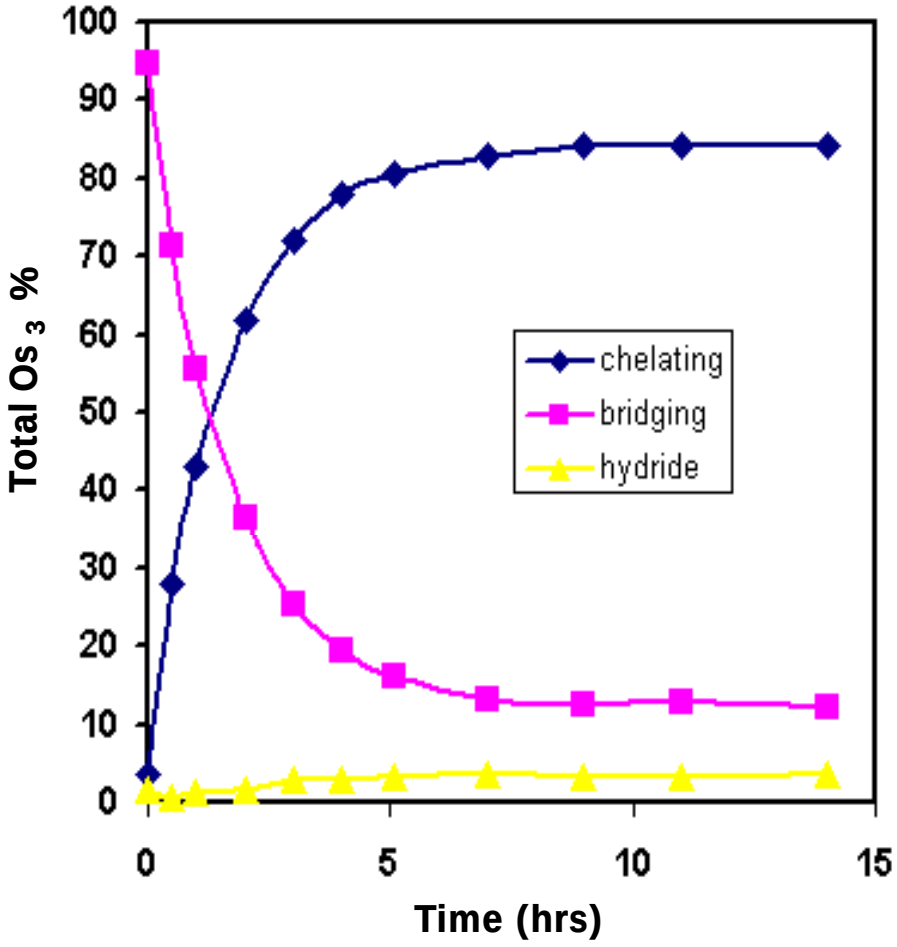

Figure 4.4. Plot for the disappearance of 1,2-$Os_3(CO)_{10}$(cDPPEn) and the appearance of 1,1-$Os_3(CO)_{10}$(cDPPEn) and $HOs_3(CO)_9$[(Z)-$PhP(C_6H_4)CH{=}CHPPh_2$] during thermolysis of 1,2-$Os_3(CO)_{10}$(cDPPEn) in C_7D_8 at 100 °C over time. (Reprinted with permission from *Organometallics* **2005**, 24, 5431-5439. Copyright 2005 American Chemical Society.)

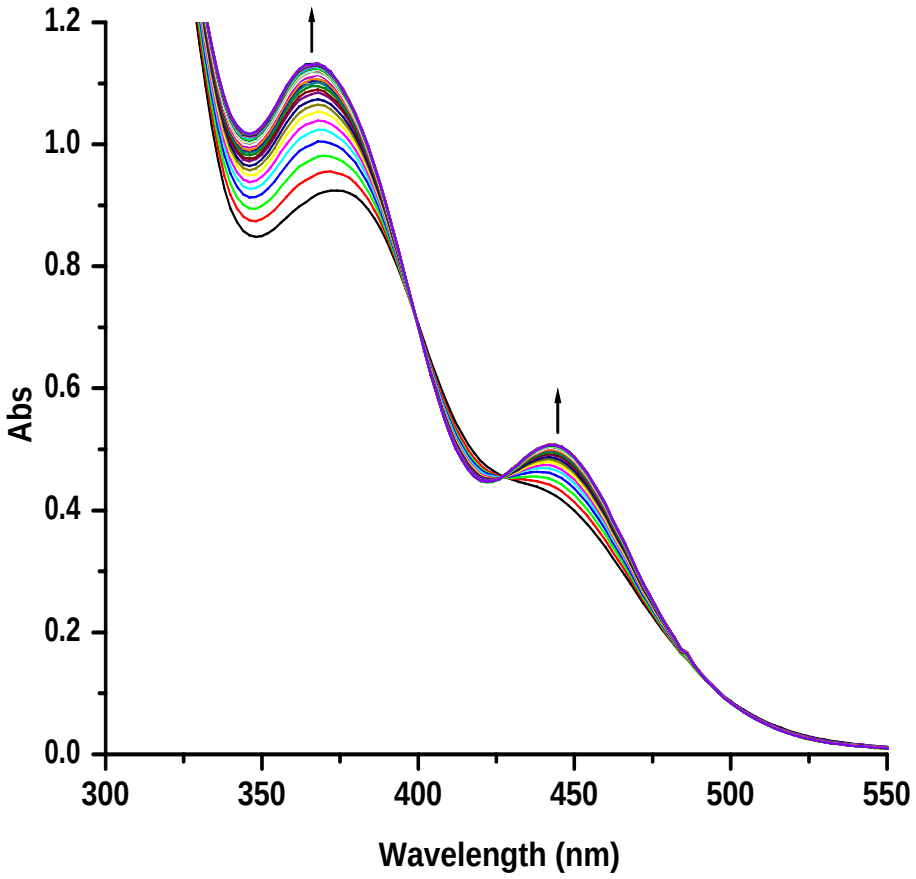

Figure 4.5. UV-VIS spectral changes for the isomerization in $Os_3(CO)_{10}$(cDPPEn) recorded at 100 °C under 1 atm CO in toluene. (Reprinted with permission from *Organometallics* **2005**, 24, 5431-5439. Copyright 2005 American Chemical Society.)

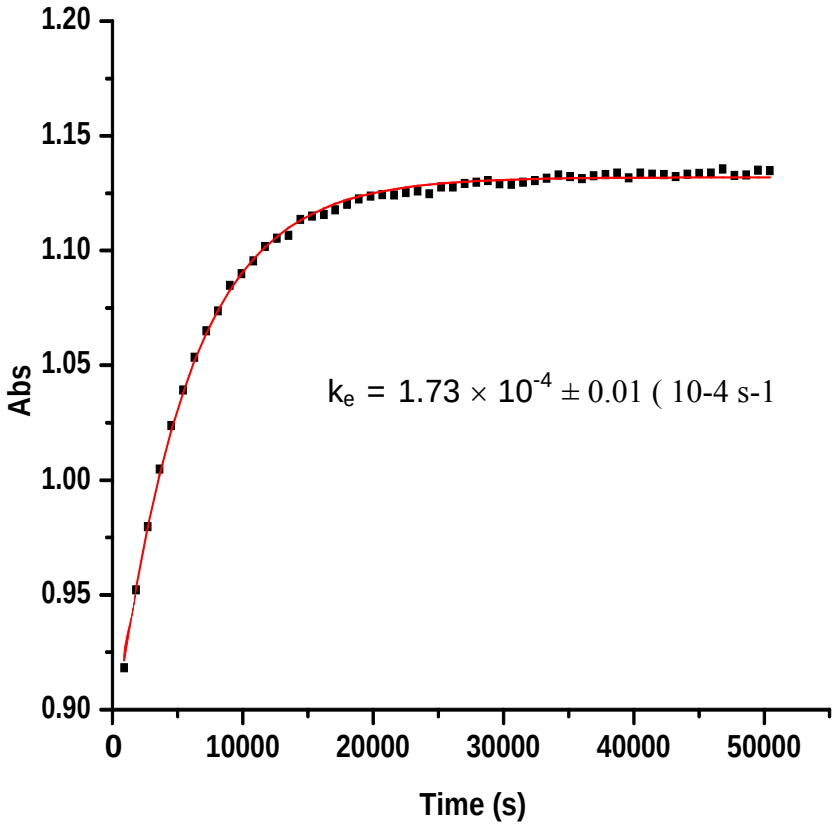

Figure 4.6. The UV-VIS absorbance versus time curves at 368nm for the experimental data (■) and the least-squares fit of k_e (solid line) for the isomerization of $Os_3(CO)_{10}$(cDPPEn) recorded at 100 °C in toluene under 1 atm CO.

Table 4.2. Kinetic Data for the Isomerization of 1,2-$Os_3(CO)_{10}$(cDPPEn) and 1,1-$Os_3(CO)_{10}$(cDPPEn) in Toluene[a]

Temp (K)	10^4k_e (s^{-1})[b]	10^4k_1 (s^{-1})	10^4k_{-1} (s^{-1})	Method
358.0	0.37 ± 0.01	0.32 ± 0.01	0.05 ± 0.01	^{31}P NMR
358.5	0.40 ± 0.01	0.35 ± 0.01	0.05 ± 0.01	UV-VIS
364.0	0.66 ± 0.01	0.58 ± 0.01	0.08 ± 0.01	UV-VIS
369.0	1.16 ± 0.02	1.01 ± 0.02	0.15 ± 0.02	UV-VIS
373.0	1.78 ± 0.04	1.56 ± 0.04	0.22 ± 0.04	^{31}P NMR
373.0	1.76 ± 0.01	1.54 ± 0.01	0.22 ± 0.01	UV-VIS
373.0	1.75 ± 0.02			UV-VIS[c]
378.0	2.92 ± 0.14	2.55 ± 0.14	0.37 ± 0.14	UV-VIS
381.5	3.82 ± 0.12	3.34 ± 0.12	0.48 ± 0.12	UV-VIS

[a]All kinetic data were collected under 1 atm of CO unless otherwise noted. The quoted UV-VIS kinetic data represent an average of two, independent measurements. [b]The quoted rate constants (k_e) represent the rate towards equilibrium, as determined by following the increase in the 368 nm band (UV-VIS) and the changes in the ^{31}P resonances for the bridging and chelating isomers (^{31}P NMR). [c]Experiment conducted in a Fischer-Porter tube under 6.8 atm CO (constant pressure). Only the determined value of k_e is reported here. (Reprinted with permission from *Organometallics* **2005**, 24, 5431-5439. Copyright 2005 American Chemical Society.)

in Table 4.2. Finally, the hydride cluster observed in Figure 4.4 at δ 43 and 54 after 11 hr of thermolysis accounted for less than 4% of the total Os_3 concentration.

The kinetics for the isomerization reaction were also studied by UV-VIS spectroscopy in toluene solution under 1 atm of CO over the temperature range of 358.5-381.5 K by following the increase in the absorbance of the 368 nm band belonging to 1,1-$Os_3(CO)_{10}$(cDPPEn). The UV-VIS spectral changes for the thermolysis of 1,2-$Os_3(CO)_{10}$(cDPPEn) in toluene carried out at 373 K are shown Figure 4.5, where clearly defined isosbestic points at 394 and 437 nm are seen to accompany the reversible transformation. The excellent fit between the least-squares regression curve and the absorbance data (Figure 4.6) confirms that the isomerization is well-behaved and free from complications. Unlike the ^{31}P NMR experiments where the thermally promoted loss of CO in 1,1-$Os_3(CO)_{10}$(cDPPEn) gives rise to small quantities of the hydride cluster $HOs_3(CO)_9[(Z)\text{-}PhP(C_6H_4)CH{=}CHPPh_2]$, the amount of hydride cluster present in the UV-VIS experiments is predicted to be negligible. The equilibrium between the chelating cluster and hydride cluster in the presence of CO mandates the suppression of the hydride cluster for reactions carried out under high concentrations of CO relative to the isomeric clusters $Os_3(CO)_{10}$(cDPPEn). A conservative 10-fold concentration excess of CO relative to the bridging and chelating clusters is predicted from available solubility data for CO in toluene.[4] The rate constants for the approach to equilibrium (k_e), along with the values of k_1 and k_{-1}, as computed with the aforementioned K_{eq} value for 1,2-$Os_3(CO)_{10}$(cDPPEn)⇆1,1-$Os_3(CO)_{10}$(cDPPEn), are given in Table 4.2. A caveat worth pointing out is that the reversible first-order behavior for the 1,2-

$Os_3(CO)_{10}$(cDPPEn)⇆1,1-$Os_3(CO)_{10}$(cDPPEn) equilibrium could have easily been misinterpreted as an irreversible first-order conversion had the UV-VIS data been analyzed in the absence of the ^{31}P NMR data. The UV-VIS data collected at 373 K furnished values for k_e, k_1, and k_{-1} in excellent agreement with those values determined by the ^{31}P NMR experiment, underscoring the validity of the data obtained from the two different experiments. That the presence of added CO does not affect the equilibrium between 1,2-$Os_3(CO)_{10}$(cDPPEn) and 1,1-$Os_3(CO)_{10}$(cDPPEn) was demonstrated by the reaction conducted under 6.8 atm of CO. Here the value of 1.75 (2) x 10^{-4} s^{-1} found for k_e is within experimental error to the corresponding reaction run under 1 atm of CO.

Eyring plots of ln (k_1/T) and ln (k_{-1}/T) versus T^{-1} allowed for the determination of the isomerization activation parameters for the forward and reverse reaction directions for $Os_3(CO)_{10}$(cDPPEn). The calculated values of $\Delta G^{\ddagger}_{373}$ = 28.4 (6) kcal/mol, $\Delta H^{\ddagger}$ = 26.5 (6) kcal/mol, and $\Delta S^{\ddagger}$ = -5 (2) eu for the forward isomerization (1,2-$Os_3(CO)_{10}$(cDPPEn)→1,1-$Os_3(CO)_{10}$(cDPPEn)) and $\Delta G^{\ddagger}_{373}$ = 29.9 (6) kcal/mol, $\Delta H^{\ddagger}$ = 26.5 (6) kcal/mol, and $\Delta S^{\ddagger}$ = -9 (2) eu for the reverse isomerization (1,1-$Os_3(CO)_{10}$(cDPPEn)→1,2-$Os_3(CO)_{10}$(cDPPEn)) reveal that the entropy of activation is small and negative in both directions and argues against a dissociative mechanism involving the release of one of the PPh_2 moieties from the cluster frame to generate an unsaturated Os_3 cluster having a pendant η^1-diphosphine moiety. Such a phosphine ligand release process that exhibits a positive $\Delta S^{\ddagger}$ value has been demonstrated in the reductive coupling of ethane from $PtMe_4$(dppe) by Goldberg,[5] where the rate-limiting chelate opening of the diphosphine ligand in $PtMe_4$(dppe) furnishes a reactive five-

coordinate intermediate that serves as the platform for the evolution of ethane.[6]

Any acceptable mechanism for the isomerization of the cDPPEn ligand about the triosmium frame must account for the observed P-ligand/CO exchange that accompanies the reaction. A terminal-bridge-terminal sequence involving a CO group(s) and a PPh_2 moiety across an Os-Os bond(s) would effectively serve to scramble the participant ligands. The highly ordered transition state mandated by any such terminal-bridge-terminal sequence is reconciled with the negative $\Delta S^{\ddagger}$ values found from Eyring analysis of the rate data. A rate-limiting process involving the dissociation or release of one of the arms of the bidentate ligand, followed by scrambling of the diphosphine ligand and subsequent ligand ring closure (bridge or chelate), can be immediately eliminated from consideration as it would violate the observed entropies of activation and insensitivity of the reaction to added CO.

The top portion of Scheme 4.6 depicts a pairwise terminal-bridge exchange in the cluster 1,2-$Os_3(CO)_{10}$(cDPPEn) involving an axial group (CO_a) and one P-moiety across the diphosphine-bridged Os-Os bond that proceeds through the doubly bridged cluster $Os_3(CO)_9(\mu\text{-CO})[(Z)\text{-}\mu,\eta^1\text{-}Ph_2PCH{=}CHPPh_2]$. This species can produce the chelating isomer 1,1-$Os_3(CO)_{10}$(cDPPEn) ultimately upon opening of the μ-CO and μ-phosphine bridges. However, the simple opening of this doubly bridged cluster cannot give 1,1-$Os_3(CO)_{10}$(cDPPEn) directly as an additional permutation(s) or turnstile rotation(s) of the remaining spectator groups associated with the phosphine-substituted osmium centers must accompany the bridge-opening reaction. A more direct diphosphine equilibration that relies on the well-known "merry-go-round" mechanism is illustrated in the bottom

portion of Scheme 4.6. Here a terminal-bridge exchange of two equatorial CO groups and one of the phosphine centers in 1,2-$Os_3(CO)_{10}$(cDPPEn) gives rise to the triply bridged cluster $Os_3(CO)_8(\mu\text{-}CO)_2[(Z)\text{-}\mu,\eta^1\text{-}Ph_2PCH{=}CHPPh_2]$, which directly furnishes 1,1-$Os_3(CO)_{10}$(cDPPEn) upon completion of the bridge-terminal exchange.[7,8] The latter mechanism for diphosphine isomerization in $Os_3(CO)_{10}[(Z)\text{-}Ph_2PCH{=}CHPPh_2]$ is favored on the basis of its simplicity.[9] Given that no dynamic diphosphine isomerization has been observed in $Os_3(CO)_{10}$(dppe),[1a] the saturated analogue of $Os_3(CO)_{10}$(cDPPEn), the stereochemistry and rigid nature of the ancillary $(Z)\text{-}Ph_2PCH{=}CHPPh_2$ ligand is believed to actually promote the scrambling of the ligand about the cluster by maintaining constant and intimate contact between the diphosphine ligand and the osmium centers.[10] It is

Scheme 4.6. Two proposed mechanisms for diphosphine isomerization in $Os_3(CO)_{10}$(cDPPEn).

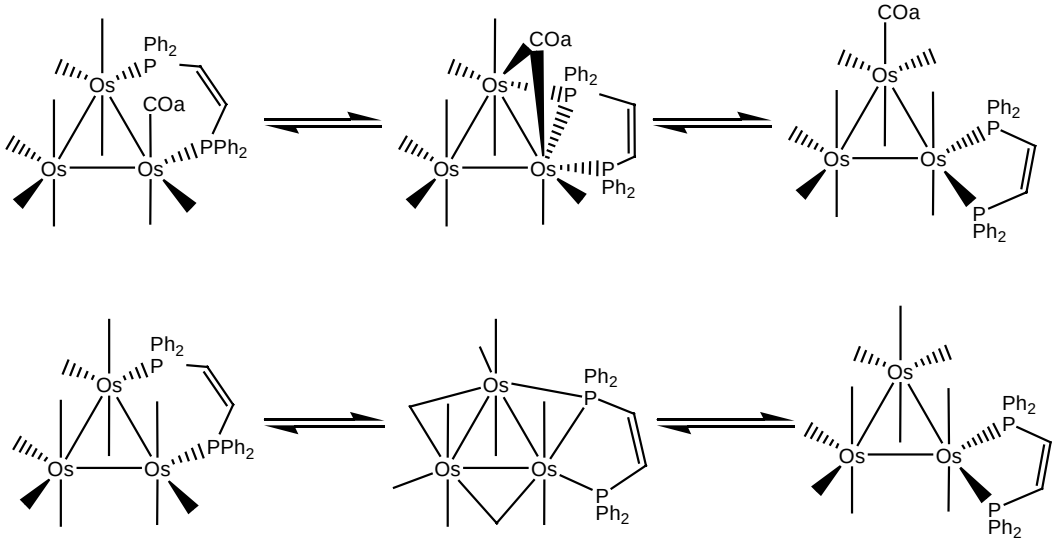

believed that this isomerization phenomenon is general in nature, at least for this genre of cluster, provided that the diphosphine ligand is rigid and possesses *cis* stereochemistry

based on observations of facile diphosphine isomerization in the cluster compounds $Os_3(CO)_{10}$(P-P) [where P-P = bpcd, 3,4-bis(diphenylphosphino)-5-methoxy-2(5H)-furanone (bmf), and 1,2-bis(diphenylphosphino)benzene].[11,12]

The dynamical migration of CO ligands about the metal centers in polynuclear clusters through terminal-bridge-terminal CO exchanges has been a phenomenologically established fact for over three decades.[13] Analogous migratory ligand behavior has only recently been observed for tertiary phosphine ligands. For example, Adams has provided conclusive NMR evidence for the intramolecular scrambling of phosphine ligands between the platinum and adjacent ruthenium centers in the mixed-metal carbide clusters $PtRu_5(\mu_6\text{-}C)(CO)_{15}P$,[14] while phosphine equilibration between the two ruthenium centers in the dinuclear compounds $Cp^*_2Ru_2(\mu\text{-}H)_2P$ has been demonstrated by Suzuki.[15,16] The postulated transformation of an η^1-phosphine ligand to that of a μ-bound phosphine in this work and the above examples is strengthened by reports showing the coordination of a tertiary P-ligand simultaneously bound to two and three metal centers.[17]

Finally, Figure 4.7 shows two free-energy diagrams for the merry-go-round isomerization for 1,2-$Os_3(CO)_{10}$(cDPPEn)$\leftrightarrows$1,1-$Os_3(CO)_{10}$(cDPPEn) at 373 K, whose major difference lies in the nature of the contribution of the putative species $Os_3(CO)_8(\mu\text{-}CO)_2[(Z)\text{-}\mu,\eta^1\text{-}Ph_2PCH{=}CHPPh_2]$. The left-hand diagram depicts a single-step isomerization where the triply bridged cluster $Os_3(CO)_8(\mu\text{-}CO)_2[(Z)\text{-}\mu,\eta^1\text{-}Ph_2PCH{=}CHPPh_2]$ functions as the transition state for the two isomers of $Os_3(CO)_{10}$(cDPPEn), while the two-step mechanism involving $Os_3(CO)_8(\mu\text{-}CO)_2[(Z)\text{-}\mu,\eta^1\text{-}Ph_2PCH{=}CHPPh_2]$ as a reactive intermediate of finite lifetime in the 1,2-

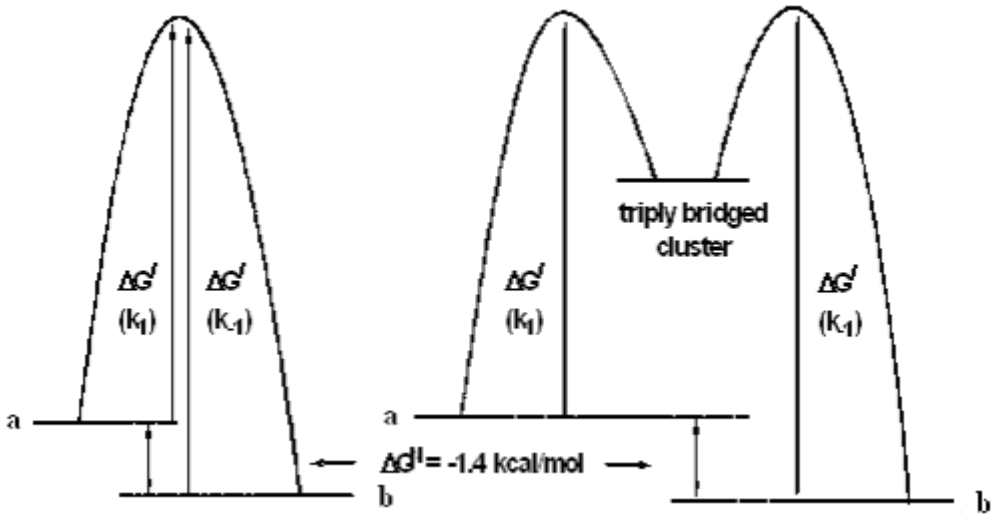

Figure 4.7. Free-energy diagrams for the merry-go-round isomerization of $Os_3(CO)_{10}$(cDPPEn) at 373 K where the triply bridged cluster $Os_3(CO)_8(\mu\text{-}CO)_2$[(Z)-μ, η^1-$Ph_2PCH{=}CHPPh_2$] functions as a transition state (left) and as a discrete intermediate of finite lifetime (right). (a) 1,2-$Os_3(CO)_{10}$(cDPPEn); (b) 1,1-$Os_3(CO)_{10}$(cDPPEn). (Reprinted with permission from *Organometallics* **2005**, 24, 5431-5439. Copyright 2005 American Chemical Society.)

$Os_3(CO)_{10}$(cDPPEn)⇆1,1-$Os_3(CO)_{10}$(cDPPEn) isomerization is shown to the right. Differentiation between the concerted (left) and the two-step (right) processes is not a trivial matter, but the data would suggest that the concerted scrambling of the diphosphine ligand is likely the correct path. The $\Delta G°$ value of -1.4 kcal/mol in favor of cluster 1,1-$Os_3(CO)_{10}$(cDPPEn), as determined from the magnitude of K_{eq} for 1,2-$Os_3(CO)_{10}$(cDPPEn)⇆1,1-$Os_3(CO)_{10}$(cDPPEn) by ^{31}P NMR spectroscopy (*vide supra*), is identical to the $\Delta\Delta G^{‡}$ value found from the kinetic experiments. This is reasonable and expected for a single-step or concerted reaction with the triply bridged cluster serving as the transition state for both 1,2-$Os_3(CO)_{10}$(cDPPEn) and 1,1-$Os_3(CO)_{10}$(cDPPEn). Theoretical calculations on the bridge-to-chelate isomerization of the $H_2PCH_2CH_2PH_2$ ligand in the dinuclear compound $Mo_2Cl_4(H_2PCH_2CH_2PH_2)_2$ reveal that a non-dissociative migration of the phosphine moieties across the Mo-Mo quadruple bond, analogous to that proposed by us in $Os_3(CO)_8(\mu\text{-}CO)_2[(Z)\text{-}\mu,\eta^1\text{-}Ph_2PCH{=}CHPPh_2]$, proceeds as a transition state and not a *bona fide* intermediate.[18,19] If the two-step process reflects the scrambling mechanism, then the fortuitous similarity in the values determined for $\Delta G°$ and $\Delta\Delta G^{‡}$ indicate that the barrier heights relating 1,2-$Os_3(CO)_{10}$(cDPPEn) and 1,1-$Os_3(CO)_{10}$(cDPPEn) to the triply bridged cluster $Os_3(CO)_8(\mu\text{-}CO)_2[(Z)\text{-}\mu,\eta^1\text{-}Ph_2PCH{=}CHPPh_2]$ must be small and identical in magnitude.

C. Fluxional Mechanism of CO Scrambling in 1,2-$Os_3(CO)_{10}$(bpcd) and 1,1-$Os_3(CO)_{10}$(bpcd)

An investigation concerning the fluxional behavior of the ancillary CO ligands in 1,2-$Os_3(CO)_{10}$(bpcd) and 1,1-$Os_3(CO)_{10}$(bpcd) was carried out by VT $^{13}C\{^1H\}$ NMR

spectroscopy. The limiting ^{13}C NMR spectrum for 1,2-$Os_3(CO)_{10}$(bpcd), which was obtained at –61.0 °C, is comparable to that of 1,2-$Os_3(CO)_{10}$(cDPPEn) and shows four sharp singlets at δ 193.07, 184.78, 178.17 and 173.12 with an integral ratio of 4:2:2:2 due to its C_{2v} symmetry (Figure 4.8). Warming the sample to –26.7 °C leads to line broadening of peaks a and c, with peaks b and d remaining sharp up to 54.7 °C. Coalescence of peaks a and c was observed at 21.2 °C. Line broadening of peaks b and d was seen at temperature above 55 °C. The coalescence temperature for peaks b and d was estimated as 90.2 °C. The fluxional behavior of the CO groups in 1,2-$Os_3(CO)_{10}$(bpcd) is similar to that of 1,2-$Os_3(CO)_{10}$(cDPPEn) except that the energy barrier is lower for the two-center merry-go-round CO exchange of the former. The exchange rate constants and the free energy of activation at coalescence for each CO exchange process in 1,2-$Os_3(CO)_{10}$(bpcd) are shown in Table 4.3.

The limiting ^{13}C NMR spectrum of 1,1- $Os_3(CO)_{10}$(bpcd) was recorded at –38.7 °C, with one triplet and three singlet resonances at δ 196.39, 185.34, 178.59, and 171.24 having a ratio of 2:4:2:2 found (Figure 4.9). VT $^{13}C\{^1H\}$ NMR analysis shows line broadening for peaks b, c, and d on warming, while peak a remains sharp up to 32.0 °C. Peaks b, c, and d coalesce at 66.8 °C, which can be explained by two simultaneously operating mechanisms, the two-center merry-go-round and turnstile exchanges (see Schemes 4.1 and 4.3). Peak a broadened at temperatures above 43.3 °C, with fast exchange found at temperatures greater than 90 °C. Table 4.3 summarizes the rate data and the free energies of activation for the two CO exchange processs.[2]

D. Diphosphine Isomerization Mechanism of $Os_3(CO)_{10}$(bpcd)

Heating the cluster 1,2- $Os_3(CO)_{10}$(bpcd) at ambient temperature (< 70 °C) leads to bpcd isomerization and formation of the chelated cluster 1,1-$Os_3(CO)_{10}$(bpcd), as depicted in Scheme 4.7. The extent of the reaction was easily assessed by ^{1}H and ^{31}P NMR spectroscopy due to the down-field shift in the methylene singlet belonging to the dione ring and the phosphorus groups of the product. Here the initial methylene resonance (in $CDCl_3$) at δ 3.06 in 1,2- $Os_3(CO)_{10}$(bpcd) is replaced by a new signal in the ^{1}H NMR spectrum at δ 3.74 for 1,1-$Os_3(CO)_{10}$(bpcd), with the associated phenyl resonances remaining invariant in terms of their general chemical shift information. The ^{31}P NMR spectrum is accompanied by a similar transformation insomuch as a new ^{31}P resonance at δ 17.97 is observed, whose large nuclear deshielding is consistent with a chelating bpcd ligand.[20] The isomeric clusters display the same R_f value on silica gel and the IR data are virtually indistinguishable given their idealized C_{2v} symmetry, negating the use of TLC analysis and IR spectroscopy as probes for the study of this reaction.

The kinetics for the conversion of cluster 1,2-$Os_3(CO)_{10}$(bpcd)→1,1-$Os_3(CO)_{10}$(bpcd) were next studied due to the small but growing number of reports on non-dissociative phosphine isomerization reactions at di- and polynuclear compounds.[14,21] The isomerization rates for 1,2-$Os_3(CO)_{10}$(bpcd)→1,1-$Os_3(CO)_{10}$(bpcd) were conveniently measured by both UV-VIS and ^{1}H NMR spectroscopies over the temperature range of 323-343 K, with the reaction rates reported in Table 4.4. The UV-VIS derived rates were obtained by following the increase in the absorbance of the 364

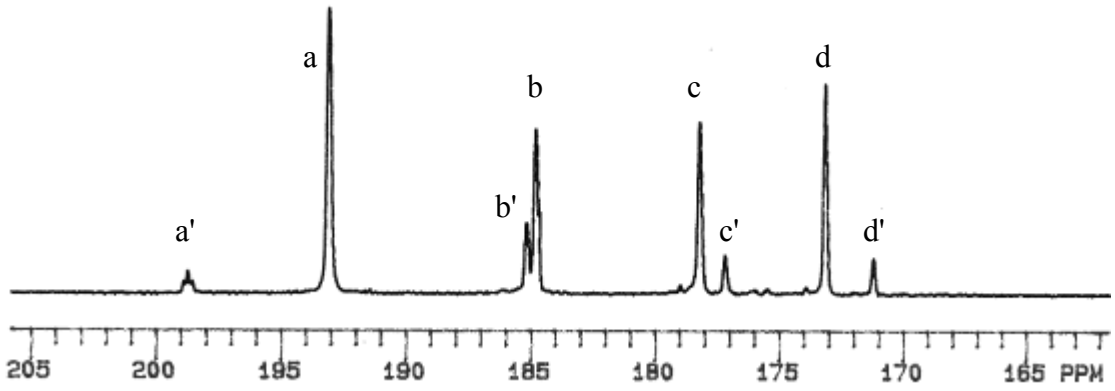

Figure 4.8. $^{13}C\{^{1}H\}$ NMR spectrum of ^{13}CO-enriched mixture of 1,2-$Os_3(CO)_{10}$(bpcd) and 1,1-$Os_3(CO)_{10}$(bpcd) with a ratio of 3:1 recorded in C_7D_8 at –61.0 °C and under 1 atm ^{13}CO. 1,2-$Os_3(CO)_{10}$(bpcd): (a) δ 193.07 (axial), (b) δ 184.78 (axial), (c) δ 178.17 (equatorial) and (d) δ 173.12 (equatorial); 1,1-$Os_3(CO)_{10}$(bpcd): (a′) δ 198.59 (axial), (b′) δ 185.03 (axial), (c′) δ 177.02 (equatorial) and (d′) δ 171.02 (equatorial).

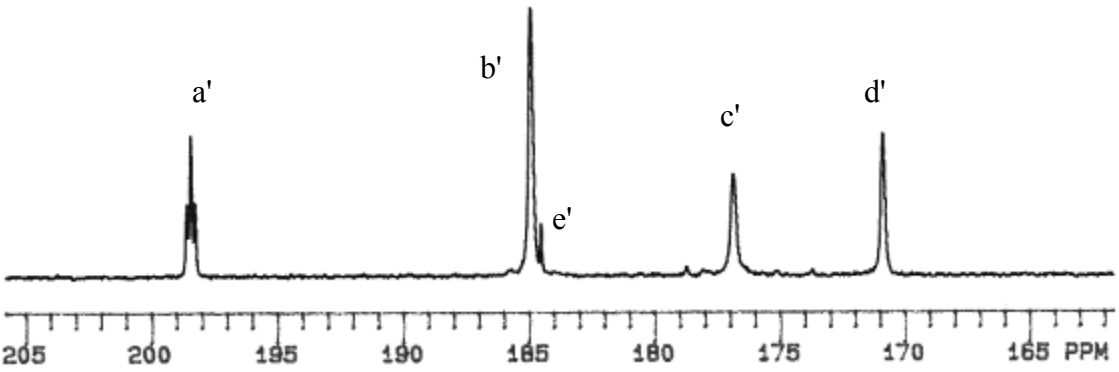

Figure 4.9. $^{13}C\{^{1}H\}$ NMR spectrum of ^{13}CO-enriched 1,1-$Os_3(CO)_{10}$(bpcd) recorded in C_7D_8 at –15.4 °C and under 1 atm ^{13}CO. (a′) δ 198.59 (axial), (b′) δ 185.03 (axial), (c′) δ 177.02 (equatorial) and (d′) δ 171.02 (equatorial); ^{13}CO: (e′) δ 184.56.

Table 4.3. The Estimated Coalescence Temperature (T_c), Rate Constant (k), and Free Energy of Activation ($\Delta G^{\ddagger}$) for CO Scrambling in $Os_3(CO)_{10}$(bpcd)

Compound	Mechanism*	T_c (°C)	k (s^{-1})	$\Delta G^{\ddagger}$ (Kcal/mol)
1,2-isomer	a	21.2	1.65×10^3	12.9
	b	90.2	1.29×10^3	16.3
1,1-isomer	a	54.7	8.89×10^2	14.9
	b	66.8	6.66×10^2	15.6
	c	90.2	1.51×10^3	16.2

*Mechanism a---two-center terminal-bridge-terminal exchange involving 6 CO ligands; b---one-center turnstile exchange involving 3 CO ligands; c---three-center exchange of three axial CO ligands.

nm band belonging to cluster 1,1-$Os_3(CO)_{10}$(bpcd). Figure 4.10 shows the UV-VIS spectral changes for the thermolysis of 1,2-$Os_3(CO)_{10}$(bpcd) in benzene solution at 323 K, where multiple, well-defined isosbestic points accompany the reaction. The fit of the least-squares regression curve and the absorbance data displayed in Figure 4.11 underscores the fact that the isomerization is well-behaved and free from kinetic complications. Complimentary ^{1}H NMR kinetic studies were also conducted in benzene-d_6 by monitoring the decrease in the methylene moiety of 1,2-$Os_3(CO)_{10}$(bpcd) at δ 1.78 (Figure 4.12). The complete consumption of this resonance was accompanied by the growth of a methylene singlet at δ 2.45 belonging to cluster 1,1-$Os_3(CO)_{10}$(bpcd). The NMR data conclusively showed that the isomerization furnished 1,1-$Os_3(CO)_{10}$(bpcd) in quantitative yield unlike the isomerization found for the related cluster $Os_3(CO)_{10}$(cDPPEn), where a reversible equilibrium that favored the chelating isomer was found (K_{eq} = 6.9 for chelate/bridge clusters over the temperature range of 358-382 K).[30] Treatment of the NMR data by traditional ln [1,2-$Os_3(CO)_{10}$(bpcd)] versus time plots or by non-linear regression analysis afforded first-order rate constants that were in excellent agreement with each other and with those data obtained from the UV-VIS studies. Moreover, plots of the total cluster concentration 1,2-$Os_3(CO)_{10}$(bpcd) and 1,1-$Os_3(CO)_{10}$(bpcd) versus time displayed smooth exponential decay and growth curves for the consumption and formation of 1,2-$Os_3(CO)_{10}$(bpcd) and 1,1-$Os_3(CO)_{10}$(bpcd), respectively. Figure 4.13 shows the stacked ^{1}H NMR spectra for isomerization of 1,2-$Os_3(CO)_{10}$(bpcd) in the presence of 10 equivalence of triphenylphosphine, which does not

complicate or participate in the ligand isomerization reaction. Inspection of the data in Table 4.4 reveals that the isomerization is unaffected by added phosphine, phosphite, and

Scheme 4.7. Sequential reactions of bpcd-coordinated triosmium carbonyl clusters involving ligand isomerization, C-H bond activation and P-C bond activation.

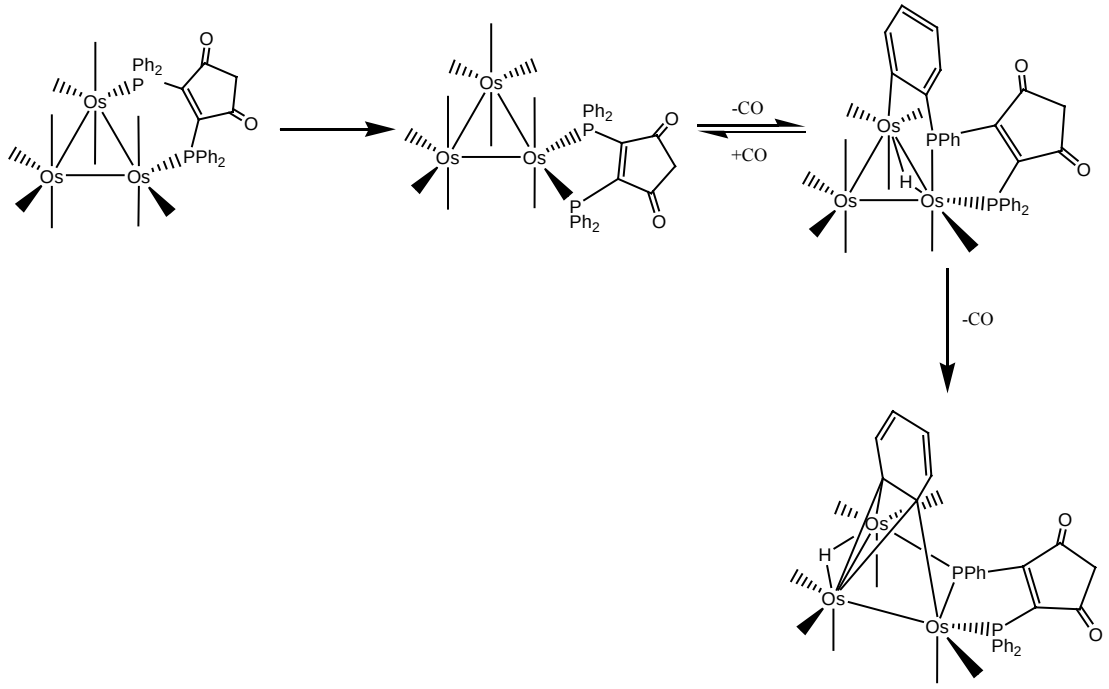

CO trapping ligands. The invariant rates in the presence of added ligands and the Eyring activation parameters [UV-VIS: $\Delta H^{\ddagger}$ = 25.0 (0.7) kcal/mol and $\Delta S^{\ddagger}$ = -2 (2) eu; NMR: $\Delta H^{\ddagger}$ = 23.9 (0.4) kcal/mol and $\Delta S^{\ddagger}$ = -4 (1) eu] strongly support a non-dissociative, rate-limiting unimolecular rearrangement of the bpcd ligand.

The above kinetic data undeniably support an intramolecular migration or transit of one of the phosphorus atoms across an Os-Os bond to afford a diphosphine-chelated

osmium center, as opposed to a process involving the dissociative release of one of the PPh_2 moieties of the bpcd ligand. This latter scenario would lead to the formation of an unsaturated cluster with an η^1 bpcd ligand that could be scavenged by any trapping ligand present; however, the expected substituted clusters $Os_3(CO)_{10}L(\eta^1\text{-bpcd})$ [L = CO, PR_3, $P(OEt)_3$] have not been observed.[22,23] Given the clean conversion of 1,2-$Os_3(CO)_{10}$(bpcd)$\rightarrow$1,1-$Os_3(CO)_{10}$(bpcd), the two most likely isomerization processes that are consistent with the kinetic data and activation parameters are shown in Scheme 4.7. A pairwise exchange of a CO ligand with an adjacent phosphorus atom, through the intermediacy of the doubly bridged cluster $Os_3(CO)_9(\mu\text{-CO})(\mu\text{-bpcd})$, gives rise to cluster 1,1-$Os_3(CO)_{10}$(bpcd). Alternatively, the merry-go-round migration involving two equatorially disposed CO ligands and a phosphorous atom can also furnish the cluster 1,2-$Os_3(CO)_{10}$(bpcd) upon bridge-terminal opening of the three bridging participants.

Distinction between these two exchange processes was sought through examination of the VT ^{13}C NMR spectra of cluster 1,2-$Os_3(CO)_{10}$(bpcd). However, the rates of CO scrambling at coalescence in 1,2-$Os_3(CO)_{10}$(bpcd) are much greater than that of ligand isomerization. Consequently, any attempt to use the ^{13}C NMR data from 1,2-$Os_3(CO)_{10}$(bpcd) to elucidate the isomerization mechanism for the slower bpcd migration to cluster 1,1-$Os_3(CO)_{10}$(bpcd) will be met with failure.[24,25] Of importance to this body of work is the fact that the bpcd ligand isomerization is facile and gives cluster 1,1-$Os_3(CO)_{10}$(bpcd) as the platform for the ensuing orthometallation described below.

E. Thermal and Photochemical Activation of 1,1-$Os_3(CO)_{10}$(bpcd) and Characterization of $HOs_3(CO)_9[\mu$-$(PPh_2)C{=}C\{PPh(C_6H_4)\}C(O)CH_2C(O)]$ and $HOs_3(CO)_8(\mu_3$-$C_6H_4)[\mu_2,\eta^1$-$PPhC{=}C(PPh_2)C(O)CH_2C(O)]$

Thermolysis of cluster 1,1-$Os_3(CO)_{10}$(bpcd) at elevated temperatures provided evidence for the activation of the bpcd ligand, as shown in Figure 4.14 for the ^{1}H NMR distribution data from a sealed-tube thermolysis conducted at 90.0 °C in toluene-d_8.[26]

Scheme 4.8. Two proposed mechanisms for diphosphine isomerization of $Os_3(CO)_{10}$(bpcd).

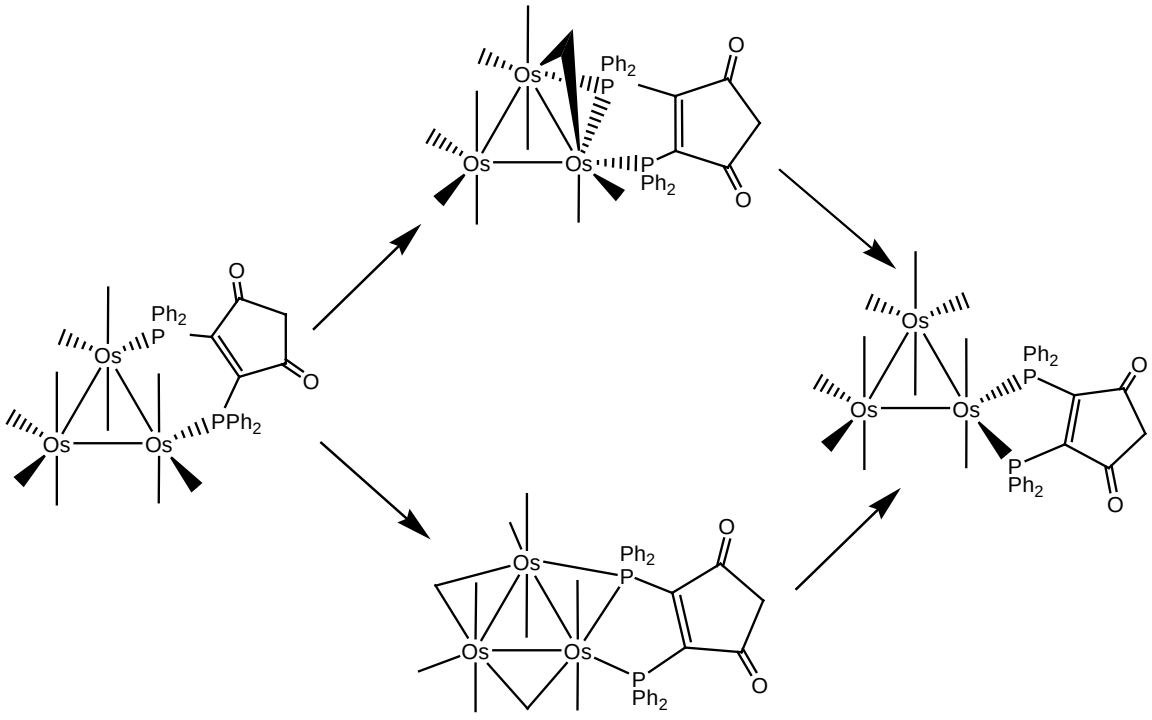

Here a rapid production of the hydrido cluster $HOs_3(CO)_9[\mu$-$(PPh_2)C{=}C\{PPh(C_6H_4)\}C(O)CH_2C(O)]$ (■) is observed, followed by the slower

formation of the benzyne-substituted cluster $HOs_3(CO)_8(\mu_3\text{-}C_6H_4)[\mu_2,\eta^1\text{-}PPhC{=}C(PPh_2)C(O)CH_2C(O)]$ (■). Heating a sealed NMR tube containing $HOs_3(CO)_9[\mu\text{-}(PPh_2)C{=}C\{PPh(C_6H_4)\}C(O)CH_2C(O)]$ under analogous conditions furnished $HOs_3(CO)_8(\mu_3\text{-}C_6H_4)[\mu_2,\eta^1\text{-}PPhC{=}C(PPh_2)C(O)CH_2C(O)]$ as the major product along with 1,1-$Os_3(CO)_{10}$(bpcd), as shown in Figure 4.15. Two important points emerging from these thermolysis experiments are that cluster 1,1-$Os_3(CO)_{10}$(bpcd) serves as the direct precursor for the formation of the hydride $HOs_3(CO)_9[\mu\text{-}(PPh_2)C{=}C\{PPh(C_6H_4)\}C(O)CH_2C(O)]$, and that this latter cluster can be converted back to 1,1-$Os_3(CO)_{10}$(bpcd) through a reversible orthometallation sequence. Carrying out the thermolyses at 110 °C with purging of the liberated CO furnishes $HOs_3(CO)_8(\mu_3\text{-}C_6H_4)[\mu_2,\eta^1\text{-}PPhC{=}C(PPh_2)C(O)CH_2C(O)]$ as the dominant product in solution. The two new clusters, whose structures are depicted below, were subsequently isolated by column chromatography and fully characterized in solution and by X-ray diffraction analysis in the case of $HOs_3(CO)_8(\mu_3\text{-}C_6H_4)[\mu_2,\eta^1\text{-}PPhC{=}C(PPh_2)C(O)CH_2C(O)]$. With the identities of the two product clusters established from the thermolysis of 1,1-$Os_3(CO)_{10}$(bpcd), the photochemical activation of 1,1-$Os_3(CO)_{10}$(bpcd) was next explored. Irradiation of 1,1-$Os_3(CO)_{10}$(bpcd) in either benzene or CH_2Cl_2 solvent with 366 nm light leads to CO loss and clean conversion to $HOs_3(CO)_9[\mu\text{-}(PPh_2)C{=}C\{PPh(C_6H_4)\}C(O)CH_2C(O)]$, as verified by NMR and UV-VIS analyses. A quantum efficiency (Φ) of 0.02 was found for this orthometallation at 18 °C in benzene, with the formation of $HOs_3(CO)_9[\mu\text{-}(PPh_2)C{=}C\{PPh(C_6H_4)\}C(O)CH_2C(O)]$ being retarded when the irradiation was conducted under 1 atm of CO. The observed CO inhibition supports the generation of the

coordinatively unsaturated cluster 1,1-$Os_3(CO)_9$(bpcd) upon optical excitation. That CO is lost from 1,1-$Os_3(CO)_{10}$(bpcd) is of interest as the related clusters $Os_3(CO)_{10}$(α-diimine)

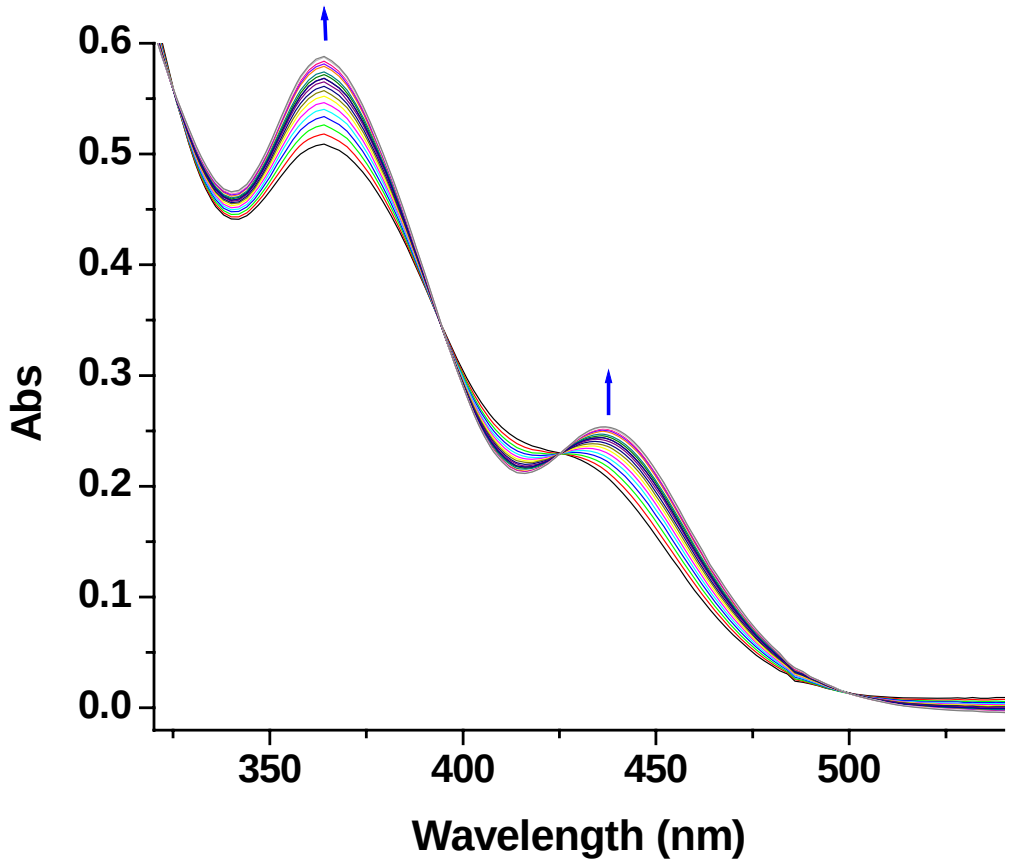

Figure 4.10. UV-VIS spectral changes for 1,2-$Os_3(CO)_{10}$(bpcd)→1,1-$Os_3(CO)_{10}$(bpcd) recorded at 323 K in benzene. (Reprinted with permission from *Organometallics* **2006**, 25, 930-945. Copyright 2006 American Chemical Society.)

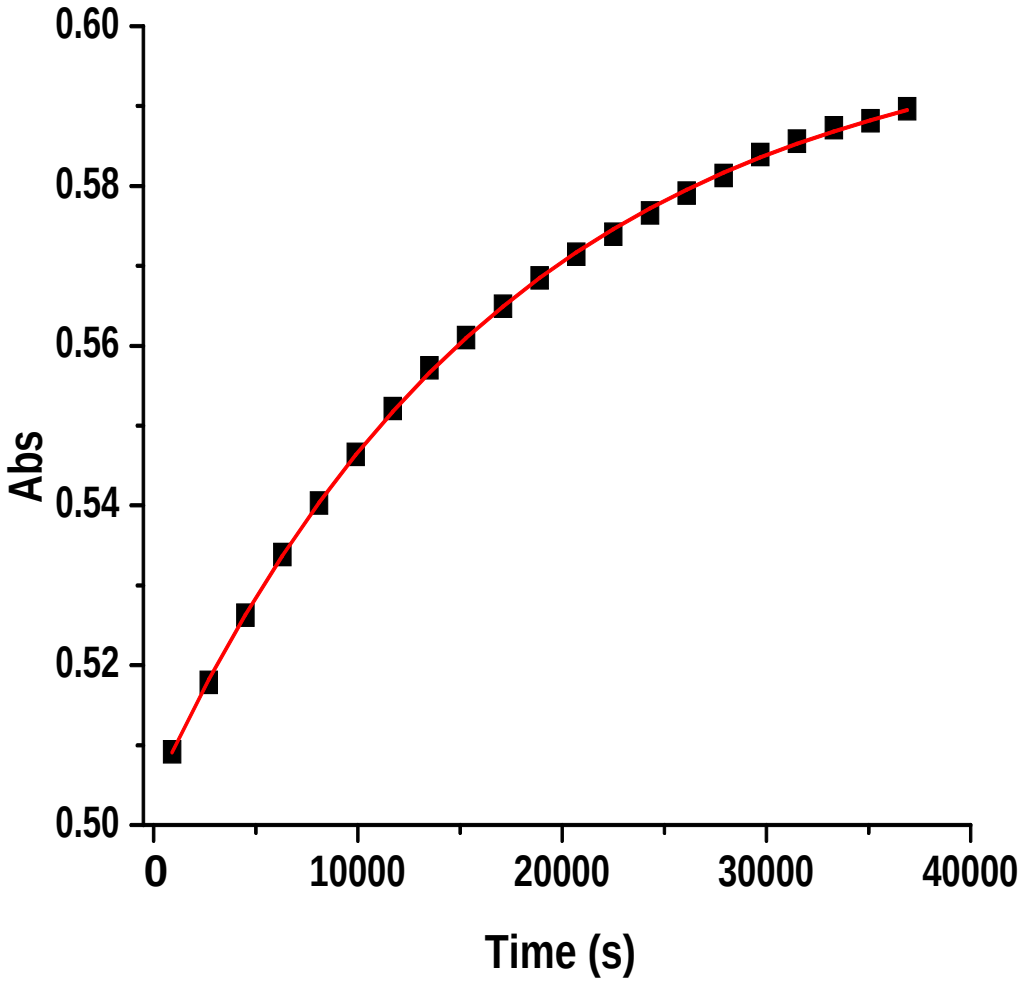

Figure 4.11. The absorbance versus time curves for the experimental data (■) and the least-squares fit (solid line) of the first-order rate constant k for 1,2-$Os_3(CO)_{10}$(bpcd)→1,1-$Os_3(CO)_{10}$(bpcd) recorded at 323 K in benzene by UV-VIS spectroscopy. (Reprinted with permission from *Organometallics* **2006**, 25, 930-945. Copyright 2006 American Chemical Society.)

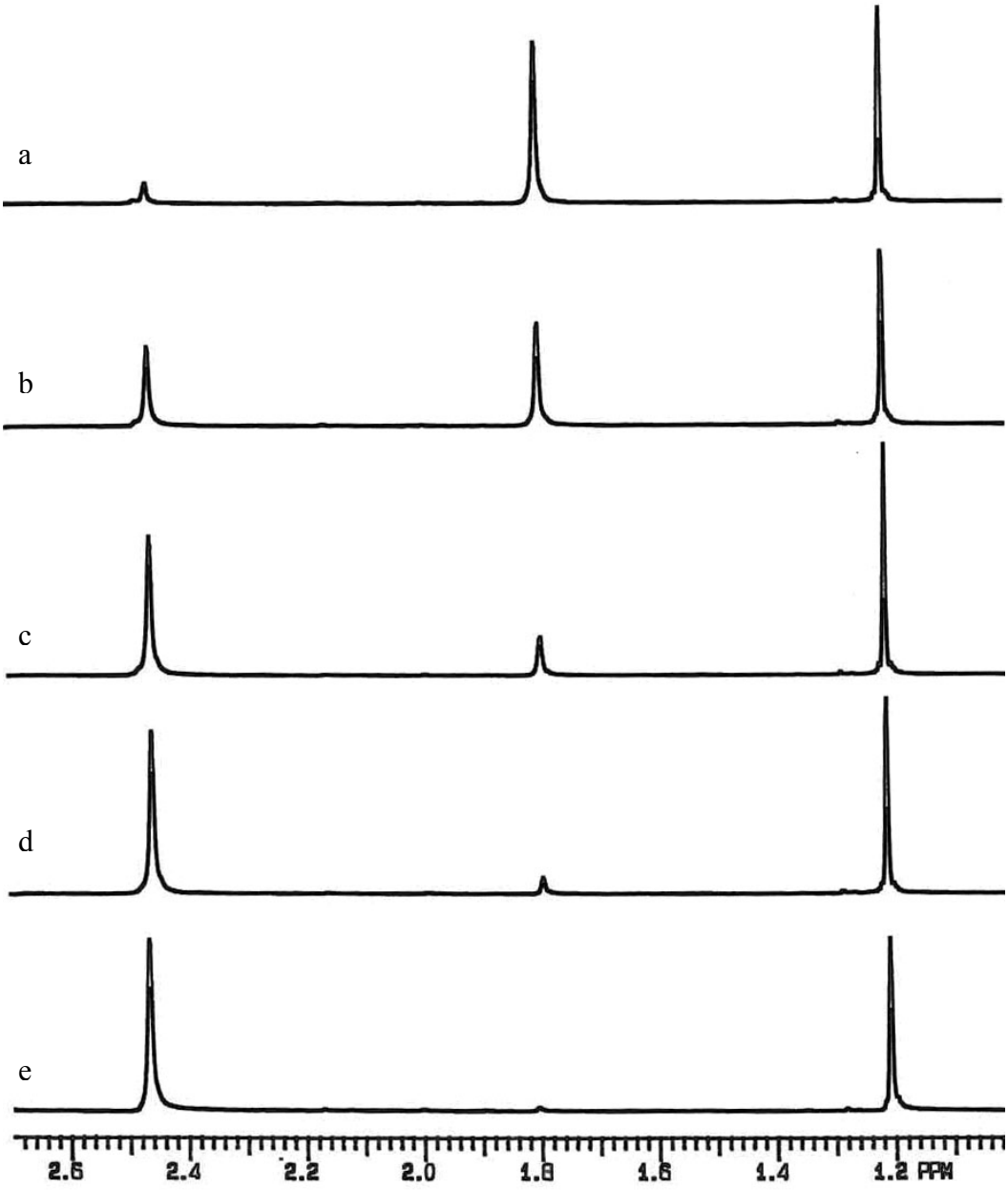

Figure 4.12. ^{1}H NMR spectra of 1,2-$Os_3(CO)_{10}$(bpcd) on heating in C_6D_6 at 65 °C with *tert*-butylbenzene as the internal standard. (a) 0.0 hr, (b) 0.5 hr, (c) 1.5 hr, (d) 2.5 hr, and (e) 3.5 hr.

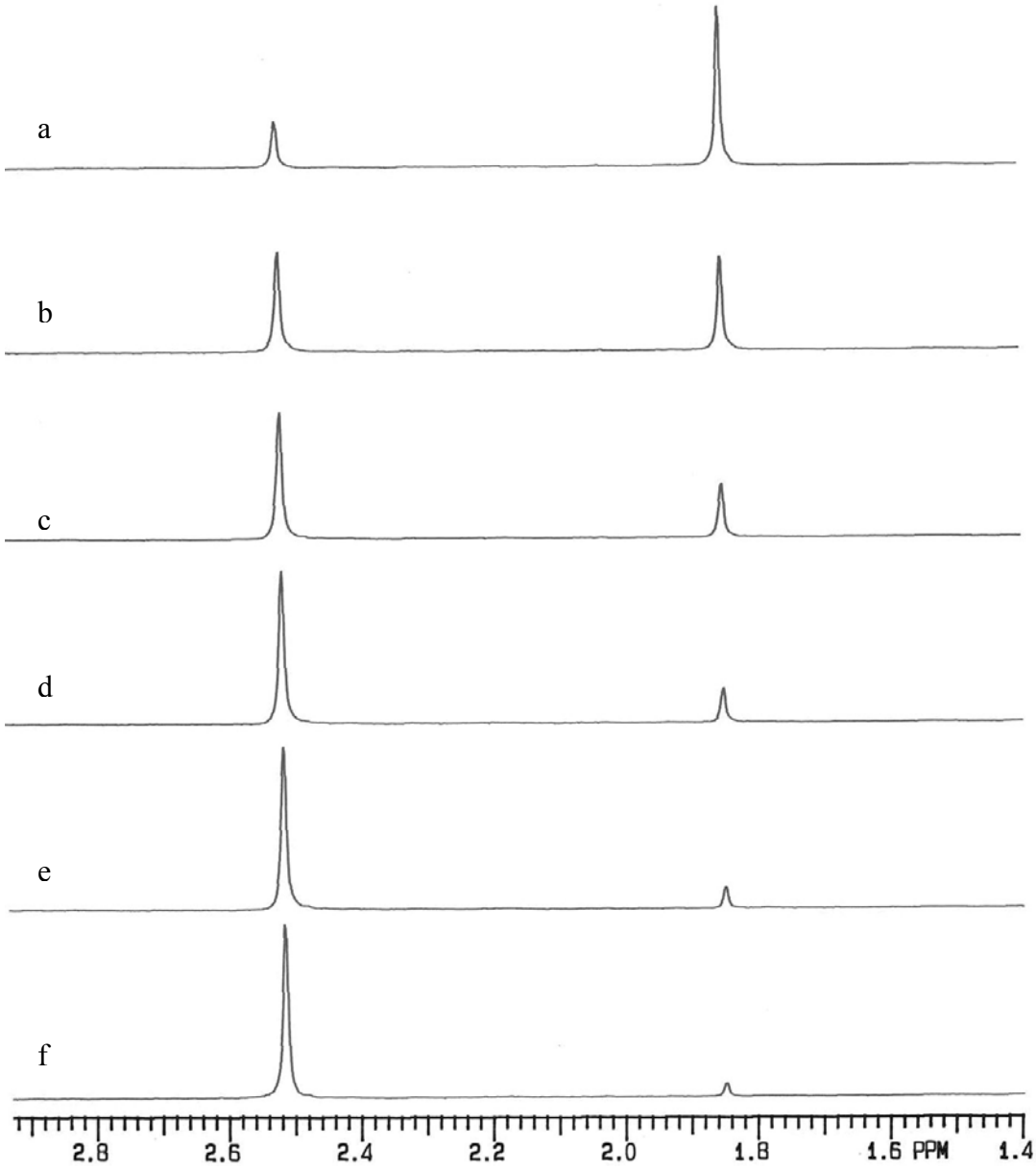

Figure 4.13. ^{1}H NMR spectra of 1,2-$Os_3(CO)_{10}$(bpcd) on heating in C_6D_6 at 65 °C in the presence of 10 equivalents of PPh_3. (a) 0.0 hr, (b) 0.5 hr, (c) 1.0 hr, (d) 1.5 hr, (e) 2.0 hr, and (f) 2.5 hr.

Table 4.4. Experimental Rate Constants for the Isomerization of 1,2-$Os_3(CO)_{10}$(bpcd) to 1,1-$Os_3(CO)_{10}$(bpcd)[a]

Temp (K)	10^4k (s^{-1})	Trapping Ligand	Method
323.0	0.58 ± 0.01		UV-VIS
323.0	0.51 ± 0.01		NMR
328.0	0.78 ± 0.03		UV-VIS
328.0	1.02 ± 0.07	6.8 atm CO	UV-VIS[b]
328.0	0.87 ± 0.01		NMR
333.0	1.91 ± 0.06		UV-VIS
333.0	1.74 ± 0.01	25 eq PPh_3	UV-VIS
333.0	1.60 ± 0.02		NMR
338.0	3.04 ± 0.23		UV-VIS
338.0	2.81 ± 0.05		NMR
338.0	2.82 ± 0.05	25 eq PPh_3	UV-VIS
338.0	3.18 ± 0.08	1.0 atm CO	UV-VIS
338.0	2.67 ± 0.01	10 eq PPh_3	NMR
338.0	2.87 ± 0.06	10 eq $P(OEt)_3$	NMR
343.0	5.82 ± 0.09		UV-VIS
343.0	4.62 ± 0.06		NMR

[a]The UV-VIS kinetic data were collected in benzene using ca. 10^{-4} M 1,2-$Os_3(CO)_{10}$(bpcd) by following the increase in the absorbance of the 364 nm band, and the NMR kinetics were conducted in benzene-d_6 with 1,2-$Os_3(CO)_{10}$(bpcd) at an initial concentration of ca. 10^{-2} M in the presence of an internal standard (either *p*-dimethoxybenzene or *t*-butylbenzene). The extent of the isomerization was followed by monitoring the decrease in intensity of the methylene singlet of the bridging isomer at δ 1.78. [b]Experiment conducted in a Fischer-Porter tube under constant CO pressure, where aliquots were removed and analyzed by UV-VIS spectroscopy. (Reprinted with permission from *Organometallics* **2006**, 25, 930-945. Copyright 2006 American Chemical Society.)

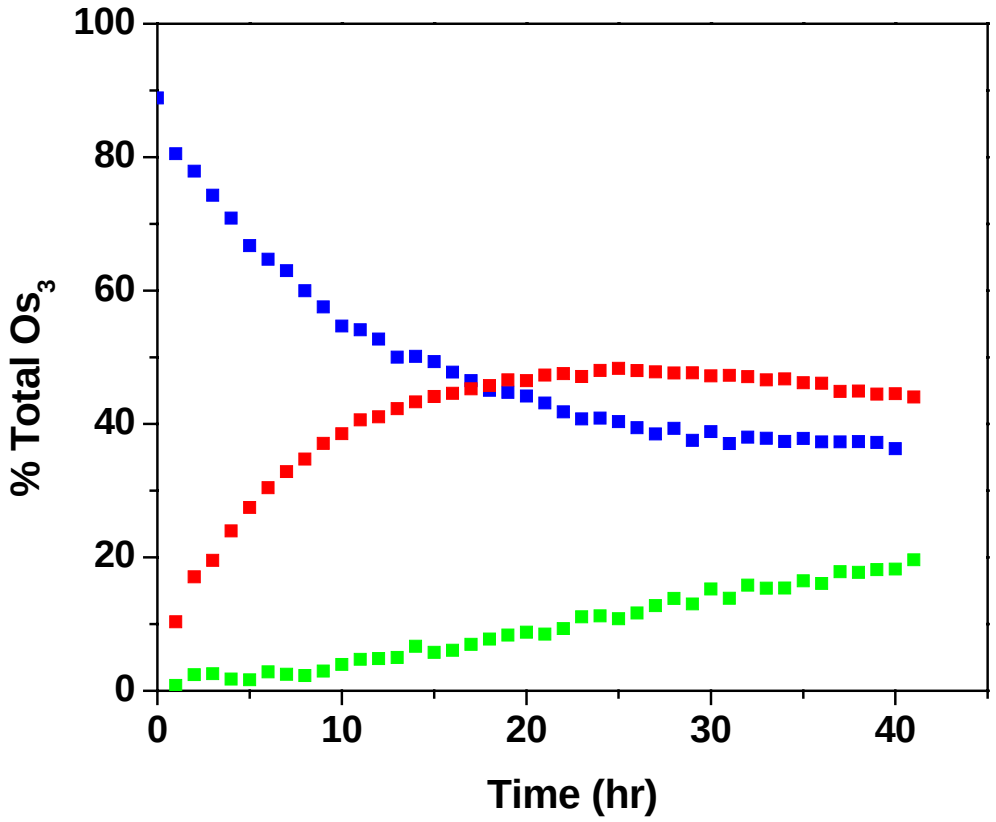

Figure 4.14. Plot of the cluster distribution of 1,1-$Os_3(CO)_{10}$(bpcd) (■), $HOs_3(CO)_9[\mu$-$(PPh_2)C{=}C\{PPh(C_6H_4)\}C(O)CH_2C(O)]$ (■), and $HOs_3(CO)_8(\mu_3$-$C_6H_4)[\mu_2,\eta^1$-$PPhC{=}C(PPh_2)C(O)CH_2C(O)]$ (■) versus time from the thermolysis starting with 1,1-$Os_3(CO)_{10}$(bpcd) in benzene-d_6 at 90.0 °C. The extent of the reaction was determined by ^{1}H NMR analysis using the methylene group from each cluster species. (Reprinted with permission from *Organometallics* **2006**, 25, 930-945. Copyright 2006 American Chemical Society.)

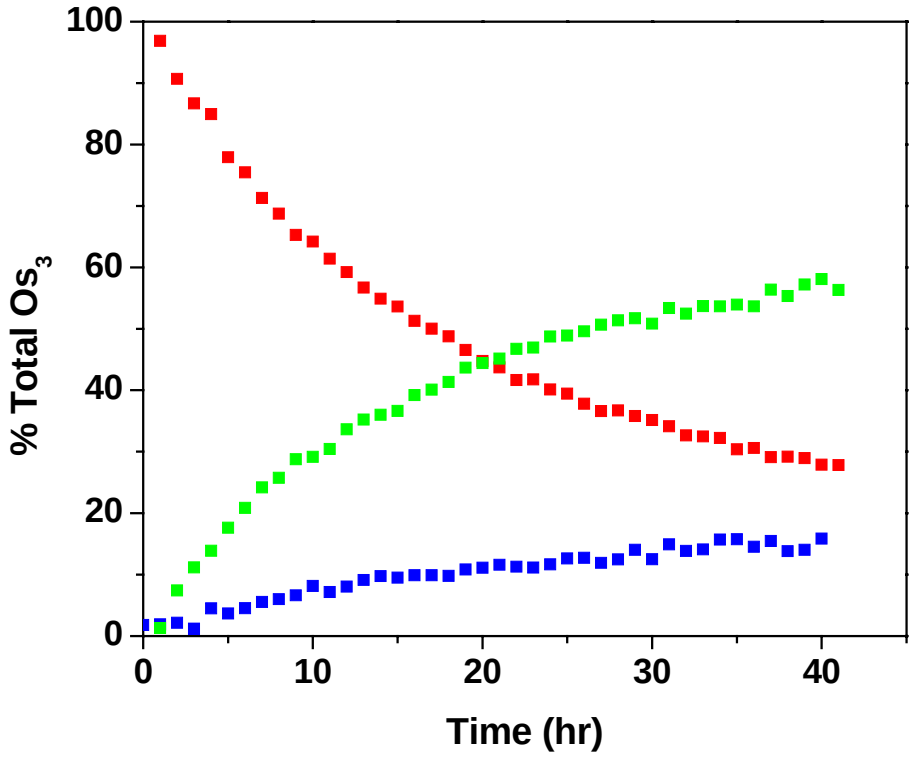

Figure 4.15. Plot of the cluster distribution of 1,1-$Os_3(CO)_{10}$(bpcd) (■), $HOs_3(CO)_9[\mu$-$(PPh_2)C{=}C\{PPh(C_6H_4)\}C(O)CH_2C(O)]$ (■), and $HOs_3(CO)_8(\mu_3$-$C_6H_4)[\mu_2,\eta^1$-$PPhC{=}C(PPh_2)C(O)CH_2C(O)]$ (■) versus time from the thermolysis starting with $HOs_3(CO)_9[\mu$-$(PPh_2)C{=}C\{PPh(C_6H_4)\}C(O)CH_2C(O)]$ in benzene-d_6 at 90.0 °C. The extent of the reaction was determined by ^{1}H NMR analysis using the methylene group from each cluster species. (Reprinted with permission from *Organometallics* **2006**, 25, 930-945. Copyright 2006 American Chemical Society.)

are resistant to dissociative CO loss on excitation, producing spectroscopically observable biradical and zwitterionic species from Os-Os bond cleavage reactions depending on the polarity of the solvent employed.[27,28] No evidence for the activation of the benzene or CH_2Cl_2 solvents was observed in our photolysis experiments when the reaction solutions were monitored by ^1H and ^{31}P NMR spectroscopy.

In keeping with the current body of knowledge on alkane and arene activation by mononuclear complexes, the demonstrated reductive C-H bond coupling in $HOs_3(CO)_9[\mu\text{-}(PPh_2)C{=}C\{PPh(C_6H_4)\}C(O)CH_2C(O)]$ is expected to proceed by way of an intermediate ;-complex, prior to the rate-limiting formation of the unsaturated cluster 1,1-$Os_3(CO)_9$(bpcd).[29] Such aspects of our reaction could readily be probed through parallel kinetic studies employing an isotopically substituted bpcd ligand where all the aryl hydrogens have been replaced by deuterium atoms. Accordingly, the diphosphine ligand bpcd-d_{20} was synthesized (Scheme 4.9), and has been used in the preparation of the deuteride cluster $DOs_3(CO)_9[\mu\text{-}(PPh_2\text{-}d_{10})C{=}C\{P(Ph\text{-}d_5)(C_6D_4)\}C(O)CH_2C(O)]$ and kinetic trapping studies of the latter by PPh_3, as shown in Scheme 4.10.

The reaction of $DOs_3(CO)_9[\mu\text{-}(PPh_2\text{-}d_{10})C{=}C\{P(Ph\text{-}d_5)(C_6D_4)\}C(O)CH_2C(O)]$ and excess PPh_3 (25 equiv.) was investigated in toluene solution by UV-VIS spectroscopy, as described for $HOs_3(CO)_9[\mu\text{-}(PPh_2)C{=}C\{PPh(C_6H_4)\}C(O)CH_2C(O)]$ (*vide supra*), with the first-order rate constants (k_D) for the consumption of $DOs_3(CO)_9[\mu\text{-}(PPh_2\text{-}d_{10})C{=}C\{P(Ph\text{-}d_5)(C_6D_4)\}C(O)CH_2C(O)]$ reported in Table 4.5. The observed inverse isotope effect of 0.88 (average value for all five runs) for the reductive C-H bond coupling is best interpreted as arising from an equilibrium isotope effect (EIE) that is

coupled with a slower, isotope insensitive step (i.e., $K \times k$). In the present study, such a scenario is easily rationalized within a multistep manifold that involves a rapid and reversible pre-equilibrium step between the hydride (deuteride) cluster and an arene ; complex (k_{rc}/k_{oc}) that precedes the rate-limiting dissociation of the arene ; bond from the osmium center (k_{diss}).[30] Scheme 4.11 illustrates this stepwise progression from $HOs_3(CO)_9[\mu\text{-}(PPh_2)C{=}C\{PPh(C_6H_4)\}C(O)CH_2C(O)]$ to the phosphine-substituted cluster 1,1-$Os_3(CO)_9P$(bpcd). While many paradigms provide unequivocal evidence for the involvement of σ-alkane and π-arene intermediates through equilibrium isotope effects in reductive coupling reactions at mononuclear complexes,[31,32] to our knowledge, the data reported here represent the first such work concerning a C-H bond forming process at a polynuclear system.[33]

F. Proof of Reversible Orthometallation through Ligand Trapping of the Unsaturated Intermediate 1,1-$Os_3(CO)_9$(bpcd)

The observation of minor amounts of 1,1-$Os_3(CO)_{10}$(bpcd) from the thermolysis of $HOs_3(CO)_9[\mu\text{-}(PPh_2)C{=}C\{PPh(C_6H_4)\}C(O)CH_2C(O)]$ (Figure 4.15) signaled that the orthometallation of the aryl ligand is reversible, and as such, this reaction was studied in more detail given its relevance to hydrocarbon activation. $HOs_3(CO)_9[\mu\text{-}(PPh_2)C{=}C\{PPh(C_6H_4)\}C(O)CH_2C(O)]$ was found to react readily with added CO (1 atm) at 75 °C in a variety of solvents to furnish 1,1-$Os_3(CO)_{10}$(bpcd) in quantitative yield when monitored by ^{1}H NMR and UV-VIS spectroscopies. The carbonylation proceeded cleanly and without the presence of spectroscopically observable intermediates. Having established the reversible C-H bond formation in the reaction of $HOs_3(CO)_9[\mu\text{-}$

$(PPh_2)C{=}C\{PPh(C_6H_4)\}C(O)CH_2C(O)]$ with added CO, the kinetic trapping of the postulated unsaturated intermediate 1,1-$Os_3(CO)_9$(bpcd) with donor ligands other than CO was next examined.[34] The reaction of the hydride cluster $HOs_3(CO)_9[\mu$-$(PPh_2)C{=}C\{PPh(C_6H_4)\}C(O)CH_2C(O)]$ with excess trapping ligand (> 10 equiv.) was investigated in toluene solution over the temperature range of 331-359 K. The progress of each reaction was followed by monitoring the decrease in the absorbance of the 396 nm band for $HOs_3(CO)_9[\mu$-$(PPh_2)C{=}C\{PPh(C_6H_4)\}C(O)CH_2C(O)]$, as illustrated in Figure 4.16 for the absorbance versus time plot (left) for the reaction with PPh_3. The UV-VIS changes for this reaction are clean, and the isosbestic points observed at 383 and 452 nm support the formation of 1,1-$Os_3(CO)_9(PPh_3)$(bpcd) as the major product (see Figure 4.16).[35] The first-order rate constants quoted in Table 4.5 were obtained from non-linear regression analysis (Figure 4.17). Examination of entries 4-7 in Table 4.5 confirms that the rate of the reaction is independent of added ligand, allowing the elimination of a rate-limiting bimolecular process involving the cluster and ligand from consideration. The activation parameters for these data are $\Delta H^{\ddagger}$ = 26.8 (0.5) kcal/mol and $\Delta S^{\ddagger}$ = 0 (2) eu.

Scheme 4.9. Preparation of bpcd-d_{20}.

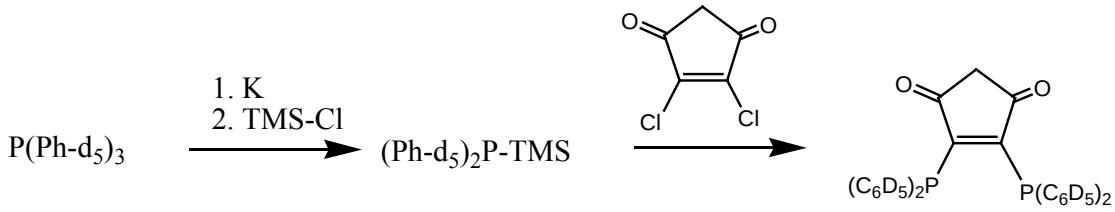

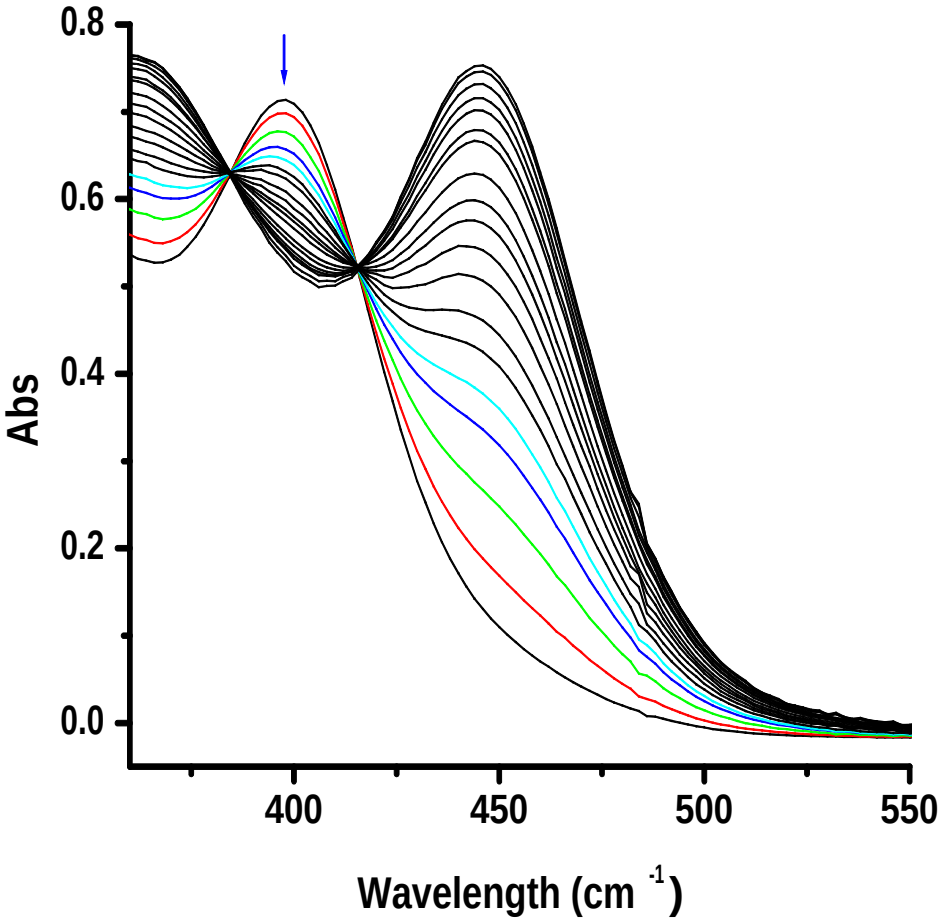

Figure 4.16. UV-VIS spectral changes for the reaction of $HOs_3(CO)_9[\mu$-$(PPh_2)C{=}C\{PPh(C_6H_4)\}C(O)CH_2C(O)]$ in the presence of PPh_3 (25 equivalents) recorded at 331 K in toluene. (Reprinted with permission from *Organometallics* **2006**, 25, 930-945. Copyright 2006 American Chemical Society.)

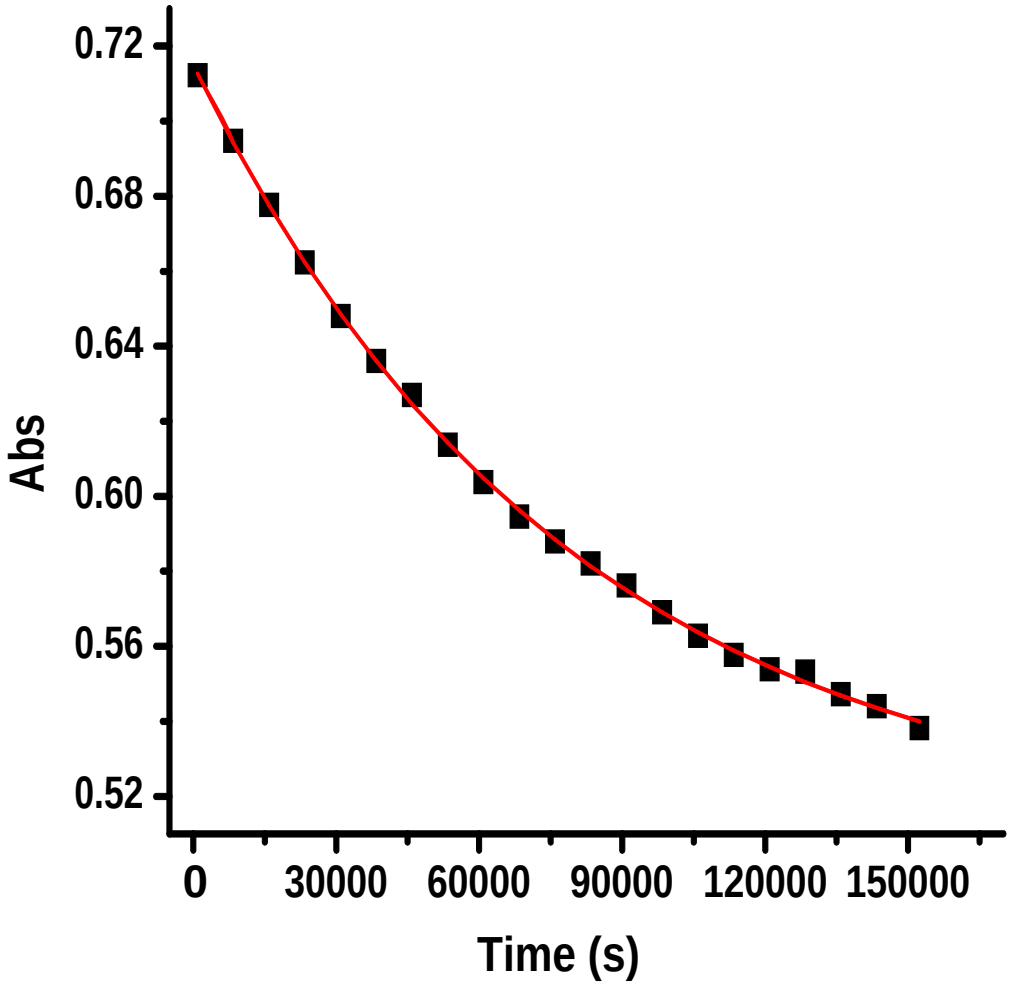

Figure 4.17. The UV-VIS absorbance versus time curves for the experimental data (■) for the decay of $HOs_3(CO)_9[\mu\text{-}(PPh_2)C{=}C\{PPh(C_6H_4)\}C(O)CH_2C(O)]$ and the least-squares fit (solid line) of the first-order rate constant k_H for the reaction of $HOs_3(CO)_9[\mu\text{-}(PPh_2)C{=}C\{PPh(C_6H_4)\}C(O)CH_2C(O)]$ and 25 equivalents of PPh_3 recorded in toluene at 331 K. (Reprinted with permission from *Organometallics* **2006**, 25, 930-945. Copyright 2006 American Chemical Society.)

Table 4.5. Experimental Rate Constants for the Conversion of $HOs_3(CO)_9[\mu$-$(PPh_2)C{=}C\{PPh(C_6H_4)\}C(O)CH_2C(O)]$ to 1,1-$Os_3(CO)_9(P)$(bpcd) and $DOs_3(CO)_9[\mu$-$(PPh_2$-$d_{10})C{=}C\{P(Ph$-$d_5)(C_6D_4)\}C(O)CH_2C(O)]$ to 1,1-$Os_3(CO)_9(P)$(bpcd-d_{20})[a]

Temp (K)	10^4k_H (s^{-1})[b]	10^4k_D (s^{-1})[b,c]	Trapping Ligand	k_H/k_D[d]
331.0	0.13 ± 0.03	0.15 ± 0.01	25 eq PPh_3	0.87
338.0	0.30 ± 0.02	0.33 ± 0.04	25 eq PPh_3	0.91
346.0	0.74 ± 0.06	0.90 ± 0.08	25 eq PPh_3	0.82
353.0	1.66 ± 0.01		10 eq PPh_3	
353.0	1.62 ± 0.01		10 eq $P(OEt)_3$	
353.0	1.62 ± 0.02	1.78 ± 0.01	25 eq PPh_3	0.91
353.0	1.64 ± 0.04		25 eq PCy_3	
359.0	3.47 ± 0.08	3.99 ± 0.07	25 eq PPh_3	0.87

[a]The UV-VIS kinetic data were collected in toluene using ca. 10^{-4} M $HOs_3(CO)_9[\mu$-$(PPh_2)C{=}C\{PPh(C_6H_4)\}C(O)CH_2C(O)]$ and $DOs_3(CO)_9[\mu$-$(PPh_2$-$d_{10})C{=}C\{P(Ph$-$d_5)(C_6D_4)\}C(O)CH_2C(O)]$ by following the decrease in the absorbance of the 396 nm band. [b]The quoted rate constants k_H and k_D represent the rates of reaction for the reductive coupling of $HOs_3(CO)_9[\mu$-$(PPh_2)C{=}C\{PPh(C_6H_4)\}C(O)CH_2C(O)]$ and its deutride isotopomer, respectively. [c]The Eyring activation parameters were determined as $\Delta H^{\ddagger}$ = 26.8 (0.8) kcal/mol and $\rho S^{\ddagger}$ = 0 (2) eu. [d]The average of the five k_H/k_D values is 0.88. (Reprinted with permission from *Organometallics* **2006**, 25, 930-945. Copyright 2006 American Chemical Society.)

G. Thermodynamic and Kinetic Orthometallation in 1,1-$Os_3(CO)_9$(bpcd) and H/D Scrambling in the Arene Intermediate

Besides the experimentally determined inverse isotope effect from the ligand trapping studies employing $HOs_3(CO)_9[\mu\text{-}(PPh_2)C{=}C\{PPh(C_6H_4)\}C(O)CH_2C(O)]$ and

Scheme 4.10. Preparation of 1,1-$Os_3(CO)_{10}$(bpcd-d_{20}), $DOs_3(CO)_9[\mu\text{-}(PPh_2\text{-}d_{10})C{=}C\{P(Ph\text{-}d_5)(C_6D_4)\}C(O)CH_2C(O)]$ and 1,1-$Os_3(CO)_9(PPh_3)$(bpcd-d_{20}).

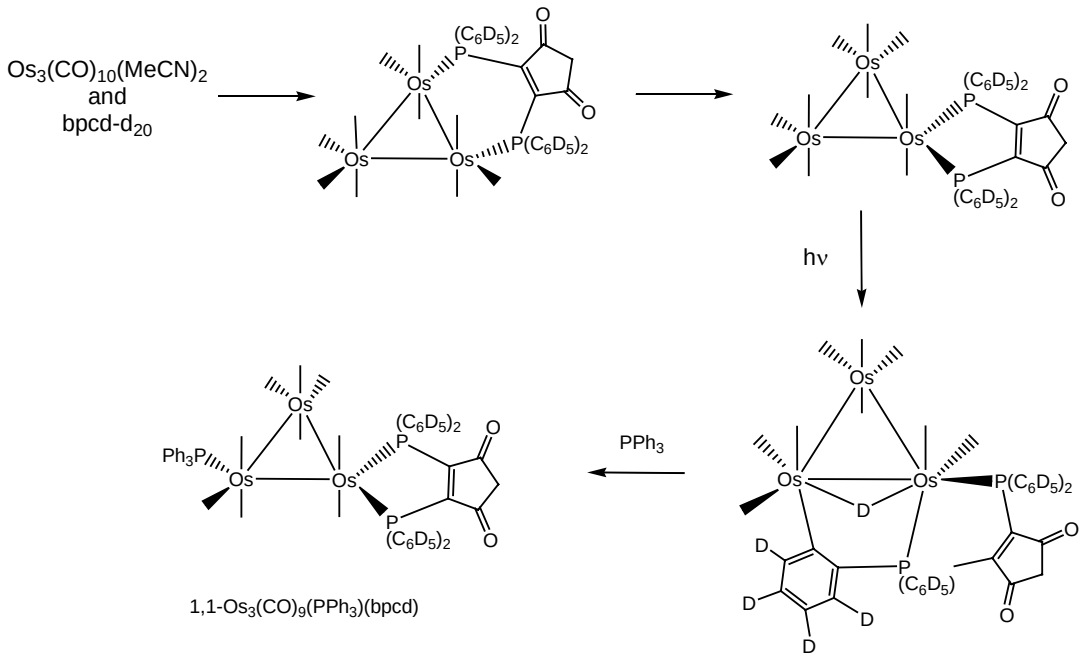

Scheme 4.11. Proposed mechanism for trapping the intermediate of reductive coupling of the hydride cluster.

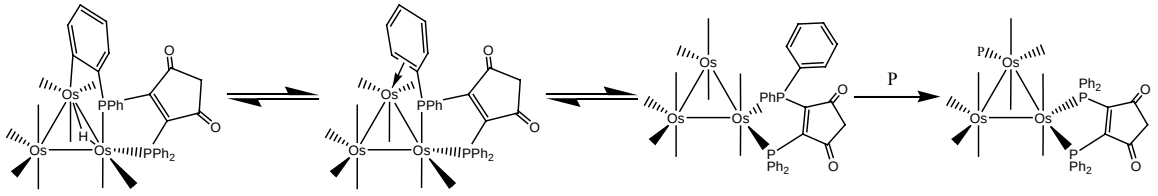

$DOs_3(CO)_9[\mu\text{-}(PPh_2\text{-}d_{10})C{=}C\{P(Ph\text{-}d_5)(C_6D_4)\}C(O)CH_2C(O)]$, intramolecular H/D scrambling between the bridging hydride or deuteride of $HOs_3(CO)_9[\mu\text{-}(PPh_2)C{=}C\{PPh(C_6H_4)\}C(O)CH_2C(O)]$ and an appropriately labeled orthometalated aryl moiety (C_6D_4 for the hydride and C_6H_4 for the deuteride) would also furnish corroborating evidence for the intermediate ; complex. Replacement of the bridging hydride in $HOs_3(CO)_9[\mu\text{-}(PPh_2)C{=}C\{PPh(C_6H_4)\}C(O)CH_2C(O)]$ by deuterium or the bridging deuteride in $DOs_3(CO)_9[\mu\text{-}(PPh_2\text{-}d_{10})C{=}C\{P(Ph\text{-}d_5)(C_6D_4)\}C(O)CH_2C(O)]$ by hydrogen would give the below isotopically substituted clusters that could be used to probe H/D scrambling in $HOs_3(CO)_9[\mu\text{-}(PPh_2)C{=}C\{PPh(C_6H_4)\}C(O)CH_2C(O)]$ (See Scheme 4.12). Unfortunately, attempts to deprotonate the hydride ligand in $HOs_3(CO)_9[\mu\text{-}(PPh_2)C{=}C\{PPh(C_6H_4)\}C(O)CH_2C(O)]$ using BuLi or Et_3N, followed by acidification with acetic acid-d_1 or D_2O, did not furnish the desired deuteride cluster $DOs_3(CO)_9[\mu\text{-}(PPh_2)C{=}C\{PPh(C_6H_4)\}C(O)CH_2C(O)]$ but led to deuterium incorporation into the methylene group of the dione ring, along with substantial decomposition of the starting cluster. Analogous methodologies have been utilized by many researchers to demonstrate isotopic exchange via a transient arene ; complex and σ alkane complex. Two classic examples that demonstrate the involvement of an arene π and , alkane intermediate in H/D scrambling sequences are the mononuclear complexes $Cp^*Rh(PMe_3)H(C_6D_5)$[31d] and $Cp^*Rh(PMe_3)D(^{13}CH_2CH_3)$,[36] respectively.

Since the hydride deprotonation/acidification route employing $HOs_3(CO)_9[\mu\text{-}$

$(PPh_2)C{=}C\{PPh(C_6H_4)\}C(O)CH_2C(O)]$ could not be used in the synthesis of a suitable probe cluster for the H/D scrambling study, an isotopically substituted alternative was sought, one where the ancillary bpcd ligand contained one *ortho* hydrogen and deuterium relative to the phosphorus atom. This was achieved by starting with the isotopically substituted phosphine PPh_3-d_{3ortho} and preparing the diphosphine ligand bpcd-d_{4ortho} through the standard protocols outlined in Scheme 4.13. The bpcd-d_{4ortho} ligand was then used in the synthesis of 1,1-$Os_3(CO)_{10}$(bpcd-d_{4ortho}), which in turn was used to in the generation of the unsaturated cluster 1,1-$Os_3(CO)_9$(bpcd-d_{4ortho}) through photochemical activation.

Near-UV irradiation of 1,1-$Os_3(CO)_{10}$(bpcd-d_{4ortho}) is expected to lead to CO loss and formation of 1,1-$Os_3(CO)_9$(bpcd-d_{4ortho}), as illustrated in the lower portion of Scheme 4.14. Coordination of one of the aryl groups to an osmium center adjacent to the bpcd-chelated osmium center furnishes a labile ; complex that is in equilibrium with the orthometalated hydride and deuteride clusters depicted in the upper portion of Scheme 4.14. On the basis of the earlier trapping studies with $HOs_3(CO)_9[\mu$-$(PPh_2)C{=}C\{PPh(C_6H_4)\}C(O)CH_2C(O)]$, the partitioning of the ; complex between the hydride and deuteride clusters is predicted to be rapid at ambient temperatures relative to the rate-limiting dissociation of the coordinated aryl ligand from the cluster since this would regenerate the high-energy unsaturated cluster. The important orthometallation equilibria may be treated in terms of the relative concentrations of the product hydride/deuteride clusters where K_{eq} = [deuteride]/[hydride]. Alternatively, K_{eq} may be expressed as a function of the individual rate constants for the forward and reverse

reactions so that $K_{eq} = [k(H)_{RC} \times k(D)_{OC}]/[k(D)_{RC} \times k(H)_{OC}]$, which may also be rearranged in terms of the reductive coupling and oxidative coupling kinetic isotope effects: $K_{eq} = [k(H)_{RC}/k(D)_{RC}]/[k(H)_{OC}/k(D)_{OC}]$. As pointed out by Jones, extraction of two of the three

Scheme 4.12. Possible H/D exchange reactions.

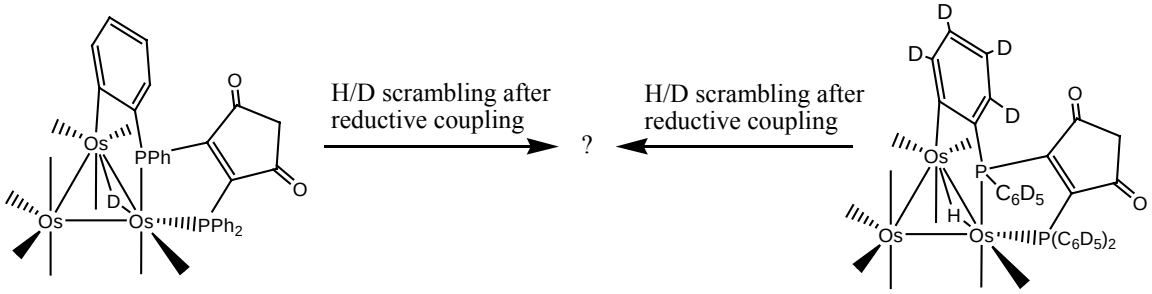

Scheme 4.13. Preparation of bpcd-$d_{4ortho.}$

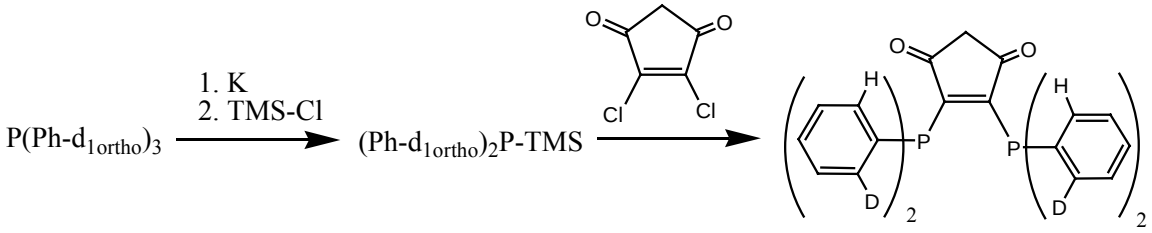

related isotope effects allows for a complete understanding of the pre-equilibrium isotope contributions to our orthometallation reaction.[29c]

Irradiation of a sealed NMR tube containing 1,1-$Os_3(CO)_{10}$(bpcd-d_{4ortho}) in toluene-d_8 at 0 °C allowed the kinetic selectivity for the orthometallation to be established. Here a 55:45 mixture of the corresponding hydride and deuteride clusters was found.[37] This product ratio affords a $k(H)_{OC}/k(D)_{OC} = 1.22$ for the C-H(D) bond activation in the orthometallation step. The observation of a small normal KIE is on par

with the value of 1.4 found for the oxidative cleavage of 1,3,5-$C_6H_3D_3$ by Cp*Rh(PMe_3).[29d] Heating kinetically generated samples of the cluster over the temperature range of 40-60 °C led to the equilibration of the hydride and deuteride clusters and a final isomer composition of 67:33 in favor of the hydride cluster and a K_{eq}

Scheme 4.14. Proposed mechanism for reductive coupling and oxidative coupling involving a π-arene intermediate.

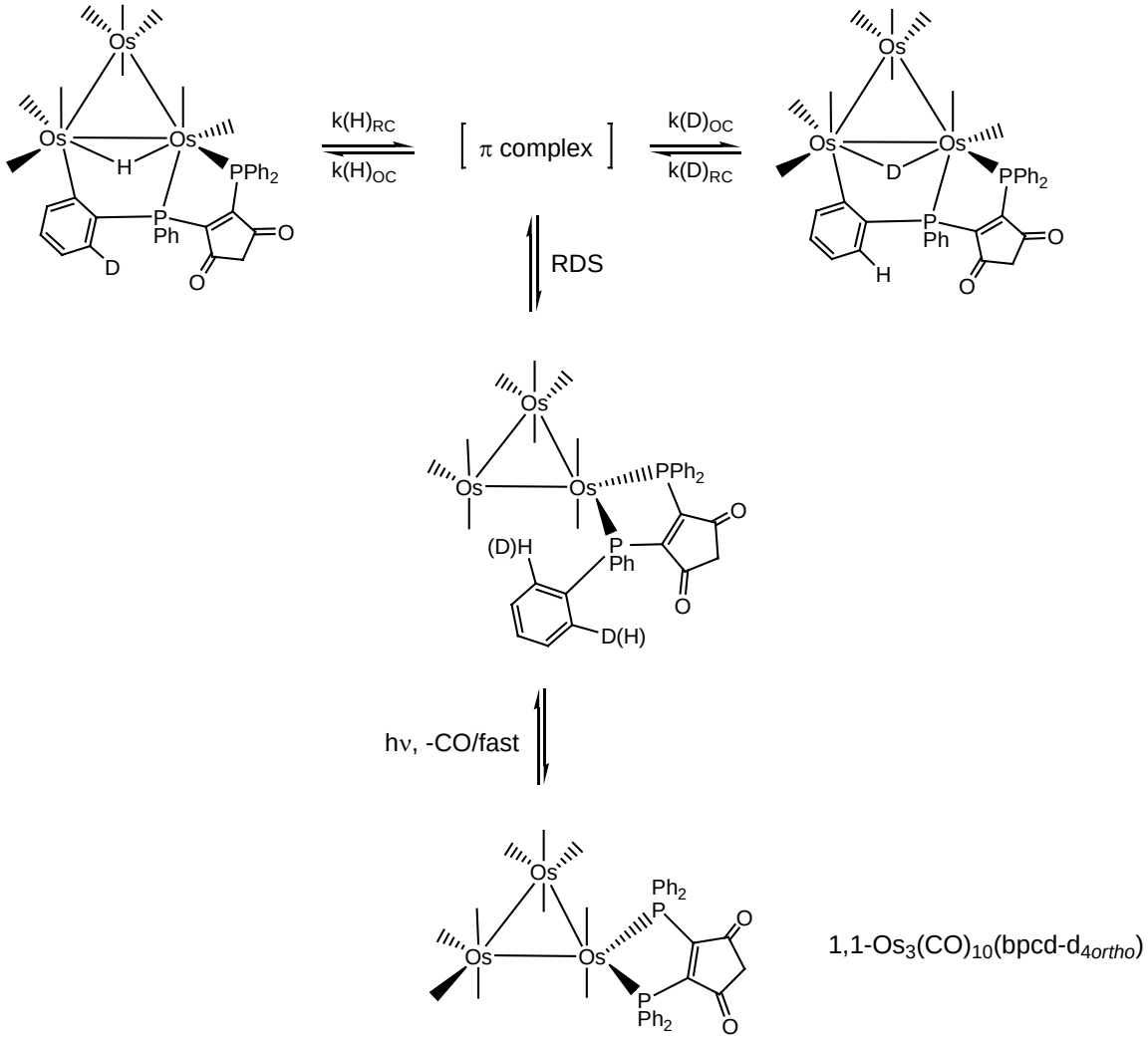

= 0.49.[38] Irradiation of 1,1-$Os_3(CO)_{10}$(bpcd-d_{4ortho}) at 40 °C in benzene-d_6 gave a K_{eq} value identical to that obtained from the thermally equilibrated cluster samples. That the hydride cluster is thermodynamically favored over the corresponding deuteride cluster is understood within the tenets of the Born-Oppenheimer approximation where changes in the vibrational energies of the participant bonds control the direction of the hydride/deuteride equilibrium in this orthometallation reaction.[39] The smaller zero-point energy difference between the bridging osmium-hydride(deuteride) bonds vis-à-vis the fully formed arene *ortho* C-H(D) bonds in the orthometalated aryl ring guarantees that the hydride-bridged cluster with its stronger arene C-D bond will dominant the equilibrium and favor the hydride-bridged cluster $HOs_3(CO)_9$[μ-(PPh_2-d_{2ortho})C=C{P(Ph-d_{1ortho})(C_6H_3D)}C(O)CH_2C(O)]. From these data we find that the reductive coupling step exhibits an inverse KIE with $k(H)_{RC}/k(D)_{RC}$ = 0.60. The gross characteristics for the reversible orthometallation in 1,1-$Os_3(CO)_{10}$(bpcd) are remarkably similar to the activation of benzene by Cp*$Rh(PMe_3)H_2$.[29d] Taken collectively, the data on the multistep conversion of the hydride clusters $HOs_3(CO)_9$[μ-(PPh_2)C=C{$PPh(C_6H_4)$}C(O)CH_2C(O)] and $DOs_3(CO)_9$[μ-(PPh_2-d_{10})C=C{P(Ph-d_5)(C_6H_4)}C(O)CH_2C(O)] to 1,1-$Os_3(CO)_9$L(bpcd) in the presence of trapping ligands are best described by the reaction coordinate depicted in Figure 4.18.[40]

H. Kinetics for the Conversion of $HOs_3(CO)_9$[μ-(PPh_2)C=C{$PPh(C_6H_4)$}C(O)CH_2C(O)] to $HOs_3(CO)_8(\mu_3\text{-}C_6H_4)[\mu_2,\eta^1\text{-}PPhC{=}C(PPh_2)C(O)CH_2C(O)]$

The relationship of cluster $HOs_3(CO)_9$[μ-(PPh_2)C=C{$PPh(C_6H_4)$}C(O)CH_2C(O)] to $HOs_3(CO)_8(\mu_3\text{-}C_6H_4)[\mu_2,\eta^1\text{-}PPhC{=}C(PPh_2)C(O)CH_2C(O)]$ was next examined.

Conceptually, an attractive route for conversion of $HOs_3(CO)_9[\mu$-$(PPh_2)C{=}C\{PPh(C_6H_4)\}C(O)CH_2C(O)] \rightarrow HOs_3(CO)_8(\mu_3$-$C_6H_4)[\mu_2,\eta^1$-$PPhC{=}C(PPh_2)C(O)CH_2C(O)]$ would involve a P-C bond cleavage of the activated aryl group in $HOs_3(CO)_9[\mu$-$(PPh_2)C{=}C\{PPh(C_6H_4)\}C(O)CH_2C(O)]$, as this would serve to liberate the benzyne ligand. However, such a path would violate the principle of microscopic reversibility that requires the regeneration of the coordinatively unsaturated cluster 1,1-$Os_3(CO)_9$(bpcd), which in turn must function as a precursor for the production of $HOs_3(CO)_8(\mu_3$-$C_6H_4)[\mu_2,\eta^1$-$PPhC{=}C(PPh_2)C(O)CH_2C(O)]$. The kinetics for the conversion of $HOs_3(CO)_9[\mu$-$(PPh_2)C{=}C\{PPh(C_6H_4)\}C(O)CH_2C(O)] \rightarrow HOs_3(CO)_8(\mu_3$-$C_6H_4)[\mu_2,\eta^1$-$PPhC{=}C(PPh_2)C(O)CH_2C(O)]$ were studied over the temperature range 363-383 K in toluene solvent by following the decrease in the 396 nm absorbance band belonging to $HOs_3(CO)_9[\mu$-$(PPh_2)C{=}C\{PPh(C_6H_4)\}C(O)CH_2C(O)]$. Regression analysis provided the first-order rate constants that are quoted in Table 4.6, from which the values of $\rho H^{\ddagger} = 29.2$ (1.1) kcal/mol and $\rho S^{\ddagger} = 4$ (3) eu were determined by Eyring analysis. The activation data are in excellent agreement with those data obtained from the ligand trapping studies employing $HOs_3(CO)_9[\mu$-$(PPh_2)C{=}C\{PPh(C_6H_4)\}C(O)CH_2C(O)]$, as expected. Under these higher temperature conditions 1,1-$Os_3(CO)_9$(bpcd), once formed, can undergo an irreversible P-C bond activation and ultimately furnish the benzyne cluster $HOs_3(CO)_8(\mu_3$-$C_6H_4)[\mu_2,\eta^1$-$PPhC{=}C(PPh_2)C(O)CH_2C(O)]$. The exact nature of the aryl group formed upon P-C bond cleavage cannot be determined on the basis of the present data, but the generation of a cluster bound η^1-Ph moiety would not be

unreasonable, as depicted below for $Os_3(CO)_9(\eta^1\text{-Ph})[\mu\text{-}(PPh_2)C{=}C(PPh)C(O)CH_2C(O)]$ (Scheme 4.15).[41] Subsequent orthometallation of the η^1-Ph moiety could then give the coordinated benzyne ligand found in $HOs_3(CO)_8(\mu_3\text{-}C_6H_4)[\mu_2,\eta^1\text{-}PPhC{=}C(PPh_2)C(O)CH_2C(O)]$.

I. Conclusions

The reaction between $Os_3(CO)_{10}(NCMe)_2$ and cDPPEn gives 1,2-$Os_3(CO)_{10}$(cDPPEn) as the kinetic product of ligand substitution. Isomerization of the bridged cluster into the chelated cluster 1,1-$Os_3(CO)_{10}$(cDPPEn) proceeds readily upon heating. The isomerization kinetics and thermodynamics have been explored by spectroscopic methods and both products subjected to structural analysis. On the basis of the kinetic data, a non-dissociative phosphine migration across one of the Os-Os bonds has been proposed.

Scheme 4.15. Possible intermediate for the conversion of $HOs_3(CO)_9[\mu\text{-}(PPh_2)C{=}C\{PPh(C_6H_4)\}C(O)CH_2C(O)]$ to $HOs_3(CO)_8(\mu_3\text{-}C_6H_4)[\mu_2,\eta^1\text{-}PPhC{=}C(PPh_2)C(O)CH_2C(O)]$.

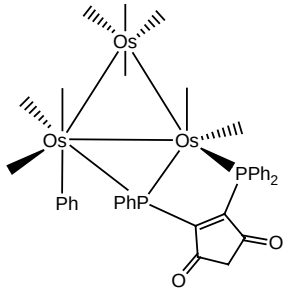

The reaction between the diphosphine ligand bpcd and $Os_3(CO)_{10}(NCMe)_2$ has been investigated and found to give 1,2-$Os_3(CO)_{10}$(bpcd) as the kinetic product of ligand substitution. Non-dissociative ligand isomerization to the chelated cluster 1,1-$Os_3(CO)_{10}$(bpcd) occurs upon heating, followed by the loss of CO and formation of the hydride cluster $HOs_3(CO)_9[\mu\text{-}(PPh_2)C{=}C\{PPh(C_6H_4)\}C(O)CH_2C(O)]$ through an orthometallation sequence. The orthometallation reaction is reversible and proceeds by way of a transient ; complex. The individual kinetic isotope effects associated with the pre-equilibrium step (hydride/π complex) have been determined, and the role of the unsaturated cluster 1,1-$Os_3(CO)_9$(bpcd) as a common precursor for the formation of both $HOs_3(CO)_9[\mu\text{-}(PPh_2)C{=}C\{PPh(C_6H_4)\}C(O)CH_2C(O)]$ and the benzyne-substituted cluster $HOs_3(CO)_8(\mu_3\text{-}C_6H_4)[\mu_2,\eta^1\text{-}PPhC{=}C(PPh_2)C(O)CH_2C(O)]$ is confirmed. In the present study, the benzyne ligand is derived from an irreversible P-C bond cleavage reaction, followed by an orthometallation of the cluster-bound phenyl moiety. Future work on the mechanistic examination of other cluster-mediated ligand degradation reactions, and the influence that the metal cluster has on the magnitude of the isotope contributions for the orthometallation step could seem mandated.

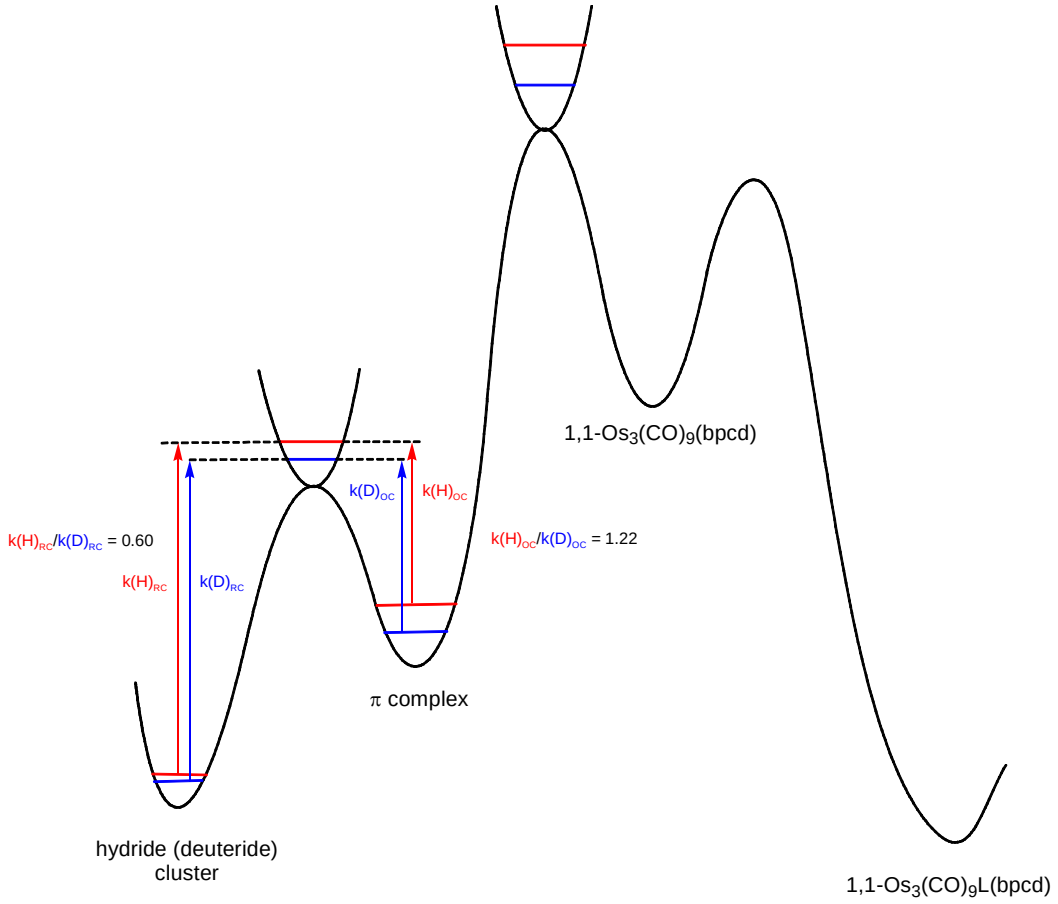

Figure 4.18. Reaction coordinate for the multistep conversion of $HOs_3(CO)_9[\mu$-$(PPh_2)C{=}C\{PPh(C_6H_4)\}C(O)CH_2C(O)]$ to $1,1$-$Os_3(CO)_9L$(bpcd) in the presence of trapping ligands. (Reprinted with permission from *Organometallics* **2006**, 25, 930-945. Copyright 2006 American Chemical Society.)

Table 4.6. Experimental Rate Constants for the Conversion of $HOs_3(CO)_9[\mu$-$(PPh_2)C{=}C\{PPh(C_6H_4)\}C(O)CH_2C(O)]$ to $HOs_3(CO)_8(\mu_3$-$C_6H_4)[\mu_2,\eta^1$-$PPhC{=}C(PPh_2)C(O)CH_2C(O)]$[a]

Temp (K)	10^4k (s^{-1})
363.0	1.31 ± 0.04
368.0	2.21 ± 0.03
373.0	3.58 ± 0.04
378.0	7.10 ± 0.10
383.0	11.0 ± 0.3

[a]The UV-VIS kinetic data were collected in toluene using ca. 10^{-4} M $HOs_3(CO)_9[\mu$-$(PPh_2)C{=}C\{PPh(C_6H_4)\}C(O)CH_2C(O)]$ by following the decrease in the absorbance of the 396 nm band. (Reprinted with permission from *Organometallics* **2006**, 25, 930-945. Copyright 2006 American Chemical Society.)

J. Chapter References

1. (a) Deeming, A. J.; Donovan-Mtunzi, S.; Hardcastle, K. I.; Kabir, S. E.; Henrick, K.; McPartlin, M. *J. Chem. Soc., Dalton Trans.* **1988**, 579. (b) Deeming, A. J.; Donovan-Mtunzi, S.; Kabir, S. E. *J. Organomet. Chem.* **1984**, *276*, C65. (c) Johnson, B. F. G.; Lewis, J.; Reichert, B. E.; Schorpp, K. T. *J. Chem. Soc., Dalton Trans.* **1976**, 1403.
2. Sandström, J. Dynamic NMR Spectroscopy. Academic Press: New York, 1982.
3. Deeming, A. J. *Adv. Organomet. Chem.* **1986**, *26*, 1.
4. (a) Van Raaij, E. U.; Schmulbach, C. D.; Brintzinger, H. H. *J. Organomet. Chem.* **1987**, *328*, 275. (b) Basickos, L.; Bunn, A. G.; Wayland, B. B. *Can. J. Chem.* **2001**, *79*, 854.
5. Crumpton-Bregel, D. M.; Goldberg, K. I. *J. Am. Chem. Soc.* **2003**, *125*, 9442.

6. For some other examples exhibiting chelate-ring opening, see: (a) Knebel, W. J.; Angelici, R. J. *Inorg. Chem.* **1974**, *13*, 627; 632. (b) Schultz, L. D.; Dobson, G. R. *J. Organomet. Chem.* **1976**, *124*, 19. (c) Dobson, G. L.; Cortés, J. E. *Inorg. Chem.* **1988**, *27*, 3308. (d) Henderson, R. A. *J. Chem. Soc., Dalton Trans.* **1988**, 509; 515.

7. In principle the VT ^{13}C NMR spectra of both 1,2-$Os_3(CO)_{10}$(bpcd) and 1,1-$Os_3(CO)_{10}$(bpcd) could provide critical data capable of differentiating the two proposed diphosphine scrambling mechanisms. Unfortunately, the complete coalescence of all carbonyl groups in 1,2-$Os_3(CO)_{10}$(bpcd) and 1,1-$Os_3(CO)_{10}$(bpcd) by 363 K does not allow the ^{13}C NMR data to distinguish between the two mechanisms depicted in Scheme 4.6.

8. The scrambling of the carbonyl groups in 1,2- $Os_3(CO)_{10}$(bpcd) and 1,1-$Os_3(CO)_{10}$(bpcd) followed terminal-bridge-terminal merry-go-round and turnstile processes found in other phosphine-substituted Os_3 clusters. For related VT NMR studies, see: (a) ref. 1a. (b) Deeming, A. J.; Stchedroff, M. *J. Chem. Soc., Dalton Trans.* **1998**, 3819. (c) Deeming, A. J.; Donovan-Mtunzi, S,; Kabir, S. E. *J. Organomet. Chem.* **1985**, *281*, C43. (d) Alex, R. F.; Pomeroy, R. K. *Organometallics* **1987**, *6*, 2437.

9. The simplicity alluded to stems from the application of Occam's razor.

10. In the case of an isomerization reaction involving a dppe ligand, an intermediate state can be envisioned where the hydrogen atoms of the ethane backbone must adoption an eclipsed conformation during the bridge⇔chelate transformation. This specific

destabilization is avoided in diphosphines possessing an unsaturated carbon backbone.

11. Unpublished results.

12. Our isomerization data for 1,2- $Os_3(CO)_{10}$(bpcd)⇔1,1-$Os_3(CO)_{10}$(bpcd) parallel those of $Os_3(CO)_{10}(Ph_2PCH_2CH_2SMe)$, where thiophosphine isomerization is believed to proceed through a bridging thioether moiety. See: Persson, R.; Monari, M.; Gobetto, R.; Russo, A.; Aime, S.; Calhorda, M. J.; Nordlander, E. *Organometallics* **2001**, *20*, 4150.

13. (a) Cotton, F. A. *Inorg. Chem.* **1966**, *6*, 1083. (b) Johnson, B. F. G.; Lewis, J.; Reichert, B. E.; Schorpp, K. L. *J. Chem. Soc., Dalton Trans.* **1976**, 1403. (c) Cotton, F. A.; Hanson, B. E. In *Rearrangements in Ground and Excited States*, de Mayo, P., Ed.; Academic Press: New York, 1980; Chap. 12.

14. Adams, R. D.; Captain, B.; Fu, W.; Pellechia, P. J. *Inorg. Chem.* **2003**, *42*, 3111.

15. Ohki, Y.; Suzuki, H. *Angew. Chem. Int. Ed.* **2002**, *41*, 2994.

16. For additional reports of phosphine-ligand isomerization in metal clusters, see: (a) Laurenczy, G.; Bondietti, G.; Ros, R.; Roulet, R. *Inorg. Chim. Acta* **1996**, *247*, 65.(b) Braunstein, P.; Boag, N. M. *Angew. Chem. Int. Ed.* **2001**, *40*, 2427. (c) Bradford, A. M.; Douglas, G.; Manojlović-Muir, L.; Muir, K. W.; Puddephatt, R. J. *Organometallics* **1990**, *9*, 409.

17. (a) Balch, A. L.; Davis, B. J.; Olmstead, M. M. *J. Am. Chem. Soc.* **1990**, *112*, 8592; *Inorg. Chem.* **1993**, *32*, 3937. (b) Pechmann, T.; Brandt, C. D.; Werner, H. *Angew.*

Chem. Int. Ed. **2000**, *39*, 3909; *Chem. Commun.* **2003**, 1136. (c) Pechmann, T.; Brandt, C. D.; Roger, C.; Werner, H. *Angew. Chem. Int. Ed.* **2002**, *41*, 2301.

18. Blasco, S.; Demachy, I.; Jean, Y.; Lledos, A. *New. J. Chem.* **2002**, *26*, 1118.

19. In a subsequent paper by the same researchers, it was disclosed that a multistep process involving the dissociative release of one arm of the diphosphine ligand, followed by phosphine migration and ligand reattachment, was energetically competitive to the concerted phosphine migration process reported in ref. 32. Since a dissociative mechanism is not supported by the kinetic data, it can be excluded from consideration. See: Demachy, I.; Jean, Y.; Lledos, A. *New. J. Chem.* **2004**, *28*, 1494.

20. (a) Garrou, P. E. *Chem. Rev.* **1981**, *81*, 229. (b) Richmond, M. G.; Kochi, J. K. *Inorg. Chem.* **1987**, *6*, 254.

21. (a) Ohki, Y.; Suzuki, H. *Angew. Chem. Int. Ed.* **2002**, *41*, 2994. (b) See also: Persson, R.; Monari, M.; Gobetto, R.; Russo, A.; Aime, S.; Calhorda, M. J.; Nordlander, E. *Organometallics* **2001**, *20*, 4150. (c) Yang, K.; Smith, J. M.; Bott, S. G.; Richmond, M. G. *Organometallics* **1993**, *12*, 4779. (d) Bott, S. G.; Yang, K.; Richmond, M. G. *J. Organomet. Chem.* **2005**, *690*, 3067. (e) Watson, W. H.; Wu, G.; Richmond, M. G. *Organometallics* **2005**, *24*, 5431.

22. This assertion concerning the formation of an unsaturated intermediate as a steady-state species is valid provided that the rate of ring closure (to either the bridged or chelated cluster) is slow relative to the rate of the ligand trapping reaction. For some related examples, see: (a) Glueck, D. S.; Bergman, R. G. *Organometallics* **1991**, *10*, 1479. (b) Mao, F.; Tyler, D. R.; Keszler, D. *J. Am. Chem. Soc.* **1989**, *111*, 130. (c)

Jones, W. D.; Libertini, E. *Inorg. Chem.* **1986**, *25*, 1794.

23. It is noted that an independently prepared sample of $Os_3(CO)_{11}(\eta^1$-bpcd) was found to be stable towards ring closure to $Os_3(CO)_{10}$(bpcd) under the conditions identical to those employed in our isomerization reaction.

24. This situation is akin to assigning the locus of CO dissociation in a metal carbonyl cluster when the rate of carbonyl scrambling about the cluster polyhedron exceeds the rate of dissociative CO loss by several orders of magnitude. See: Richmond, M. G.; Kochi, J. K. *Inorg. Chem.* **1986**, *25*, 1334.

25. The VT ^{13}C NMR behavior of 1,1-$Os_3(CO)_{10}$(bpcd) has also been studied in toluene-d_8 solution, with comparable CO fluxionality, vis-à-vis 1,2-$Os_3(CO)_{10}$(bpcd), observed.

26. The small amount of $HOs_3(CO)_9[\mu$-$(PPh_2)C{=}C\{PPh(C_6H_4)\}C(O)CH_2C(O)]$ in the thermolysis starting with cluster 1,1-$Os_3(CO)_{10}$(bpcd) does not adversely affect the outcome of the reaction.

27. (a) van Outersterp, J. W. M.; Oostenbrink, M. T. G.; Nieuwenhuis, H. A.; Stufkens, D. J.; Hartl, F. *Inorg. Chem.* **1995**, *34*, 6312. (b) Bakker, M. J.; Hartl, F.; Stufkens, D. J.; Jina, O. S.; Sun, X.-Z.; George, M. W. *Organometallics* **2000**, *19*, 4310. (c) Vergeer, F. W.; Kleverlann, C. J.; Stufkens, D. J. *Inorg. Chim. Acta* **2002**, *327*, 126. (d) Vergeer, F. W.; Kleverlaan, C. J.; Matousek, P.; Towrie, M.; Stufkens, D. J.; Hartl, F. *Inorg. Chem.* **2005**, *44*, 1319.

28. For $Os_3(CO)_{12}$ photochemistry involving CO loss, see: Bentsen, J. G.; Wrighton, M. S. *J. Am. Chem. Soc.* **1987**, *109*, 4518 and references therein.

29. (a) Jones, W. D.; Feher, F. J. *Acc. Chem. Res.* **1989**, *22*, 91. (b) Arndtsen, B. A.; Bergman, R. G.; Mobley, T. A.; Peterson, T. H. *Acc. Chem. Res.* **1995**, *28*, 154. (c) Jones, W. D. *Acc. Chem. Res.* **2003**, *36*, 140. (d) Churchill, D. G.; Janak, K. E.; Wittenberg, J. S.; Parkin, G. *J. Am. Chem. Soc.* **2003**, *125*, 1403. (e) Jones, W. D. *Inorg. Chem.* **2005**, *44*, 4475. (f) Lersch, M.; Tilset, M. *Chem. Rev.* **2005**, *105*, 2471.

30. No kinetic distinction between an arene π or an agostic interaction involving the *ortho* C-H(D) bond can be made based on the data at hand. However, given the preponderance of structural and solution examples of η^2-bound arene complexes, the intermediate in the present orthometalation reaction will be treated similarly. See: (a) Cheng, T.-Y.; Szalda, D. J.; Bullock, R. M. *Chem. Commun.* **1999**, 1629. (b) Johansson, L.; Tilset, M.; Labinger, J. A.; Bercaw, J. E. *J. Am. Chem. Soc.* **2000**, *122*, 10846. (c) Reinartz, S.; White, P. S.; Brookhart, M.; Templeton, J. L. *J. Am. Chem. Soc.* **2001**, *123*, 12724.

31. For some representative examples, see: (a) Parkin, G.; Bercaw, J. E. *Organometallics* **1989**, *8*, 1172. (b) Buchanan, J. M.; Stryker, J. M.; Bergman, R. B. *J. Am. Chem. Soc.* **1986**, *108*, 1537. (c) Janowicz, A. H.; Bergman, R. B. *J. Am. Chem. Soc.* **1983**, *105*, 3929. (d) Jones, W. D.; Feher, F. J. *J. Am. Chem. Soc.* **1986**, *108*, 4814. (e) Jensen, M. P.; Wick, D. D.; Reinartz, S.; White, P. S.; Templeton, J. L.; Goldberg, K. I. *J. Am. Chem. Soc.* **2003**, *125*, 8614. (f) Wick, D. D.; Reynolds, K. A.; Jones, W. D. *J. Am. Chem. Soc.* **1999**, *121*, 3974. (g) Bullock, R. M.; Headford, C. E. L.; Hennessy, K. M.; Kegley, S. E.; Norton, J. R. *J. Am. Chem. Soc.* **1989**, *111*, 3897.

32. Based on the totality of the available data for reductive coupling processes not

proceeding via free-radical paths, a single-step reaction having a product-like or late transition state can be neglected in favor of a multistep sequence for the formation of the aryl C-H bond in $HOs_3(CO)_9[\mu\text{-}(PPh_2)C{=}C\{PPh(C_6H_4)\}C(O)CH_2C(O)]$.

33. For related C-H bond activation reactions at Ru_3 and Os_3 clusters, see: (a) Calvert, R. B.; Shapley, J. R. *J. Am. Chem. Soc.* **1977**, *99*, 5225. (b) Duggan, T. P.; Golden, M. J.; Keister, J. B. *Organometallics* **1990**, *9*, 1656.

34. Studies on the kinetic trapping of the unsaturated cluster $1,1\text{-}Os_3(CO)_9(bpcd)$, as generated from $HOs_3(CO)_9[\mu\text{-}(PPh_2)C{=}C\{PPh(C_6H_4)\}C(O)CH_2C(O)]$, in the presence of CO (low pressure) show saturation kinetics arising from the competitive capture of $1,1\text{-}Os_3(CO)_9(bpcd)$ by the arene ; bond and CO. Watson, W. H.; Wu, G.; Richmond, M. G. *Organometallics* **2006**, *25*, 930.

35. A preparative reaction between $HOs_3(CO)_9[\mu\text{-}(PPh_2)C{=}C\{PPh(C_6H_4)\}C(O)CH_2C(O)]$ and excess PPh_3 (1:10 mole ratio) has been conducted and $1,1\text{-}Os_3(CO)_9(PPh_3)(bpcd)$ isolated by column chromatography. On the basis of ^1H and ^{31}P NMR data, the major stereoisomer present (> 90%) found in solution contains a chelating bpcd ligand and one equatorially bound PPh_3 ligand that is attached to an adjacent osmium atom. ^{31}P NMR (C_6D_6, 298 K): δ 16.62 (1P, d, bpcd, $J_{P\text{-}P}$ = 12 Hz), 15.47 (1P, d, bpcd, $J_{P\text{-}P}$ = 12 Hz), -6.64 (s, 1P, PPh_3). ^1H NMR (C_6D_6, 298 K): δ 6.85-8.00 (35 H, multiplet), 2.43 (2H, s, methylene).

36. Periana, R. A.; Bergman, R. G. *J. Am. Chem. Soc.* **1986**, *108*, 7332.

37. The presence of the bridging deuteride ligand in $DOs_3(CO)_9[\mu\text{-}(PPh_2\text{-}$

d_{2ortho})C=C{P(Ph-d_{1ortho})(C_6H_4)}C(O)CH_2C(O)] was also verified by ^{2}H NMR analysis that revealed a broadened, high-field resonance at ca. -16 ppm.

38. The difference in the EIE values (0.88 vs 0.49) obtained from the two different ligands (bpcd-d_{20} and bpcd-d_{4ortho}) presumably reflects the effect of isotopic substitution at the α, β, and γ aryl C-H(D) bonds (relative to the orthometalated carbon) of the two ligands.

39. (a) Bullock, R. M.; Bender, B. R. Isotope Methods in Homogeneous Catalysis, in *Encyclopedia of Catalysis*, Horváth, I. T., Ed.; Wiley: New York, 2003. (b) Wolfsberg, M. *Acc. Chem. Res.* **1972**, *7*, 225.

40. Technically, the observed reductive coupling step requires a short-lived terminal Os-H(D) ligand prior to the formation of the coordinated ; complex based on microscopic reversibility. VT ^{1}H NMR analysis of $HOs_3(CO)_9$[μ-(PPh_2)C=C{PPh(C_6H_4)}C(O)CH_2C(O)] showed no evidence for hydride fluxionality over the temperature range 298-340 K, as only a sharp high-field triplet at δ -15.91 (in benzene-d_6) was observed. In terms of the reaction coordinate depicted in Figure 4.18, the reductive coupling is shown arising directly from the bridging clusters to the corresponding π complex directly for simplicity. It is acknowledged that the situation is more complex with an small equilibrium isotope expected between the bridging hydride(deuteride) clusters and the terminal hydride(deuteride) isomers that furnish the ; complex.

41. For structurally characterized clusters possessing an η^1-phenyl moiety, see: (a) Bruce,

M. I.; Humphrey, P. A.; Skelton, B. W.; White, A. H. *J. Organomet. Chem.* **1996**, *526*, 85. (b) Deeming, A. J.; Smith, M. B. *J. Chem. Soc., Dalton Trans.* **1993**, 3383. (c) de Araujo, M. H.; Vargas, M. D.; Braga, D.; Grepioni, F. *Polyhedron* **1998**, *17*, 2865. (d) Briard, P.; Cabeza, J. A.; Llamazares, L.; Riera, V. *Organometallics* **1993**, *12*, 1006. (d) Chen, G.; Deng, M.; Lee, C. K.; Leong, W. K. *Organometallics* **2002**, *21*, 1227. (e) Leong, W. K.; Chen, G. *Organometallics* **2001**, *20*, 2280.